University of Nevada, Reno

Igneous and Hydrothermal Geology of the Central Cherry Creek Range, White Pine County, Nevada

A thesis submitted in partial fulfillment of the requirements

for the degree of Master of Science in Geology

by

David J. Freedman

Dr. Michael W. Ressel, Thesis Advisor

May, 2018

THE GRADUATE SCHOOL

We recommend that the thesis
prepared under our supervision by

DAVID JOSEPH FREEDMAN

entitled

Igneous and Hydrothermal Geology of the Central Cherry Creek Range,
White Pine County, Nevada

be accepted in partial fulfillment of the
requirements for the degree of

MASTER OF SCIENCE

Michael W. Ressel, PhD, Advisor

John L. Muntean, PhD, Committee Member

Douglas P. Boyle, PhD, Graduate School Representative

David W. Zeh, PhD, Dean, Graduate School

May, 2018

Abstract

The central Cherry Creek Range exposes a nearly intact, 8-km thick crustal section of Precambrian through Eocene rocks in a west-dipping homocline. Similar tilts between Eocene volcanic rocks and underlying Paleozoic carbonates demonstrate that tilting and exhumation largely occurred during post-Eocene extensional faulting, thus allowing for relatively simple paleo-depth determinations of Eocene intrusions and mineral deposits. The study area is cored by the Cherry Creek quartz monzonite pluton (35 km^2 exposure; ~132 km^2 coincident magnetic anomaly), which was emplaced into Precambrian and Cambrian meta-sedimentary strata between 37.9-36.2 Ma and is exposed along the east side of the range. The pluton and overlying Paleozoic strata are cut by abundant 35.9-35.1 Ma porphyritic silicic dikes.

A range of polymetallic mineralization styles are hosted by the intrusive rocks along two deeply-penetrating, high-angle faults and their intersections with favorable Paleozoic units. Geochemical, geochronological, petrographic, and field mapping show progression among hydrothermal ore deposits from the mesozonal intrusion-proximal through the epizonal intrusion-distal environments. Data indicate that both the intrusions and hydrothermal deposits at Cherry Creek are exclusively Eocene, and were developed prior to the westward tilt that affects rocks above and below the Eocene unconformity. The deepest-formed and highest-temperature deposits are intrusion-related Sn-W-(Mo) greisen and Au-rich polymetallic vein mineralization that occurred at paleodepths of 7-8 km and developed during the emplacement of the Cherry Creek pluton based on $^{187}Re/^{187}Os$ and $^{238}U/^{206}Pb$ ages. Carbonate replacement deposits containing Ag-Pb-Zn-(W) occurred at intermediate depths of ~4-5 km during the Eocene, whereas distal-disseminated Au-Ag and Carlin-Type Au deposits (CTDs) formed slightly later than high-temperature deposits in shallower environments, from 1-3 km below the Eocene

unconformity. The close timing and spatial associations suggest a link between all deposits and the development of the Cherry Creek intrusive complex.

These findings imply that Eocene CTDs relate to large deep-seated plutons and/or batholiths, not to shallow porphyry-type plutons, and that shallow CTDs are potentially zoned with deep Sn-W-Mo greisen and high-temperature Au-rich vein and replacement deposits. Late Eocene magmatic-hydrothermal events at Cherry Creek regionally coincided with a major metallogenic period in the Cordillera that resulted in the formation of economically important CTDs.

Acknowledgements

This thesis would not have been possible without the help of many people over the last three years. First, thanks to David Tretbar and Summit Mining International for going above and beyond to fund the project, provide support in Cherry Creek during the 5 months of field work, and for his continued interest in the project. Thanks to my thesis committee, especially to my adviser Dr. Mike Ressel for his patience and enthusiasm during the writing process. Thanks to Dr. John Muntean for his tireless hard work towards the success of the CREG program and its students. Thanks to Dr. Doug Boyle who served as outside committee member. Thanks to Will Ostrenga and Jamie Robinson for their great company and geologic conversation in the field. Thanks to Dr. Paul O'Sullivan, Dr. Rob Creaser, and Kathleen Zanetti for their assistance with the geochronology presented in this thesis. Thanks to my classmates in CREG, especially to Micah Claypoole, Rob Selwood, and Patrick Quillen who saw the whole thing.

Table of Contents

List of Tables

List of Figures

Introduction

During the late Eocene, the Great Basin experienced a period of intense magmatism and hydrothermal mineralization, forming a variety of metallic mineral deposits. Intrusion-associated deposits such as Cu-Au-Mo and Mo porphyries, polymetallic and Au skarns, and distal-disseminated Au-Ag formed in clear conjunction with upper crustal granitic intrusions and their associated magmatic-hydrothermal processes during this 42-36 Ma window, although the origin of other deposit types in this period are more controversial. Arguments over the genesis of Carlin-type gold deposits (CTGDs), a class of sedimentary-hosted, disseminated deposit defined by decalcification, silicification, and an association with Au-As-Hg-Sb-Tl (Hofstra and Cline, 2000), are especially significant. CTGDs are well studied in the Carlin, Cortez, Battle Mountain-Eureka, and Getchell trends that have made Nevada one of the world's leading gold producers. One unresolved point of the magmatic-hydrothermal origin hypothesis of Carlin-type deposits is the lack of typical magmatic-hydrothermal zoning along the conduits that would have allowed for fluids to reach the shallow environment from deep plutonic sources below the depth of typical porphyry systems (Cline et al., 2005, Muntean et al., 2011). No major Carlin-type districts expose more than 2 or 3 km of crustal section, and their underlying hydrothermal architecture and mesozonal roots remain buried and have not been studied.

The central Cherry Creek Range (Figure 1) and the adjoining northern Egan Range are composed of a west-dipping homocline that reveals 7 to 8 km of Precambrian through Permian strata. On the east side of the Cherry Creek Range, Neoproterozoic phyllite and quartzite at the base of the section was intruded by the 35 km^2 Eocene Cherry Creek pluton, and on its west side the Eocene unconformity atop Pennsylvanian-Permian sedimentary rocks is overlain by nearly concordant Eocene volcanic rocks (McKee et al., 1973). This 8-km-thick section between the

Cherry Creek pluton and the Eocene volcanic rocks is exposed by Miocene and younger extensional faulting that exhumed and tilted the range but largely left its Eocene architecture intact (Best and Christiansen, 1991a). In Cherry Creek, the presence of a nearly complete stratigraphic section and a major Eocene intrusive center containing abundant base and precious metal mineralization, and a lack of pre-Eocene intrusive activity, make the central Cherry Creek Range an ideal location in which to study the age, distribution, and origin of various Eocene deposits, including Carlin-type gold deposits.

Few studies have examined the relationships between deeply and shallowly seated mineralization from the same crustal column, but many have addressed the significance of vertical zoning in hydrothermal systems at the district-scale such as Kalamazoo, Arizona (Park, 1957) Maricunga, Chile (Muntean and Einaudi, 2001) and Yerington, Nevada (Dilles, 1987). In the central Cherry Creek Range, the 8-km thick section provides an opportunity to examine the Eocene crust from surface to a deeply-seated pluton. Large mesozonal plutons like those exposed at Cherry Creek have been hypothesized to source and drive the circulation of Carlin-type fluids elsewhere in Nevada (Muntean et al., 2011; Ressel and Henry, 2006). Properties of the Eocene hydrothermal geology exposed in the central Cherry Creek Range suggest that the differences in metal contents, deposit styles, and alteration are functions of their structural level and distance from the deep-seated Cherry Creek pluton. The presence of polymetallic greisen and phyllic alteration in the Cherry Creek pluton signifies that high-temperature hydrothermal conditions prevailed at Eocene paleodepths depths of ~8 km based on estimates of the pre-tilt thickness of overlying strata. Strong spatial and geochemical associations of these magmatic-hydrothermal deposits with quartz vein-controlled mineralization in the flanking and overlying phyllites and quartzites indicate that hydrothermal communication between the pluton and

deeply buried sedimentary rocks was established in the late Eocene, allowing ore-forming fluids to ascend to higher structural levels. The main conduits that allowed for fluid ascent are two major subparallel, high-displacement ENE-striking faults that mostly predate the Eocene intrusions. Above the level of the pluton, hydrothermal alteration and mineralization are localized along these faults and their intersections with other structures in Cambrian carbonate strata. The character of carbonate-hosted mineralization contrasts with the intrusion-proximal deposits, and with carbonate-hosted mineralization at still higher structural levels. The deposits closest to the Eocene paleosurface bear similarities to Carlin-type deposits elsewhere in the range and northeast Nevada. The fact that these varied deposits exist one above the other in the Cherry Creek Range suggests that they may have similar genetic origins, such as a common deep-seated magmatic source for heat and metals.

This study tests the hypothesis that magmatic-hydrothermal fluids associated with igneous phases of the Cherry Creek pluton were responsible for the polymetallic zonation in the district as a function of structural depth in the Eocene. The practical goals of the project are to determine the relationships between magmatism and the diverse mineral deposits in the central Cherry Creek Range, and to test the hypothesis that magmatic-hydrothermal fluids associated with igneous phases of the Cherry Creek pluton were responsible for the metal zonation in the district as a function of structural depth in the Eocene. This study 1) assesses the range of spatial patterns, petrographic and chemical conditions, and ages of the igneous rocks of the central Cherry Creek Range, 2) establishes the geologic relationships, distribution, composition, and age of mineralization associated with deep hydrothermal activity, and 3) draws spatial, temporal, and chemical comparisons between deep and shallow mineralization.

Geologic History of the Great Basin

The geologic construction of Nevada began with accretion of Proterozoic terranes onto Archean continental lithosphere. In northeastern Nevada and northwestern Utah, the boundary between Archean and Proterozoic crustal segments is inferred to be an arcuate east-west trending suture that separates the Archean Wyoming Craton in the north from tectonic mélange of the Proterozoic Mojave and Yavapai-Mazatzal provinces in the south. These blocks formed the western side of Laurentia, which was incorporated into the supercontinent Rodinia during the Mesoproterozoic. When breakup of Rodinia began in the Neoproterozoic, rifting along the western margin of Laurentia separated the crust of eastern and central Nevada from adjoining Precambrian continental rocks of uncertain affinity and delineated the western margin of the Paleozoic North American continent.

Between the Neoproterozoic and early Mesozoic, sedimentation along this margin resulted in deposition of siliciclastic and carbonate strata of miogeoclinal affinity in shelf and slope environments from west-central Utah to central Nevada, while areas to the west accumulated oceanic basinal sediment. Accumulations of strata during this time amounted to as much as twelve kilometers in the shelf environment of eastern Nevada (Poole et al., 1993). East-west directed convergence eventually ended miogeoclinal deposition and triggered the Antler and Sonoma orogenies in the Devonian and Permian. In western and central Nevada, these events resulted in the emplacement of the Roberts Mountains and Golconda allochthons eastward from the oceanic basin toward the continental margin. Eastern Nevada occupied the foreland of these events, and experienced shallow-marine and basinal sedimentation in the Mississippian through Permian and locally into the Triassic (Dickinson, 2006).

Tectonism shifted in the Mesozoic with the activation of the Pacific subduction zone along the western margin of North America. East-directed subduction caused arc-related magmatism to occur starting in the Late Triassic, forming an extensional backarc environment in west-central Nevada, which was later inverted and thrust eastward along the Luning-Fencemaker fault system towards central Nevada. Episodic subduction-related magmatism continued in the arc and backarc through the Cretaceous, resulting in the emplacement of Jurassic (~155-165 Ma) and Cretaceous (~130-90 Ma) plutons including some that formed far inboard of the continental margin. Evidence of a limited degree of synkinematic metamorphism and magmatism in eastern Nevada is found in close association with plutons as young as Late Cretaceous in eastern Nevada's Snake Range (Hose and Blake, 1976), suggesting that latest Cretaceous mid-crustal deformation associated with the Sevier orogeny accompanied latest Mesozoic S-type magmatism. Others have invoked a period of Late Jurassic ductile deformation and metamorphism as well (Thorman and Peterson, 2004).

During the Late Cretaceous, low-angle subduction and arc magmatism began nearer the continental margin and migrated eastward towards the continental interior. This magmatic incursion was accompanied by retroarc thrusting along the Sevier orogenic belt, which reached as far as Utah by the Paleogene (Armstrong, 1968). The Sevier Orogeny triggered significant crustal shortening along thin-skinned thrusts that manifested particularly along bedding in the Paleozoic rocks of the miogeocline. Although thrusting was most significant along the leading edge of the Sevier belt in western and central Utah, its western hinterland in Nevada was also shortened, particularly at depth (e.g., Decelles, 2004). The locus of hinterland deformation was mainly in deeply buried rocks of Neoproterozoic and older age (Armstrong, 1968). Deep-seated thickening coincided with magmatism and mid to upper crustal metamorphism at greenschist to

amphibolite conditions (Long and Soignard, 2016; Miller and Gans, 1989). The surface expression of the Sevier hinterland uplift was subdued and largely limited to broad folding that exposed Mesozoic and upper Paleozoic rocks by the Early Cenozoic. These surfaces correspond to regional unconformities that represent the Eocene-Oligocene paleosurface.

The eastern extent of contractional deformation related to shallow-angle subduction reached eastern Utah and Colorado, manifesting in the basement-rooted deformation of the Laramide orogeny in the Late Cretaceous through Eocene. The end of subduction on the western margin of the continent coincided with the end of regional tectonic compression and foundering of the Farallon plate beneath the continent. Renewed magmatism accompanied asthenospheric upwelling in the early to middle Cenozoic as leading edge of the plate sank into the mantle. Magmatism swept in from the margins of the plate, ending a period of quiescence in the western hinterland and converging from the north and east in northeast Nevada and the south in southern Nevada. Plutonic and volcanic rocks of calc-alkaline affinity are related to this sweep of magmatism that was widespread across much of western North America. This early Cenozoic pulse of magmatism overprinted earlier phases of Jurassic and Cretaceous plutonism that had occurred in the subduction backarc and arc environments of central and eastern Nevada. The most extensive areas of early Cenozoic magmatism occurred between western Montana, Idaho, Colorado, and southwestern Nevada from the late Paleocene to middle Miocene (McKee and Moring, 1996) resulting in the eruption of ash-flow tuffs and lavas that young to the southwest. This slab retreat-related volcanism blanketed much of Nevada and western Utah with widespread Eocene to early Miocene ash-flows, tuffs, and locally extensive lavas that were deposited along the subdued paleosurface that had been quiescent since the Sevier orogeny. The composition of volcanic rocks was dominantly high-potassium, calc-alkaline

rhyolite to andesite. Contemporaneous intrusive igneous rocks were emplaced at plutonic and hypabyssal levels (Best and Christiansen, 1991a; Axen et al., 1993).

Limited backarc extension accompanied this Eocene and Oligocene magmatism in eastern Nevada and western Utah, and regional strain would remain subdued until the Miocene (Best and Christiansen, 1991b). This first phase of Cenozoic extension in the Great Basin, like the Sevier deformation that preceded it, probably involved the middle crust and left the upper crust relatively intact. In eastern Nevada, exhumation of the modern Snake, Ruby-East Humboldt, and Raft River core complexes began at this time (Dickinson, 2006), overprinting the area's Mesozoic magmatic rocks and contractional structures. Limited zones in the Sevier hinterland experienced extension of the upper crust (Druschke et al., 2009), as evidenced by sedimentation in the Elko and other Eocene basins even before the eruption of lavas (Ressel and Henry, 2006), although the origin of these basins is currently debated. The locus of magmatism continued to advance towards southern Nevada until the Miocene, when the end of slab-rollback processes by northwestward propagation of the Mendocino triple junction effectively ended arc magmatism.

By the early Miocene, initiation of transform motion along the San Andreas fault delineated a new boundary of the western North American plate. A transtensional stress state induced by this motion affected Nevada as well as parts of Utah, Wyoming, Idaho, California, and Oregon. This change in regional stress supplanted local backarc tension and triggered the onset of Basin and Range extension and transtension. Block faulting of the upper crust

collapsed the thickened Sevier orogen, forming the modern topography of the province. Eastern Nevada's core complexes that had begun to form in the mid Cenozoic were further exhumed, and the upper crust across the region was variably dissected and tilted by kilometer-scale normal faulting. Basaltic and bimodal magmatism occurred in association with backarc environments in the Cascades region in the Neogene, and contemporaneously in the Great Basin's northern Nevada rift (Zoback et al., 1994).

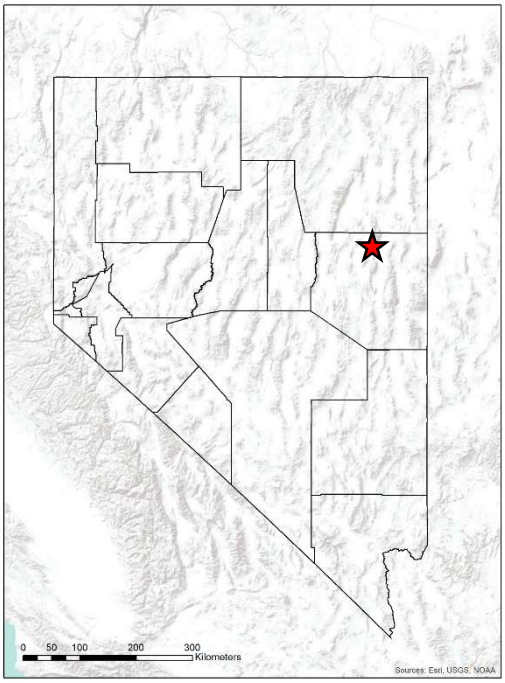

Figure 1. DEM map with outlines of the counties of Nevada. The study area is denoted by a red star in north-central White Pine County

Local Geology

Stratigraphy

The rocks of the Cherry Creek and northern Egan ranges are composed of a west-dipping homocline that exposes eight kilometers of Proterozoic through Permian miogeoclinal strata and Eocene volcanic rocks (Adair, 1961). The oldest rocks at Cherry Creek are exposed along the western edge of Steptoe Valley and the youngest rocks are exposed along the eastern edge of Butte Valley (Figure 2, 3).

The Late Precambrian McCoy Creek Group (MCG) is 1,500 m thick in the central Cherry Creek Range and contains 5 units of thin- to medium-bedded quartzite and phyllite strata that alternate between 150 and 850 m thick (Fritz, 1960). These strata correlate with units of the McCoy Creek Group elsewhere in eastern Nevada and western Utah, and in this study are termed MCG units C through unit G (Woodward, 1967; Misch and Hazzard, 1962). The MCG is overlain by the Cambrian Prospect Mountain Quartzite (PMQ), which is a ~1200-m-thick, medium-grained, thick- to medium-bedded, cross-bedded and laminated quartzite with thin lenses of pebble conglomerate (Adair, 1961). Above the PMQ, the upper Lower Cambrian Pioche Shale is composed of 200 m of silty shale interbedded with thin siltstone and limestone beds up to 5 m thick. The Middle Cambrian rocks include the Burrows, Burnt Canyon, Dome, Swasey, Wheeler, Marjum, Weeks, and Orr formations (Adair, 1961). This Middle Cambrian miogeoclinal sequence contains 1,900 m of alternating massive and thinly bedded limestones, dolomites, marls, and shales that are equivalent to the more widely known Pole Canyon, Lincoln Peak, and Johns Wash formations (Hose et al., 1976). The Upper Cambrian rocks include the silty, 225-m-thick Dunderberg Shale and the 550-m-thick, thin-bedded Notch Peak Limestone.

Ordovician rocks in the Cherry Creek Range are composed of 1,100 m of cherty, thin-bedded, detrital and fossiliferous limestone and some shales assigned to the Pogonip Group, and the thin (< 15 m) Eureka Quartzite. The Silurian Fish Haven and Lake Town dolomites are grouped in the central Cherry Creek Range to an undivided 500 m sequence of fine-grained, crystalline dolomite. The 1150-m-thick undivided unit of Devonian rocks that overlie the Lake Town dolomite include the Sevy, Simonson, and Guilmette dolomites, which also include some subordinate limestones and are differentiated from the Silurian rocks by their finer grain size and thin-bedded characteristic (Hose et al., 1976). The 995 m Carboniferous section is best exposed in the western extremes of the Cherry Creek Range, and consists of the thinly-bedded and commonly nodular Pilot Shale, Joana Limestone, Chainman Shale, and Ely Limestone (Fritz, 1960, 1968). The uppermost Paleozoic rocks belong to the Permian Arcturus Formation and are predominately siltstones and shales, with small amounts of chert.

A major unconformity overlies the Permian and Pennsylvanian carbonate rocks in the central and western Cherry Creek Range. It is marked by the base of a 200-m-thick succession of volcanic rocks including rhyolitic ash and pyroclastic flows and dacitic to andesitic lavas, as well as a few minor rhyolite vitrophyres and tuffs. These near-vent volcanic rocks have 35-50˚ northwest dips, indistinguishable from the dips of Paleozoic rocks exposed less than 300 m away. The absence of an angular unconformity indicates that the tilting of the Cherry Creek Range was accomplished following the deposition of these oldest volcanic rocks. Biotite from two rhyolite vitrophyres within this unit give Eocene K-Ar ages (35.46 ± 1.9 Ma; 35.4 ± 1.4 Ma; McKee et al., 1971).

Igneous Geology

The foremost igneous feature of the Cherry Creek district is the Cherry Creek pluton, a >35 km^2 Eocene quartz monzonite that intrudes Proterozoic and Lower Cambrian phyllite and quartzite along the range's eastern border with Steptoe Valley (Figures 3 and 5; Adair 1961; Hose et al. 1976). The Cherry Creek pluton is continuous with exposures of coarse-grained granitic rocks in the adjoining northern Egan Range on the south side of Egan Canyon, and similar igneous rocks form a segmented band at least 16 km long (Adair 1961). A small (~1 km^2) tonalite stock is also present in the northeast corner of the Cherry Creek district at the mouth of Silver Canyon. Previous published ages on the igneous rocks of the Cherry Creek pluton include three fission-track ages from biotite quartz monzonite exposed in Egan Canyon: one from zircon (36±4 Ma) and two from sphene (45±4 Ma; 40±4 Ma) and two K-Ar biotite ages from biotite quartz monzonite located 5 to 7 km south of Egan Canyon (Armstrong, 1970).

Porphyritic dikes of felsic to mafic composition are abundant in the Cherry Creek pluton as well as in the overlying sedimentary rocks. Of these, felsic dikes are the most abundant type, followed by andesitic and dioritic dikes. Although their frequency diminishes with stratigraphic height, the dikes intrude all structural levels of the district from the pluton to within a kilometer of the base of Eocene volcanic rocks. The position, orientation, and density of dikes is controlled in part by the presence of brittle structures. In rocks of the Cherry Creek pluton, the dikes mainly strike north-northeast and dip moderately to the east, parallel to the predominant joint array affecting the pluton. Above the roof of the pluton, the dikes are hosted mainly in northwest- and northeast-striking high-angle faults, the largest of which is the Exchequer fault.

Eocene volcanic rocks on the west side of the range are informally termed the Johnson Spring volcanics for the small basin in which they occur in the northwest corner of the district.

The map pattern of the Johnson Spring volcanic rocks and their internal flow structures suggests that they have undergone a 40-50˚ westward tilt, roughly parallel to and similar in magnitude to average tilts in pre-Cenozoic rocks to the east. Biotite from two rhyolite vitrophyres on the west side of the range give Eocene K-Ar ages (35.46 ± 1.9 Ma; 35.4 ± 1.4 Ma; McKee et al., 1973).

Structural Geology

I. Pre-intrusion faults

Black Metal, Exchequer, and Gilligan faults

Three Early Cenozoic, east-northeast-trending, high-angle faults are largely responsible for the distinctive S-shape of the central Cherry Creek Range where this study was focused (Figures 2 and 3). The Black Metal and Exchequer faults, together with the smaller Gilligan fault collectively have nearly 2.5 km of apparent dextral displacement across a corridor 10 km wide from Cocomongo Mountain on the south to Exchequer Peak on the north (Adair, 1961). The faults are pre- or broadly syn-intrusion, based on crosscutting relationships between them, small porphyritic dikes, and the plutonic rocks exposed along the eastern range front (Figure 5).

The most persistent of these are the Exchequer and Black Metal faults, which respectively accommodate 650 m and 1500 m apparent dextral displacement and are linked by several smaller NW-striking faults. The Black Metal fault, the most northerly of these faults, strikes N75°E and dips between 60 and 85 degrees to the northwest. The Exchequer fault, the central, strikes N70°E and dips between 64 and 80 degrees to the northwest. The Gilligan fault, located over 6 km to the south of the Exchequer fault, forms a smaller and more poorly exposed structural zone oriented N55°E and dipping between 60 and 80 degrees to the northwest. The corridor defined by these three faults is the setting for most of this study.

Bedding-parallel faults

One significant class of features is a set of pre-intrusion bedding-parallel faults. These bedding-parallel faults manifest most strongly at stratigraphic horizons marked by quartzite-shale or limestone-shale facies changes. The fault planes are usually localized to lithologic contacts between shale and thickly-bedded carbonate or siliciclastic rocks, but in places they ramp upward through basal layers of the hanging wall or cut uppermost layers of the footwall and thin the section. Seven bedding-parallel fault horizons have been documented in the Cherry Creek district (Adair, 1961), and many are marked in places by mineralized, tabular breccia bodies. Much of the brecciation in these mineralized bodies, especially in the middle Cambrian rocks, appears from their lack of milled fragments and matrix-supported nature to be dissolution or hydrothermal breccias. This theory is supported by the variable thickness and consistency of the breccia bodies; even within a single horizon they reach thicknesses of 15 m and yet pinch along strike to nothing. Brecciation is most strongly developed in the limestone footwalls, and gouge is often along the faults' upper margins (Heard, 1881; Adair, 1961). Starting from the bottom, the three contacts that localize breccia bodies are: 1. Cambrian Prospect Mountain Quartzite – Cambrian Pioche Shale, 2. Cambrian Swasey Limestone – Cambrian Wheeler Shale, and 3. Cambrian Marjum Limestone – Cambrian Dunderberg Shale. Other, less conspicuous examples are present elsewhere, including at intraformational facies changes in the thick Swasey and Orr Formations, at the Mississippian Pilot Shale – Chainman Shale contact, and in Proterozoic McCoy Creek rocks to the south of the study area (Adair, 1961; Fritz, 1960). The absolute timing of bedding-fault movement is uncertain, but they are demonstrably older than all other structural or igneous features in the district including the high-angle Exchequer and Black Metal faults and the thin porphyritic dikes, which cut them. None are intruded by sills or

otherwise contain igneous rock. The small stratigraphic omissions along these faults indicate that they have extensional kinematics (Adair, 1961), and the faults do not significantly disrupt the normal stratigraphic order of units.

II. Post-intrusion structures

Joints

A strongly developed array of joints in granitic rocks of the Cherry Creek pluton is the most conspicuous of the post-intrusion structures. In porphyritic quartz monzonite between Cherry Creek and Egan Canyons, the major joint sets are consistently oriented with strikes between N10°E and N30°E with dips between 20 and 40˚ to the east. The intrusive rock is normally deeply weathered, and exposure is generally very poor. Joint spacing varies between 50 cm and 25 m. Several more small zones of jointing are present only in single outcrops.

North-dipping faults

At least two west-striking and moderately north-dipping faults are present in the main body of porphyritic quartz monzonite to the south of Cherry Creek Canyon. Similar strike orientations are present in a few small faults that cut quartzite and phyllite on the north slope of Bull Hill (Figure 4), although they dip more nearly vertical. Another set of north-dipping faults are mineralized at the Star property in El Rey Canyon. Most of these post-intrusion faults are at least weakly mineralized. The hydrothermal aspects of these features are described in more detail below.

East-dipping faults

Along the easternmost edge of the Cherry Creek Range adjacent to Steptoe Valley, rocks of the Cherry Creek pluton are juxtaposed against quartzite and carbonate rocks of Lower Paleozoic and possibly Neoproterozoic age. The faulted contact between the quartz monzonite

and these fractured but unmetamorphosed units is sharp and in all cases dips to the east-southeast between 40 and 55˚. The fault is best exposed along 2.5 km of the range front between Salvi Ranch and Egan Canyon (Figure 5), where historic exploration trenches reveal it between weathered outcrops of quartzite on the east and intrusive rock on the west. In this study, the feature is referred to as the Salvi fault. Isolated outcrops of quartzite exposed through Quaternary alluvial fans define the range-bounding Salvi fault, which is traced along the eastern range front from just south of the Salvi Ranch northward through the town of Cherry Creek and continuing northeast along the eastern edge of the Silver Canyon stock, more than 10 km away. The hydrothermal features of the Salvi fault are discussed at length in the section on hydrothermal geology.

III. Basin and Range faults

Many young, north-trending normal faults also occur in the Cherry Creek Range, and are easily recognizable due to their continuity and the fact that they cut all other structures including those that host mineralization. None of these young Basin and Range faults are mineralized, although hot and cold springs emanate from many points on the range front at the eastern toe of the Cherry Creek Range. Substantially larger Basin and Range faults tilt the section to the west, revealing the complete hydrothermal architecture between pluton and Eocene paleosurface.

Hydrothermal Geology

The Cherry Creek district shows abundant evidence of hydrothermal mineralization in the intervening strata between the pluton on its eastern side and the base of volcanic strata 10 km to the west. The district's deepest exposures of igneous rock have experienced localized

metasomatism, hydrothermal alteration, and sulfide mineralization. Precambrian and early Cambrian quartzite units up to 1.5 km thick host siliceous polymetallic veins above the pluton's roof. Hydrothermally-altered porphyritic dacite and rhyolite dikes occur in close association with horizons of structurally-controlled polymetallic Ag mineralization in west-dipping Cambrian carbonate and siliciclastic rocks. The top two kilometers of Paleozoic carbonate stratigraphy host laterally extensive Au-bearing jasperoid mineralization and felsic porphyry dikes that inhabit structural corridors and lithologic contacts. This hydrothermal footprint encompasses nearly eight kilometers of stratigraphy and is responsible for the metallic mineralization that has allowed over 40 historical mines to operate on the district. Elements of the hydrothermal system have been described in previous studies (Adair, 1961; Morabbi, 1980) but questions on the conditions of mineralization and the relationships among deposits remain outstanding.

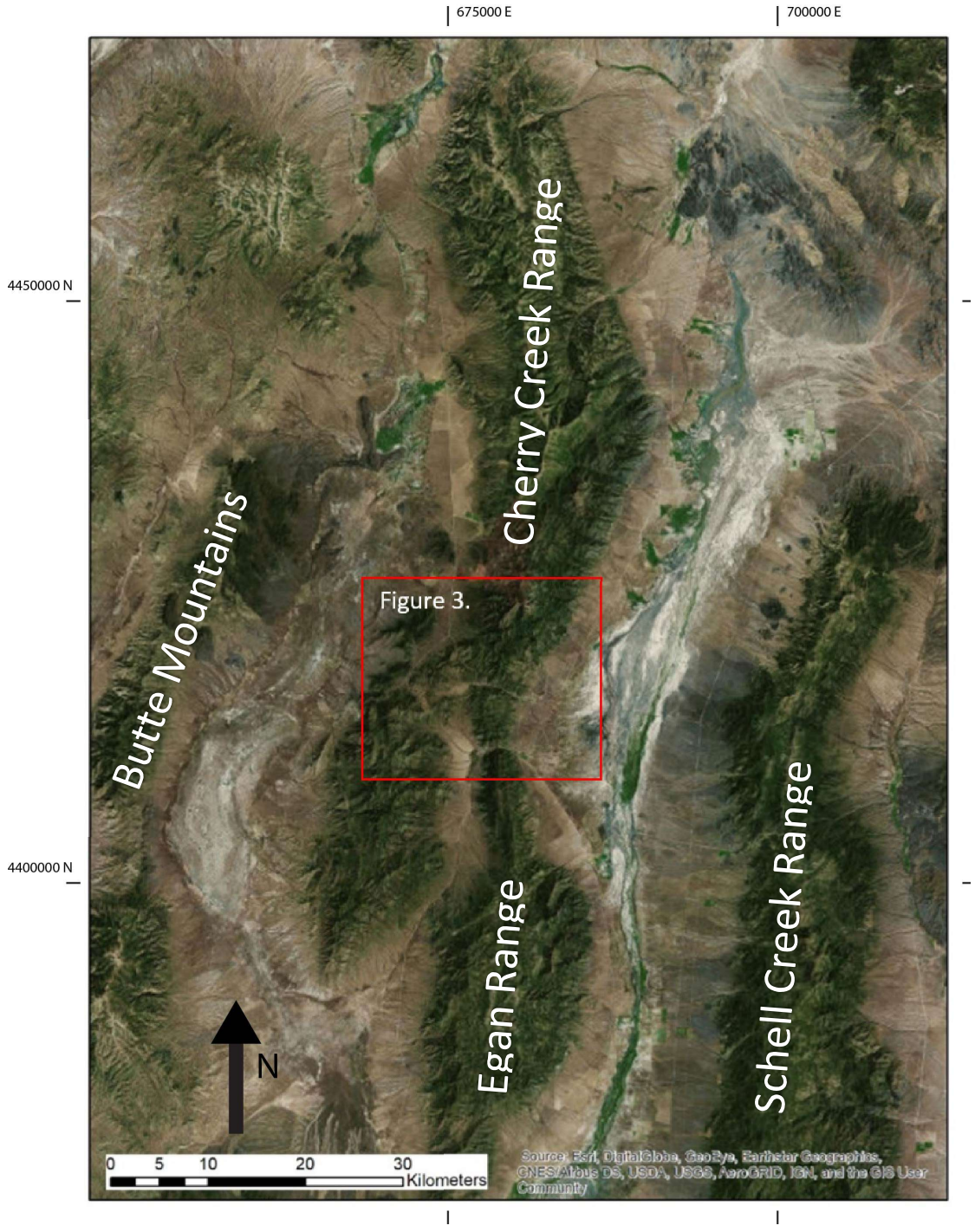

Figure 2. Satellite image of Cherry Creek Range and surrounding area. Steptoe Valley and the Schell Creek Range are to the east of the Cherry Creek Range. Butte Valley and the Butte Mountains are to the west.

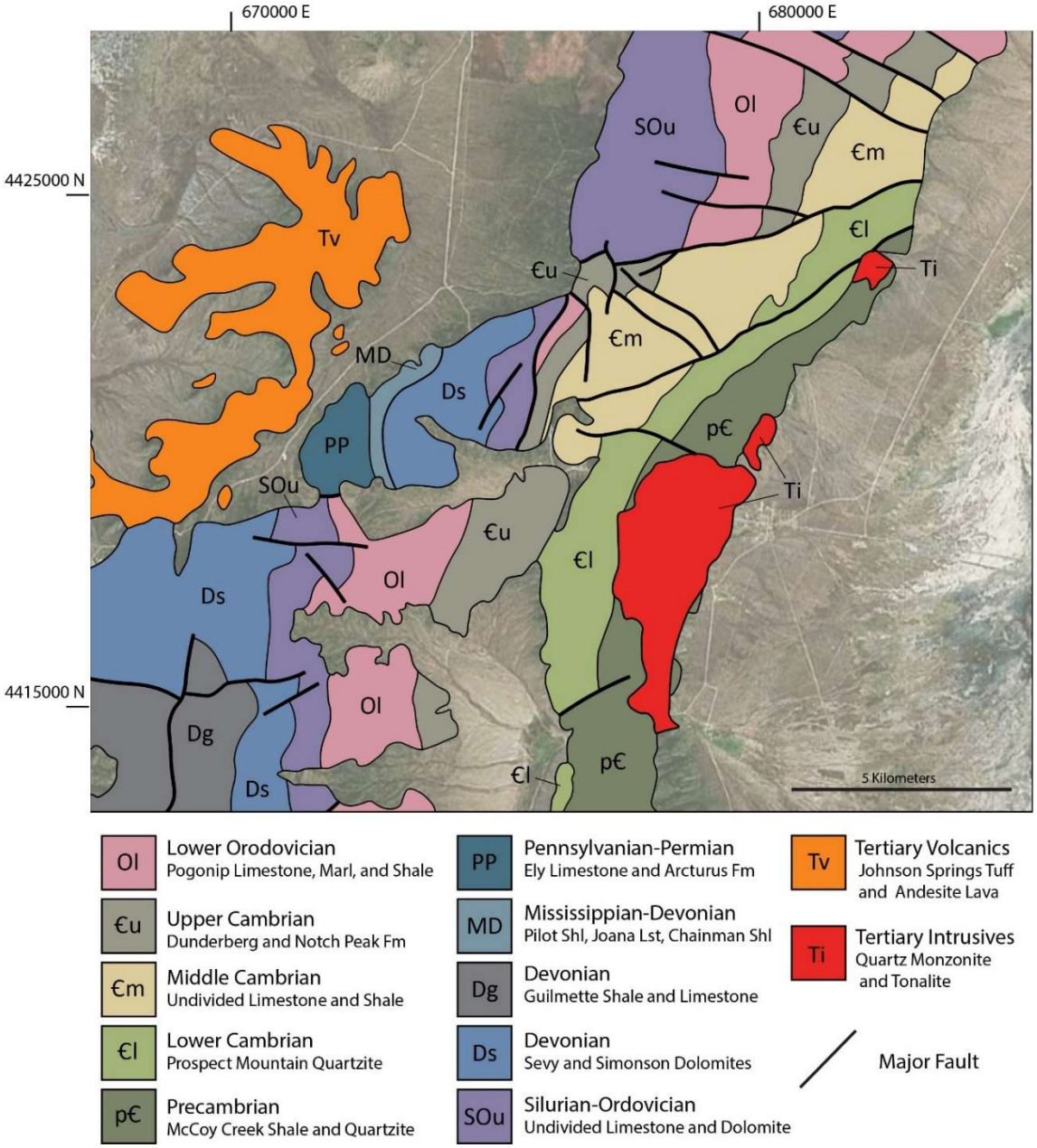

Figure 3. Local geological map of the Central Cherry Creek Range. Adapted from Hose and Blake (1976)

Methodology

Field Mapping and Petrology

During the two field seasons in the summers of 2015 and 2016, mapping, field petrology, and sampling were conducted on the Cherry Creek study area. The primary goals of these activities were 1) to identify and describe the igneous lithologies of the Cherry Creek pluton, 2) to determine the distribution of these lithologies, and 3) to take representative samples for geochronological, geochemical, and petrological analysis. Outcrop mapping of igneous rocks at 1:5,000-scale was conducted using a Brunton pocket transit compass and plotted on a satellite photo and topographic base with mylar overlays for lithological and structural layers. In addition to comprehensive mapping on the east side of the study area, further goals of the two field seasons were to determine the distribution of dikes in the high Cherry Creek Range, particularly around the TiCup project in 2015 during exploration by Summit Mining geologists, and to take samples for geochronological analysis. During 2016, the altered and mineralized rocks of the Cherry Creek pluton were mapped in reconnaissance-style and sampled for geochemical and geochronological analysis. Visits were made to many historical mines in the Cherry Creek area during independent mapping, with project adviser Dr. Mike Ressel, and with Summit Mining geologists. Examinations were made of the dumps, workings, and surrounding geology to describe the salient features of mineralization. In addition, longtime Cherry Creek resident, miner, and prospector Art Ruggles provided invaluable first-hand knowledge of the mines, their production, and their history. During July and August of 2016, the study area was expanded to encompass the Flint Canyon prospect on the west side of the central Cherry Creek Range as exploration by Summit Mining moved into drilling and more

became known about the subsurface relationships of this area. D.H. Adair's 1961 geologic map of the Cherry Creek and northern Egan Range at 1:20,000 scale and W.H. Fritz's 1968 geologic map of the north Egan and west Cherry Creek Range were essential in providing context and a range-scale framework for this study.

Geochemistry

135 outcrop and dump grab samples were collected in the field for geochemical analysis. These samples included unaltered igneous rocks, altered igneous rocks, and mineralized igneous and sedimentary rocks from across the Cherry Creek field area. The samples were trimmed in the field to remove weathered rock, tagged with GPS coordinates, and packed in individual cotton bags pending shipment. All 135 samples were submitted to ALS Laboratories for 66-element analysis including suites for major oxides and several trace-element groups using their whole-rock characterization package CCP-PKG-01. Analyses were completed by ALS Laboratories in Vancouver, British Columbia (major and trace elements) and Reno, Nevada (fire-assay gold). ALS crushed and pulverized the samples, and cycled a blank of geochemically "clean" quartz between samples. Crushing and pulverizing was done using Cr-steel jaw crushers and pulverizing rings. Ten-gram sample pulps were melted using lithium metaborate flux in a reduction furnace, quenched to glass, digested with four acids, and analyzed using ICP-MS and ICP-AES. Gold was determined by fire-assay of 30-gram pulps followed by analysis of the bead by atomic absorption spectroscopy.

In addition to the 135 samples collected by the author, this study also incorporates 805 geochemical analyses of altered and mineralized rock-chip samples from the Summit Mining database, which includes many ICP-MS and ICP-AES trace- and major-element determinations

using a 4-acid (hydrofluoric, perchloric, nitric, and hydrochloric) digestion (ALS ME-MS81 method). Analysis of whole rock and ore chemical data was conducted using Reflex IoGAS and Microsoft Excel software. Assessment of ore geochemistry included simple 1-variable statistics, correlation matrices, cumulative frequency plots, and box and whisker plots.

For the classification of unaltered igneous rocks, this study employed Microsoft Excel and Reflex ioGAS software. Using ioGAS, major-element oxides were normalized to 100% anhydrous and plotted on standard rock classification diagrams. Trace elements and rare earth elements were used for further classification and discrimination using normalized spider plots. For igneous rocks, the signatures of alteration and mineralization were determined by comparing the baseline element concentrations with those of altered and mineralized rock. The baseline values were known from the extensive classification, mapping, and geochemistry conducted during the first phase of the study. Calculations of enrichment and depletion were made using Microsoft Excel and plotted using a custom template based on the isocon diagram (Grant, 1986) and configured to display gains and losses in elemental concentration. In most cases, these plots represent single samples selected as representatives of an alteration assemblage or mineralization type. The many dikes that occur in association with ore deposits at various sites in the range provided an opportunity to evaluate alteration and mineralization outside of the pluton with a similar approach, and in most instances the trace-element suite alone is considered.

In sedimentary-hosted mineralization, data were filtered to focus on quartz veins, quartz-cemented breccias, and pervasively silicified rocks to avoid the complexity of reconciling baseline and enrichment values across different lithologies. Analyses of mineralization focused on 25 trace elements that were selected based on their variation across the district, their

behavior in correlation matrices, and their status as pathfinders or important ore elements. The distributions of these elements were evaluated for normality, skewness, and mineralization range using box plots, cumulative frequency plots, and direct statistical measurements in Reflex ioGAS. Geochemical signatures of mineralization in sedimentary rock-hosted veins were determined by Spearman rank correlation matrices and the relative abundance of key elements. For this study's purpose, the Spearman rank is more appropriate than a simple Pearson value correlation for determining elemental associations because of discrepancies among detection limits of different elements. Spearman correlation is measured in ρ (rho), which falls between -1 for a perfect negative correlation and +1 for a perfect positive correlation.

Petrography

Over the span of the 2015 and 2016 field seasons, 105 rock samples were collected for petrographic studies of the lithologies, alteration, and mineralization of the Cherry Creek district. At the University of Nevada (UNR), the hand samples were cut into slabs using a hydraulic saw with a 36-inch diamond-impregnated masonry blade. These samples were catalogued and described using a binocular scope at 10-30x magnification at the UNR Center for Research in Economic Geology (CREG) lab. Forty rock samples were selected as a representative set for petrographic analysis from the range of primary igneous rocks and secondary igneous-hosted alteration in the study area. Fifteen samples of coarse crystalline and porphyritic igneous rocks represent the range of compositions and textures for unaltered intrusive phases related to the Cherry Creek pluton and coincident intrusions. Another twenty-five samples represent the range of mineralization and alteration mineralogies and textures that affect the igneous rocks in zones of pronounced hydrothermal activity. Rocks were cut into slabs at the

and submitted to Wagner Petrographic in Lindon, Utah for thin-section cutting and polishing to 0.03mm thickness. The thin sections were examined and described using a transmitted and reflected light petrographic microscope and SEM at UNR.

Geochronology

$^{238}U/^{206}Pb$ Geochronology

Fifteen U-Pb zircon crystallization ages were determined from a spatially and compositionally representative set of the district's plutonic and porphyritic dike rocks. Rock samples from the field were cleaned, crushed, sieved, and washed, and zircons were separated sequentially using a Frantz LB-1 barrier magnetic separator and methylene iodide heavy liquids at GeoSep Services in Moscow, Idaho. Zircons were hand-picked based on the criteria of euhedral shape and relative lack of melt and mineral inclusions. Selected zircons were mounted in epoxy, spatially referenced, and ablated using a 20 μm-diameter laser spot and a Thermo Scientific Element 2 magnetic sector mass spectrometer at the Washington State University Geoanalytical Laboratory in Pullman, Washington. Spectroscopy targeted masses 202, 204, 206, 207, 208, 232, 235, and 238. Mass spectrometry and data reduction were conducted by Paul O'Sullivan using GeoSeps software. The igneous ages reported in this study were obtained by weighted mean averaging of ages and errors using conventional $^{207}Pb/^{235}U$ vs $^{206}Pb/^{238}U$ concordia diagrams on Et_Redux software (Bowring, 2016).

$^{40}Ar/^{39}Ar$ Geochronology

Hydrothermal activity in the Cherry Creek district resulted in discrete areas of feldspar-destructive phyllic and argillic alteration of granitic rocks of the Cherry Creek pluton and

porphyritic dikes that intrude overlying, quartzite and carbonate rocks. More intensely altered igneous rocks proximal to mineralization are generally bleached white to grey and are texturally much less distinctive than corresponding fresh samples, with feldspars phenocrysts altered to white clays and mafic minerals commonly altered to tan or white clay minerals. Clay minerals affecting feldspars and mafic minerals are commonly sericite (illite and/or muscovite) based on high 2nd-order maximum birefringence, micaceous habit, and bird's eye extinction. Petrographic and textural distinctions among altered igneous rocks were accompanied by strong geochemical changes, including the removal of many major elements through leaching of primary minerals and the addition of many ore elements through precipitation of metal-bearing sulfides.

Samples with feldspar-destructive alteration were analyzed with an ASD Terraspec reflectance spectrometer to determine the identity of fine-grained clays. The results of this analysis were used in determining samples for isotopic dating of illite and muscovite, the major hydrothermal alteration products of feldspar. Illite and muscovite were identified in thin section and separated from altered porphyritic and coarse-crystalline igneous rocks by carefully hand-picking sericitized feldspar phenocryst sites from cut slabs using a tungsten-carbide scribe. This coarse separate was gently crushed in folded paper, and hard, coarse grains were hand-picked using tweezers and a binocular scope at 10-30x magnification to remove remnant feldspar and quartz. The sericite extracted in these phenocryst sites was further concentrated by paper shaking, with platy sericite selectively adhering to the paper. Sericite separates were sent to the Nevada Isotope Geochronology Laboratory (NIGL) at the University of Nevada, Las Vegas for $^{40}Ar/^{39}Ar$ step-heating isotopic analysis.

At NIGL, samples were wrapped in aluminum foil and stacked in 6 mm-diameter fused silica tubes with neutron fluence monitors placed every 5-10 mm along the tube. Neutron-

induced argon interferences were monitored using synthetic K-glass and optical-grade CaF_2 that were included with the samples. Loaded tubes were packed in an aluminum container and irradiated at the USGS 1 MW TRIGA Reactor in Denver, CO for 7 hours. Corrections were made based on repeated analysis of K-glass and CaF_2 fragments, which were measured as $(^{40}Ar/^{39}Ar)_K$=1.36 ($\pm$ 12.80%) x 10^{-2} for K and $(^{36}Ar/^{37}Ar)_{Ca}$ = 3.01 (± 0.80%) x 10^{-4} and $(^{39}Ar/^{37}Ar)_{Ca}$ = 8.31 (± 0.44) x 10^{-4} for CaF_2. Consistent single-crystal neutron fluence during the fusions indicated that no neutron fluence gradients were present within individual packets of crystals. Standards of Fish Creek Tuff sanidine were fused using a 20W CO_2 laser in a high-vacuum extraction line and analyzed by step-heating in a double vacuum resistance furnace. Peak intensity measurements were made with a Balzers electron multiplier by peak hopping through 7 cycles in which peak heights were determined by linear regression based on gas admission. Line blanks for ^{40}Ar and ^{36}Ar were used in the step heating and laser fusion analysis.

The preferred method of spectral analysis for $^{40}Ar/^{39}Ar$ is to calculate an isochron age, which is a statistically significant age incorporating at least 3 but preferably 4 or more steps of similar age. Isochrons are evaluated by a least squares (MSWD) calculation or statistical goodness of fit. In the absence of an isochron age, the next preferred method is to calculate a plateau age, which consists of “ideal” step heating behavior where 3 or more consecutive, statistically-identical steps yielding >50% of total ^{39}Ar of a single age. In the absence of both a usable isochron and plateau age, the final method of analysis is to use a total gas age incorporating the total argon released throughout the step heating process to calculate an aggregate age from all steps. The total gas ages are determined by a weighted mean based on the proportion of ^{39}Ar released.

$^{187}Re/^{187}Os$ Geochronology

One phase of mineralization in the central Cherry Creek district contains substantial coarse molybdenite (MoS_2). A sample of molybdenite-bearing quartz-sericite-pyrite-altered rock from the Maryanne mine dump was submitted to the University of Alberta $^{187}Re/^{187}Os$ laboratory for molybdenite separation and Re/Os isotopic analysis. About 2 kg of the mineralized rock were washed and crushed with metal-free equipment and molybdenite was separated through gravity and magnetic circuits described in detail by Selby and Creaser (2004). Concentrations of ^{187}Re and ^{187}Os were determined using the isotope-dilution mass spectroscopy method using a Carius-tube, solvent extraction, anion chromatography, and negative thermal ionization techniques. Isotopic measurements were made using a ThermoScientific Triton multi-collector thermal ionization mass spectrometer (TIMS) equipped with solid-carbon Faraday cups. Molybdenite age reference HLP-5 powder (Markey et al., 1998), with an accepted age of 221.0 ± 0.1 Ma, was analyzed in the same batch as Cherry Creek sample 10081 and produced an identical age to its accepted age.

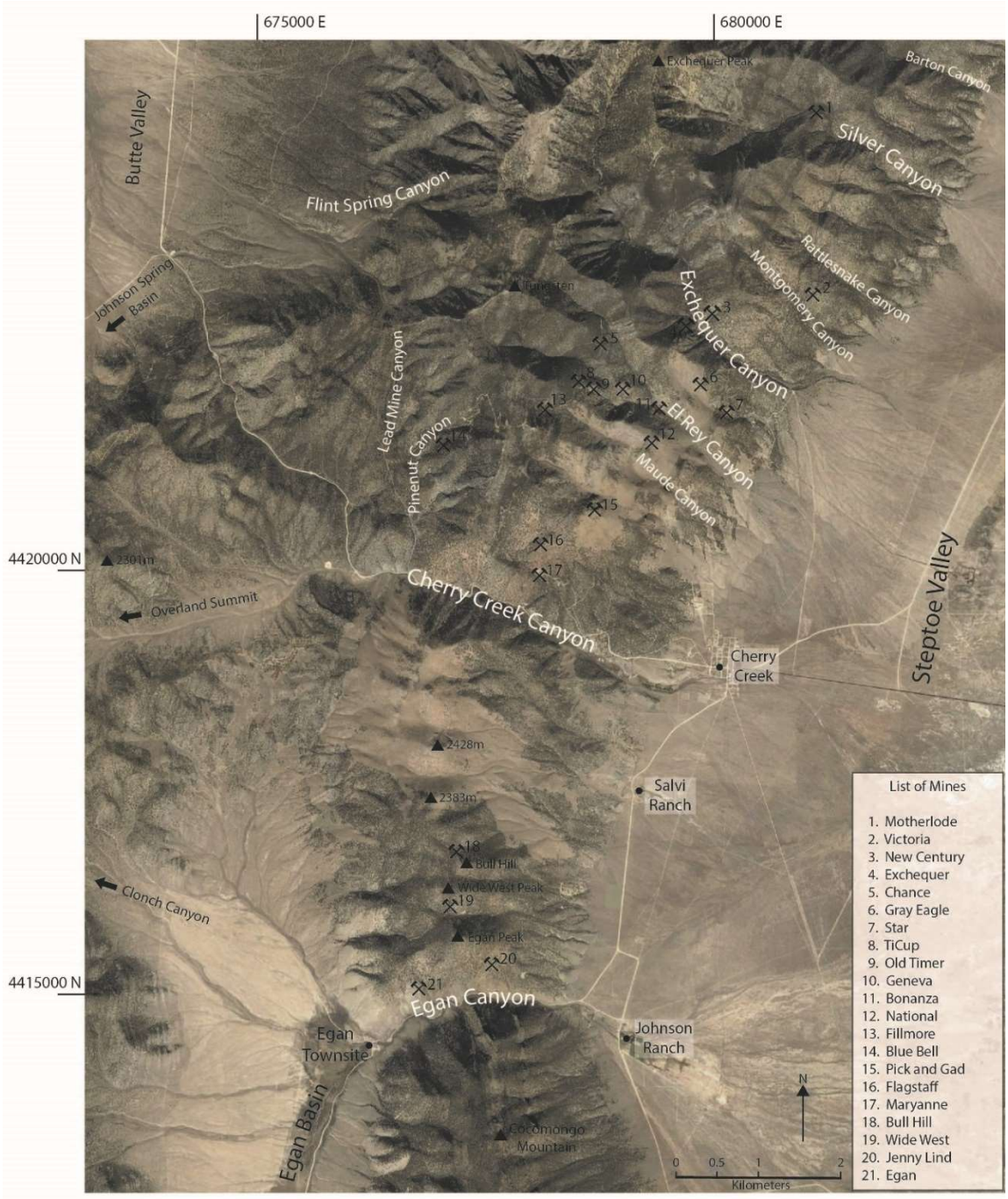

Figure 4. Location map of the Cherry Creek study area.
Map area approximates the area of the Cherry Creek mining district in the Central Cherry Creek Range, northeast Nevada. Geographic names referred to in text and historic mines are also shown. Base map is from Google Earth.

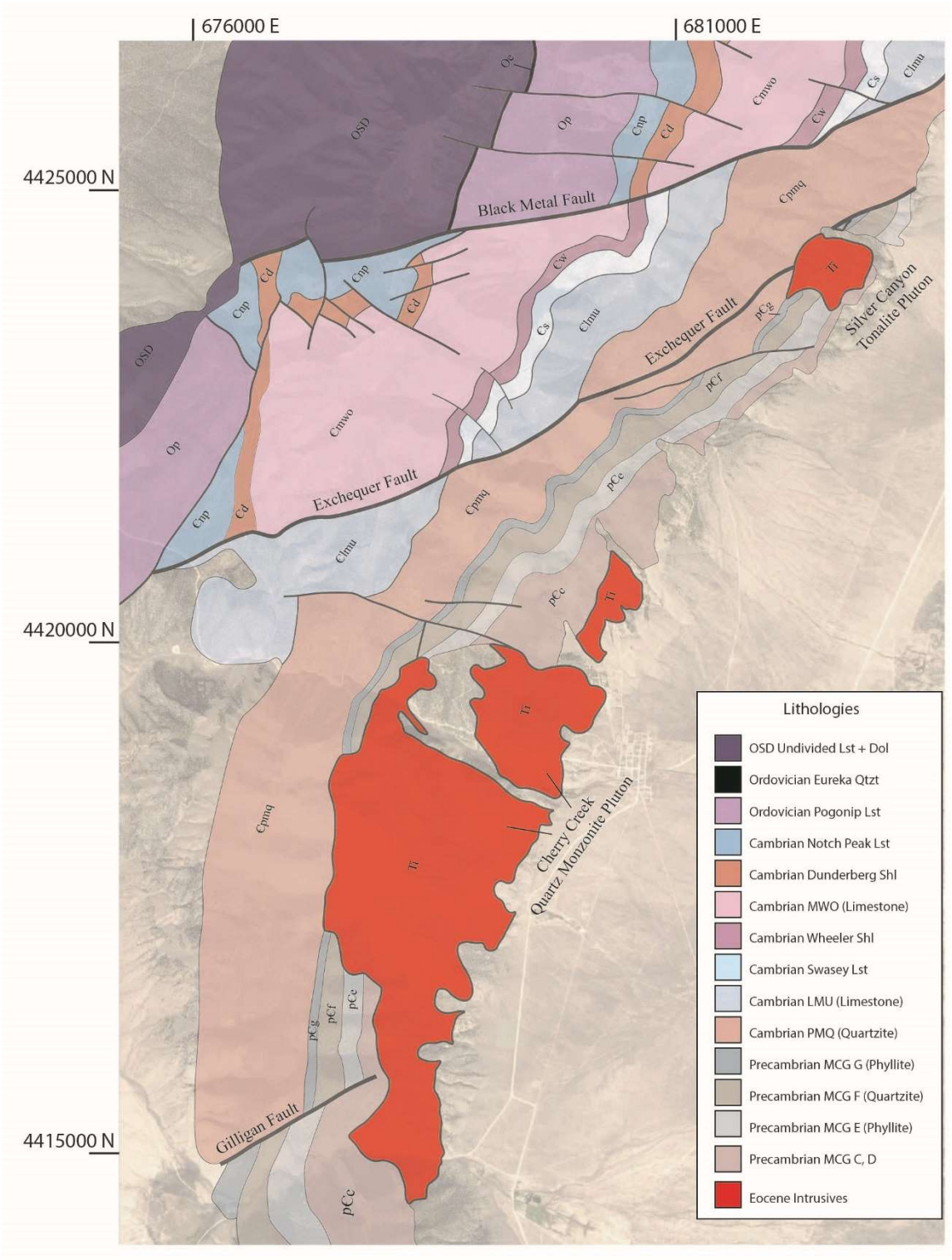

Figure 5. District scale geologic map of the central Cherry Creek Range overlain on satellite background. Geology simplified from Adair (1961)

Igneous Geology

Porphyritic Quartz Monzonite of the Cherry Creek Pluton

Field Relationships and Petrographic Description

The main body of porphyritic quartz monzonite crops out over 10 km^2 along the eastern flank of the Cherry Creek Range and northern Egan Range between El Rey Canyon on the north and Egan Canyon on the south (Figure 6). The rocks of the pluton are deeply weathered and generally form subdued topography, cropping out from grus and talus-covered slopes as rounded monoliths up to 50 meters in diameter. The best exposed examples of the Cherry Creek pluton are in the hills to the immediate south of Cherry Creek Canyon. Only in a few places are the primary contacts between the pluton and surrounding sedimentary strata revealed; more typically they are covered by quartzite scree shed from the overlying Cambrian rocks. The best examples of the exposed intrusive contact are in the south wall of Cherry Creek Canyon and at the north and east sides of Bull Hill as well as both walls of Egan Canyon in the northern Egan Range. The main exposed body of the pluton measures 5.25 km on its long NNE axis and between 0.5 and 1.85 km on its short WNW axis.

The upper contacts of the Cherry Creek pluton in the study area (Figure 3) are exclusively with quartzite and phyllite units of the massive Lower Cambrian Prospect Mountain Quartzite (PMQ) and the more thinly bedded phyllite and quartzite units of the Upper Precambrian McCoy Creek Group (MCG). The roof of the pluton undulates through 750 meters of the surrounding strata, truncating units of the upper MCG and reaching a maximum stratigraphic position at the base of the massive PMQ in a 2-km wide salient in the hills west of

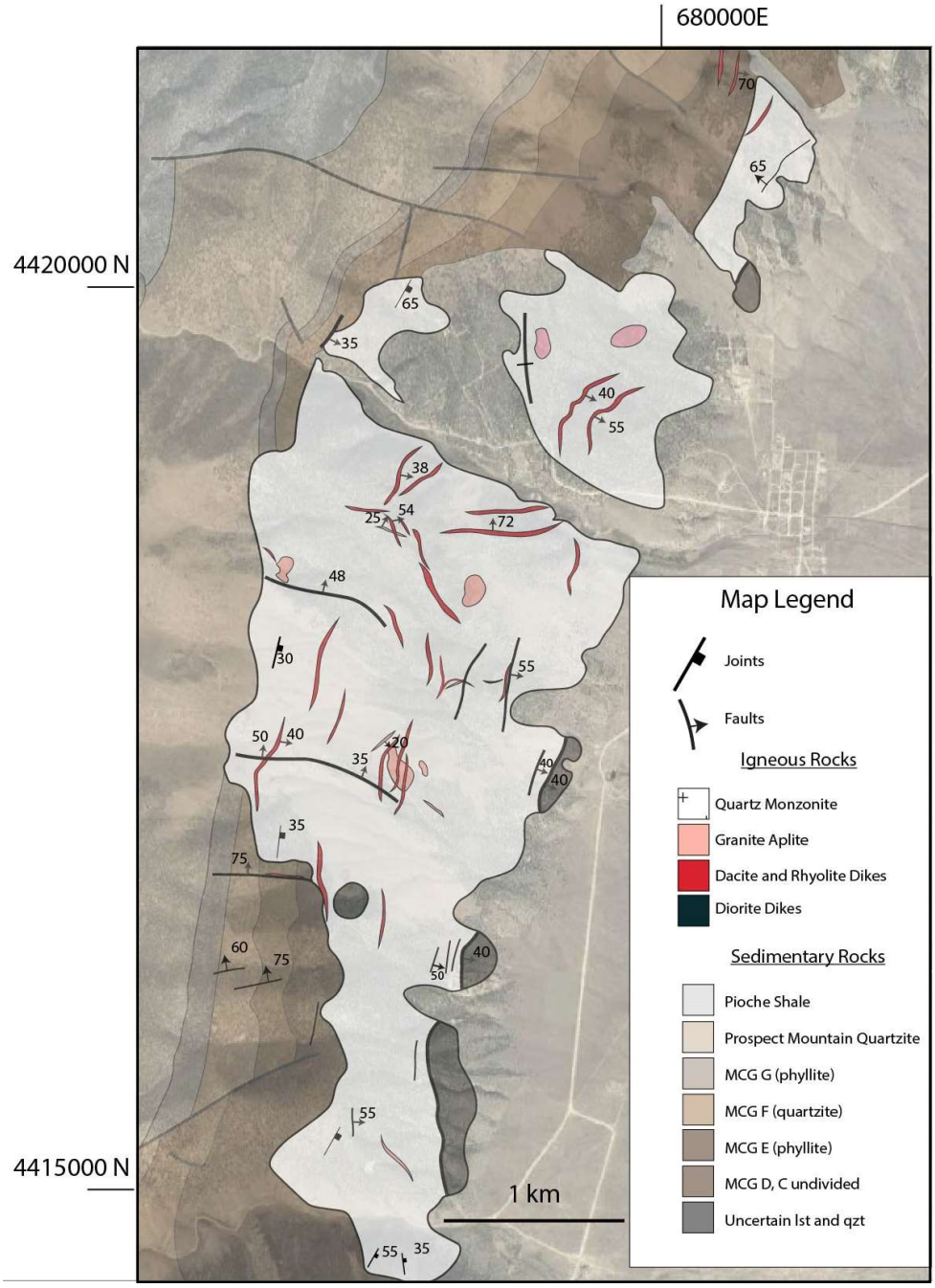

Figure 6. Inset map of the Cherry Creek pluton showing major features of the pluton including dikes and faults. From mapping by Adair (1961) and the author.

Salvi Ranch to the south of Cherry Creek Canyon. At this position, the roof contact lies approximately parallel to the north-northeast strike of overlying bedding in the PMQ over 2 km. Less than 600 m to the north of this position the contact is exposed in the walls of Cherry Creek Canyon where it dips to the west between 40 and 50 degrees under a heavily cemented 225-meter-thick unit of coarse grained quartzite and pebble conglomerate near the top of the MCG that is possibly correlative to the Shingle Creek quartzite described elsewhere in northeast Nevada by Misch and Hazzard (1962). On the north side of Cherry Creek Canyon and at Bull Hill in the northern Egan Range (Figure 4), the roof of the pluton retreats still farther to the east until it resumes a NNE trend parallel to one of a few thin quartzite units in what is likely the Strawberry Creek Formation (Woodward, 1967). Although the stratigraphic range which the pluton intrudes is large, the north-northeast trend of the pluton is consistent with an overall stratigraphic control on its emplacement. One small roof pendant of heavily-fractured quartzite surrounded by quartz monzonite has a nearly flat contact, although the internal bedding relationships of this block are uncertain.

The eastern contact of the pluton, which borders Steptoe Valley, is locally juxtaposed against probable Cambrian quartzite and carbonate rocks by a series of east-dipping faults. The contact between the quartz monzonite and these fractured but unmetamorphosed units is sharp, and in all cases dips to the east-southeast between 40 and 55 degrees. This feature has been interpreted as the largest of a series of down-to the east-southeast, post-intrusive normal faults, and are discussed more thoroughly in the subsequent sections on structural and hydrothermal geology.

Several sets of jointing affect the quartz monzonite pluton. The oldest and best developed joints are a set with strikes between N10°E and N25°E and dips between 20 and 50˚

to the east-southeast. This jointing is widespread, but is commonly obscured by the deep weathering that affects much of the pluton. It is best exposed in the north wall of Egan Canyon and in a series of large monolithic outcrops on the rib of intrusive rock that comprises the south wall of Cherry Creek Canyon. The orientation of this joint set is consistent with the general orientation of numerous dacite dikes that cut the core of the pluton between Maude Canyon and the hills west of Salvi Ranch (Figure 6). The dikes are discussed more in the next subsection on hypabyssal rocks.

Most of the Cherry Creek pluton is comprised of a light grey, medium to coarse-grained, porphyritic quartz monzonite (Figure 7; Table 1). The quartz monzonite is composed of about equal amounts of plagioclase feldspar and potassium feldspar, along with smaller amounts of quartz hornblende, and biotite. Texturally, quartz monzonite has a generally hypidiomorphic granular groundmass with grains that vary from 2 to 7 mm diameter. Euhedral phenocrysts of potassium feldspar reach up to 5 cm long and can comprise as much as 7 to 10% of the rock, although they are not always present. Some potassium-feldspar phenocrysts have small inclusions of biotite (Figure 7b). Phenocryst-poor zones are more granitic in composition, with quartz constituting up to 25%, although their contacts with strongly porphyritic zones are generally gradational and complex. Many <1 m diameter rounded xenoliths of granodiorite are locally present in the quartz monzonite pluton, although there is no apparent pattern to their distribution. No border effects of decreased grain size, flow structures, or unidirectional solidification textures were identified in any of the contact zones between quartz monzonite and siliciclastic rocks.

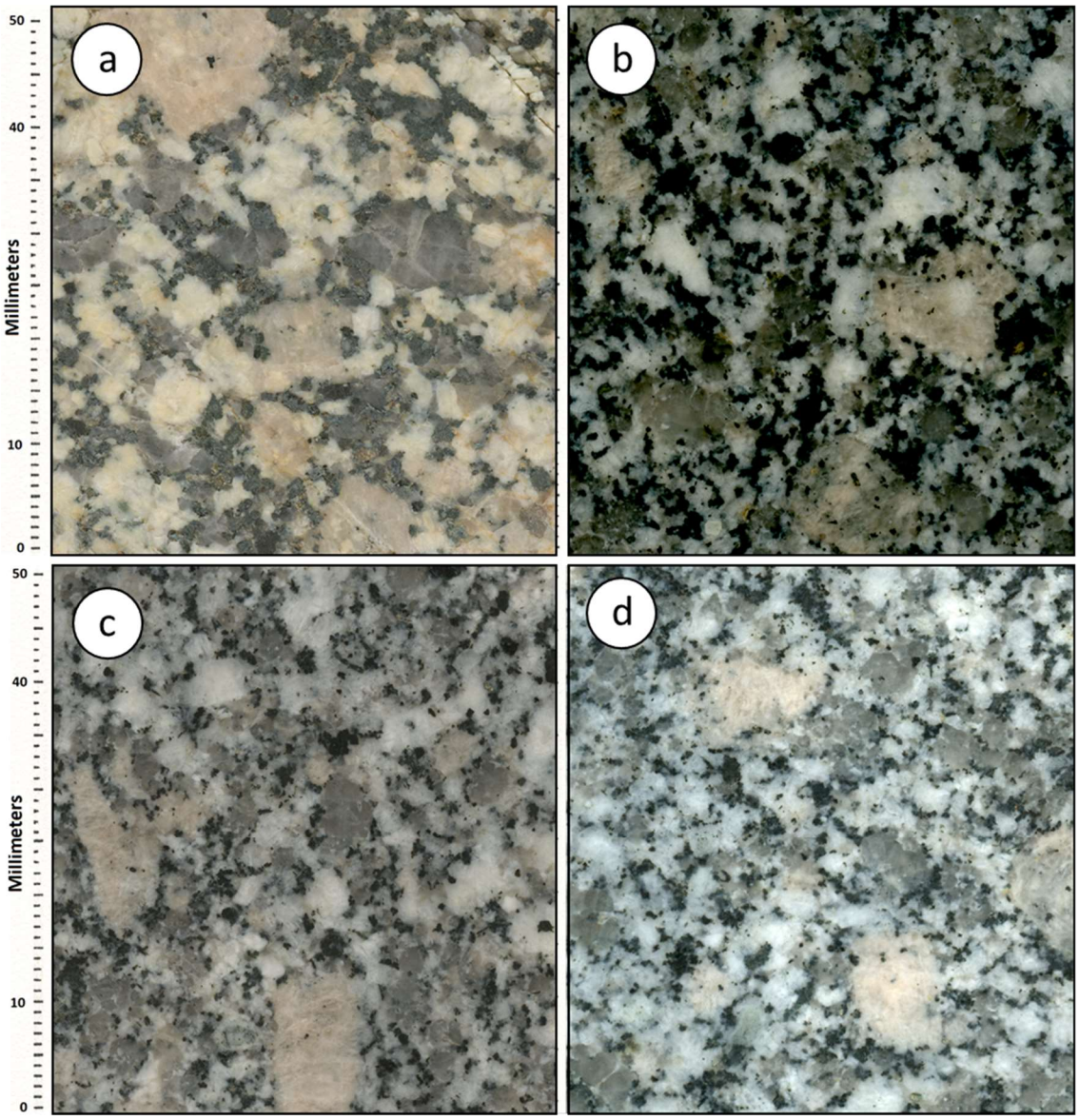

Figure 7. Petrographic photo of typical quartz monzonite textures. Note the blocky potassium feldspar phenocrysts in photos A, B, and C, and the sparser and more malformed phenocrysts in photo D.

In thin section, the quartz monzonite is hypidiomorphic, being formed of medium-grained euhedral plagioclase and biotite along with large tabular potassium feldspar phenocrysts set in interlocking subhedral to anhedral grains of quartz and potassium feldspar. The accessory minerals include apatite, zircon, titanite, magnetite, and chloritized amphibole. Plagioclase (30-40%) and alkali feldspar (30-40%) occur in roughly equal proportion to each other, whereas quartz (15-25%) and biotite and chlorite-altered hornblende (10-15%) are less abundant. Plagioclase is commonly zoned with greater concentrations of sodium or potassium in rims and distinct albite twins. Quartz crystals in a few samples have strained, undulatory extinction. The rock is holocrystalline, although some samples of medium-grained quartz monzonite display small patches of complex myrmekitic intergrowths of quartz in plagioclase, similar to the granophyric intergrowths of quartz with K-feldspar developed in aplitic samples of quartz monzonite like those discussed below in the subsection on hypabyssal rocks.

Geochemistry

The quartz monzonite is subalkaline and weakly peraluminous (Figure 13; Table 2). Ratios of total alkalis versus silica in quartz monzonite plot across the granite-granodiorite boundary of the Middlemost (1994) classification system, although classification based on modal mineralogy perhaps better characterizes its composition, considering the large amount of calcic plagioclase present. In Harker (X-Y) plots of the major oxides, the quartz monzonite plots near the bottom of linear trends for MgO, TiO_2, MnO, and Fe_2O_3 among the igneous rocks of this study, indicating its more fractionated character (Figure 14). A chondrite-normalized rare-earth element (REE) plot shows strong negative slopes towards the heavy rare earths and weak Eu anomalies, probably owing to modest early fractionation of plagioclase. The quartz monzonite

is particularly depleted in the heavy rare earths Yb and Lu relative to most other intrusive rocks, indicating its more evolved composition that likely resulted from early hornblende removal.

Geochronology

Five samples of quartz monzonite were selected from the Cherry Creek pluton for U/Pb isotopic dating of zircon (Figure 15; Table 3). Samples 10060, 10084, and 10111 represent the least-altered rocks from the pluton, which were collected from monolithic outcrops on the south side of Cherry Creek Canyon. Sample 10060 is from a porphyritic phase that contains abundant potassium feldspar megacrysts, and yielded a weighted mean age of 36.72 ± 0.3 Ma (2σ) based on 27/30 grains. Sample 10084 is from a relatively coarse-grained and quartz-rich phase that verges on granitic composition, and yielded a weighted mean age of 37.76 ± 0.3 Ma based on 28/30 grains. Sample 10111 is from a relatively fine-grained and relatively more mafic phase that verges on quartz monzodiorite, and yielded a weighted mean age of 37.67 ± 0.3 Ma based on 24/30 grains. Sample 10107 is from altered quartz monzonite along the northern margin of the pluton that lies on the periphery of a north-east striking fracture set related to the mineralization at the Maryanne Mine, and yielded a weighted mean age of 37.89 ± 0.28 Ma based on 23/30 grains. Sample 10059 is from propylitically altered quartz monzonite on the far north end of the exposed pluton in El Rey Canyon, and yielded a weighted-mean age of 36.18 ± 0.31 Ma based on 26/30 grains.

Tonalite of the Silver Canyon Stock

Field Relationships and Petrographic Description

A small, 1.5km^2 stock of medium-grained, medium to dark grey tonalite is exposed at the mouth of Silver Canyon, 3 km to the northeast of the Cherry Creek townsite (Figure 3). The stock is deeply weathered and outcrops are extremely friable. The whole area is covered with grus and heavily vegetated. The outcrop pattern of the stock is roughly circular. It is bounded on its west side by cliffs of massive, moderately west-dipping PMQ, on its north and south by phyllite and quartzite units of the upper MCG; and on its east by a planar, N20°E/40°SE contact with quartzite of uncertain origin. Its contacts with MCG sedimentary rocks are undulatory. Phyllitic units around the stock are heavily recrystallized and embayed by tongues of tonalite that extend from the main body, especially on the south side of the stock. Between phyllitic units, a peninsula of white quartzite on the south side of the stock projects northeast towards the stock's center, with the tonalite extending to the south on either side of this resistant unit. An apophysis on the north side of the Silver Canyon stock follows 75 m along the uppermost phyllite unit of the MCG before pinching out against quartzite. This northern tongue of tonalite projects along the footwall of the Exchequer Fault Zone (EFZ), which juxtaposes MCG on the south against massive PMQ on the north. Another, smaller strand of the EFZ lies to the south; in this way, the tonalite stock at Silver Canyon is localized within its splay zone.

One 15 m^2 outcrop of quartz-poor, medium-grained diorite exists along the southeast border of the Silver Canyon stock; the diorite is bounded on the north by tonalite and on the south by an undulatory intrusive contact with arenaceous phyllite. The stock is cut by northeast-striking dikes with easterly dips, the largest of which are variably altered hornblende-pyroxene porphyritic andesites. A north-northeast-striking andesite dike on the west side of the

stock crosses from phyllite into tonalite before tracking north-northwest and eventually vanishing under scree near the western contact of the stock. A series of small (< 30 m x 2 m) diabase dikes form a small swarm in the tonalite near its faulted eastern border with quartzite. Several elongate outcrops originally mapped as mafic dikes proved to be thin calc-silicate screens, also with northerly trends. The largest of these screens measures 15 m x 2 m.

The Silver Canyon tonalite stock is dark grey on fresh surfaces and phaneritic, with a fine-grained (0.5-1 mm) equigranular texture of plagioclase (50%), quartz (20%), intergrown amphibole (20%) and biotite (10%), and lesser K-feldspar that is consistent across the entire body (Figure 8; Table 1). Most of the tonalite is weakly magnetic. The tonalite is hypidiomorphic and intergranular with subhedral plagioclase and amphibole set in a matrix of anhedral interstitial quartz and minor potassium feldspar. The plagioclase is conspicuously zoned. The mafic minerals in the tonalite are almost always altered: intergrown amphibole and biotite has an extremely shreddy appearance due to the presence of a fringe of chlorite. It is possible that some intergrowths of amphibole and biotite may be relicts of potassic alteration. Accessory phases include magnetite, which is associated with the other mafic minerals, apatite, and zircon.

Geochemistry

On Harker plots the tonalite is substantially less evolved than the quartz monzonite (Table 2), as shown by its higher Fe_2O_3, CaO, MgO, and TiO_2 contents. The tonalite is also significantly less potassic but does contain more alumina, probably as result of its substantial amphibole component. The tonalite's chondrite-normalized rare earth plot has the shallowest slope towards the heavy rare earths; it is depleted in La, Ce, and Pr relative to most other igneous rocks in the study. Unlike the Cherry Creek quartz monzonite, the Silver Canyon tonalite

has no appreciable negative Eu anomaly, suggesting little plagioclase was fractionated. It is the only major igneous lithology to retain a negative slope through even the heavy REEs. The lack of a Eu anomaly coupled with lower heavy REE concentrations implies that the magma may have been water-saturated, inhibiting early plagioclase crystallization but promoting amphibole crystallization and fractionation.

Geochronology

Two samples were selected from the Silver Canyon stock for U/Pb zircon age dating. Sample 10053 is a representative from typical, relatively unaltered tonalite that makes up most of the stock (Figure 15). All 30 zircon grains from 10053 yielded concordant ages with a weighted mean of 37.33 ± 0.34 Ma. Sample 10075 is from the small diorite enclave that occurs in the southeastern corner of the stock. 16 zircons selected from 10075 yielded concordant ages with a weighted mean of 40.16 ± 0.93 Ma, thus apparently representing an older pulse of intrusion than the main tonalite and the oldest recognized Eocene magmatism in the Cherry Creek district.

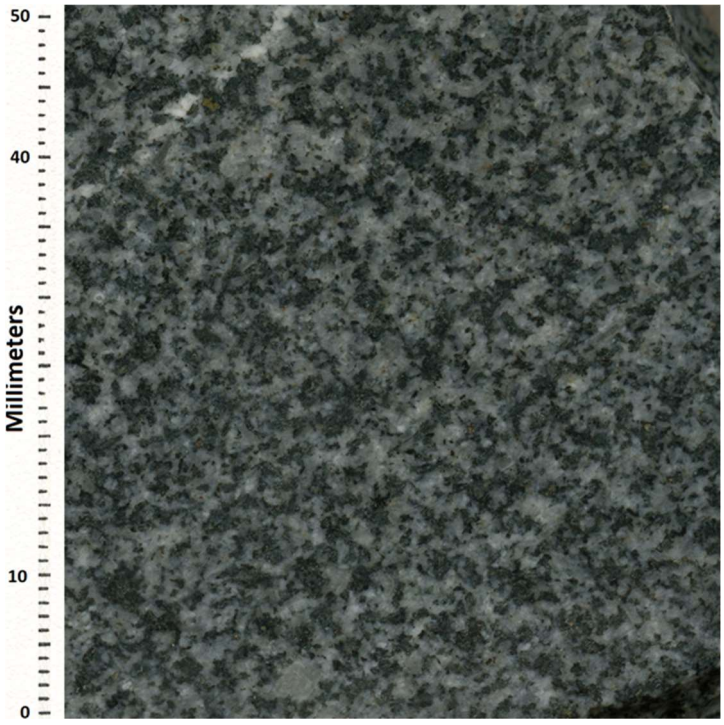

Figure 8. Scan of slabbed Silver Canyon tonalite

Porphyritic Rhyolite and Dacite Dikes

Field Relationships and Petrographic Description

Strongly porphyritic rhyolite and dacite dikes are the most abundant type of dikes in the Cherry Creek study area. They intrude host rocks of all lithologies, including especially the Cherry Creek quartz monzonite pluton and the MCG rocks that inhabit the deepest stratigraphic levels of the district. They are less abundant but still prevalent in Cambrian quartzite and carbonate rocks higher in the section, where they are effectively localized to fault zones. Thus, their pre-tilting vertical extent may be as much as 4 km above the top of the Cherry Creek pluton, and some of these dikes have strikes lengths on the order of kilometers, especially along the east flank of the Cherry Creek Range.

The densest population of felsic dikes is found between the center and eastern margin of the exposed Cherry Creek pluton, where dikes form a north-northeast-trending swarm ~2.5 km long by 0.4 km wide. This zone is located between the north side of Cherry Creek Canyon and the hills west of Salvi Ranch in the northern Egan Range (Figure 2). The individual dikes usually strike northeast to north-northeast and dip moderately southeast; they are commonly 1 to 5 m thick and form blocky, elongate outcrops that can be traced for 10s of meters. In the south wall of Cherry Creek Canyon, two dikes have westerly strikes and dip steeply to the north, antithetically to the main swarm of dikes.

The north-northeast orientation and overall distribution of dikes in the Cherry Creek pluton closely mirrors the pluton's predominant joint array, especially on its east side immediately west of the Cherry Creek townsite, where tightly spaced, meter-scale jointing is in places so tight as to give the pluton a "sheeted" appearance. The dikes are harder and more

resistant than rocks of the pluton, and thus form small rib-like outcrops that can be traced for 10s to 100s of meters.

The felsic dikes define several important crosscutting relationships. With most dikes localized by joints in the Cherry Creek quartz monzonite, an obvious implication is that the dikes postdate cooling and brittle fracturing of the pluton. In a few cases dikes cut one other, indicating that multiple phases of dike intrusion took place. In the low hills west of Salvi Ranch, at least three porphyritic rhyolite dikes cut a lobate body of aplite (Figure 6), while another truncates a small diorite dike and is in turn cut by a considerably mineralized north-striking fault. In a small exposure to the north, another dacite dike cuts across a northwest-striking aplite dike. It is clear from these relationships that at least some of the felsic dikes are among the youngest igneous features in the area.

Between Cherry Creek and El Rey Canyons, the roof of the pluton dips to the east, revealing Precambrian rocks of the MCG that extend for 5.5 km along the range front to the northeast before being truncated by the Exchequer Fault near the mouth of Silver Canyon. At least 10 small porphyritic dacite dikes strike northeast and dip moderately to the southeast within this interval, cutting the MCG rocks nearly orthogonally to their bedding. The dikes, especially those in Maude and El Rey Canyons, are often heavily altered and intimately associated with mineralized rocks around many of the historic mines.

The abundance of felsic dikes generally diminishes upward with increasing distance from the pluton and increasing stratigraphic level. With decreasing abundance, the dikes are progressively more controlled by large faults. As such, the dikes almost always have high dip angles, but the strike direction varies from northeast to northwest depending on the orientation of the faults that they inhabit. Felsic dikes are exposed in the Exchequer Fault in at least three

places: at the Exchequer-New Century mine, at the Geneva mine, and at the Fillmore mine. These relationships and their connections to hydrothermal geology are discussed in the subsequent section on hydrothermal geology.

The amount of petrographic variability in the felsic dikes of the district is considerable (Figures 9 and 10). The dikes have mineralogies that fall between dacitic and rhyolitic in composition and textures that fall between phenocryst-rich porphyritic and equigranular aphanitic, also with a range of groundmass features that differ even within a single area. This petrographic variation indicates that the dikes developed from different source magma chambers at different times, or possibly from different phases from the same chamber, and illustrates the complexity of post-Cherry Creek pluton magmatism. About 70% of dikes are dacitic, commonly with variable amounts phenocrystic potassium feldspar (20-40%), plagioclase (20-40%), quartz (10-30%), biotite (10-20%), and amphibole (10-20%), constituting 30-60% of rock volume, with the remainder being aphanitic groundmass. The phenocrysts are fine to coarse grained, with biotite, plagioclase, and amphibole being euhedral to subhedral, while potassium feldspar is subhedral and quartz generally forms subrounded, anhedral “eyes” up to five millimeters in diameter. The groundmass is very fine-grained and ranges texturally from aphanitic to aplitic and intergrown, in which plagioclase and

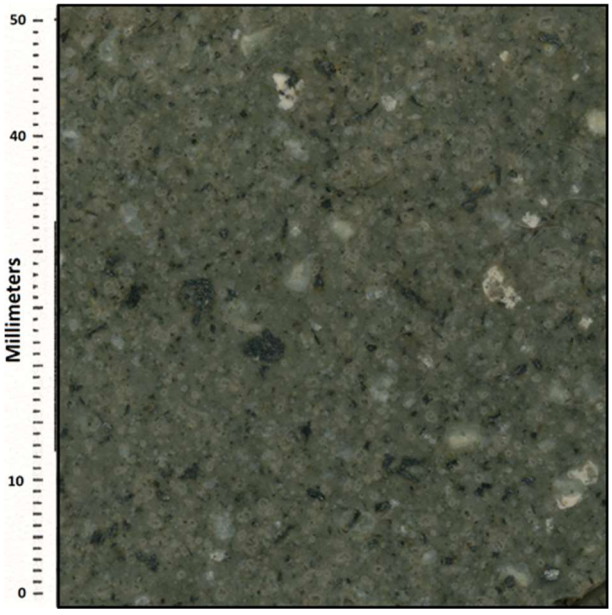

Figure 9. A probable devitrified dacite dike from the Exchequer fault, Exchequer Canyon. Note the unaltered phenocrysts of hornblende and biotite (black), and glassy plagioclase (white)

quartz show graphic and vermicular granophyric textures. However, in many samples and especially those having experienced phyllic alteration, groundmass textures are totally bleached and obscured in hand sample, and only slightly more discernible in thin section. In rare cases, such as in the dacite dike at the Exchequer Mine, potassium feldspar and quartz occur as mm-scale spherulites that may have resulted from solid-state devitrification. This texture is particularly abundant in one dike near the top of Flint Spring Canyon on the west side of the range. The distribution of these textures is very irregular, and often dikes within the same area or even portions of the same dike are strikingly different. Another example of rhyodacite from the Flint Spring Canyon area is far coarser, with 7-10 mm quartz eyes and distinctive glomerocrysts of tightly packed mm-scale albitized feldspar crystals. A few dikes are weakly foliated.

Another 20% of dikes are rhyolitic, with very fine-grained phenocrysts of quartz (40%), potassium feldspar (35%), plagioclase feldspar (20%), and rare biotite (5%), constituting 25-50% of the rock and the rest being an aphanitic groundmass. Phyllic alteration in these dikes often overprints the groundmass and obscures primary textures, which appear to mostly be subhedral to anhedral hypidiomorphic. In most cases, feldspar grain boundaries in the groundmass are delineated by vague shapes of fine-grained sericite. Some of the most fine-grained varieties

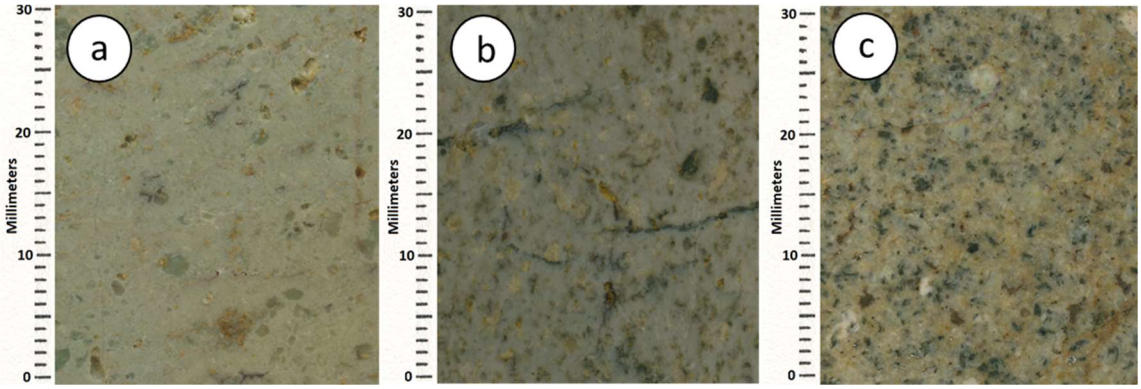

Figure 10. Representative examples of dacite dikes from Cherry Creek Canyon demonstrating the variation in phenocryst size and abundance.

have perlitic fractures suggesting that they may have been glassy. These examples are the rhyolitic end members of this lithology.

Geochemistry

Concentrations of major elements in the felsic dikes are considered here for the "average" compositions as well as for phenocryst-rich and phenocryst-poor end members (Table 2; Figures 13 and 14). The average unaltered felsic dike is a low-silica rhyolite with higher silica contents and higher ratios of silica to Al_20_3, Fe_2O_3, CaO, and TiO_2 than the Cherry Creek quartz monzonite in addition to most other igneous phases. The dacites have the highest alkali content overall, and highest alkali content relative to Fe_2O_3 and MgO. They are weakly to strongly peraluminous, and all have alkali-to-silica ratios consistent with granite (rhyolite) or borderline granitic-quartz monzonitic compositions based on total alkalis-silica diagram (TAS) for plutonic rocks by Wilson (1989) and Middlemost (1994). In both cases they plot adjacent to the quartz monzonite phase but clearly define their own populations.

Rare-earth element geochemistry for dacite dikes is typical for felsic calc-alkaline rocks, and like the other igneous suites, porphyritic rhyolite and dacite dikes have parallel REE patterns on chondrite-normalized plots with strong negative slopes in the light rare earths. The felsic dikes all have pronounced negative Eu anomalies, with rhyolite dikes displaying stronger anomalies than dacite. The slope in heavy rare earths is weakly negative to Er, and many examples from this suite also have a weak to moderately pronounced upward "hook" with positive slopes from Er to Yb and Lu.

Geochronology

Six samples of porphyritic rhyolite and dacite dikes (Table 3; Figure 15) from across the district were dated using U/Pb zircon methods. Samples 10079, 10091, and 10108 represent fine-grained examples of typical porphyritic rhyolites that cut coarse-grained and aplitic phases of the Cherry Creek pluton in the main exposure of the pluton west of Salvi Ranch; these dikes are the youngest dikes to cross cut the pluton in that area and none are altered. These dikes yield weighted mean zircon ages of 35.59 ± 0.28 Ma (10079, 30/30 grains), 35.26 ± 0.37 Ma (10091, 30/30 grains), and 35.07 ± 0.34 Ma (10108, 27/30 grains). Three other samples (10080, 10102, and 10129) represent felsic dikes that occur in proximity to hydrothermally altered rocks in varying levels of the Cambrian stratigraphy to the west of the Cherry Creek pluton. Sample 10080 is an unaltered rhyolite hosted in quartzite near the western margin of the pluton in El Rey Canyon, and yields a weighted mean zircon age of 35.44 ± 0.36 Ma based on 30/30 grains. Sample 10102 is a weakly altered dacite that occurs along the western edge of a jasperoid body near the Chance Mine at the head of El Rey Canyon, and yields a weighted mean age of 38.20 ± 0.50 Ma based on 23/30 grains. Sample 10129 is a strongly argillized dacite that occurs along the west side of a series of jasperoids in Flint Spring Canyon, and yields a weighted mean age of 35.44 ± 0.36 Ma based on 30/30 grains.

Granite Aplite and Aplitic Quartz Monzonite

Field Relationships and Petrographic Description

Two varieties of aplitic rocks exist in the field area. Aplite exists within the main body of the Cherry Creek quartz monzonite pluton, and occurs within a broadly north-northeast-trending, 0.2 km by 4.5 km zone that roughly follows the center of the exposed pluton between Egan Canyon and the north wall of Cherry Creek Canyon. Most of the aplite occurs as thin dikes and small lobate intrusions that have sharp contacts with the surrounding rocks. These bodies of aplite are 30-150 cm in thickness and less than 50 m in strike length. They strike to the north-northwest and dip to the east-northeast between 30 and 50 degrees. A few dip moderately to the south. The densest population of aplite dikes is in the hills west of Salvi Ranch, where they associated with several phases of metasomatic or hydrothermal alteration that are described below. In two cases, the aplite dikes (Figure 11) are clearly cored with coarse cm-scale pegmatites bearing potassium feldspar and quartz. The dump of the Maryanne Mine on the north side of Cherry Creek Canyon contains a substantial amount of aplite and pegmatite, although no features of this type are exposed at the surface in

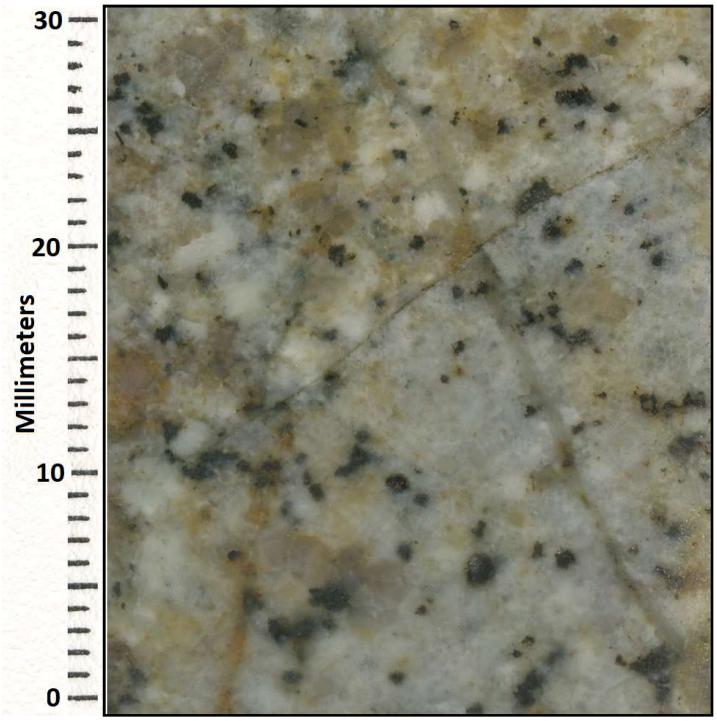

Figure 11. Petrographic example of aplitic quartz monzonite. Note the grading in phenocryst density over 2cm from top left to bottom right, which is typical of the margins of these irregular aplitic bodies

that area. Another variety of aplite is found in the groundmass of quartz monzonite, in which euhedral or subhedral phenocrysts of plagioclase, potassium feldspar, quartz, and biotite roughly the size of the phaneritic groundmass in normal quartz monzonite are set within an aphanitic aplitic groundmass (Figure 11). The apparent distribution of aplitic quartz monzonite is limited to a few exposures on the north side of Cherry Creek Canyon. It is likely that the extent of this rock type is much greater in the area, but likely obscured by preferential weathering and overprinting alteration.

The aplitic dikes are granitic in composition and weakly porphyritic, being made up of <10% fine-grained phenocrysts comprised of potassium feldspar (50%), quartz (30%), plagioclase feldspar (20%), and variable biotite (<7%). The bulk of the rock is composed of a fine-grained to aphanitic groundmass, which is conspicuously saccharoidal in hand sample. In thin section, the groundmass is equigranular and allotriomorphic, and is composed essentially of feldspar and quartz that are occasionally intergrown with granophyric or myrmekitic textures.

Where aplitic textures are developed in the groundmass of quartz monzonite, the same fine grained, intergrown, allotriomorphic quartz and feldspar aggregates are present, although the phenocrysts are more typical of standard quartz monzonite. The phenocrysts in aplitic quartz monzonite make up 60-80% of the total rock volume, and their size is consistent with the phaneritic groundmass in the standard variety. Adair (1961) reported one locality in the north Egan Range where aplitic groundmass textures contained two populations of phenocrysts, one of which had typical 3-7 mm phaneritic crystals like the groundmass of normal quartz monzonite and the other both 3-7 mm crystals and 2-3 cm megacrysts of potassium feldspar.

Geochemistry

The aplite is weakly peraluminous, subalkalic (Table 2; Figures 13 and 14), and plots within the granite field of the TAS diagram based on divisions by Debon and Le Fort (1983) and Middlemost (1994). It is set apart from the porphyritic dacite and rhyolite dikes by its relatively high silica content, relatively low total alkali content, and non-porphyritic granular texture. Being the most siliceous igneous rock, the aplite plots on the edge of major element trends in most Harker plots. It has the lowest ratios of Al_2O_3, Fe_2O_3, MgO, and TiO_2 to silica, and the lowest total percentages of those oxides compared to the average for other felsic dikes in the study.

The aplite diverges most strongly from the other igneous lithologies in its REE content, as shown relative to chondrite-normalized concentrations on the spider diagram below (Sun and McDonough 1995). The aplite has anomalously low values relative to the other igneous lithologies for the entire REE elemental suite. It maintains a negative slope from La to Er with a small inflection at Gd, and unlike most other samples it includes no negative Eu anomaly. On the heavy rare earth end of the REE diagram the aplite has a strong positive slope from Er through Yb and Lu. These features combine to give a pronounced “hook” to the profile of rare earth elements in the aplite.

Geochronology

Two samples have bearing on the geochronology of the aplite bodies at Cherry Creek (Table 3; Figure 15). Sample 10093 is a strongly sodic-calcic altered example of coarse-grained intrusive rock, originally interpreted to be a monzonite but now understood to be an alteration phase affecting quartz monzonite that is spatially associated with the margins of several aplite dikes. The crosscutting relationships necessitate that the protolith of this rock is at least as old

as the aplite dikes. Sample 10093 yields an age of 36.62 ± 0.26 Ma based on 28 zircon grains. Sample 10125 is an example of one of the highly irregular bodies of quartz monzonite distinguished by the aplitic texture of its groundmass. Sample 10125 yields an age of 37.23 ± 0.35 Ma based on 25 grains.

Porphyritic Dacite and Andesite Dikes

Field Relationships and Petrographic Description

Intermediate dikes are the second most abundant type of dike in the Cherry Creek study area. They are distinguished from the porphyritic rhyolite and dacite dikes described in the previous section by a lack of quartz phenocrysts. Eight exposures were located, most of which are spatially associated with the Silver Canyon tonalite stock and occur within a kilometer of it. These dacite and andesite dikes do not have the same association with veins as do the felsic dikes, and at most they are weakly altered (Figure 12). It is possible that some of the heavily clay-altered dikes are indeed andesites, particularly in the Flint Spring Canyon area; however, this cannot be confirmed. One intermediate dike cuts the southwestern margin of the Silver Canyon tonalite stock and adjacent MCG phyllite (Unit F) along a south-southwest strike.

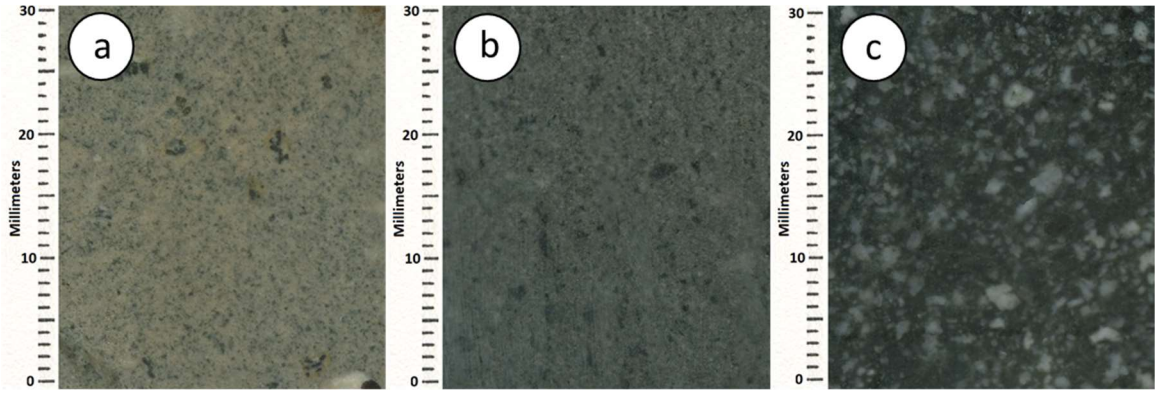

Figure 12. Scanned slabs of andesite dikes displaying the differences in phenocryst size and abundance

Another small intermediate dike cuts a polymetallic vein at the Star property on the south side of Exchequer Canyon, and a third occupies a small fault zone in Montgomery Canyon. Three weathered and fine-grained andesite dikes dip to the east, towards the tonalite stock, within the Cambrian Prospect Mountain Quartzite in Silver Canyon. No intermediate dikes were found cutting quartz monzonite in the Cherry Creek pluton. The andesite dikes are dark grey in color, fine to medium grained, and weakly porphyritic. Most are weakly flow foliated, and 40-90% of the rock volume is made up of phenocrysts (<4mm) that include euhedral to subhedral plagioclase, subhedral to anhedral amphibole, with very minor or no quartz and variably intergrown amphibole and biotite set within a dark, equigranular, fine-grained groundmass of the same minerals. The medium-grained examples of andesite are very phenocryst rich, with fine-grained groundmass minerals making up <20% of the rock. None of the andesite dikes are altered.

Geochemistry

The andesites are weakly peraluminous to metaluminous (Figures 13 and 14; Table 2), and plot in the granodiorite or granodiorite-quartz monzonite boundary zone in TAS plutonic divisions from Middlemost (1994), and in the quartz diorite field in those from Wilson (1989). In Harker plots, intermediate dikes occupy the intermediate space between quartz monzonite and dacite on one end and tonalite and gabbro on the other. The intermediate dikes have relatively high K_2O in most cases, and they are more potassic than the Cherry Creek quartz monzonite while being less siliceous. Their K_2O values essentially plot between quartz monzonite and dacite.

Intermediate dikes have moderate negative REE profiles that are relatively depleted in light rare earths compared to the felsic dikes. However, the main difference between

intermediate and felsic dikes are in the magnitude of their Eu anomalies. Intermediate dikes have weak negative Eu anomalies and a weak positive slope between Eu and Gd, whereas porphyritic rhyolite and dacite dikes have much more pronounced Eu anomalies. Intermediate dikes retain a negative slope from Gd through Yb and most samples have a moderate positive slope from Yb to Lu.

Diorite and Diabase Dikes

Field Relationships and Petrographic Description

Diorite and diabase dikes are the least abundant type in the Cherry Creek study area. They form dark green outcrops less than 2 m in thickness, and generally less than 30 m in strike length. At least 3 of them cut a small dacite dike and the Silver Canyon tonalite stock that hosts it at the northeast end of the study area near the mouth of Silver Canyon. Two others occur as small, north-northeast trending dikes <20 cm in thickness on the north side of Cherry Creek Canyon in porphyritic quartz monzonite. Due to the general appearance and thinness of the dikes they are very difficult to distinguish from the variegated dirty quartzite and arenaceous phyllite beds in the McCoy Creek Group, and as a result their abundance has almost certainly been underestimated. Cross cutting relationships indicate that, at least in the Silver Canyon rocks, the diorite dikes are the youngest igneous features in the map area. Fine-grained diorite and diabase dikes are not dated in the Cherry Creek study area. However, they cut all other intrusive rocks suggesting that they were emplaced after intrusion of the youngest dated porphyritic rhyolite dikes at ~35 Ma.

The diorite dikes are fine-grained equigranular, composed of plagioclase (60%), pyroxene (25%), amphibole (15%) olivine (5%) and magnetite (5%). A few have a considerable

amount of biotite. Most of the diorite dikes are altered and contain secondary epidote and chlorite.

Geochemistry

The diorite dikes are metaluminous (Table 2; Figures 13 and 14) and plot with tonalite in the diorite field of TAS divisions by Wilson (1989). Harker oxide plots indicate that the diabase dikes have the highest Fe_2O_3 and CaO values and the lowest K_2O and SiO_2 values, except for one sample that has nearly 6% K_2O. The diorite dikes have a universally negative slope through the rare earth elements relative to chondrite-normal values. They have a weak Eu anomaly, and the slope from Eu through the rest of the heavy rare earths remains negative to Er after which the pattern is flat.

Unit	Texture	Groundmass	Phenocrysts	Accessory	Distinguishing Features	Occurrence
Aplitic Quartz Monzonite	Fine to Medium Grained Porphyritic Aplitic groundmass	intergrown Kspar Quartz Plagioclase	1-4mm Plagioclase (30) 1-4mm K Feldspar (30) 1-4mm Quartz (25) 1-4mm Biotite (15)	Magnetite Amphibole Titanite Zircon Apatite	aplitic groundmass myrmekite	small lobes hosted in Cherry Creek pluton
Porphyritic Quartz Monzonite	Fine to Medium Grained Phaneritic Porphyritic	Plagioclase (35) K Feldspar (35) Quartz (25) Biotite (<5)	5cm- K Feldspar	Magnetite Titanite Zircon Apatite	Kspar phenocrysts	Elongate N-S 10km^2+ Stock El Rey Canyon (N) to Egan Canyon (S)
Tonalite	Fine Grained Phaneritic	0.5-2mm Plagioclase (50) 0.5-1mm Quartz (25) 0.5-2mm Hornblende (15) 0.5-2mm Biotite (10)		K Feldspar Biotite Magnetite Apatite Zircon	Plagioclase Monzonitic Enclaves Chloritized Amphibole	Circular 1.5km2 Stock Mouth of Silver Canyon
Aplite Dikes	Aphanitic to Fine Grained Porphyritic Allotriomorphic	K Feldspar (50) Plagioclase (20) Quartz (30)	Kspar (50%) quartz (30%) plagioclase (20%)	biotite	aplitic texture	Dikes and Irregular Lobes <5m thickness Cut by Dacite Porphyry Dikes
Dacite and Rhyolite Dikes	Cryptocrystalline Aphanitic Porphyritic Aplitic Porphyritic		K Feldspar Plagioclase Quartz Biotite Hornblende	Zircon Apatite Magnetite	Chilled Border Zones Gradational Grain Size Groundmass Myrmekite Quartz-Feldspar Spherulites	<1km Long, 2-20m Thick Dikes NE Trend in Pluton w/ SE Dips Swarm Centered on Cherry Creek Canyon N, NW, NE Trending in Fault Zones
Gabbro Dikes	Fine Grained to Very Fine Grained Phaneritic	Plagioclase Hornblende Augite Magnetite		olivine		Thin 10mx1m Dikes NE Trending in Tonalite

Table 1. Characteristics of igneous rocks at Cherry Creek

Table 2. Geochemistry of examples of unaltered igneous rocks from Cherry Creek

	qtz monzonite	qtz monzonite	granite	tonalite	granite aplite	andesite	andesite	dacite porphyry	dacite porphyry	gabbro	gabbro
Type	stock	stock	stock	stock	dike	dike	dike	dike	dike	dike	dike
Site	Salvi	Salvi	Cherry Cr Cyn	Silver Canyon	Salvi	Rattlesnake Canyon	Montgomery Canyon	Cherry Cr Cyn	Salvi	Silver Canyon	Silver Canyon
Sample No.	10084	10110	10060	10074	10085	10253	10288	10057	10109	10076	10063
SiO2 (%)	71.82	71.57	69.80	61.87	76.11	66.03	64.72	73.17	72.19	59.86	59.75
Al2O3 (%)	14.07	14.39	15.15	17.22	12.26	15.75	16.68	13.87	14.64	15.58	15.68
Fe2O3 (%)	3.19	3.05	3.50	5.91	2.01	4.38	4.57	2.24	2.88	6.14	6.21
CaO (%)	2.43	1.75	2.84	4.84	1.02	3.34	4.65	1.51	1.01	5.59	5.70
MgO (%)	0.68	0.79	0.85	2.80	0.30	1.38	2.07	0.39	0.40	4.34	4.42
Na2O (%)	3.09	3.57	3.27	3.47	2.80	2.70	3.11	2.90	1.92	3.33	2.86
K2O (%)	3.87	3.97	3.63	2.39	5.10	4.68	2.80	5.20	6.12	2.93	2.95
Cr2O3 (%)	BDL	BDL	BDL	0.01	BDL	BDL	BDL	BDL	BDL	0.03	0.03
TiO2 (%)	0.41	0.46	0.49	0.91	0.19	0.61	0.70	0.24	0.27	0.98	0.98
MnO (%)	0.05	0.06	0.06	0.09	0.03	0.07	0.08	0.05	0.03	0.09	0.10
P2O5 (%)	0.16	0.15	0.19	0.22	0.06	0.20	0.17	0.07	0.07	0.33	0.32
SrO (%)	0.04	0.05	0.05	0.06	0.01	0.05	0.07	0.02	0.03	0.08	0.08
BaO (%)	0.11	0.13	0.13	0.11	0.04	0.16	0.15	0.11	0.16	0.17	0.20
C (%)	0.05	0.05	0.02	0.06	0.03	0.44	0.22	0.20	0.24	0.51	0.62
S (%)	0.01	BDL	0.01	BDL	0.01	0.05	0.01	0.02	0.01	0.01	BDL
Ba (ppm)	1030	1180	1060	971	425	1415	1405	896	1500	1450	1625
Ce (ppm)	96.1	101.5	102.5	94.7	36.7	120	96	101	139.5	105	101
Cr (ppm)	20	20	20	50	20	20	20	30	20	220	220
Cs (ppm)	2.26	4.11	2.87	1.48	1.76	5.83	3.69	3.58	7.84	0.82	1.16
Dy (ppm)	3.86	3.63	3.94	4.63	1.55	4.88	3.92	4.41	4.3	4.14	3.93
Er (ppm)	1.97	1.84	1.89	2.51	0.89	2.61	2.11	2.44	2.43	2.02	1.87
Eu (ppm)	1.38	1.42	1.42	1.59	0.63	1.51	1.62	0.98	1.32	1.76	1.64
Ga (ppm)	22.3	21.5	22.3	22.4	19.7	21.1	23.8	20	19.6	21.9	22
Gd (ppm)	5.18	5.32	5.35	5.8	1.63	5.93	5.31	5.08	5.65	5.7	5.47
Ge (ppm)	<5	<5	<5	<5	<5	<5	<5	<5	<5	<5	<5
Hf (ppm)	5.6	6	5.5	5.8	3.7	7.5	5.6	5.8	9.2	5.5	5.3
Ho (ppm)	0.74	0.68	0.7	0.9	0.31	0.96	0.71	0.82	0.89	0.79	0.78
La (ppm)	53.4	56.4	58.5	50.6	20.4	61.3	49.8	54.2	78.2	58.5	57
Lu (ppm)	0.3	0.25	0.21	0.3	0.19	0.42	0.31	0.39	0.38	0.3	0.26
Nb (ppm)	21.3	21.2	20.4	17.2	16	20.9	17.1	23.6	23.5	19.6	18.6
Nd (ppm)	39.2	40.4	40.3	39.6	13.5	46	38.3	38.2	50.4	43.1	40.8
Pr (ppm)	10.45	10.9	11	10.3	3.82	12.9	10.5	10.9	14.25	11.5	11.1
Rb (ppm)	157.5	206	147	58.9	192.5	189.5	76.7	233	285	93.5	82.6
Sm (ppm)	6.73	7.37	6.74	6.97	2.37	7.66	6.78	6.59	8.46	6.69	7.04
Sn (ppm)	3	5	5	2	1	2	2	3	13	2	1
Sr (ppm)	348	443	396	566	120	426	692	195.5	239	682	730
Ta (ppm)	2.1	1.7	1.4	1	1.4	1.3	1	2.1	1.8	1	1
Tb (ppm)	0.74	0.71	0.76	0.78	0.25	0.83	0.74	0.72	0.8	0.75	0.73
Th (ppm)	25.6	26.5	25.1	15.35	19.65	24	13.85	39	38.1	20.1	18.85
Tm (ppm)	0.29	0.26	0.23	0.33	0.14	0.39	0.33	0.31	0.36	0.29	0.3
U (ppm)	5.4	4.6	3.38	2.12	8.02	5.57	2.94	10.85	7.07	4.72	4.36
V (ppm)	37	37	44	114	22	64	51	17	11	120	116
W (ppm)	2	8	4	1	2	3	1	2	8	1	1
Y (ppm)	20.2	18	18.3	22.5	8.6	26.3	21.5	24.2	23.1	20.5	20.3
Yb (ppm)	1.93	1.57	1.51	2.27	1.07	2.35	2.01	2.47	2.38	1.89	1.86
Zr (ppm)	180	207	193	219	101	282	215	188	344	214	205
As (ppm)	1.3	0.5	0.3	1.4	0.7	2.1	1.2	1.7	0.8	0.9	1.3
Bi (ppm)	0.13	0.06	0.23	0.05	0.12	0.05	0.09	0.43	0.1	0.01	0.02
Hg (ppm)	0.013	0.008	0.009	<0.005	0.014	0.019	0.011	0.013	0.007	<0.005	<0.005
In (ppm)	0.029	0.014	0.034	0.018	0.017	0.034	0.019	0.067	0.015	0.015	0.022
Re (ppm)	<0.001	<0.001	<0.001	<0.001	<0.001	0.001	<0.001	0.001	<0.001	<0.001	<0.001
Sb (ppm)	0.15	0.23	<0.05	0.15	0.1	1.21	0.91	0.1	0.14	0.31	0.38
Se (ppm)	0.3	0.3	0.3	0.5	0.2	<0.2	<0.2	0.5	0.5	0.4	0.3
Te (ppm)	0.01	<0.01	0.01	<0.01	<0.01	<0.01	0.01	<0.01	<0.01	<0.01	<0.01
Tl (ppm)	0.28	0.16	0.44	0.02	0.12	0.19	0.18	0.35	0.28	0.02	0.02
Au (ppm)	<0.001	0.001	<0.001	0.001	0.001	0.004	<0.001	<0.001	0.006	0.001	0.011
Ag (ppm)	<0.5	<0.5	<0.5	<0.5	<0.5	0.6	0.6	<0.5	<0.5	<0.5	1.4
Cd (ppm)	<0.5	<0.5	<0.5	<0.5	<0.5	<0.5	<0.5	0.5	0.7	<0.5	<0.5
Co (ppm)	2	3	4	12	2	8	7	2	2	16	15
Cu (ppm)	17	2	5	5	27	8	4	5	5	2	3
Li (ppm)	20	20	30	20	<10	20	30	30	30	20	40
Mo (ppm)	<1	<1	<1	1	4	2	2	1	<1	<1	<1
Ni (ppm)	<1	<1	1	6	1	3	3	1	1	37	36
Pb (ppm)	23	16	20	20	29	37	20	49	40	18	20
Sc (ppm)	4	4	5	12	3	8	9	3	3	13	13
Zn (ppm)	51	44	62	79	27	79	91	114	107	78	79

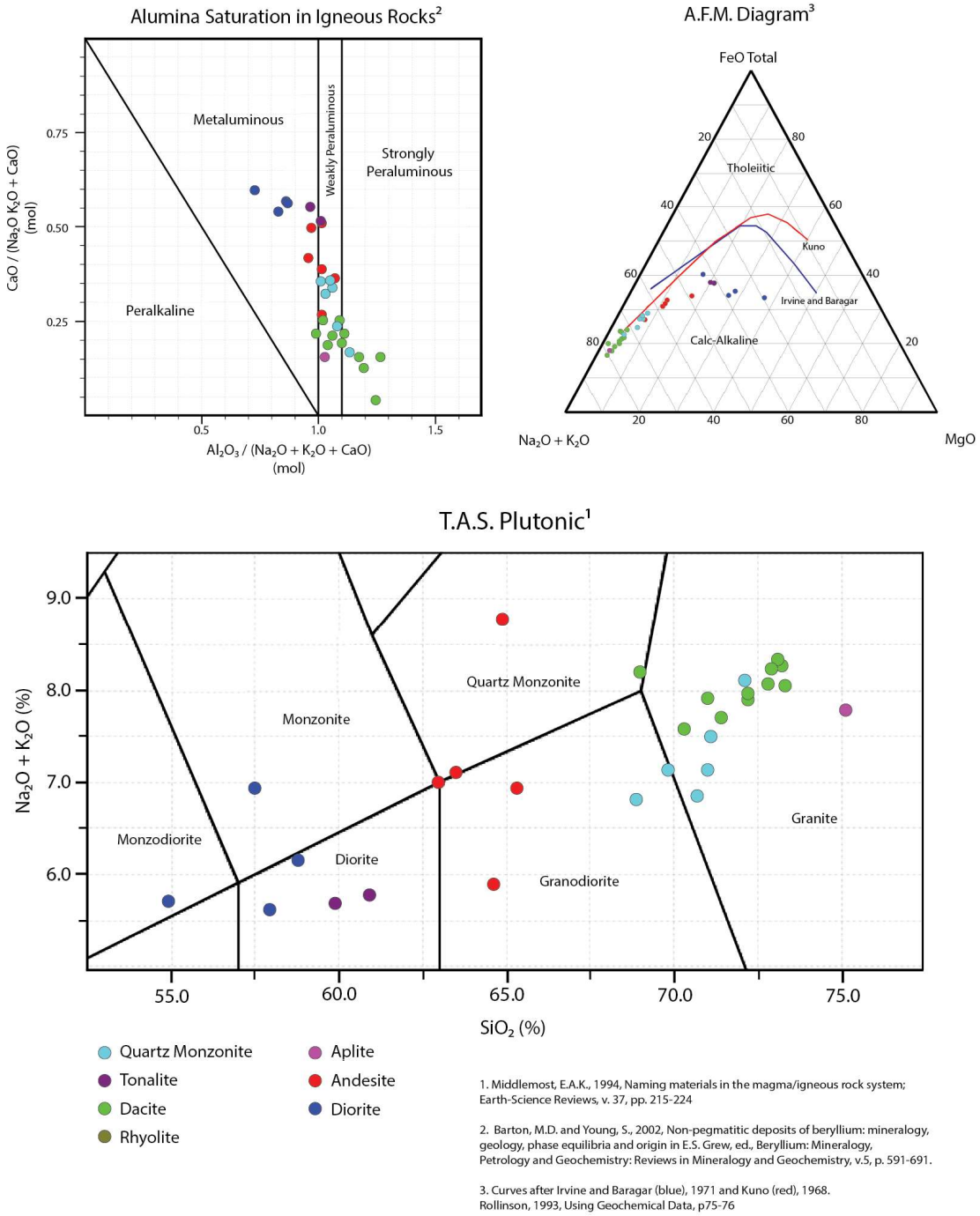

Figure 13. Geochemical classification diagrams for igneous rocks of Cherry Creek

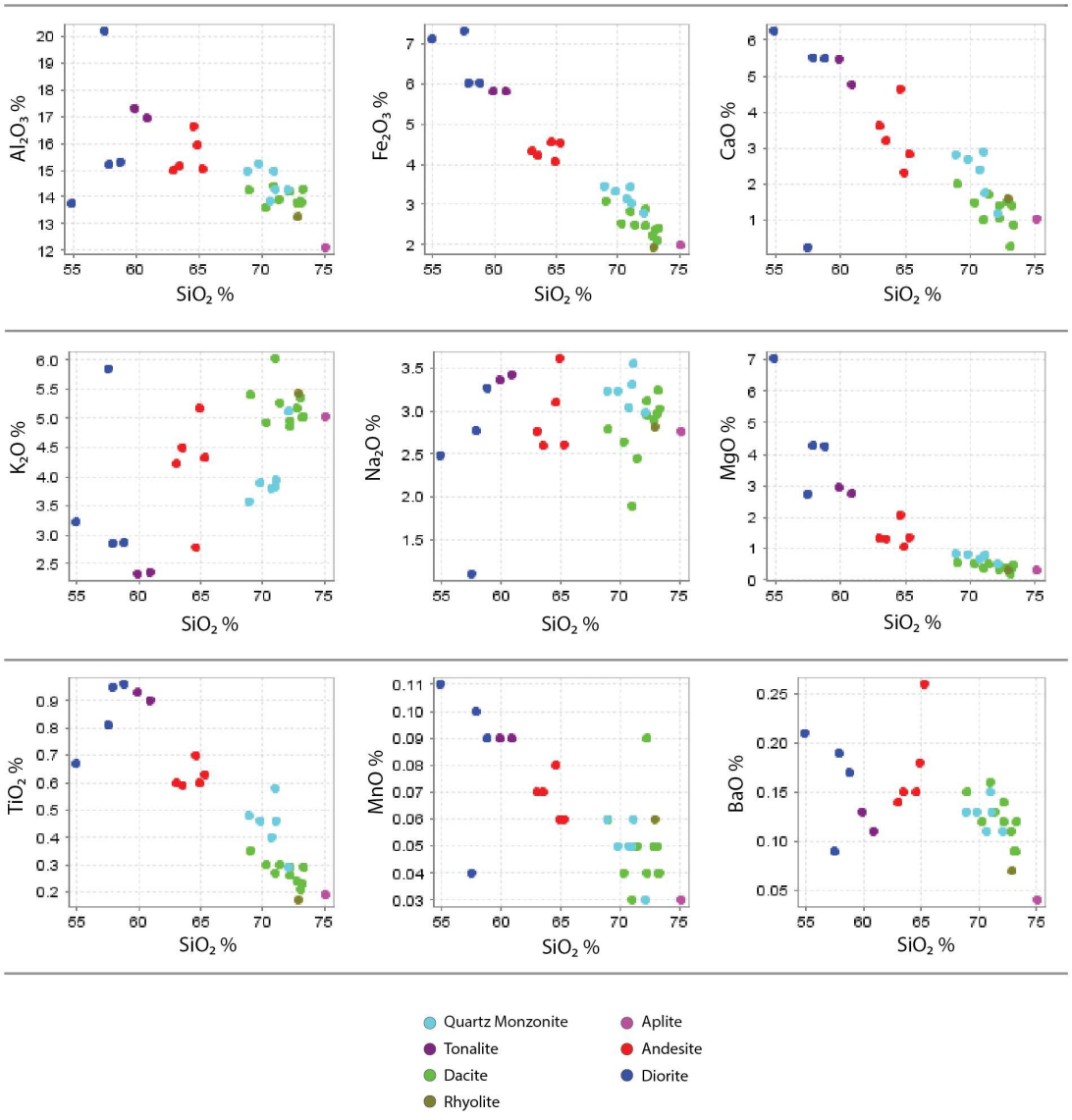

Figure 14. Harker variation plots for major element oxides

Quartz Monzonite Ages

Sample No.	206Pb/238U	2σ Error (Ma)	MSWD	No.
10107	37.89	0.28	2.6	23
10084	37.76	0.3	0.95	28
10111	37.67	0.3	1.4	24
10125	37.23	0.35	1.4	25
10060	36.72	0.3	1.1	27
10093	36.62	0.26	1.01	28
10059	36.18	0.31	1.3	26

Tonalite Ages

Sample No.	206Pb/238U	2σ Error (Ma)	MSWD	No.
10075	40.16	0.93	1.5	16
10053	37.33	0.34	0.96	30

Dike Ages

Sample No.	206Pb/238U	2σ Error (Ma)	MSWD	No.
10102	38.2	0.5	0.65	23
10079	35.59	0.28	0.56	30
10080	35.44	0.41	0.45	30
10129	35.44	0.36	1.2	29
10108	35.07	0.34	0.8	27
10091	35.26	0.37	0.9	30

Table 3. Summary of $^{206}Pb/^{238}U$ zircon ages for igneous rocks of Cherry Creek

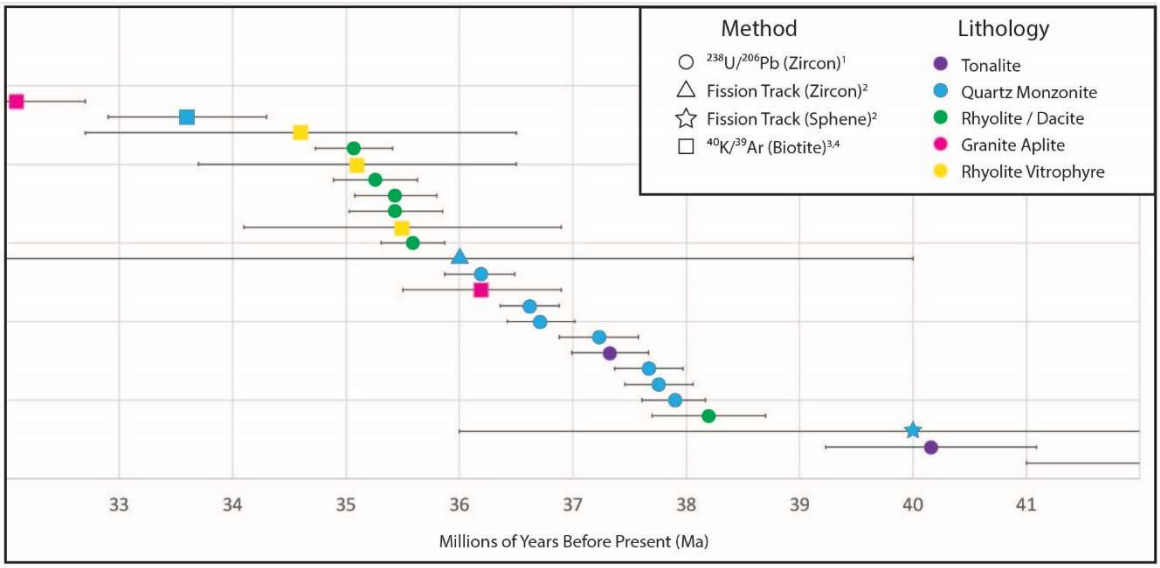

1. This study
2. Hose, R.K., Blake, M.C., and Smith, R.M., 1976, Geology and Mineral Rescources of White Pine County, Nevada: Nevada Bureau of Mines and Geology Bulletin, v. 85, p. 105.
3. Armstrong, R.L., 1970, Geochronology of Tertiary igneous rocks, eastern Basin and Range Province, western Utah and eastern Nevada, U.S.A.: Geochimica et Cosmochimica Acta, v. 34, p. 203–232
4. McKee, E.H., Silberman, M.L., Marvin, R.E., and Obradovich, J.D., 1973, A summary of radiometric ages of Tertiary volcanic rocks in Nevada and eastern California. Part I: Central Nevada.:

Figure 15. Geochronology of igneous rocks at Cherry Creek, including analyses from previous studies

Hydrothermal Geology

One defining aspect of the Cherry Creek district is the spatial and compositional range of hydrothermally altered rocks that occur across an 8-km section of exposed stratigraphy. Evidence of hydrothermal alteration and mineralization is found at the extreme eastern and western margins of the range alike, and occurs at intervals across the >10 km width of the range. The passage of hydrothermal fluids through rocks in the Cherry Creek district has both created ore deposits and altered the chemistry and mineralogy of their host rocks. The footprint of this hydrothermal activity is substantial, and has resulted in the alteration of sedimentary and igneous rocks alike (Figure 16). As such, the district's endowment of Ag, Au, W, Cu, Pb, and Zn is associated with a diverse suite of hydrothermal ore deposits.

The distributions and compositions of altered rocks of the pluton represent the mineralization age and style in the structurally deepest levels of the Cherry Creek Range. The first half of this chapter discusses the signatures of these hydrothermal effects in the pluton, and the second discusses the controls, zonation, and extent of hydrothermal mineralization in the rocks between the realms of Eocene plutonism and the Eocene paleosurface. Special attention is paid to the structural, lithological, and temporal variation that occur along the Exchequer and Black Metal faults, which are the main throughgoing mineralized structures in the study area. Evidence of magmatism along the Exchequer fault is widespread in the many mineralized dikes that are hosted within the fault zone, and for this reason it is the best place to investigate the association between hydrothermal and igneous geology. For this reason, among others, the Exchequer has been the primary focus of study. The following sections include observations from reconnaissance-style

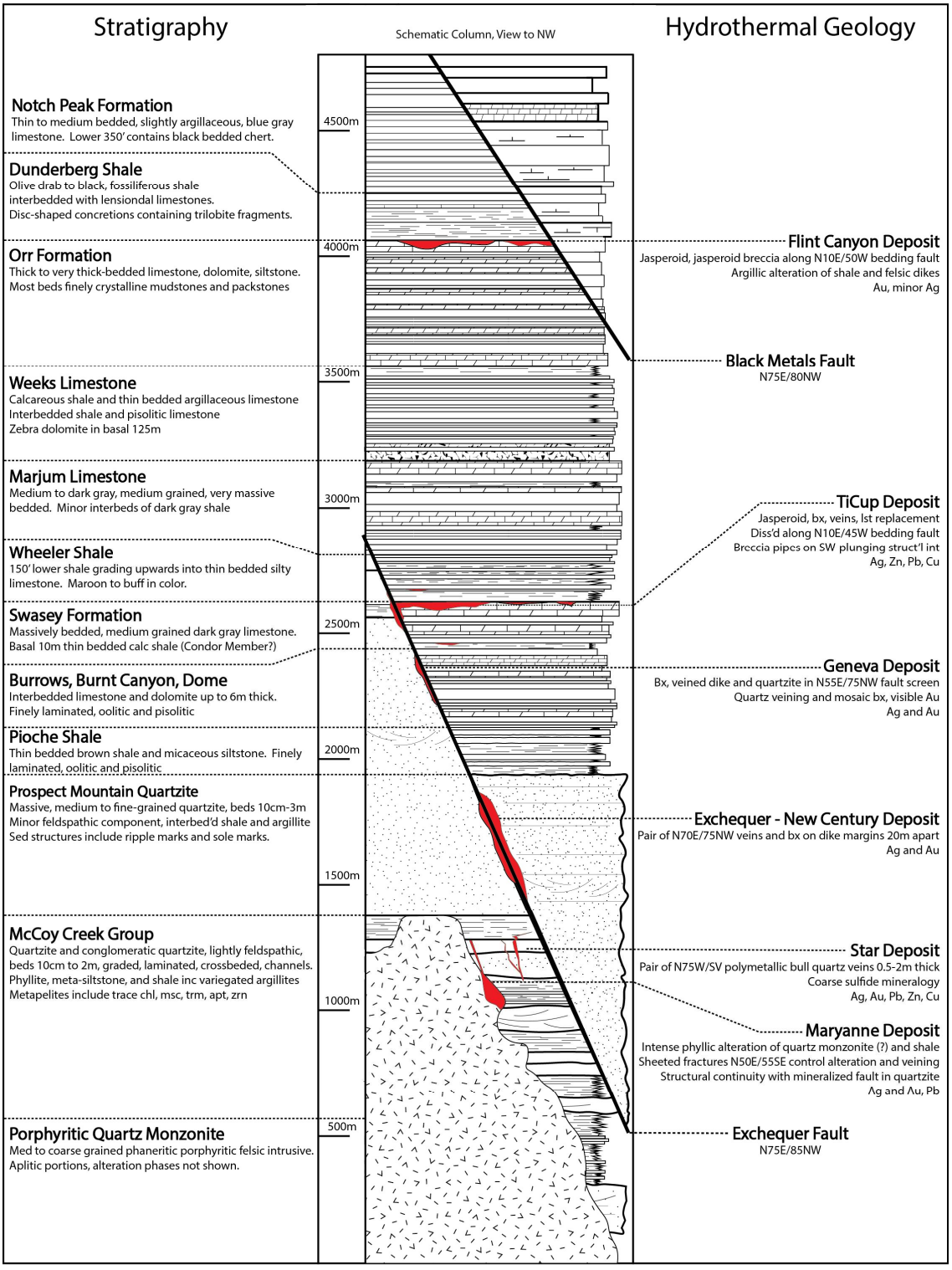

Figure 16. Composite stratigraphic column of Precambrian and Cambrian rocks of the Cherry Creek district. Stratigraphic designations are made on the left side of the column, and the characteristics of hydrothermal rocks and faults listed on the right. Hydrothermal deposits are represented on the column by the color red.

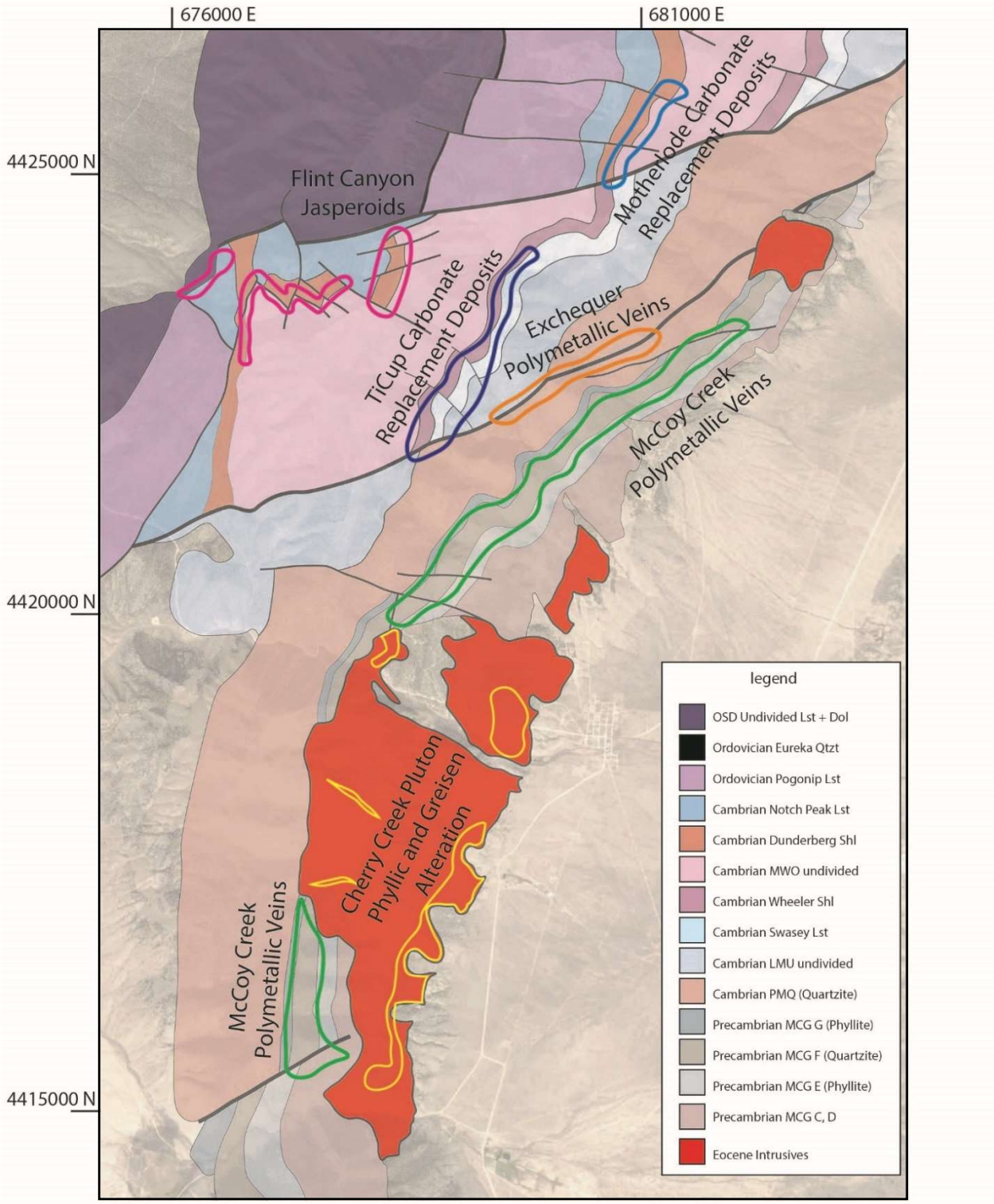

Figure 17. Geologic map of the central Cherry Creek Range showing major zones of hydrothermal mineralization

petrographic analysis, geochemical analysis, geochronology, and mapping. Wherever possible, accounts from historical reports have been included to provide information on historic mines.

Contact-Metamorphic and Skarn Rocks

Contact Metamorphism

Despite the significant size of the Cherry Creek pluton, the apparent thermal and metasomatic effects of its intrusion are relatively minor, in large part because of the massive, quartz-dominant lithologies in its hanging wall. Intrusive contacts between the pluton and quartzite and phyllites of the McCoy Creek Group (MCG) are very rarely exposed, and only in a few places are contact metamorphic features exposed in the study area. The Cambrian Prospect Mountain Quartzite (PMQ) forms the upper contact of the Cherry Creek pluton in most places, and it displays little evidence of contact metamorphic effects beyond recrystallization of quartz grains. Primary depositional structures including cross bedding, fining-upwards sequences, and channel structures are readily discernible. While cementation has destroyed most granular textures in the unit, no dynamic lineations or foliations were noted in the quartzite. Sulfide-barren quartz veins are common, as is a weak, fine-grained pyritic overprint that is especially common in fractured rock of the major fault zones. Whether these features are the result of hydrothermal or contact-metamorphic effects is unclear.

Metapelitic rocks of the upper MCG are composed of slate, phyllite, and minor hornfels either owing to regional metamorphism in the Cretaceous (Long and Soignard, 2016) or the intrusion of the Cherry Creek pluton in the Eocene. These units are best exposed in Egan Canyon and between Maude and Silver Canyons, although the only exposed contacts between them and the Cherry Creek pluton are located to the south of Cherry Creek Canyon.

Three horizons of carbonate rocks are present in the phyllite-dominated McCoy Creek strata of the study area. The two best-exposed examples are found to the northwest of the Cherry Creek townsite, in a section of phyllite (Unit G) bordering unaltered quartz monzonite (Figures 5 and 6). The lenses are small, in both cases being <5 m thick and <25 m in strike length. The carbonate minerals making up these marble beds are recrystallized to significantly coarser sizes than their host phyllite, and are composed of dark grey calcite mottled with light brown dolomite. Being soft-weathering, both lenses are only revealed by strings of prospect pits that follow their hanging wall contacts. It is possible these correlate with carbonate beds in the Osceola Argillite, as described elsewhere in eastern Nevada by Woodward (1967).

Skarns

Skarns are exceedingly rare in the study area, and only one is well-exposed at the surface in the upper 50 m of the McCoy Creek Group. The exposed skarn is composed of quartz, garnet, epidote, and minor tremolite with well-developed, cm-scale banding (Figure 18a). The skarn body is somewhat incongruous, being located roughly 150 meters from the apparent upper contact of the Cherry Creek pluton's quartz monzonite phase in the Cherry Hills area south of Cherry Creek Canyon (Figure 2). The geometry of the upper contact here is apparently

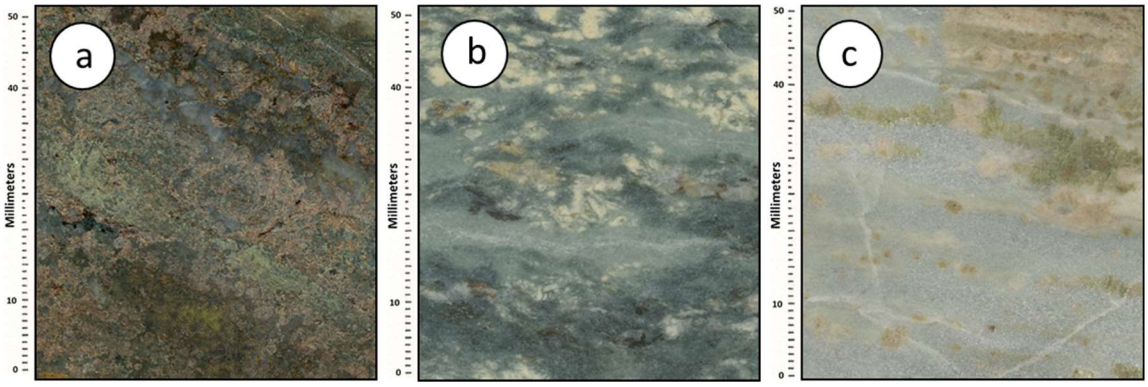

Figure 18. Petrographic examples of zoned skarn mineralization from Cherry Hills. From north to south and inferred proximal to distal, andradite-tremolite-epidote skarn (a), chlorite-phlogopite skarn (b), and weakly epidotized marble (c).

planar, as the approximate contact can be traced along the strike of the overlying quartzite beds. The skarn is a lensoidal 15 by 25-meter body that pinches along strike. Transects of the same stratigraphic horizon to the south revealed another small lensoidal carbonate body about 125 meters away, which contains other cm-scale foliated skarn lithologies (Figure 18; Table 4), including 1) fine- to medium-grained chlorite, phlogopite, and sericite, with some calcite (Figure 18b), and 2) a recrystallized, foliated marble with only weak development of skarnoid minerals possibly attributable to isochemical metamorphism, including porphyroblastic dolomite and epidote (Figure 18c).

Skarn material in the dump at this site also includes limited amounts of altered mafic igneous rock, overprinted by cm-scale bands of fine-grained chlorite (<0.5 mm), phlogopite (0.5-2 mm), scheelite, and quartz. In addition, much of the rock is also darkened by weakly disseminated and very fine-grained mafic minerals (probably biotite) that occur in mm-scale bands. This lithology was not located in outcrop, and its age and context are somewhat enigmatic.

Table 4. Composition of Cherry Hill garnet-epidote skarn

Garnet-Epidote Skarn
Cherry Hill
10058

	SiO2	Al2O3	Fe2O3	CaO	MgO	Na2O	K2O	Cr2O3	TiO2	MnO	P2O5	C	S
(%)	39.4	10.3	18.7	26.7	0.81	0.03	0.13	0.01	0.28	0.67	0.04	0.04	0.01
	Au	Ag	Zn	Pb	Cu	As	Ba	Sb	W	Bi	Sn	Mo	Ni
ppm	0.007	<0.5	44	9	3	3.9	229	0.19	55	0.33	237	4	8

Hydrothermal Deposits in the Cherry Creek Pluton

Quartz-Muscovite Greisen and Phyllic Alteration in the Salvi Fault Zone

The Salvi Fault Zone (SFZ) is located along the eastern edge of the Cherry Creek quartz monzonite pluton between the Cherry Creek townsite and Egan Canyon (Figure 2). It consists primarily of an east-dipping plane that juxtaposes quartz-monzonite in the footwall against bedded, probable Lower Cambrian quartzite and carbonate strata in the hanging wall. The SFZ is best exposed along a 2.5 km stretch between Salvi Ranch and Egan Canyon, where exploration trenches have revealed the fault between weathered outcrops of quartzite and intrusive rock. A few isolated outcrops of quartzite in the hanging wall form small, subdued hills standing no more than a few meters above the surrounding alluvial fan to the west of Salvi Ranch along County Road 23 between Cherry Creek and Egan canyons (Figure 2).

The igneous footwall of the Salvi fault is highly fractured, with a 50 to 100 m-wide set of subparallel, N10°E/35°SE to N40°E/55°SE fractures extending at least 3.5 km along the eastern margin of the Cherry Creek pluton (Figure 19). A few small faults with similar orientations cut the quartz monzonite stock and a dacite dike as far as 200 m from the SFZ. The main strand of the fault is coated with lineated clay gouge and calcite displaying normal-sense kinematic indicators raked between 25 and 50 degrees to the south-southwest. To the immediate west of the Cherry Creek townsite dense, sheeted fractures are present but the fault is not exposed.

Within 75 m of the SFZ, most fractures are mineralized and many host granoblastic quartz veins, although few joint sets to the west are mineralized. The veins are controlled by a N10°-40°E orientation, and accompanied by disseminated and selvage-controlled greisen and phyllic alteration. Although quartz veins are widespread in the footwall

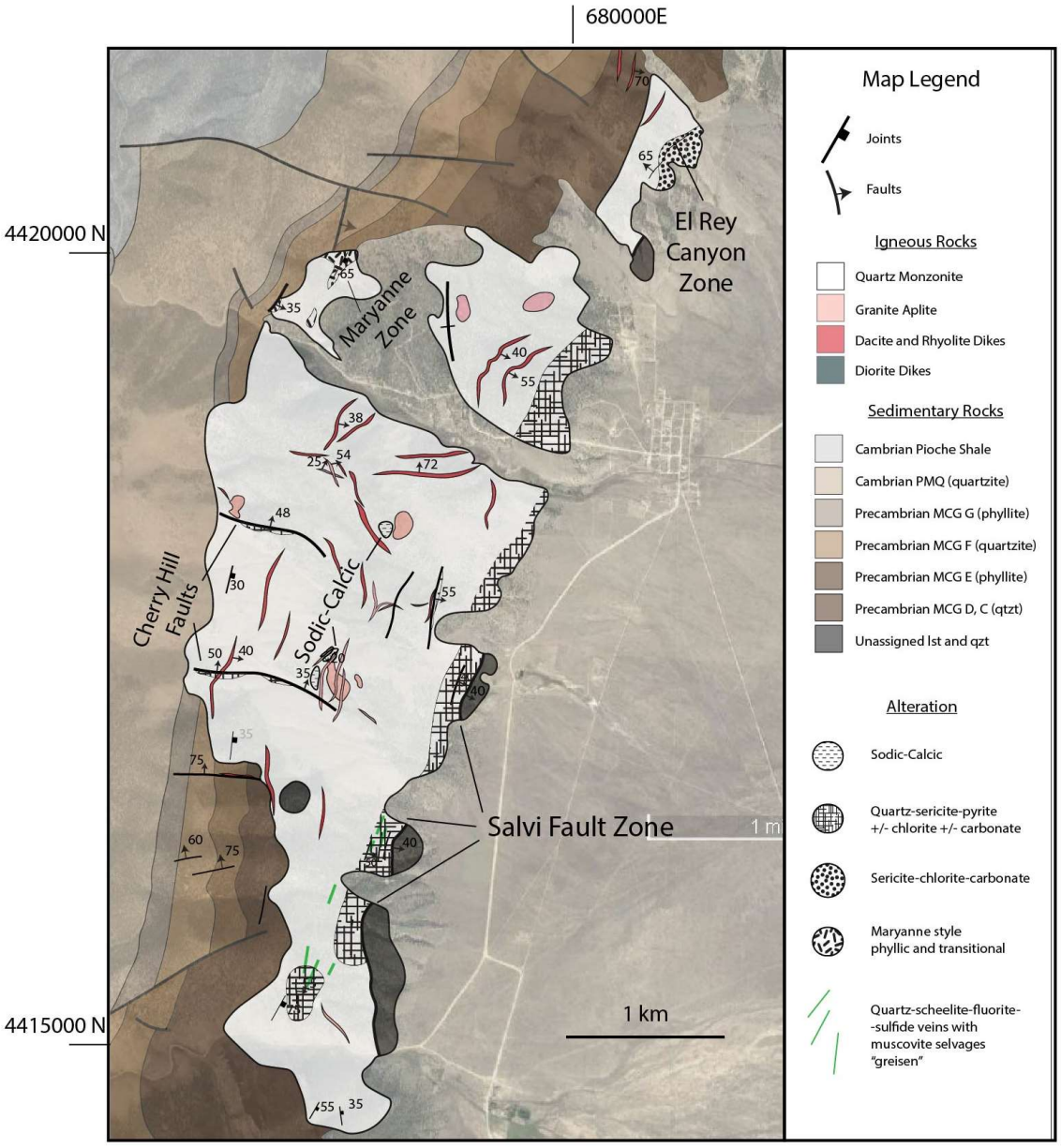

Figure 19. Schematic map of the Cherry Creek pluton showing major zones of altered rock. Based on mapping by the author and D. Adair (1961).

of the SFZ, the strongest development of alteration is limited to the exposures south of Cherry Creek Canyon.

The hanging wall of the SFZ is heavily fractured but chaotic, with no recognizable fabric. In it, quartzite is usually weakly veined with some granoblastic quartz, and the carbonates are unmetamorphosed but have been intensely brecciated and cemented with calcite. It is possible that a large amount of post-mineral offset may have obscured the primary relationships.

I. Greisen Alteration (Quartz-Muscovite)

Quartz-muscovite mineralization within the main body of quartz monzonite is essentially limited to a thin, 50 x 500-m strip of the SFZ hanging wall where it occurs in small zones of isolated veinlets (Figures 19 and 20). It is characterized foremost by the presence of thin (5-25 mm), undulatory and lobate quartz veins with muscovite selvages up to 35 mm thick. The veins have undulating walls and attain maximum densities of 35% of rock mass. The vein quartz is normally anhedral and granoblastic, with individual grains up to 8 mm in diameter. In places, the quartz is smoky. Other constituents of the vein material include hematite, which comprises up to 40% of the vein material over small intervals and commonly assumes the cubic shape suggestive of a psuedomorphic replacement of mm-scale pyrite. Minor amounts of fluorite and

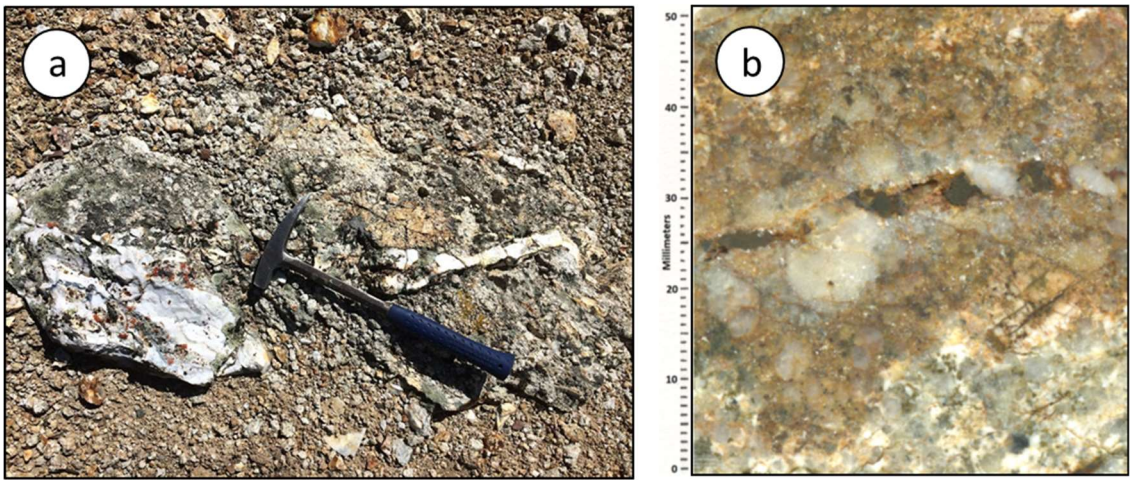

Figure 20. Intense quartz veining with muscovite selvage in outcrop (a) and hand sample (b)

scheelite are locally present in the veins. Small, <1-mm-thick veinlets of muscovite and chlorite are also widespread. Due to the prevalence of coarse muscovite and its coincidence with quartz, scheelite, and fluorite, this alteration is best classified as vein-controlled greisen (Figure 20).

In the best examples of quartz-muscovite alteration, the wall rock abutting muscovite selvages has cloudy, buff-colored feldspars and is weakly to moderately sericitized. It contains a trace amount of disseminated pyrite up to 1-mm and a few thin fracture coatings of iron oxide. Further outboard of the veins the wall rock is strongly bleached, and alteration transitions into a strongly silicic, phyllic, and sulfidic style like that described in detail below. It is unknown exactly how these alteration assemblages are related, but the greisen veining is suspected to represent a more intense and higher temperature expression of the same mineralizing process. A few extremely lobate veins of chalcedonic quartz (Figure 20b) are also present in the area, and seem to be associated with intensely kaolinized quartz monzonite. The relationships and extent of this alteration is unclear as it has only been found in one small area in the north side of Egan Canyon.

Geochemistry

Major-element trends of quartz-muscovite-veined quartz monzonite show strong enrichment of K_2O and minor enrichment of CaO mainly at the expense of Na_2O, and Fe_2O_3, which are strongly to moderately depleted relative to unaltered quartz monzonite (Figure 21). Ba, C, and S are weakly enriched, and Fe_2O_3, P_2O_5, MnO, and SrO are weakly depleted.

The most substantial increases in trace-element concentrations in greisen-veined quartz monzonite are mainly in W, which represents a large proportion of the total trace element enrichment and has experienced a 100x increase from unaltered levels (Figure 21). In addition, major elevations also occur in the concentrations of Sn, Bi, and Sb. Other trace elements added include As, Te, Ni, Mo, Cu, and Ag. No fluorine analyses were done, but the presence of fluorite as a primary vein mineral indicates significant fluorine metasomatism.

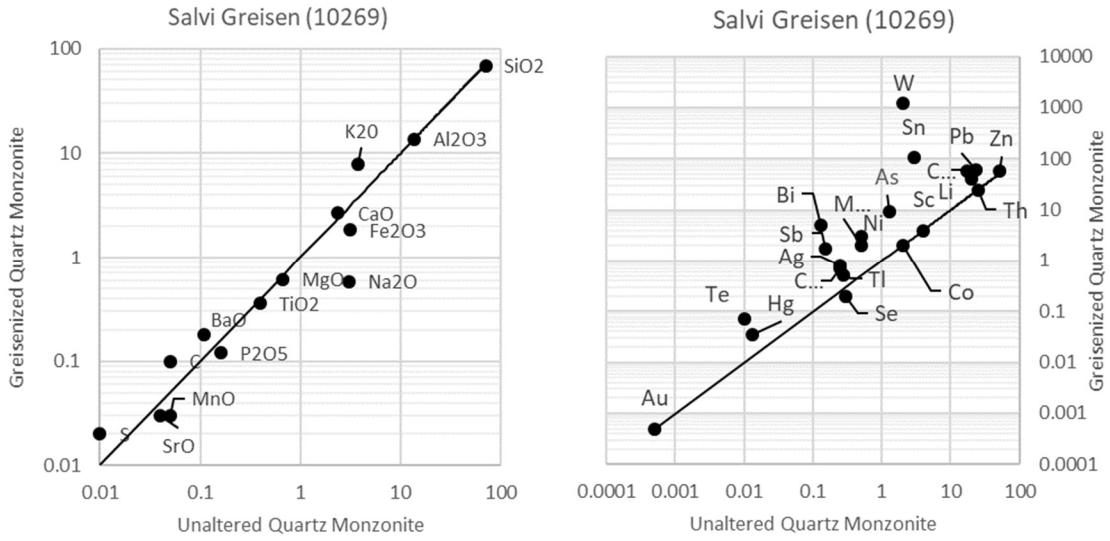

Figure 21. Isocon diagrams for greisen-veined quartz monzonite

II. Phyllic Alteration (Quartz-Sericite-Pyrite-Chlorite-Carbonate)

A form of phyllic alteration is the most widespread style associated with quartz vein mineralization along the SFZ on the east side of the Cherry Creek pluton (Figure 19). The veins that accompany phyllic alteration manifest as anhedral, granoblastic quartz veins and lobes comprising on average 10 to 30% of the rock volume, and at maximum attaining 80% density over small $1m^2$ zones. The heavily fractured wall rock is affected by moderate to very strong quartz-sericite-chlorite-calcite alteration in feldspar sites, and cubes of pyrite up to 4 mm diameter are sparse but commonly present. Overall, this phyllic-altered quartz monzonite is only weakly sulfide-bearing. Mafic sites in the altered quartz monzonite are usually filled with chlorite or partially chloritized biotite. A few outcrops of intensely phyllic-altered quartz monzonite are foliated, with elongate sericite and chlorite separating isometric, <1-cm diameter quartz grains. The same samples are flooded with irregular, anastomosing lobes and veinlets of quartz up to a few centimeters in diameter. Centimeter-scale iron-oxide lobes apparently deformed into sigma clasts can be found within matrices of quartz, chlorite, and sericite (an s-c fabric; Figure 22). A few grains of pyrite are fractured and fragmented within a cataclastic matrix of fine-grained rounded quartz.

The footprint of phyllic alteration extends at least 4.25 km along a N20°E trend, achieving a maximum width of about 150 m and extending from Egan Canyon to the north wall of Cherry Creek Canyon. The best exposures of this mineralization style are found immediately to the west of the Cherry Creek townsite, west of Salvi Ranch, and on the south side of the road to the Wide West Mine on the north side of Egan Canyon (Figure 4). This veining is spatially associated with quartz-muscovite veining but significantly more widespread. Away from the SFZ, sericitization decreases in intensity although weak sericitization and chloritization of biotite

is widespread in the Cherry Creek pluton. A few northeast-striking and east-dipping faults are marked by thin quartz veins and localized intense phyllic alteration up to 400 m from the SFZ. Outside of the trenches and a few small outcrops, most exposures are intensely weathered and bleached white, although notable changes in the color and texture of soil are consistently recognized.

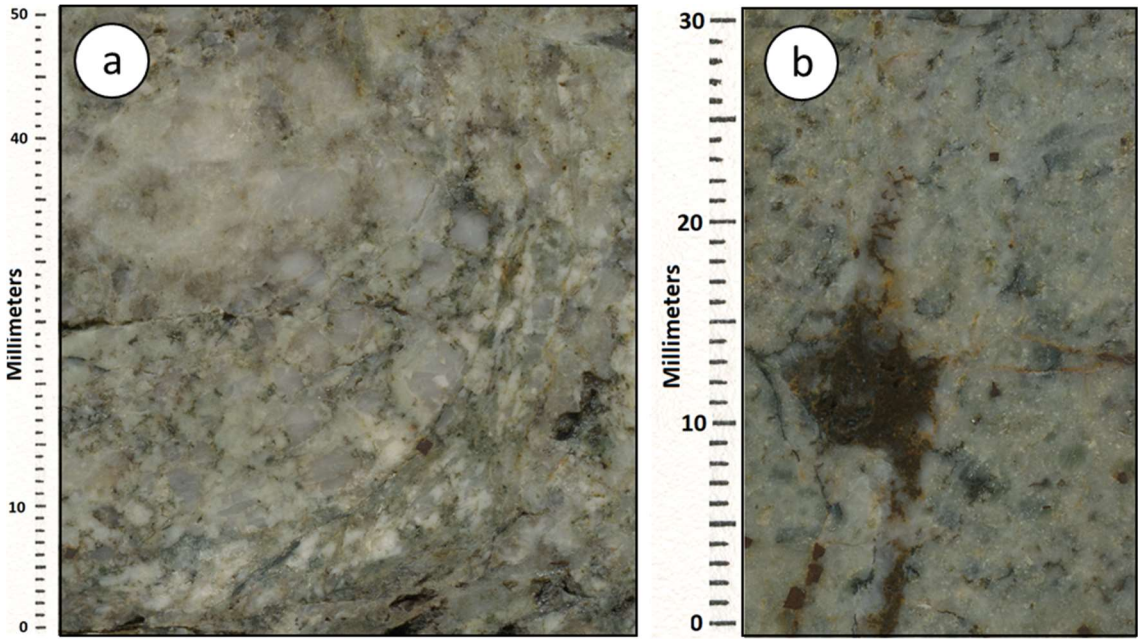

Figure 22. Intensely phyllic-altered quartz monzonite in the footwall of the Salvi fault.
Note the foliation present in elongated sericite and chlorite (a) and possible sigma clast (b) showing dextral motion along a sub-vertical trace.

Geochemistry

Major-element concentrations in samples of phyllic (quartz-sericite-pyrite-chlorite-carbonate)-altered quartz monzonite have experienced weak addition of SiO_2. Na_2O is almost entirely depleted, and moderate to minor depletions occur in CaO and MgO. The concentration of Fe_2O_3 is variable, being weakly depleted in some samples and heavily enriched in others. Heavily veined samples show a weak depletion in K_2O but other samples show a weak enrichment, probably due to rock dilution by quartz veining. S and C are elevated significantly, and reach concentrations of 0.5%.

Au, As, Hg, Ag, Pb, Zn, W, Sb, Bi, Mo, and Sn were added during phyllic alteration along the SFZ (Figure 23). One sample (10106) of phyllic-altered quartz monzonite contained 0.238ppm Au, although it was not heavily mineralized with base metals or Ag. The strength of base metal mineralization is associated with the presence of cubic Fe-oxide casts of pyrite.

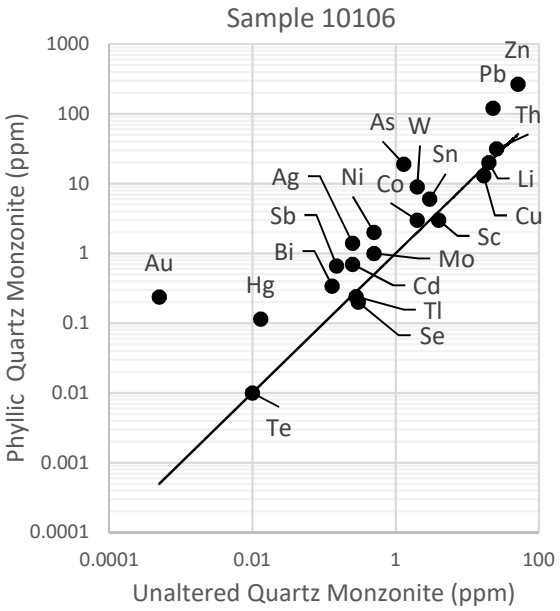

Figure 23. Isocon diagram of phyllic-altered quartz monzonite from Salvi fault zone

Phyllic Alteration and Quartz-Mineralized Faults at Cherry Hill and Bull Hill

At least two west-trending and moderately north-dipping faults are present in the main body of porphyritic quartz monzonite to the south of Cherry Creek Canyon. The faults are mineralized and occur 1 km apart about 400 meters to the east of Peak 2428 m, hereafter referred to as Cherry Hill (Figure 4). These mineralized faults form two chevron-shaped hills that have weathered distinctively into angular shapes and contrast strongly with the normal, spheroidal weathering pattern of the unaltered quartz monzonite around them. Both mineralized faults at Cherry Hill strike N75˚W and dip to the north between 35˚ and 50˚. The main outcrops of these features align with each other, and are separated by 1 km in which intervenes a large exposure of unaltered porphyritic and fine-grained quartz monzonite. The southern vein is better exposed, and crops out over 100 meters along trend to the east and downslope. A series of small prospect pits reveal weak mineralization commonly marked by quartz veins and minor to moderate alteration further to the east where the fault is only poorly exposed. Strong silicification can be tracked at least 300 m to the east along this trend. The northern vein has been similarly prospected and can be traced for 150 m to the east before it disappears under alluvium.

In outcrop, the two veins at Cherry Hill are very similar (Figure 24). Their upper surfaces are comprised of a 1-2 m thick vein of quartz-cemented polyphase breccia that incorporates weakly outlined angular quartz clasts (30-50%) and sericitized and silicified quartz monzonite and dacite (5-10%) in a matrix of white sucrosic quartz (Figure 24a). In the footwall, altered quartz monzonite is extremely friable and soft-weathering, with variable degrees of sericitization of feldspars and generally weak but variable quartz veining over at least 75 cm. The rock is highly

Figure 24. Field Photos from Cherry Hill area.
The vein itself (a) is very siliceous and contains multiple generations of quartz fragments. The footwall quartz monzonite (b) is weakly altered and veined, and heavily weathered.

weathered but biotite is still recognizable. Prospect pits dug along the fault reveal it being cut by an array of tightly spaced shear fractures oriented between N45°W/55°NE and N35°W/50°NE. A few structural intersections below the fault are more highly mineralized and containing significantly more iron oxides. In one prospect pit, a small amount of quartz veining and weak alteration clearly postdates intrusion of the dacite.

Geochemistry

The best samples of altered rocks along the footwalls of the north-dipping Cherry Hills faults have similar trends of enrichment and depletion (Table 7). The primary enrichment in weakly veined and sericitized quartz monzonite forming most of the footwall (sample 10113) is in SiO_2, which is elevated to nearly 80% of rock mass. Intense and almost complete depletion of Na_2O and CaO occurs, and Fe_2O_3 is also strongly depleted. In phyllic-altered dacite (10114) from

a prospect 15 m to the east, SiO_2 is barely elevated while the depletions of CaO and, to a lesser extent, Na_2O are still present.

Trace-element trends are also for the most part similar (Figure 25). Neither the bulk of quartz monzonite nor the dacite dike is strongly altered, and enrichments in the trace elements are only rarely more than 4 times unaltered levels. In sericitized quartz monzonite, the main enrichments are found in W, Bi, Sn, Ag, and Ni. In dacite, the most substantial addition is in Ag, whereas weaker additions exist in Hg, W, Sn, and Zn (Figure 25). In comparison, a strongly phyllic-altered sample (10117) from the thin and more iron-rich, fracture controlled mineralization from the footwall contains a slightly different elemental signature. Although it contains abundant SiO_2 and is strongly depleted in Na_2O and CaO like the rest of the footwall, it contains substantially more Fe_2O_3 and S. The fact that both Al_2O_3 and TiO_2 are strongly depleted and in roughly the same proportion is indicative of dilution through quartz veining. In addition, the trace element suite is characterized by a more diverse assemblage with abundant additions of Bi, Te, Pb, Ag, Mo, Cu, and smaller amounts in As, Zn, and Sn, W, Se, and Au.

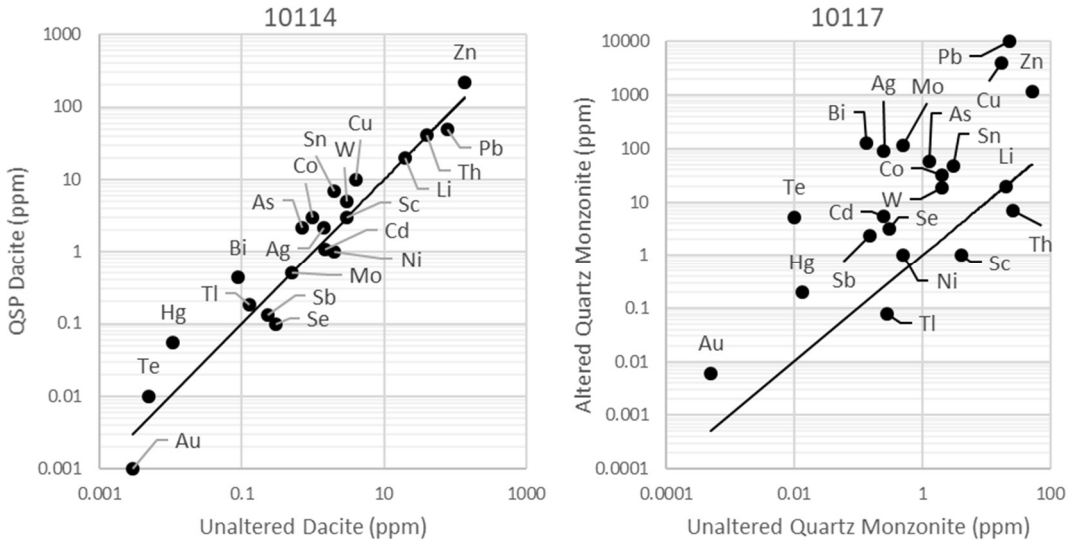

Figure 25. Isocon diagrams for mineralized dacite (10114) and quartz monzonite (10117) at Bull Hill

Phyllic Alteration and Pluton-Hosted Sulfide Mineralization at the Maryanne Deposit

The Maryanne deposit is the best example of intense, feldspar-destructive igneous hosted alteration on the north side of Cherry Creek Canyon. The Maryanne mine was one of the last deposits mined in the Cherry Creek district, and operated only from 1917-1923 during which it produced $35,000 of Ag and Au from an orebody that assayed 35 to 100 ounces per ton Ag (Schrader, 1931). The relationships demonstrated in the mineralization at the Maryanne and its upslope extension at the Flagstaff deposit are critical to understanding the architecture of deep hydrothermal activity in the Cherry Creek Range.

The Maryanne area inhabits the northern shoulder of the 2 km-wide embayment where quartz monzonite of the Cherry Creek pluton intrudes westward into the upper strata of the MCG (Figure 4). To the immediate north and west of the upper Maryanne tunnel lie heavily fractured quartzite of MCG Unit F. A short distance to the northeast, the soft weathering unit E forms small saddles above the cliffs of unit D, beyond which lies Steptoe Valley (Figure 5). Ag-Au mineralization at Maryanne was localized along a set of sheeted N45°E/50°SE fractures that cut the roof of the pluton and continued for 200 meters to the northeast along the intersection between the nearly flat intrusive contact and the trace of northeast-trending fractures (A. Ruggles, personal communication). The main mineralized structure, a N40°E/65°SE fault, passes virtually uninterrupted into the quartzite above. There, the fault is mineralized by a 1-3-meter-thick zone of fracturing and quartz veining clearly visible in a series of prospect pits that lead uphill from the upper Maryanne portal. The Maryanne deposit is localized by a 100 by 200-meter zone of intensely fractured and brecciated rock at the intersection of the intrusive contact and the southeast-dipping fault, although weaker alteration also can be traced down dip to the south and away from the roof of the pluton.

Alteration and Mineralization

Hydrothermal alteration of igneous rocks in the Maryanne area is pervasive, although its intensity and mineralogy varies significantly. The most distinctive style of alteration in quartz monzonite at the Maryanne site is a form of intense, quartz-rich and sulfidic phyllic alteration localized along the uppermost portion of the Maryanne area. Discrete quartz veining is relatively rare, but where present, individual veins are mostly straight and normally < 5 mm thick, at maximum comprise <15% of rock volume. Most veins have outer walls lined with sulfides, which less commonly form cm-wide halos around the veins. More typical of the mineralized rocks at the Maryanne is widespread flooding by fine-grained quartz. The margins of quartz-flooded zones are extremely irregular, and often they are gradational with aggregated mm-scale blebs of sericite that contain crystals ranging in coarseness from 0.2mm to <0.01mm (Figure 26c, d). These blebs usually make up between 20 and 70% of the rock volume, with the matrix composed of veins or flooded zones of quartz up to 1.5 cm in width (<60%), sulfides (<30%), and open-space vugs lined with slender, terminated quartz crystals (<5%). Several generations of quartz replacement and flooding are evident, and at least one generation contains fine-grained secondary quartz with a distinctive blue-grey appearance due to an abundance of finely disseminated sulfide and sericite. Elongate mm- to cm-scale vugs partially infilled with terminated quartz crystals occur in some areas. The sulfide mineralogy of phyllic alteration at the Maryanne deposit is comprised chiefly of pyrite with much lesser galena. Disseminated sphalerite, chalcopyrite, and molybdenite are also present in variable amounts in strongly altered igneous rock.

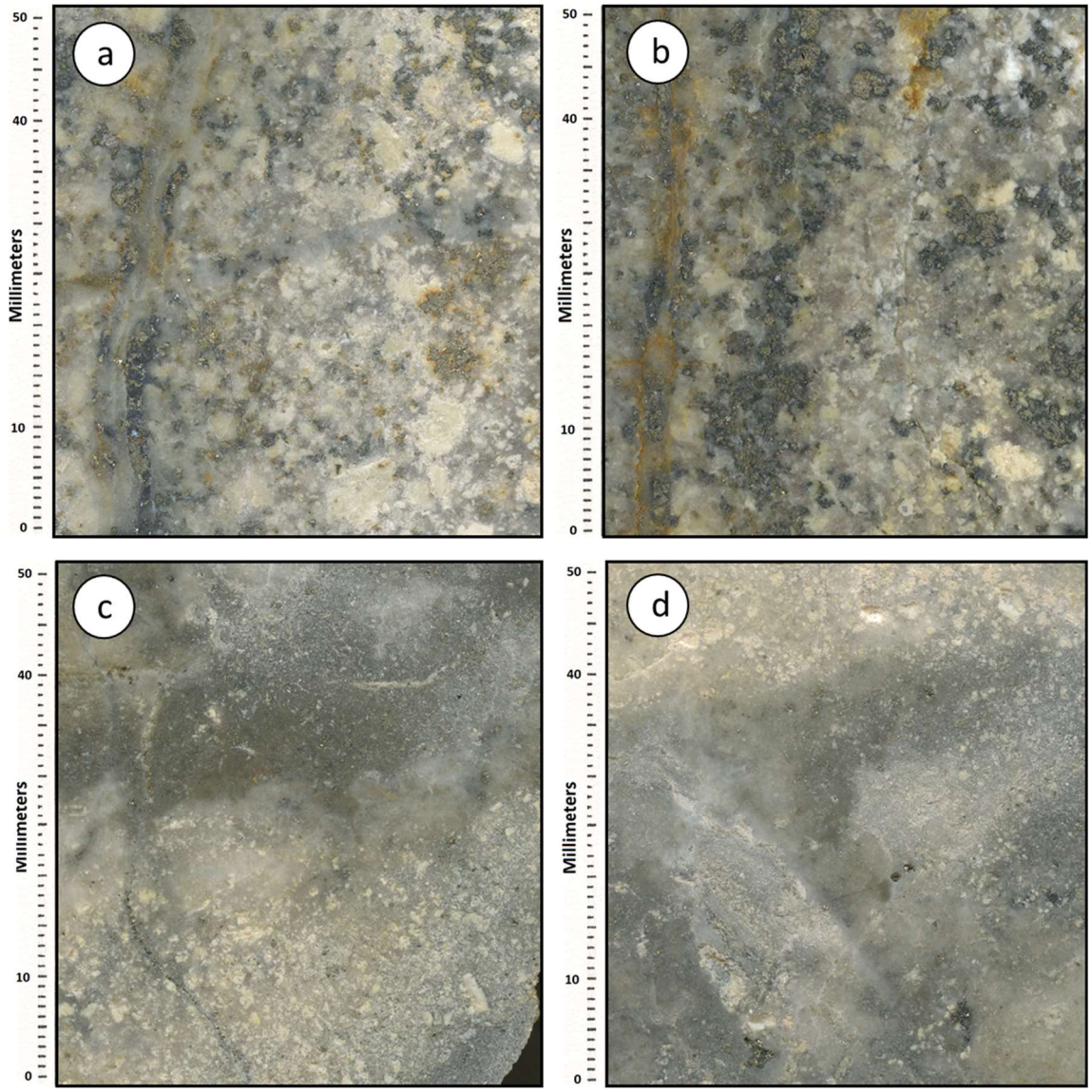

Figure 26. Scanned images of rock slabs showing style of phyllic alteration at the Maryanne mine. Veins normally occur with sulfides along their walls in association with strongly disseminated phyllic alteration in the wallrock (a). Some veins have bulbous envelopes of pyrite, chalcopyrite, galena, and rarely, molybdenite (b). Quartz flooding textures (c,d) are usually marked by grading in the density of sericitized blebs at the mm or cm scale. Some flooded quartz is darkened with fine-grained sulfides, mainly pyrite. Note the destruction of igneous texture in the most strongly silicified rocks.

To the south, down dip, and away from the roof of the CCP, alteration in the Maryanne system changes character significantly. The primary feature of these areas is the presence of 1 to 10-meter spaced fractures or joints that dip to the southeast at moderate angles, being generally subparallel to but more weakly formed than the sheeted fractures around the Maryanne mine itself. In each of the estimated 350- to 400-meter-long underground tunnels, variable intensities of hydrothermal alteration are present. It is hypothesized that these features represent a distal setting to the intense Maryanne mineralization.

Quartz monzonite-hosted alteration in this lower (southern) segment of the Maryanne hydrothermal system is defined by a disseminated mineral assemblage of sericite-chlorite-calcite ± pyrite ± smectite. The intensity of this alteration ranges from complete, to very weak fracture-controlled alteration (Figure 27). The most intense examples of this alteration contain pyrite, while in weakly altered samples the most prevalent iron mineral is siderite.

The northern or upper extension of the Maryanne system is a 150-m-long and 0.5-2-m-wide mineralized fault oriented N40°E/65°SE that cuts quartzite in the MCG and terminates against a later N60°W fault. This site of quartzite-hosted mineralization is known as the Flagstaff

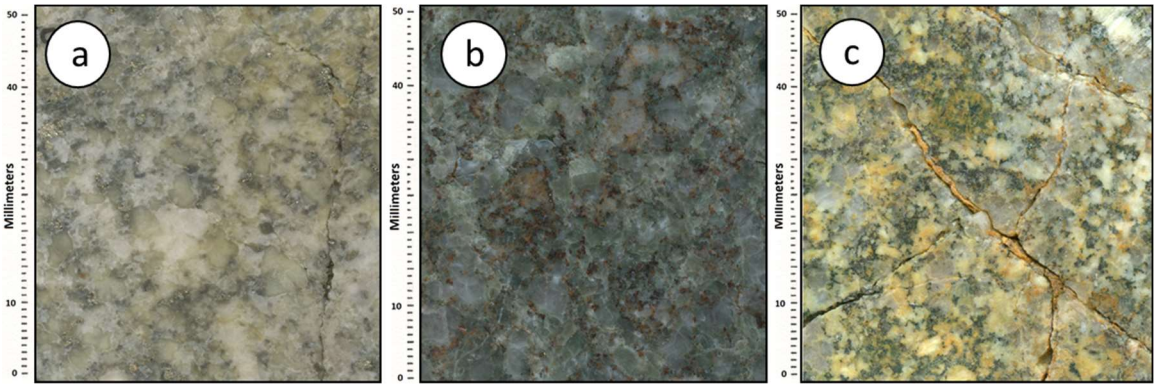

Figure 27. Slabs of sericite-chlorite-carbonate-altered quartz monzonite from the Maryanne area. Pyrite- and sericite- alteration (a) from the main Maryanne structure, chlorite- and calcite-rich alteration (b) from the lower “Brady” tunnel, and weakly sericitized and chloritized quartz monzonite cut by siderite-coated fractures (c) from the uncompleted SE access tunnel in Cherry Creek Canyon.

occurrence. The significance of the Flagstaff occurrence is that it demonstrates continuity of a single mineralized structural set that crosses from quartz monzonite into quartzite, and indicates that mineralization occurred after crystallization of the pluton and resulted in similarly-expressed quartz veining in both. Samples of these quartzite-hosted veins at the Flagstaff attain considerable high grades of Au (6 ppm) and Ag (240 ppm) but have produced little ore compared to the Maryanne (Groves, 1982). The attitude of the Maryanne fault is nearly orthogonal to the N40°E/50°NW bedding of the hosting quartzite; this relationship is a common one in veins cutting the MCG.

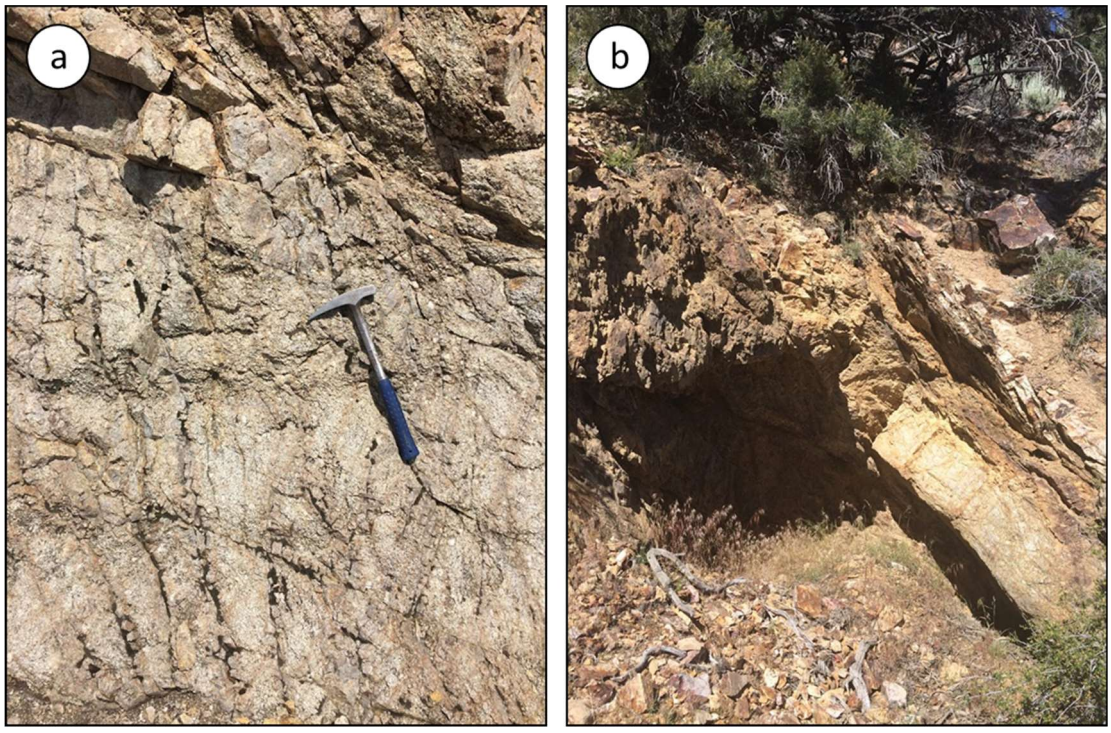

Figure 28. Structural features of the Maryanne-Flagstaff fault zone.
Sheeted N50°E/55°SE fractures on the east side of the mineralized Maryanne igneous zone (a) lie parallel to a through-going mineralized fault (b) that can be traced at least 150 meters uphill to the Flagstaff claims.

Geochemistry

Major element trends of altered igneous rocks of the Maryanne system vary, and are largely dependent on the intensity of alteration and proximity to the main structural intersection described above that is interpreted to control mineralization (Table 7). The best examples of intensely phyllic-altered quartz monzonite from the Maryanne ore zone are characterized by enrichments in Fe_2O_3 and SiO_2 and depletions in Na_2O, CaO, and MnO. In contrast to trends in the other assemblages, samples in which phyllic alteration and veining are strongly developed in the Maryanne system show a distinctively higher enrichment in TiO_2 and depletion in Al_2O_3 relative to fresh quartz monzonite, and enrichments in sulfur exceed two orders of magnitude to reach a maximum of nearly 2.5% (sample 087). As such, the highly sulfidic nature of the intense phyllic Maryanne alteration is distinctive from the phyllic and greisen alteration described along the SFZ.

More weakly altered igneous rock containing assemblages that include sericite-chlorite-carbonate rock at the southern Maryanne workings show generally weak enrichments in CaO and MnO and strong depletions in Na_2O. The most notable feature of this alteration phase is the behavior of Ba, which is 2 to 5 times elevated over levels in the intense phyllic alteration phase upslope. In addition, carbon is strongly elevated and sulfur is variably elevated. These trends reflect the changing alteration mineralogy between the two zones of the Maryanne zone, particularly in the relative intensity of sericitization and leaching of feldspars, the prevalence of carbonate versus sulfide minerals, and the abundance of quartz veins.

Trace-element trends in the Maryanne area are somewhat more complex, at least partially due to the wide variety of mineralization textures, vein abundances, and host rocks over the observed 800-meter strike length of the system from the floor of Cherry Creek Canyon

to the Flagstaff deposit at the ridgetop to its north. The best examples of intense phyllic alteration are characterized by very strong enrichments of two to three orders of magnitude in Ag, Au, and Mo, and one to two orders of magnitude in Sb, As, Bi, Sn, Te, Ni, W, Pb, and Hg. In chlorite-sericite-carbonate-altered quartz monzonite along the lower end of the Maryanne system metallic mineralization is far less significant. In samples without significant amounts of sulfide minerals, no trace elements are elevated by more than one order of magnitude, although small enrichments do exist in Sr, Cs, Zn, Pb, Sb, and Ag (Figure 29).

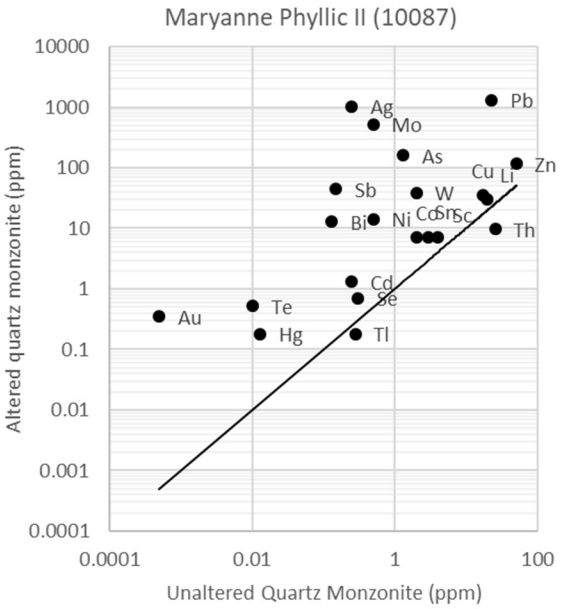

Figure 29. Isocon diagram for phyllic-altered quartz monzonite at the Maryanne deposit

The continuity between igneous- and quartzite-hosted mineralization on the up-dip extension of the Maryanne deposit is the best evidence in the Cherry Creek district of hydrothermal dispersion from the pluton into the surrounding sedimentary rocks. Phyllic-altered igneous rocks from the Maryanne area and mineralized quartzite breccias from the Flagstaff area both exhibit strong enrichments in Ag, Bi, Au, Mo, As, Pb, and Sn, and weaker

Phyllic Quartz Monzonite Maryanne Deposit 10088													
	SiO2	Al2O3	Fe2O3	CaO	MgO	Na2O	K2O	Cr2O3	TiO2	MnO	P2O5	C	S
(%)	81.2	8.68	3.76	0.06	0.51	0.04	2.75	0.01	0.48	0.02	0.06	0.03	2.26
	Au	Ag	Zn	Pb	Cu	As	Ba	Sb	W	Bi	Sn	Mo	Ni
ppm	0.302	835	113	1680	29	208	281	38.2	21	8.65	22	192	5

Table 5. Chemical composition of Maryanne phyllic sample 10088

enrichments in W, Cu, Zn, and Ba. These similar elemental enrichments suggest that mineralization occurring in the feldspar-destructive and neutralizing environment of the Maryanne deposit and mineralization occurring outboard of the pluton in the cooling environment of the Flagstaff produced the same signature. This relationship is especially important for the implications of quartzite-hosted polymetallic veins elsewhere in the district.

Geochronology of Mineralization and Alteration in the Maryanne system

One of the primary goals of this study is to constrain the timing of mineralization, particularly as it relates to the timing of intrusions. Due to the intensity and distinctive character of the mineralization surrounding the Maryanne occurrence, two dates of hydrothermal sericite and one date of molybdenite were obtained. One sample (10088) of sulfide-rich phyllic altered igneous rock from the Maryanne mine contained abundant quartz, sericite, and sulfides including coarse-grained molybdenite (Figure 30). Two aliquots of molybdenite from sample 10088 were dated using $^{187}Re/^{187}Os$ methods at 38.7 ± 0.4 Ma and 38.3 ± 0.2 Ma (Table 6).

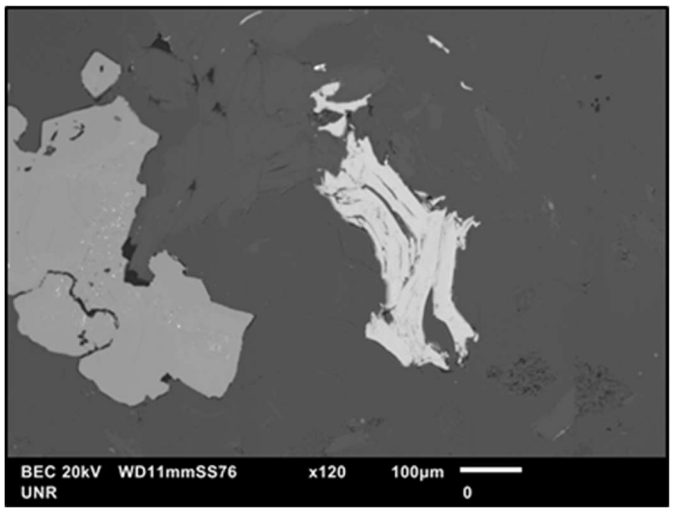

Figure 30. SEM imagine of molybdenite grain in phyllic-altered quartz monzonite, Maryanne deposit

Table 6. Re-Os isotopic and age data for molybdenite at the Maryanne deposit

Sample	Re (ppm)	± 2σ	^{187}Re (ppm)	± 2σ	^{187}Os (ppb)	± 2σ	Model Age	± 2σ
10088a	22.98	0.07	14.44	0.04	9.315	0.075	38.7 Ma	0.4 Ma
10088b	35.80	0.10	22.50	0.07	14.374	0.024	38.3 Ma	0.2 Ma

Two samples of phyllically-altered quartz monzonite from the Maryanne were also selected for $^{40}Ar/^{39}Ar$ dating (Figure 31). The first sample, a duplicate of dump sample 10088, was selected as a representative of the strong phyllic alteration characterizing the productive, Au-Ag ore-bearing mineralization at the core of the Maryanne system. In thin section, the optical characteristics of this sericite indicates the presence of muscovite up to 200 microns. Indeed, the coarseness of much of the sericite allows individual grains to be readily discerned in a 20x hand lens. The total gas age of sericite from sample 10088 is 38.05 ± 0.08 Ma. The second sericite separate (sample 10081), is from weaker phyllic alteration in southern section of the Maryanne area, which is distinguished by the presence of abundant chlorite and carbonate minerals. The optical characteristics of sericite in thin sections of 10081 indicate moderate to complete replacement of plagioclase by fine-grained illite. The total gas age of sericite from sample 10081 is 38.89 ± 0.06 Ma.

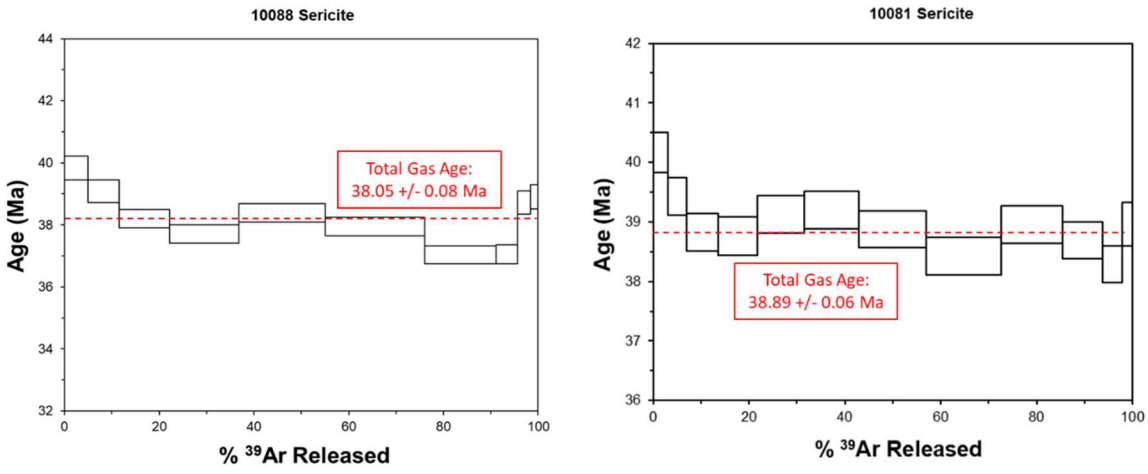

Figure 31. Step-heating $^{40}Ar/^{39}Ar$ analyses for sericite from Maryanne phyllic (left) and Maryanne sericite-chlorite (right) alteration

Sericite-Carbonate-Chlorite Alteration in El Rey Canyon

A heavily weathered and poorly exposed body of quartz monzonite that crops out on the ridge between Maude and El Rey canyons (Figure 4) represents the most northerly exposure of the CCP. The total exposure of this body is less than one square kilometer. The alteration in El Rey Canyon is readily discernible from unaltered quartz monzonite in the gravely grus that covers much of the ridge, but is best exposed in a small drainage on its south side. The dimensions of alteration in this drainage are 25 by 15 m, and essentially only visible in a few prospects and one shaft that follow weak quartz veining along the thin outcrops.

The structural setting of alteration on the south side of El Rey Canyon is unique because of the dominant S65°W/70°NW fracture orientation that controls thin quartz veining around one series of small workings and pits that seem to follow it to the northeast. In the walls of the workings, the two most pronounced fracture sets are N70°E/30°SE and N10°E/45°SE. As the ultimate extent of this alteration is unknown, the main structures exposed in and around the historic workings have been interpreted as the primary controls on alteration.

Alteration and Mineralization

The dominant style of mineralization in southern El Rey Canyon is a strong to moderate sericite-carbonate-chlorite-clay (SCC) assemblage that affects coarse-grained quartz monzonite (Figure 32). Although it occurs in association with thin, mm to cm scale

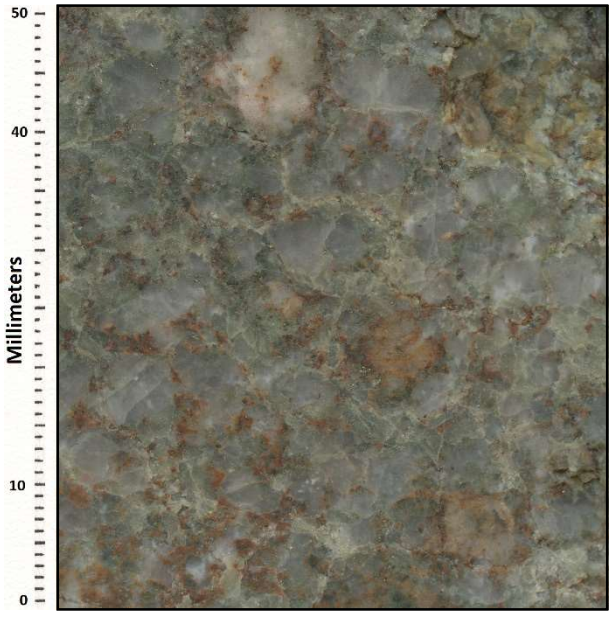

Figure 32. Scan of slabbed sericite-chlorite-carbonate altered quartz monzonite from El Rey Canyon

veinlets of quartz, it is unclear from the poorly exposed and heavily weathered exposures the degree to which quartz veins control the intensity of wall rock alteration. One of the distinctive features of this alteration is the abundance of carbonate as calcite and siderite, which make the rock strongly effervescent and easily recognizable in the field. This alteration resembles the chlorite and calcite-bearing phyllic alteration observed in the lower workings of the Maryanne mine and in sections of the mineralized Salvi Fault Zone.

Geochemistry

Sericite-chlorite-carbonate altered rock in El Rey Canyon shows enrichments of CaO and MnO, and depletions of Na_2O, SrO, and MgO (Table 7). Carbon is also elevated by an order of magnitude in this assemblage, reflecting the presence of carbonate. The concentrations of the trace elements Bi, Pb, Ag, Se, and As are weakly elevated, with none more than 10 times higher than concentration in unaltered samples (Figure 33).

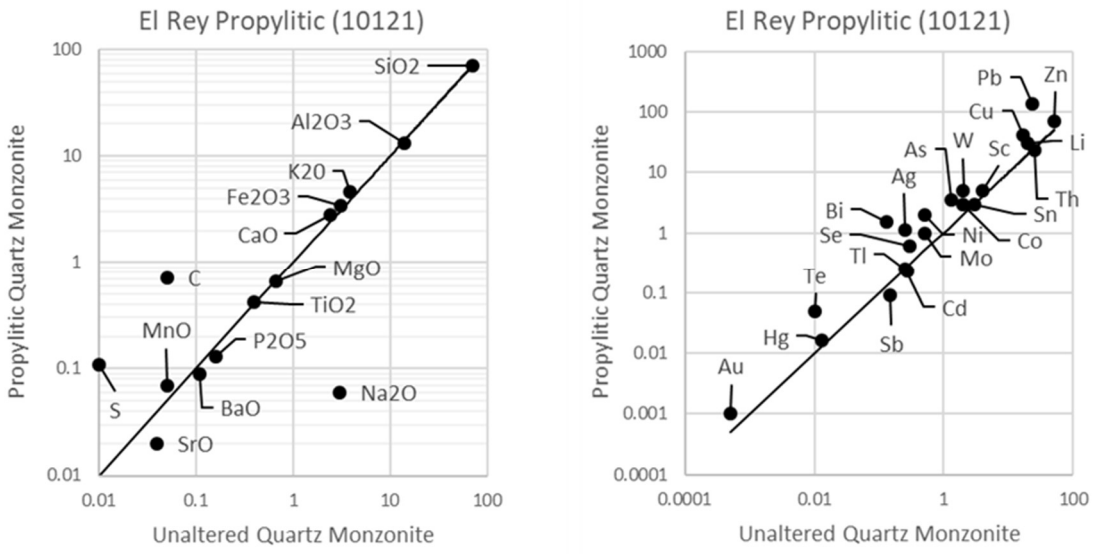

Figure 33. Isocon diagram for propylitically-altered quartz monzonite in El Rey Canyon

Sodic-Calcic Alteration in Quartz Monzonite

Apart from the structurally-controlled mineralization that follows west and northeast-striking faults, very little of the main body of quartz monzonite is hydrothermally altered. Notable exceptions are the localized zones of sodic-calcic alteration in the central and southern areas of the Cherry Creek pluton in the northern Egan Range. The best exposed examples can be found in the hills west of Salvi Ranch where a few small dikes of aplite cut quartz monzonite.

The mineralogy of sodic-calcic altered rock is dominated by albite and amphibole, with the amphibole sites largely segregated into irregular coarse blebs and bands. Most of the larger zones of amphibole have experienced chlorite and carbonate alteration, and a few also contain short and stubby crystals of augite. Albitic zones have irregular, diffuse, anhedral internal grain boundaries and are uniformly buff-colored and milky in appearance. Other accessory minerals include sphene, zircon, and apatite.

Sodic-calcic alteration is best-developed along some of the aplite dikes where it extends at least 1.5 m into the hanging wall and 50 cm into the footwall (Figure 34). Sodic-calcic alteration in the Cherry Creek study area is intense, pervasive, and texturally destructive, and gives the rock a conspicuous blocky appearance and orange-pink color.

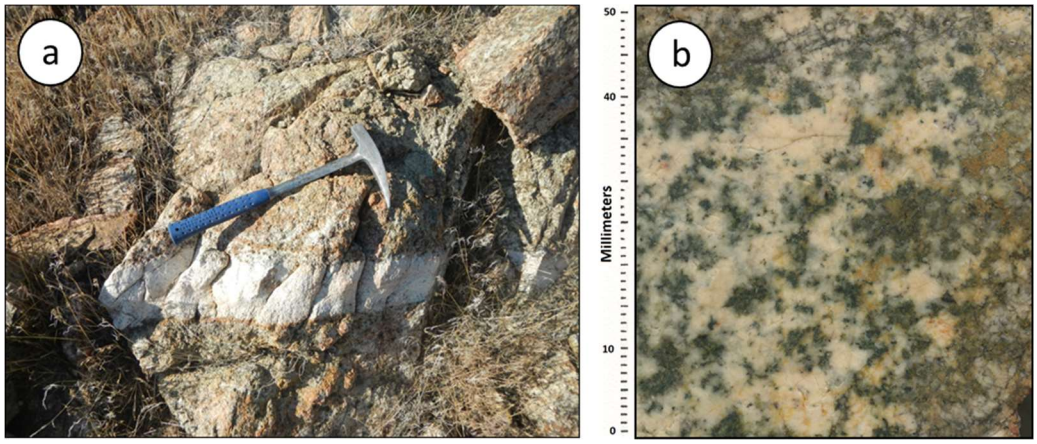

Figure 34. Outcrop (a) and slab (b) photos of sodic-calcic altered quartz monzonite in Cherry Creek. The white stripe in outcrop is an aplite dike, several of which are flanked by sodic-calcic alteration

Geochemistry

Sodic-calcic-altered rock has experienced an enrichment of Na_2O, MgO, TiO_2, and CaO, and depletion of K_2O, Fe_2O_3, and SiO_2 (Figure 35). Strontium and carbon are also added. Au, W, and Sn are the main enriched trace elements, although themselves only weakly anomalous. The sodic-calcic alteration is not understood to be associated with any veining or metallic mineralization. More likely, the association between the sodic-calcic alteration and the aplite dikes suggests a post-magmatic origin although the processes invoked in Cherry Creek are poorly understood.

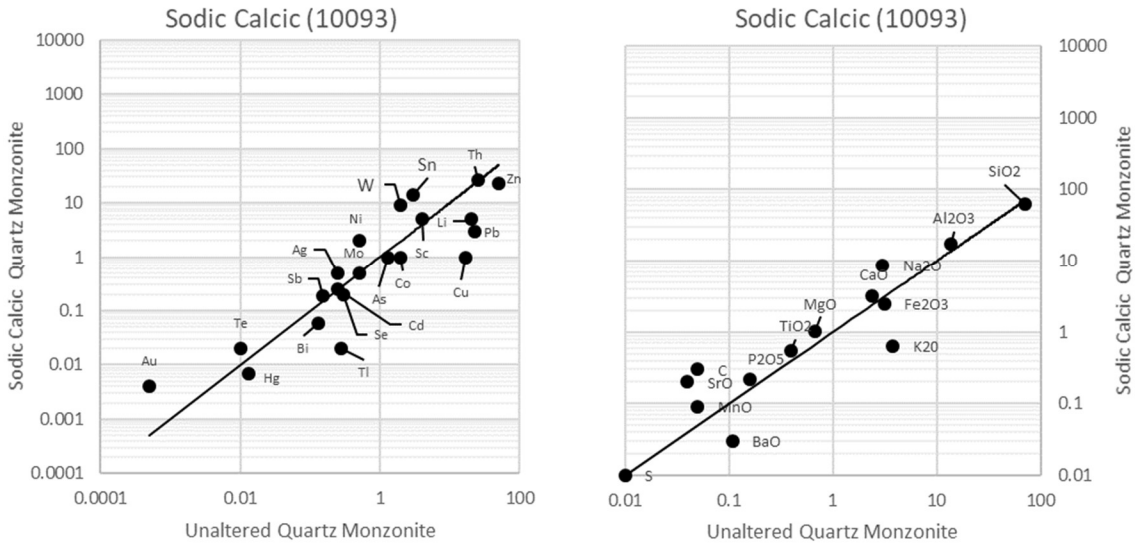

Figure 35. Isocon for sodic-calcic-altered quartz monzonite

QUARTZ MONZONITE

ALTERATION	unaltered	unaltered	greisen	Veined QSP	Brecciated QSP	Veined QSP	Maryanne QSP	Propylitic	Sodic-Calcic
HYDROTHERMAL ZONE			Salvi Fault Zone	Salvi Fault Zone	Bull Hill	Bull Hill	Maryanne	El Rey	PLUTON CORE
SAMPLE NO	10084	10110	10269	10106	10117	10113	10087	10121	10093
NOTE	equigranular	porphyritic	Veins	Foliated	Heavily Fractured	See 0117	disseminated		blocky
Major Elements: Oxides									
SiO2 %	70.7	71.1	68.6	74	77.4	79.2	82.5	70.5	63.6
Al2O3%	13.85	14.3	13.7	12.55	4.83	12.65	7.06	13.4	17.4
Fe2O3%	3.14	3.03	1.84	2.56	11.8	1.55	3.79	3.44	2.49
CaO%	2.39	1.74	2.69	1.65	0.11	0.22	0.07	2.84	3.26
MgO%	0.67	0.78	0.61	0.55	0.27	0.56	0.42	0.66	1.01
Na2O%	3.04	3.55	0.58	0.11	0.08	0.05	0.06	0.06	8.69
K20%	3.81	3.94	7.87	4.87	2.55	4	2.23	4.59	0.63
TiO2%	0.4	0.46	0.36	0.33	0.12	0.42	0.69	0.42	0.55
MnO%	0.05	0.06	0.03	0.11	0.15	0.03	0.01	0.07	0.09
P2O5%	0.16	0.15	0.12	0.11	0.12	0.15	0.03	0.13	0.22
SrO%	0.04	0.05	0.03	0.01	0.01	0.005	0.005	0.02	0.2
BaO%	0.11	0.13	0.18	0.11	0.15	0.04	0.02	0.09	0.03
C%	0.05	0.05	0.1	0.37	0.06	0.03	0.03	0.71	0.3
S%	0.01	<0.01	0.02	0.13	0.05	0.01	2.43	0.11	0.01
Minor Elements: Metals									
Sn ppm	3	5	107	6	48	15	7	3	14
Th ppm	25.6	26.5	24.4	31.4	6.88	24.3	9.68	23.5	26.9
W ppm	2	8	1200	9	19	24	38	5	9
As ppm	1.3	0.5	9.4	19.1	58.1	1.5	160.5	3.6	1
Bi ppm	0.13	0.06	4.94	0.34	126	0.76	12.75	1.55	0.06
Hg ppm	0.013	0.008	0.034	0.115	0.198	0.017	0.178	0.016	0.007
Sb ppm	0.15	0.23	1.75	0.66	2.39	0.16	44.3	0.09	0.19
Se ppm	0.3	0.3	0.2	0.2	3.1	0.1	0.7	0.6	0.2
Te ppm	0.01	0.005	0.07	0.01	5.28	0.005	0.52	0.05	0.02
Tl ppm	0.28	0.16	0.52	0.24	0.08	0.27	0.18	0.23	0.02
Au ppm	0.0005	0.0005	0.0005	0.238	0.006	0.001	0.349	0.001	0.004
Ag ppm	0.25	0.25	0.8	1.4	88.5	1.1	1030	1.1	0.5
Cd ppm	0.25	0.25	0.7	0.7	5.3	0.25	1.3	0.25	0.25
Co ppm	2	3	2	3	32	1	7	3	1
Cu ppm	17	2	58	13	3940	13	35	42	1
Li ppm	20	20	40	20	20	20	30	30	5
Mo ppm	0.5	0.5	2	1	117	1	522	1	0.5
Ni ppm	0.5	0.5	3	2	1	2	14	2	2
Pb ppm	23	16	62	121	10168	35	1310	140	3
Sc ppm	4	4	4	3	1	4	7	5	5
Zn ppm	51	44	58	266	1160	43	116	70	23

Table 7. Geochemical compositions of representative samples of altered rocks in the Cherry Creek pluton

Hydrothermal Deposits in Quartzite and Phyllite

McCoy Creek Polymetallic Veins

The most widely distributed type of deposit in the Cherry Creek study are strongly polymetallic, structurally-controlled quartz veins and breccia bodies found between Egan Canyon on the southern end of the study area and Montgomery Canyon on the northern end. These deposits are hosted in rocks of the Proterozoic McCoy Creek Group, at the deepest stratigraphic and structural level exposed in the Cherry Creek Range. The most important McCoy Creek polymetallic vein deposits (MCPV) are the Star in El Rey Canyon, the Wide West on Wide West Peak, and the Jenny Lind in Egan Canyon (Figure 4). Both the MCPV and the Cherry Creek pluton are located at an inferred paleodepth of 7.5-8.5km, based on the thickness of overlying strata and their positions in the footwall of the Exchequer fault. The Star mine, the largest producer of this class, operated initially from 1872-1883, then sporadically to 1893. It produced $5,000,000 in ore, mostly from Au. Ore at the Star mine averaged about 0.25 troy ounces per ton gold, about 20 troy ounces per ton silver, and 16% combined lead and zinc, and a few high-grade zones exceeded 800 ounces per ton silver (Hill, 1916). The final mine reports indicated proven reserves of 15,200 tons of ore at about 30 ounces per ton silver, and an additional resource amounting to four million ounces of silver (Schrader, 1931).

Character of MCPV Mineralization

Vein and breccia-hosted deposits of the MCPV fall broadly into two end-member styles of mineralization, one type sulfide- and base-metal-poor, and the other sulfide- and base-metal rich. The only instances of sulfide-poor mineralization are recognized from the southern end of the study area, specifically around Wide West Peak, however polymetallic veins are also found

there in abundance. Therefore, these end-members do not fall neatly into the northern and southern camps. The dike-vein relationships described above are only found in the sulfide-rich variety of the MCPV.

Sulfide-poor, gold-bearing veins in the Egan Canyon area are composed of several generations of coarse, anhedral, milky white quartz (Figure 36). At least the earliest phase of quartz-vein material is weakly sulfide-bearing, containing up to a few percent pyrite, mixed limonite and pyrite, arsenopyrite, and galena. The sulfides occur as randomly-oriented, isolated elongate blebs and thin, discontinuous, mm-scale veinlets that follow small fractures. The rock has a weak orange-red color, probably owing to the presence of disseminated iron oxides formed from weathering of primary pyrite. Elongate, amorphous white quartz lobes up to 2 cm in thickness are common, and contain up to 10% sulfide material, mainly pyrite. Open vugs lined with terminated, mm-scale quartz crystals stained red with iron oxides are distributed along the core of late mm- to cm-wide quartz veins that crosscut all other phases.

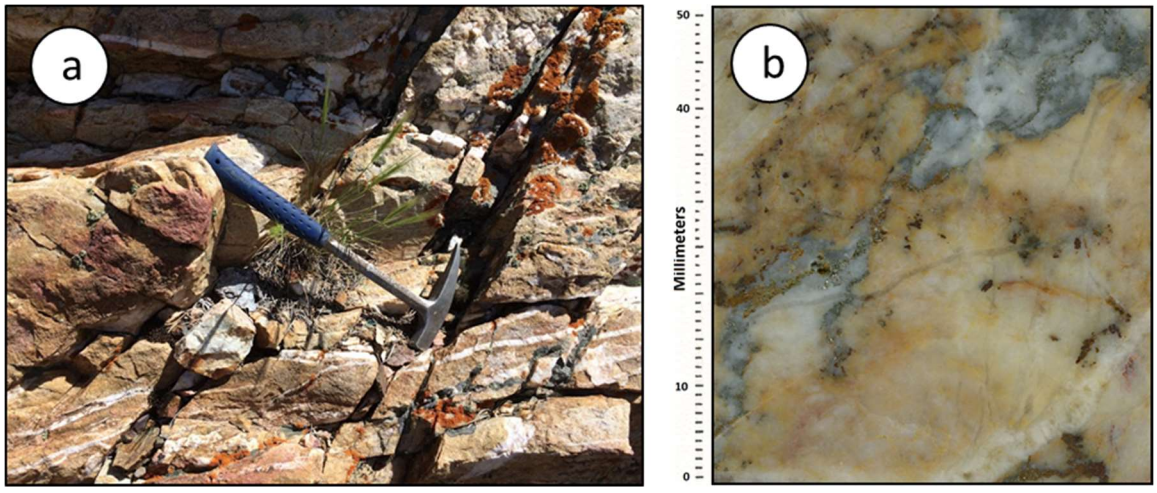

Figure 36. Outcrop (a) and cm-scale (b) examples of sulfide-poor MCPV at the Bull Hill deposit

The sulfide-rich variety of MCPVs is exemplified by mineralization at the Star deposit, and is far more common than the sulfide-poor variety described above. Sulfide-rich MCPVs are characterized by high concentrations of silver and gold that occur in well-defined, but discontinuous, quartz veins. Precious- and base-metal mineralization is coarse grained and varies between quartz-rich (up to 90%) and sulfide rich (up to 80%). Samples of mineralization collected from the dumps of the Star mine contain variable amounts of coarsely banded galena, sphalerite, pyrite, tetrahedrite, and lesser chalcopyrite set within white quartz gangue (Figure 37). Heavily brecciated and oxidized samples contain argentite, stromeyerite, and chalcopyrite, which are partly replaced by supergene proustite, stephanite, pyrargyrite, and polybasite, the supergene minerals occurring as pseudomorphs and veinlets that fill fractures in the principal veins and wall rock (Schrader 1931). Other important ore minerals included argentite and possibly stromeyerite, and although pyrargyrite constituted the majority of the historical

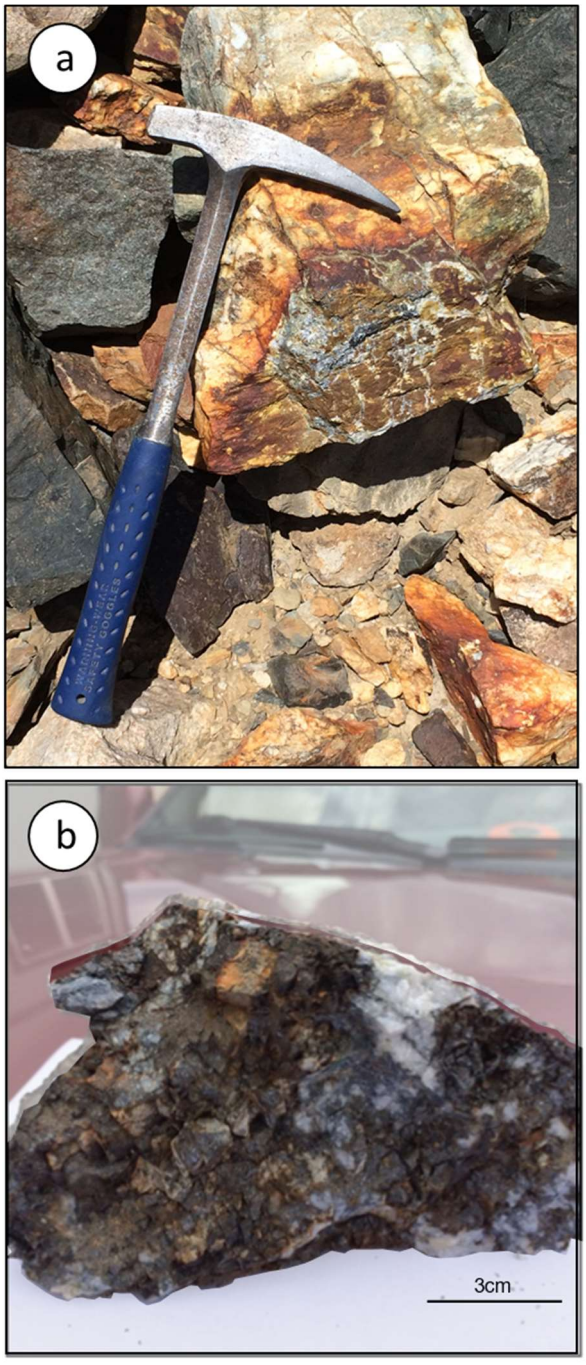

Figure 37. Example of sulfide-rich MCPV from the Star mine containing coarse galena, sphalerite, and pyrite.

silver production wires of native silver were also abundant in siliceous vein material at depth (Schrader, 1931). Au occurs mostly in association with pyrite and sphalerite. Scheelite and arsenopyrite occur in association with calcite gangue. Most outcrops of MCPV have any least some gossan related to weathering of massive sulfide. These are particularly abundant in the southern section of the field area.

This polymetallic and sulfide-rich type easily comprises the majority of MCPV, although few are as well-developed as at the Star mine, and none have the same primary east-west structural control. The historic Star deposit, the most strongly polymetallic orebody on the district, is defined by a pair of mineralized veins, each approximately 0.5 to 2 m in thickness and striking N72°-78°W and dipping between 80°N and 80°S. The veins broaden with depth, and have a known horizontal range of 700 m and vertical range of 300 m over which they are well-developed in the quartzite but finger out in the shales (Hill, 1916). The veins are partially brecciated and cut by small near-vertical faults that strike northeast, parallel to the bedding of country rock, particularly where they intersect mineralized porphyritic dacite dikes. The Grey Eagle deposit, located west of the Star in thin bedded shale and quartzite, is a 400-meter-long vein oriented N60°E/45°NNW, obliquely to the bedding of the sedimentary rocks. This dominant N60°E/45°NNW orientation is similar to that of the Exchequer fault that lies 500 m to the northeast, and yet the deposit has a stronger compositional affinity to the mineralization at the Star rather than that of the Exchequer. Other examples of the sulfide-rich mineralization can be seen at the National mine in Maude Canyon, at the Junebug mine on the north side of El Rey Canyon, and at the Victoria mine in Montgomery Canyon (Figure 4).

Stratigraphic and Structural Controls on Mineralization

The deposits described in this section demonstrate a strong affinity for a thin, 225-meter-thick package of rocks near the top of the MCG. This package, McCoy Creek Unit F, is composed of medium-bedded, coarse-grained to conglomeratic, white and grey quartzites correlative with the Shingle Creek Conglomeratic Quartzite of the Snake Range (Woodward, 1967). Unit F is flanked above and below by 250 m thick packages of phyllite that are very weakly mineralized. To a lesser extent, the deepest exposed quartzites in Unit C of the MCG are also important hosts, especially in the southern group of MCPV around Bull Hill.

This phenomenon of stratigraphic control by the quartzite of MCG Unit F is clear near the Gilligan vein, which follows a large N70°E/70°N fault-controlled breccia zone that is mineralized in the quartzite but barren in the adjacent phyllites. Similar relationships exist at the Wide West and Bull Hill deposits to the north of the Gilligan. Both deposits are localized to small, steeply south-southeast-dipping fractures in the quartzite that vanish or are unmineralized in the shales above and below. Between the north side of Bull Hill and Cherry Creek Canyon, MCG Unit F is truncated by the Cherry Creek pluton (CCP) which intrudes up-section to the base of the Cambrian Prospect Mountain Quartzite over an interval of 3 km. MCPVs are widespread in the rocks to the north of Cherry Creek Canyon, starting on the margin of the pluton at the Flagstaff Mine and extending to the north another six km to the north to the mouth of Silver Canyon. The MCPV on the north side of Cherry Creek Canyon also occur within Unit F, although their controlling orientation is consistently N40-55°E/50-70°SE and they have a stronger association with dacite dikes than the deposits to the south. The Star deposit in El Rey Canyon is an exception, occurring as a pair of 0.5 to 2-m-thick, vein-filled

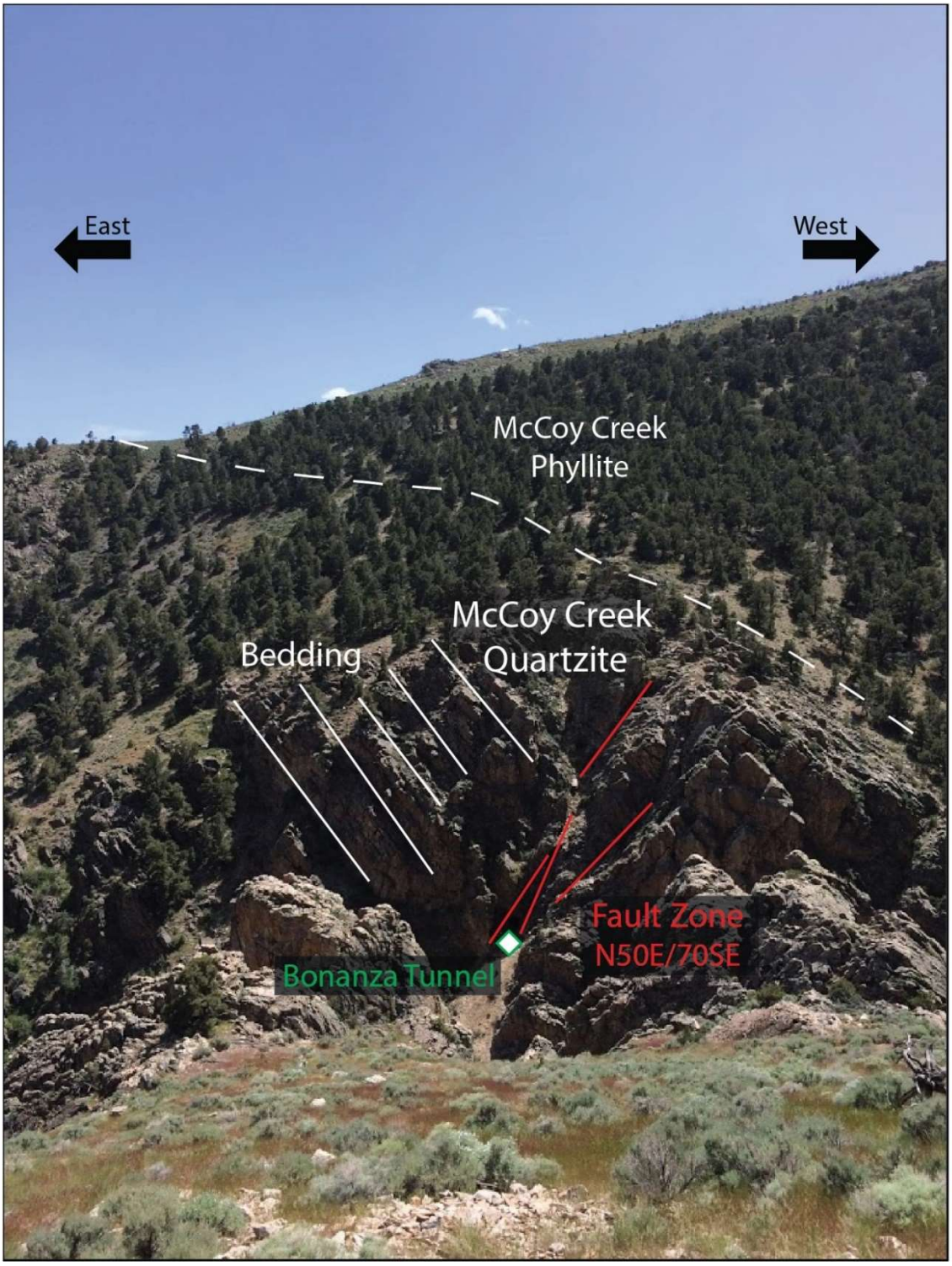

Figure 38. Annotated photograph of structural relationships at the Bonanza Mine

N80-90°E/85°S-85°N fractures in MCG Unit F and being cut by secondary N45°E/85°SE fractures (Schrader, 1931).

Association with Dikes

Polymetallic veins in the MCG rocks exposed on the east side of the Cherry Creek Range are associated with porphyritic dacite and some rhyolite dikes. Most of these dikes are altered to sericite-chlorite-pyrite, and a few are highly mineralized along their margins with polymetallic quartz veins and breccia-fill (Figure 40). Dikes and veins are similarly oriented, generally between N40°E/50°SE and N55°E/70°SE, and commonly occur together. The best examples of this can be seen at the National mine in Maude Canyon and at the Junebug mine and prospects on the north and south sides of El Rey Canyon. Intensely mineralized dikes are present at many localities and are often cut by steeply southeast-dipping cross faults, including at the Star and Victoria occurrences.

Proximity to the Cherry Creek Pluton

The MCPV represent the best examples of intrusion-proximal veins on the Cherry Creek district. Located in the lower reaches of the stratigraphic section, the MCPV have an affinity for thick beds of quartzite and are uncommon in the overlying and underlying shales and phyllites. Importantly, the MCPVs lie in rocks that are structurally deeper than the roof of the CCP, which in places is at the top of McCoy Creek Unit G. In other words, the fact that the CCP truncates all visible units of the MCG near Cherry Creek Canyon means that the deposits lying within rocks of the MCG to the north and south of the CCP likely formed lateral to the pluton. Whether the nearest contact of the Cherry Creek pluton is along strike of the MCG rocks or down dip is irrelevant, as the pre-tilt orientation of the range would have rendered the MCG roughly flat and at a consistent depth. For this reason, the MCPV can reasonably be interpreted as having

formed outboard of the pluton but at the same structural level. Overall, it seems that the development of MCPVs is controlled more by their stratigraphic and lithologic position, in the quartzite of MCG Unit F outboard of the pluton, than any specific structural set. Furthermore, it is interesting to note that deposits in which veins are associated with dikes are exclusively of the sulfide-rich MCPV variety. This crosscutting relationship indicates that episodes of veining post-date the emplacement of the dikes.

Figure 39. Annotated photograph of field relationships at the Star Mine's western shaft

Geochronology

The mineralized dacite at the Victoria mine is affected by the MCPV elemental signature, and has experienced hydrothermal alteration of its primary igneous mineralogy to a mixture of sericite, chlorite, and pyrite. Petrography and SWIR spectroscopy of sample 10264 indicates that phyllic alteration of feldspar sites has resulting in the formation of illite and muscovite, as well as minor montmorillonite and chlorite (See Appendix B). A separate of sericite from sample 10264 yielded a total gas $^{40}Ar/^{39}Ar$ age of 38.87 ± 0.10 Ma, including 5 steps with overlapping ages between 38.16 and 37.81 Ma, totaling 50.1% of the total ^{39}Ar released (Figure 41).

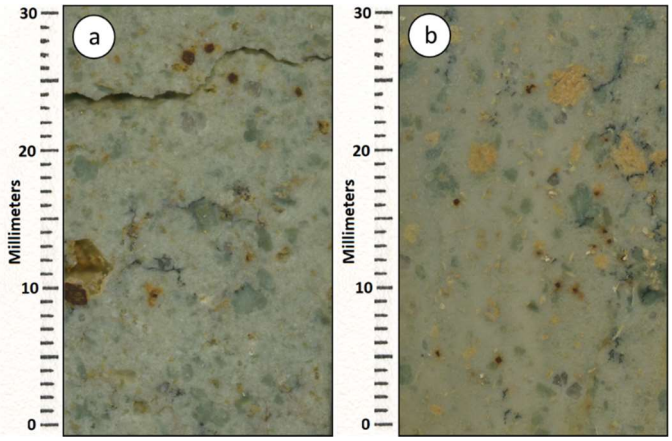

Figure 40. Scans of slabbed sericite-quartz-pyrite-chlorite altered dacites affected by MCPV fluids

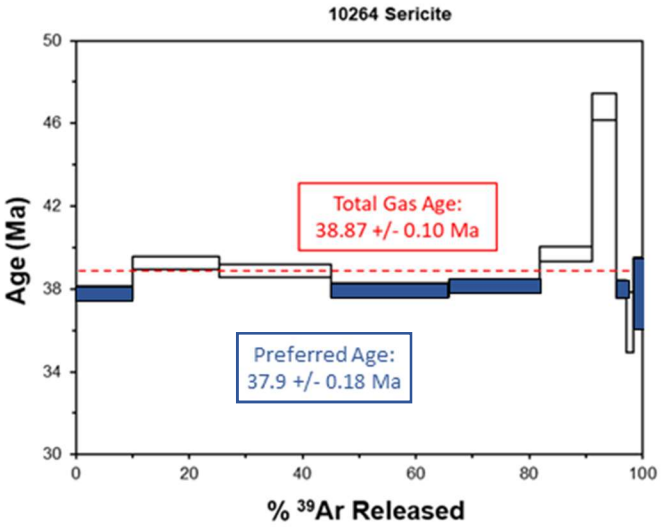

Figure 41. ^{39}Ar step-heating diagram for sericite from phyllic-altered dacite dike at Victoria Mine

Geochemistry

Spearman rank correlation matrices for sulfide-bearing quartz veins and quartz breccias in the MCPV indicate universal strong to moderate (ρ=0.5-0.8) positive associations among the precious and base metals Au, Ag, Cu, Zn, and Pb. Very strong (ρ>0.75) positive elemental associations exist between these metals and Sb, while they are also moderately associated with As. Mn is associated with Ag and the base metals but not with Au (ρ=0.08). Sn also bears an association with this signature; it is strongly correlated with Pb (ρ =0.72), moderately correlated with Ag (ρ=0.40) and Zn (ρ=0.47), and weakly correlated with Au (ρ=0.13) and Cu (ρ=0.17).

Bi and Mo are strongly associated with each other (ρ=0.69) and weakly to moderately associated with Ba, although they are moderately negatively correlated with Au, Ag, and the base metals. W has weak negative correlations with Sn (ρ=-0.30) and Bi (ρ=-0.29) but weak positive correlations with Ba (ρ=0.36) and Tl (ρ=0.36). Besides correlating with W, Ba and Tl have weak to moderate negative associations with the base metals and moderate to strong negative correlations with Au and Ag. The ratio of Ag:Au is 180:1 based on median and 130:1 based on mean values, indicating that the highest grade samples are skewed towards lower

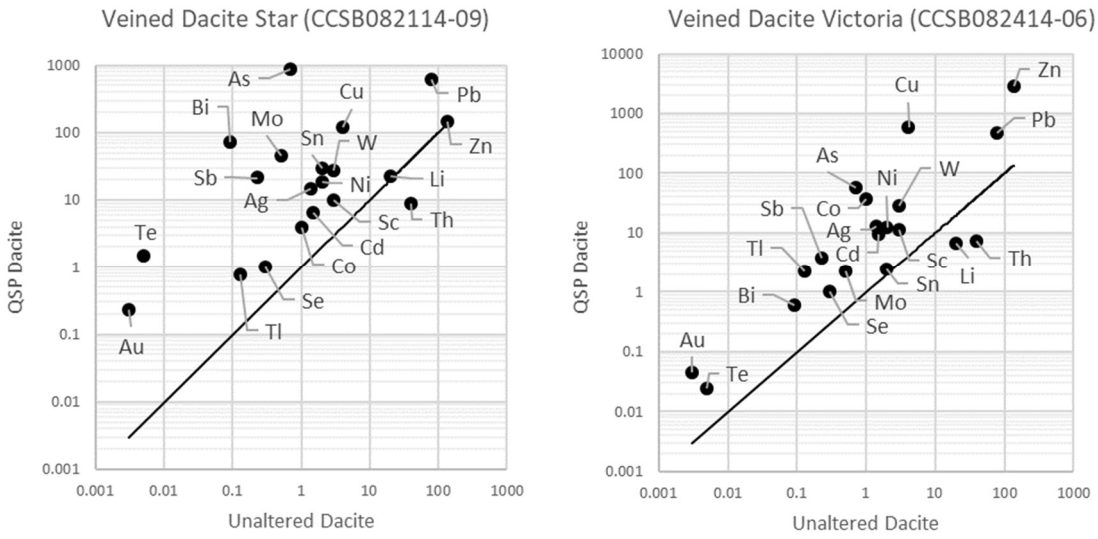

Figure 42. Trace element isocon diagrams for dike-hosted MCPV mineralization

Ag:Au values. In the best examples of mineralized dikes associated with the MCPV, the geochemistry is characterized by major additions of As, Bi, Sb, Ag, Au, W, Cu, and Pb, and variable additions of Sn, Zn, and Te (Figure 42). The MCPV have high base metal contents in the 100 to 10,000 ppm-range and typically contain Pb>Zn>Cu, reflecting the relative abundances of the major sulfides (Table 8). They contain concentrations of Bi, Sn, Mo, Au, and W commonly in the 5-10 ppm range. Overall, the MCPV are best distinguished from other mineralized features by the concentration of S, Bi, Sn, and Au, and their strong association between Au, Ag, Sb, As, and the base metals.

Table 8. Summary statistics for McCoy Creek Polymetallic Veins in ppm (N=19)

Contituent	Mean	Median	Minimum	Maximum	IQR
Au	7.70	1.03	0.01	61.40	5.88
Ag	1190.67	246.00	0.98	8710.00	1900.77
Sb	374.00	60.80	0.53	2710.00	422.82
As	239.05	139.00	2.10	868.00	247.80
Cu	1569.91	302.00	7.60	11250.00	2074.30
Pb	19279.84	3670.00	8.00	200001.00	15653.00
Zn	16456.79	798.00	23.00	139500.00	11575.00
W	11.21	4.70	0.40	45.20	12.60
Te	1.52	0.16	0.05	16.60	0.59
Tl	0.17	0.12	0.03	0.77	0.18
Mn	176.42	93.00	27.00	1240.00	173.00
Ba	106.32	100.00	10.00	260.00	150.00
Sn	12.04	6.60	0.60	53.30	8.70
Bi	39.76	1.35	0.19	474.00	13.46
Mo	4.71	2.27	0.13	25.70	4.76
S (%)	1.66	0.13	0.01	9.79	2.30

	Au	Ag	Cu	Pb	Zn	W	Sn	Bi	Mo	As	Sb	Ba	Mn	Tl
Au	1													
Ag	0.78	1												
Cu	0.68	0.76	1											
Pb	0.58	0.78	0.57	1										
Zn	0.59	0.72	0.74	0.76	1									
W	-0.19	-0.02	0.28	-0.23	0.34	1								
Sn	0.13	0.40	0.17	0.72	0.47	-0.30	1							
Bi	-0.36	-0.35	-0.27	-0.35	-0.45	-0.29	0.19	1						
Mo	-0.32	-0.34	-0.13	-0.45	-0.41	-0.07	-0.14	0.69	1					
As	0.49	0.35	0.41	0.45	0.58	0.05	0.49	0.04	0.21	1				
Sb	0.82	0.92	0.82	0.76	0.81	0.16	0.28	-0.55	-0.39	0.45	1			
Ba	-0.59	-0.60	-0.22	-0.44	-0.30	0.36	-0.14	0.34	0.49	0.01	-0.47	1		
Mn	0.08	0.29	0.39	0.31	0.53	0.60	0.09	-0.62	-0.24	0.28	0.43	0.18	1	
Tl	-0.65	-0.59	-0.43	-0.37	-0.30	0.36	-0.10	0.00	0.03	-0.27	-0.41	0.74	0.18	1

Figure 43. Elemental Spearman Rank Correlation Matrix for McCoy Creek Veins (N=19)

Exchequer Polymetallic Veins

The east-northeast-striking Exchequer fault zone (EFZ) is the most heavily mineralized fault in the Cherry Creek district, particularly along its trace through the Prospect Mountain Quartzite in the northeast sector of the study area. The Exchequer is a major fault that shows over 600 m of apparent right-lateral offset through most of the study area. Although the Exchequer is not mineralized along its entire extent, the presence of strong mineralization commonly in zones of increased brecciation and fracturing in Prospect Mountain Quartzite in the hanging wall along 1.5 km of strike length between the Exchequer and TiCup mines indicates it served as a major conduit during hydrothermal activity. The entire mineralized zones are shattered, being filled with tightly spaced feather cleavage and intense silica-cemented quartzite crackle-breccia bodies that follow the northeast direction of the fault zone (Figure 44). Many of these zones, and especially those where hydrothermal alteration has been most intense, also host altered dikes; as seen at the Exchequer, Geneva, and Fillmore mines.

Alongside the MCPV, polymetallic veins hosted in Prospect Mountain Quartzite along the EFZ are among the most thoroughly exploited type of deposit in the Cherry Creek district (Figure 45). The best examples of these Exchequer polymetallic veins (EPV) are in Exchequer Canyon. Prior to 1931, these veins produced more than $3,000,000 of Ag from ore containing about 22 ounces per ton silver and 0.05 ounces per ton gold. The most active years were between 1870 and 1885. Proved and possible reserves in 1931 amounted to 132,000 tons at 25 to 35 ounces per ton Ag (Schrader 1931). Unlike the previously discussed examples of veins in the deeper MCG strata that occur in association with small and discontinuous faults, the EPV are localized mainly along the range-scale Exchequer fault. Within this interval past geologists have identified at least four divergent fault planes, two of which are major hosts of mineralization in

the Exchequer and New-Century deposits; these are the Exchequer (NE) and Blue (SE) veins (Adair, 1961; Groves, 1982). Mineralization in the Exchequer Canyon section of the Exchequer fault is well constrained by the excellent reports of the early 1900s on the district as well as site-specific reports from the Exchequer and New Century mines from exploration efforts in the early 1980s. Very little rock is exposed or available on the surface that would have been considered ore, and no efforts were made in the study to access the deep underground beyond the 300-meter-long 1st level. For this reason, the description of the Exchequer ore itself is largely based on previous reporting.

Structural and Lithologic Controls

The Exchequer-New Century section around Exchequer Canyon represents the largest and most consistently mineralized length of the Exchequer fault. This section inhabits an easterly deflection of the EFZ, which is oriented along a north-dipping, N70°E plane marked by fractured and veined Prospect Mountain Quartzite in either wall and extending for at least 750 m. Over this interval the fault strand is occupied by a 7 to 10-meter-thick and variably altered porphyritic and partially devitrified dacite dike. The dike, which inhabits the N70°E, 85°N Exchequer fault zone, itself is also responsible for localizing polymetallic hydrothermal mineralization (Figure 46). Both sides of the dike are mineralized in this interval (Groves, 1982). The geometry of the fault zone near the Exchequer mine is significant because it incorporates an eastern deflection of the normally NE-striking fault zone. Siliceous mineralization takes the form of veinlets and breccia matrix that incorporate fine-grained pyrite and a weakly disseminated, fine-grained polymetallic sulfide haze, extending in places to encompass a steeply inclined 3-meter-thick tabular body of mineralized igneous rock and igneous-siliciclastic breccias. Both the felsic dike and the vein system follow the 070°/85°N attitude of the Exchequer fault zone for at

least 1300 m along strike, in which interval the walls of the dike are followed by quartz veins and gouge (Groves, 1982).

The bulk of Au-Ag mineralization in the Exchequer area was likely related to quartz infilling of breccia and fracture zones rather than disseminated or replacement style. The heavily fractured quartzite and silicified crackle breccia that crop out at the surface are heavily stained with limonite, and extend at least 1.25 km to the northwest and 1 kilometer to the northeast, where it was heavily prospected with blast holes and small trenches. The limited amount of mineralized material on the surface is very siliceous, and comprised of sucrosic and bull quartz, most of which has been shattered by post-mineral deformation. The sulfide content of the Exchequer veins is much lower than the MCPV and typically less than 5%. Most sulfide

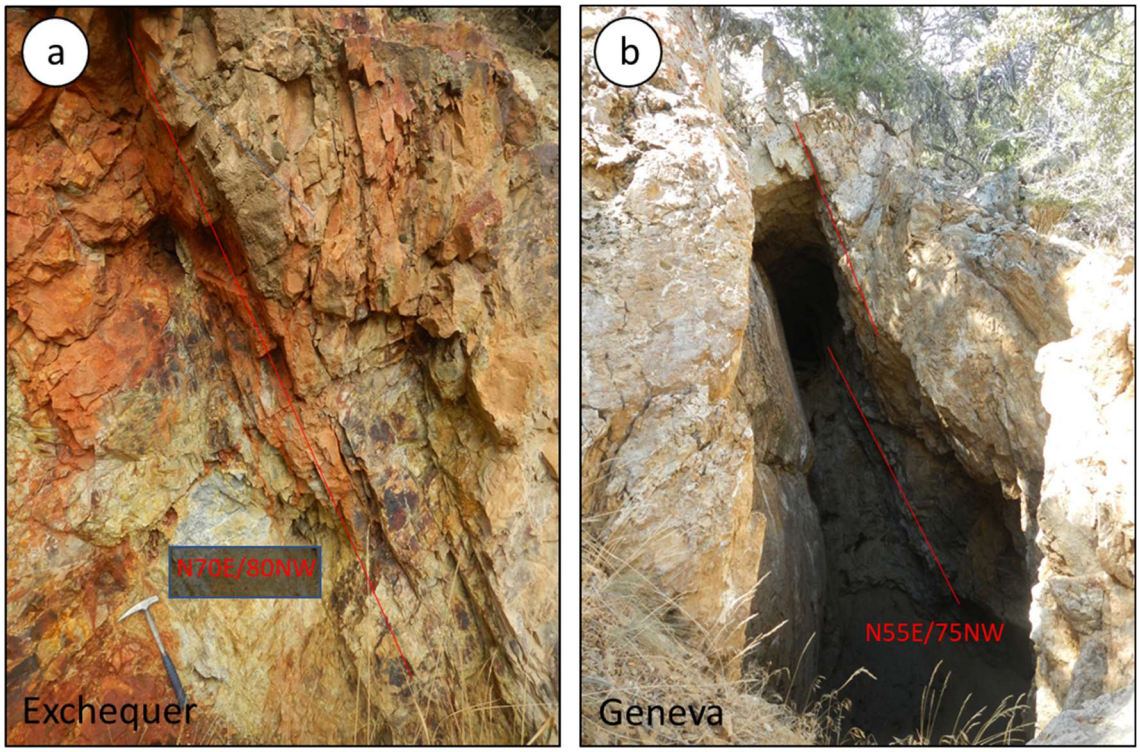

Figure 44. Field photographs of the Exchequer fault in mine workings at the Exchequer (a) and Geneva (b) mines Both mines are located on the main stand of the Exchequer fault at their respective positions along it: The Exchequer mine in Exchequer Canyon is 1500 meters northeast from the Geneva mine in upper El Rey Canyon. The two mines both stope the NW-dipping fault zone where it is inhabited by fractured dikes. A third iteration of this relationship is present at the Fillmore mine, which is discussed in the subsequent section on carbonate

mineralization is fine grained (<1 mm) and finely disseminated, in many places having a distinctively hazy appearance not unlike some quartz from the Maryanne deposit. Of total sulfides, 80-90% or more is cubic pyrite, with variable but minor amounts of galena, chalcopyrite, sphalerite, and arsenopyrite. One prospect from the eastern extension of this zone contains molybdenite. Reports indicate that the historical ore also included substantial amounts of cerargyrite, stromeyerite argentite, and tetrahedrite (Schrader, 1931), although none of these were identified by the author. Examinations of the Exchequer dike in outcrop to the west of the Exchequer mine failed to indicate any pervasive or continuous alteration in dacite beyond the immediate vicinity of the workings. Several samples of dike float that were collected from the mine dumps were weakly mineralized, and a few contained weakly disseminated pyrite. The best examples of mineralized dacite were collected from the Geneva.

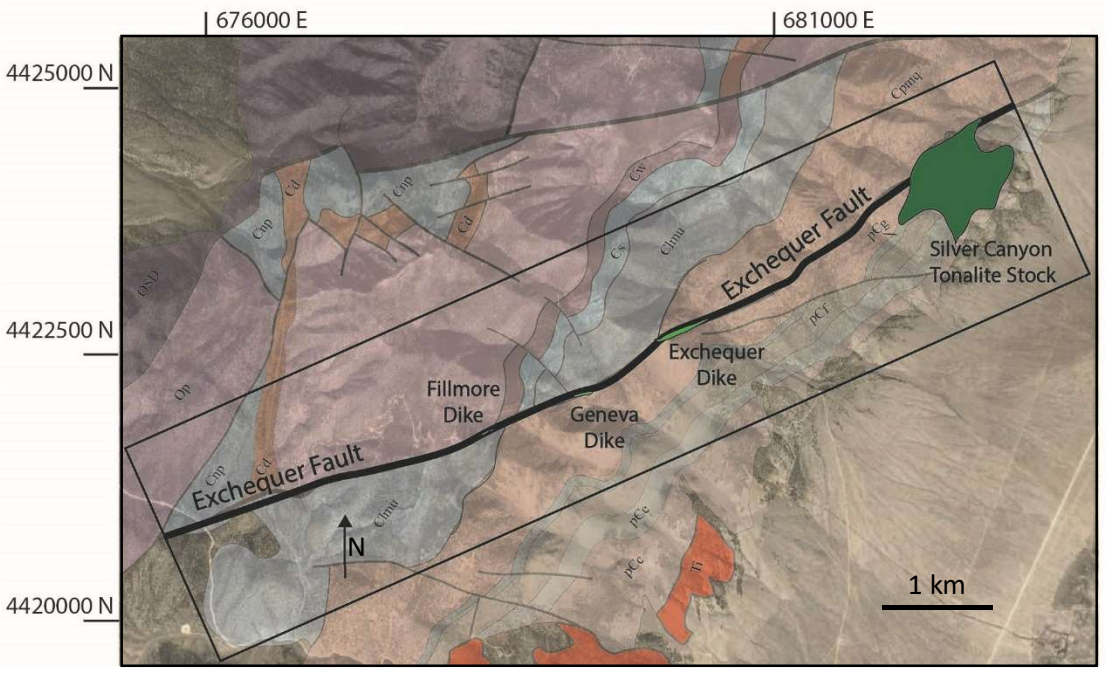

Figure 45. Map inset from Figure 5 showing dikes and plutons (in green) along the Exchequer fault

The Geneva

The Geneva mine lies in the intervening ground along the Exchequer fault between the Exchequer mine 1.25 km to its SE and the TiCup mine 500 m to its NW. The Geneva is hosted within a heavily fractured and veined dacite porphyry dike, which is oriented parallel to the trace of the Exchequer fault and dips steeply to the north. The Geneva was among the first deposits worked in the district, and reports indicate that a small amount of high-grade Au and Ag were produced from it in the mid to late 19th century (Heard, 1881). The adits were not thoroughly explored by the author in 2016, although the abundant waste rock is coated with considerable amounts of malachite and limonite. The composition of one sample of veined dacite from the Geneva property versus unaltered dacite is displayed in the isocon above. The trace-element geochemistry of this sample is defined by extreme relative enrichments in Ag and Sb, very strong enrichments in Au, Pb, and Cu, and strong enrichments in As, Te, Zn, Cd, and Ni.

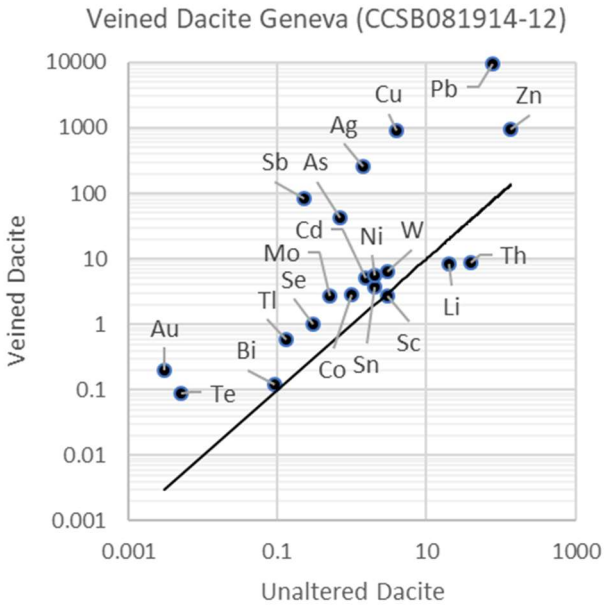

Figure 46. Isocon diagram showing enrichment of trace elements in mineralized Geneva dacite dike (CCS8081914-12)

Geochemistry

Mineralization in the veins and siliceous breccia of the Exchequer polymetallic veins (EPV) on average contains substantially less sulfide minerals than the MCPV. Very strong ($\rho>0.8$) correlations exist among Au, Ag, Cu, Pb, and Sb, while the same elements correlate moderately with Zn and moderately to weakly with As, Bi, and Sn and are weakly negatively correlated with

Ba, Mn, and Tl. W has a weak positive correlation with Zn (ρ=0.16) and a weak negative correlation with Au (ρ=-0.30) but does not correlate with Ag, Cu, or Pb. Mn and Tl have moderate positive correlations with each other (ρ=0.54), as well as with Sn (ρ=0.40-48). Tl correlates positively with W (ρ=0.6) and weakly with Ba (ρ =0.25), As (ρ=0.24), and Bi (ρ=0.19), while Mn correlates positively with Bi (ρ=0.43), and weakly with Ba and Mo (ρ=0.13). Ba is weakly associated with As (ρ=0.20). The Exchequer veins include substantial ranges of mineralization for Pb, Zn, Ag, and Cu, although they attain lower maximum grades and are more weakly mineralized than the MCPV. In addition, the strong Bi-Sn-Mo signature of the MCPV is considerably subdued and generally totals less than 5 ppm in the EPV (Table 9).

Table 9. Summary statistics for Exchequer polymetallic veins in ppm (N=24)

Contituent	Mean	Median	Minimum	Maximum	IQR
Au	2.40	0.21	0.01	22.90	1.36
Ag	437.97	33.08	0.41	2580.00	304.95
Sb	21.84	4.49	0.37	100.50	10.49
As	98.82	69.85	0.80	364.00	126.80
Cu	104.53	75.05	1.90	475.00	162.65
Pb	3309.04	492.00	3.00	25200.00	2027.95
Zn	376.91	108.00	5.00	2850.00	372.00
W	5.45	3.55	0.40	18.20	6.30
Te	0.09	0.08	0.07	0.12	0.03
Tl	0.24	0.19	0.07	0.51	0.20
Mn	100.42	57.00	17.00	905.00	63.25
Ba	235.42	165.00	60.00	810.00	245.00
Sn	0.83	0.40	0.20	6.40	0.20
Bi	1.45	0.33	0.02	6.76	2.71
Mo	3.69	3.22	0.40	9.40	3.17
S (%)	0.51	0.05	0.01	4.50	0.64

	Au	Ag	Cu	Pb	Zn	W	Sn	Bi	Mo	As	Sb	Ba	Mn	Tl
Au	1													
Ag	0.96	1												
Cu	0.80	0.81	1											
Pb	0.93	0.96	0.80	1										
Zn	0.55	0.61	0.63	0.70	1									
W	-0.30	-0.01	0.00	0.00	0.16	1								
Sn	0.12	0.18	0.38	0.25	0.38	0.32	1							
Bi	0.24	0.19	0.37	0.33	0.45	0.04	0.64	1						
Mo	0.10	0.04	0.22	0.04	-0.04	-0.09	0.22	0.38	1					
As	0.35	0.45	0.48	0.52	0.82	0.38	0.55	0.57	0.09	1				
Sb	0.91	0.93	0.83	0.94	0.63	0.08	0.35	0.32	0.09	0.58	1			
Ba	-0.15	-0.24	-0.31	-0.29	0.11	0.12	-0.01	0.09	-0.06	0.20	-0.27	1		
Mn	-0.27	-0.24	0.11	-0.20	-0.04	0.16	0.48	0.43	0.13	0.03	-0.06	0.13	1	
Tl	-0.44	-0.24	-0.07	-0.18	0.01	0.60	0.40	0.19	-0.03	0.24	-0.12	0.25	0.54	1

Figure 47. Elemental Spearman rank correlation matrix for Exchequer polymetallic veins (N=24)

Hydrothermal Deposits in Carbonate and Shale

Polymetallic Carbonate and Carbonate Breccia Replacement Deposits

The prolific silver deposits responsible for the early success of the Cherry Creek district occur in a series of carbonate-hosted orebodies at the head of El Rey Canyon (Figure 4). These are polymetallic deposits that inhabit silicified breccia zones associated with several middle and Upper Cambrian limestone-shale contacts. The best developed of these horizons is found at the contact between Swasey Limestone and Wheeler Shale, about 1.75 km to the west-southwest of the Exchequer deposit and developed by the TiCup, Chance, and Old Timer mines. The TiCup mine was established in 1868 and was mined mainly in the 1870s and from 1907 to1912, producing $3,000,000 in silver from ore that averaged 14 to 27 ounces per ton with high-grade up to 3,500 ounces per ton (Schrader, 1931). The main production in the TiCup mine was from a 350-m-long shaft inclined between- 10 and 50 degrees to the west (Hill, 1916). Well after the peak of silver production, tungsten was discovered at various locations around the TiCup patents in 1918, most notably at what would become the Old Timer and Chance tungsten mines (Adair, 1983). Other occurrences including the Gypsy and Old Timer were worked starting in the 1940s until 1956 when the government contract expired, and although prospecting continued, no tungsten ore has been produced since. Total production of tungsten is estimated at about $1,000,000 (Adair, 1983). The 1941 mill in Cherry Creek Canyon is the best-preserved relict of the tungsten era. Since tungsten production ceased, several exploration programs have investigated other Ag prospects in the area. In 1964, Atlas Minerals drilled a series of 12 holes into the northern extension of the TiCup horizon, and during the 1980s a few trenches and one small pit were dug on Ag and W prospects.

Mineralized Carbonate Breccias at the TiCup and Doctor's Cut

The TiCup horizon manifests as a tabular body of crackle and matrix-supported mosaic breccias up to 4 m in thickness, incorporating 10-75% of angular, heterolithic clasts of limestone and minor shale in quartz matrix. Limestone in and around the breccia body is variably silicified, in places so completely as to form jasperoid. Clasts of dirty limestone and shale are often abundantly pyritic and silicified, with finely disseminated sulfides <0.2 mm in size composing up to 15% of rock volume. Brecciated and altered limestone typically contains very small amounts of disseminated sulfides, but the breccia matrix often contains up to a few percent of isolated mm- to cm-scale fragments of stromeyerite and acanthite. Some of the most heavily silicified examples of jasperoid breccia contain highly embayed green clasts of massive, fine-grained chlorite, which themselves contain up to 20% gritty pockets of limonite that are lined with relict pyrite and arsenopyrite. The most intensely mineralized zones contain small amounts of pyroxene and amphibole (including anthophyllite) in association with limonite and weathered

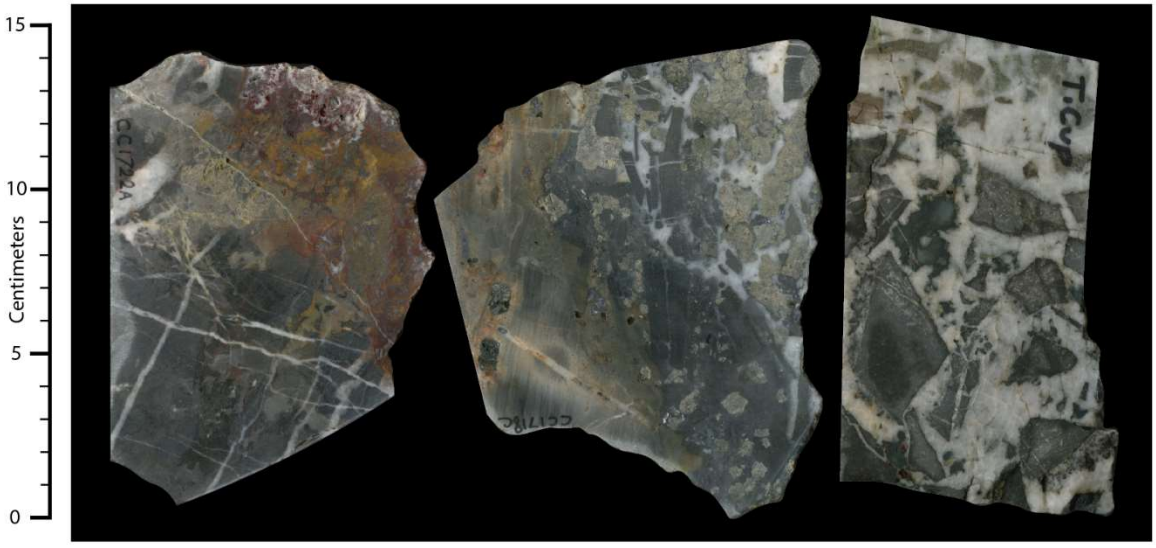

Figure 48. Mineralized breccias from carbonate breccia replacement deposits along the TiCup horizon. Quartz-veined and limonite-bearing jasperoid (left) is widespread along the TiCup horizon. Less common and localized to fault intersections with the TiCup are massive sulfide-bearing carbonate replacement breccias (center) and skarn-bearing carbonate replacement breccias (right).

pyrite and chalcopyrite (Figure 49). Where observed, these minerals were highly embayed, and overgrown by abundant coarse-grained chlorite. This mineralization occurs as irregular, sharp breccia clasts in quartz matrix or small, mm-scale blebs within larger clasts of silicified limestone. Other examples of mineralization incorporate sub-rounded, cm-scale clasts of coarse-grained massive sulfides including sphalerite and galena in massive sulfide, also suspended in a siliceous matrix (Figure 48). The heavily fractured footwall of the TiCup horizon, which is comprised exclusively of Swasey Limestone, hosts lensoidal swarms of quartz and calcite veinlets up to 2 m in thickness. In some cases, > 150 m swarms of veins of quartz clearly follow bedding-parallel weaknesses at the cm-scale of single beds and correspond to the intensity of jasperoid in the surrounding rock. As such, the veins and breccias that can be observed along the TiCup horizon are likely dissolution features that exploit the lithologic contact and pre-existing zones of brecciation. No igneous rocks or clasts of igneous rock have been noted within the mineralized breccia horizon itself.

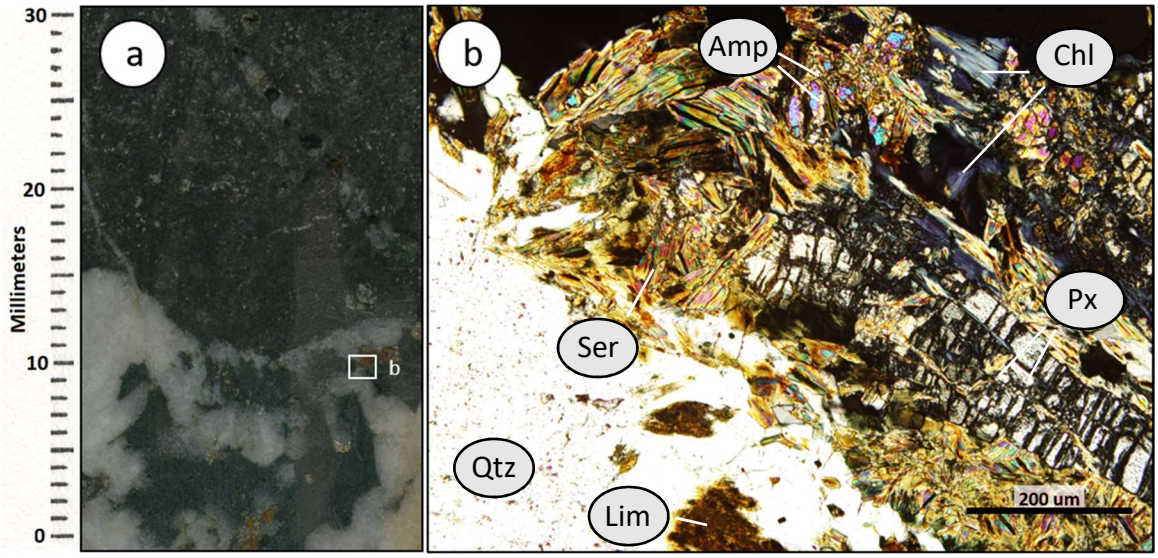

Figure 49. Scan (a) and photomicrograph (b) of skarn altered clasts in breccia from the TiCup horizon. Note the siliceous nature of the matrix-fill on the lower left in photo a and b, with green, chlorite-amphibole dominated, strongly embayed clasts occurring with jasperoid-altered limestone (top). Photo b demonstrates the apparent paragenesis of skarn, including blocky pyroxene partially replacement by amphibole (anthophyllite?) and later by chlorite. Opaque minerals are pyrite and chalcopyrite.

Jasperoid occurs in the immediate footwall of the lithologic contact, with the intensity of silicification diminishing away from the lithologic contact. In weakly and unaltered rocks of the footwall, small veinlets of quartz and calcite are subparallel to bedding and can attain densities of 50% over small intervals a few feet in thickness. Calcite crystals in the veins cutting footwall jasperoid and limestone are often >4 centimeters long and are commonly associated with scheelite. The oxidized breccia bodies can attain extremely high grades of Ag (up to 3,500 ounces per ton: Heard, 1881) with variable Zn, Pb, Cu, and minor Au in mineralogy that includes stromeyerite, tetrahedrite, galena, pyrite, and local sphalerite. Gold grades are inconsistent in the TiCup horizon and only a few samples exceed 100 ppb. The historical silver resource consisted of a black, silver-copper sulfide mineral believed to be stromeyerite ($AgCu_2S$), which

Figure 50. Mineralized carbonate breccia from the Doctor's Cut prospect. Note the blue copper oxides coating fracture surfaces (a) and rimming grains of stromeyerite (b). Photo by M. Houhoulis

can still be found in hand sample at a number of prospects (Figure 50). Sporadic scheelite is associated with thin quartz veinlets cutting jasperoid in the footwall of the Ticup horizon.

Tungsten Deposits

The tungsten resource of the Cherry Creek Range was the last to be exploited, and following its discovery in 1918 it was mined mainly in the 1940s until production ceased in the 1950s (Adair, 1983). The dominant ore mineral, scheelite, is associated with calcite gangue. The best-developed tungsten deposits in Cherry Creek occur in calcite-cemented limestone breccia zones, the most prolific of which developed alongside silver deposits at the TiCup horizon. The Old Timer and Chance mines were the largest producers of tungsten (Holmes, 1950). Many of the tungsten orebodies co-inhabit structures originally prospected for silver, most notably at the TiCup horizon, where they are associated with siliceous rather than calcareous gangue. For a more thorough treatment of this topic the reader is referred to G.H. Holmes' 1950 Bureau of Mines Report referenced below.

The style of scheelite mineralization in association with calcite gangue is widespread along the western slope of the Cherry Creek Range. From the first occurrences of this style in the TiCup area described above, mineralization of this type can be found in many locations within the Marjum, Weeks, and Orr formations. Similarly to the structural and lithological settings of siliceous mineralization described above, calcitic W ± Pb-Zn ore occurs in the hanging wall of the Exchequer fault at least three siltstone-limestone and limestone-shale contacts. The largest of these deposits, the site of the 50s era Nora mine, was in the footwall of the Dunderberg Shale (HW) – Orr Limestone (FW) contact in Lead Mine Canyon (Adair, 1961). Two km to the north in Flint Spring Canyon this same contact is mineralized with Au-bearing jasperoid.

Structural and Stratigraphic Controls on Mineralization

The best-developed examples of this carbonate replacement style of mineralization are located within a 500 by 500-meter triangle of heavily fractured rock bounded between the Exchequer fault, a series of steep, northwest-striking sympathetic faults, and the moderately west-dipping Swasey Limestone-Wheeler Shale contact, known as the TiCup horizon. The discovery outcrop, which in 1868 led to the establishment of the TiCup mine, was in the heavily fractured triangle of limestone at the intersection of the Wheeler-Swasey contact and the Exchequer fault (Heard, 1881).

The largest and most pervasive structure in the area is the N70°E/75°NW oriented Exchequer fault zone (EFZ), which tracks into the TiCup area from Exchequer Canyon and is marked by the juxtaposition of shale and thin- to medium-bedded carbonate in the hanging wall against medium to massive bedded quartzite in the footwall. As described above, the trace of the EFZ in this interval is usually accompanied by a zone of subparallel fractures and intervening

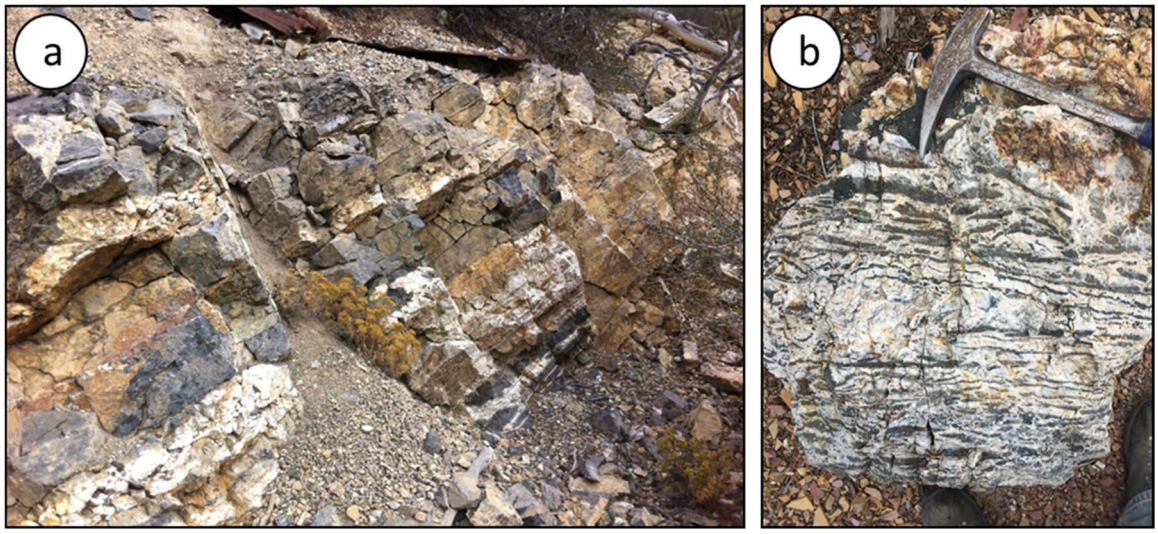

Figure 51. Field photos from the TiCup property. Note the prevalence of bedding-parallel quartz veins, quartz-cemented breccias, and dissolution textures in both the N10°E/45°W Doctor's Cut prospect (a) and "zebra" mineralization of quartz (white) and silicified limestone (black) from the TiCup Horizon.

brecciation up to 25’ thick, such as those that characterize the Geneva and Fillmore mines (Adair, 1961). The main distinction that differentiates the environment of carbonate-replacement deposits from the quartzite-breccia and vein-hosted EPV is the lithology of the Exchequer hanging wall.

At the head of El Rey Canyon, 1.75 km along strike of the EFZ from the Exchequer mine, the sequence of hanging-wall Cambrian carbonate rocks in the Exchequer hanging wall advances up section from the finely laminated carbonates of the Burnt Canyon and Dome Formations to the medium-grained and thickly-bedded Swasey Limestone. At the base of the Swasey lies the poorly exposed calcareous Condor shale member, above which the Swasey is composed of cliff forming, massive-bedded limestone. This lithologic transition is the first of at least four limestone-shale contacts that host varying degrees of brecciation and mineralization in the

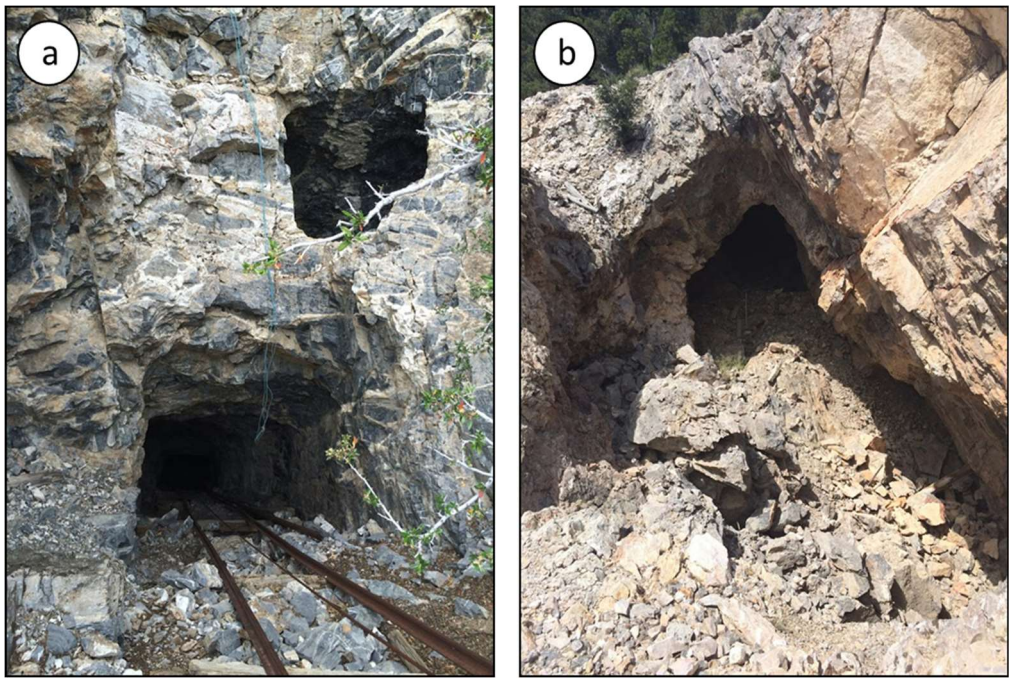

Figure 52. Bedding-parallel breccia zones at the Chance (a) and Nora (b) mines. Southern Incline of the Chance Mine (a) plunges 30˚to the west in the carbonate and quartz-cemented breccia zone beneath the TiCup Horizon. Note the matrix-supported character of the 3-m-thick breccia zone. Collapsed 10-m-thick stope at the Nora mine (b) follows a bedding-parallel calcite-cemented breccia zone in limestone of the Orr Formation on the east side of Lead Mine Canyon.

Cambrian carbonate section. The largest of these bedding-parallel mineralized zones is developed along the N10°E/45°W contact between the Swasey Limestone and overlying Wheeler Shale, although at least three other, smaller and less continuous examples of bedding-parallel, N10°E/45°W hydrothermal horizons exist at intraformational boundaries on either side of that contact. These smaller horizons include the Doctor's Cut: a siltstone-shale contact in the Wheeler Formation, and the Old Timer: a limestone-shale contact in the Swasey Formation.

Along these horizons, the most significantly brecciated and mineralized bodies of rock are localized by intersections between the moderately west-dipping bedding and steeply north-dipping high-angle faults. These intensely brecciated bodies (Figure 53) are associated with the highest Ag grades in the area (Heard, 1881), whereas such more laterally extensive swarms of quartz veins and jasperoid are disseminated along the bedding horizons outboard of the breccia bodies. The largest structural intersection, between the TiCup horizon and the Exchequer fault, delineates a more than 330 m long breccia pipe that is the site of the historic TiCup inclined shaft. 800 m to the northeast of the Exchequer fault, several high-angle and northwest-striking faults cut the N10°E/45°NW TiCup bedding horizon at the Chance mine and are marked by calcite and quartz-cemented jasperoid breccias. Still further from the Exchequer fault, the intensity of mineralization and the density of high-angle faults diminishes along the Wheeler-Swasey contact towards the north.

Motherlode Extension

Along strike of the TiCup horizon to the northeast of the Chance mine, jasperoid significantly diminishes in intensity except for a few small pods of weak silicification along small and discontinuous northwest-trending faults cutting the Swasey-Wheeler contact.

Three and a half kilometers to the north of the Chance mine, the TiCup horizon is truncated in Silver Canyon by the Black Metal fault: the largest of the major range-scale northeast-striking faults of the district. At this point, the apparent 1400 m dextral offset across the Black Metal fault juxtaposes the Swasey-Wheeler contact on the south against the Orr-Dunderberg contact on the north. This horizon represents another weakly faulted limestone-shale lithologic contact, and is cut by a series of steep, west-northwest-striking faults related to the Black Metal fault that essentially complete the analogue between this area and the TiCup.

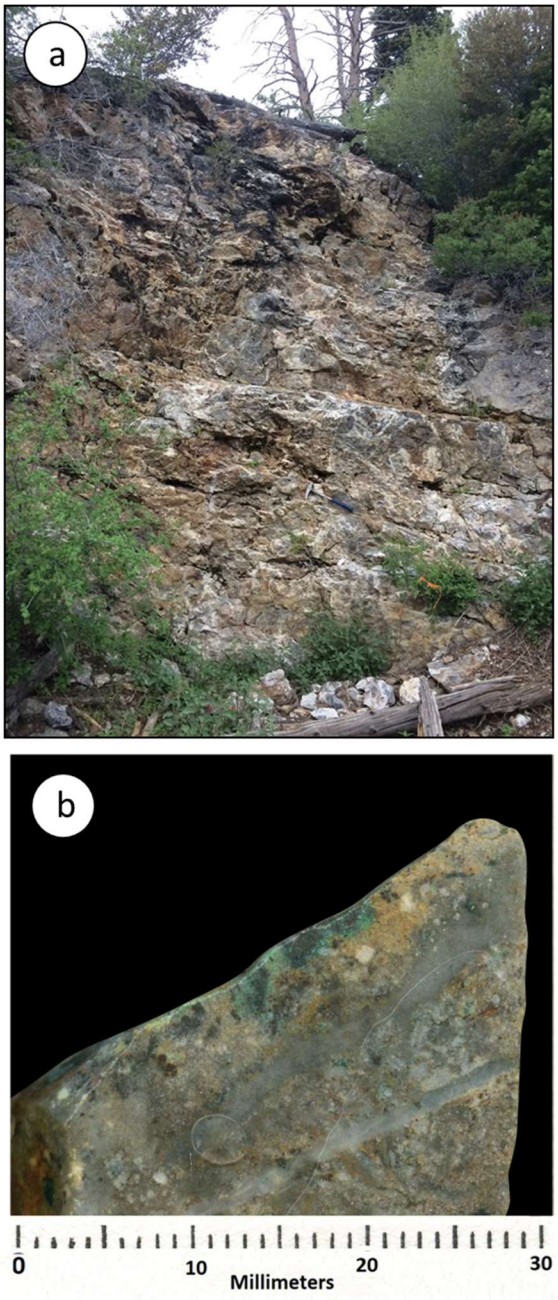

Figure 53. Field (a) and slab (b) photos from the Motherlode horizon in Silver Canyon. Large jasperoid breccia bodies (a) up to 10 meters thickness are common in the Motherlode area, and usually contain limited amounts of weathered stromeyerite (b)

This zone is known as the Mother Lode, and hosts mineralization characterized by brecciation, quartz veining, and jasperoid that strongly resemble what is seen at TiCup. Compared to the TiCup, the geology is well exposed at the surface in a few open cuts and prospects. The jasperoids that occur at the Mother Lode are typically 5-15 m thick and are commonly strongly brecciated. Most have abundant late quartz veins, with densities up to 15%. A few samples contain substantial amounts of weathered stromeyerite, and much of the dump material is coated with exotic copper oxides.

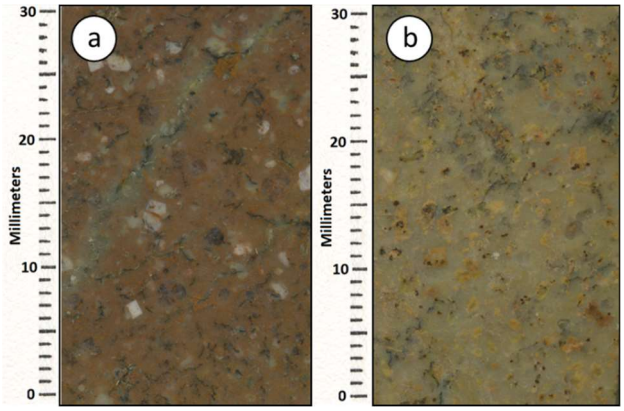

Figure 54. Slabs of relatively fresh (a) and phyllic-altered (b) dacite dike from the Fillmore mine (10256)

Dikes in the TiCup Zone

Three altered dacite dikes are present in the TiCup area. Of these, two cross the shallowly dipping structural grain of the TiCup horizon near the Chance mine, and one occupies fractured limestone in the hanging wall of the Exchequer fault at the Fillmore mine. The dikes at the Chance mine are between 1 and 2.5-m-thick, with an average attitude of N75°W/75°NE, and are weakly to moderately altered. In the dacite dike near the Fillmore

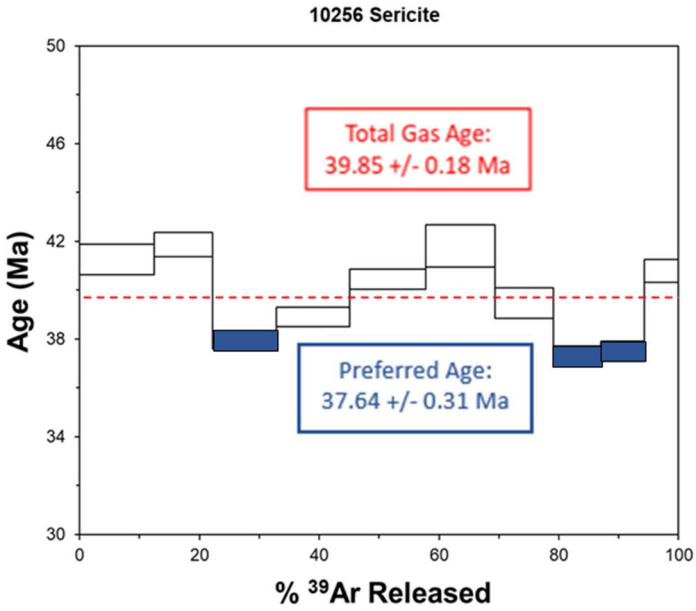

Figure 55. Step-Heating 40Ar/39Ar results for Fillmore dacite dike (10256) sericite

mine at the western end of the area, the primary igneous mineralogy of potassium feldspar, plagioclase feldspar, and amphibole is partially altered to fine-grained sericite, chlorite, and pyrite, the latter of which forms cubes up to 3 mm in diameter (Figure 55). Small 1-2-millimeter rounded eyes of quartz are still visible. The dikes primary aphanitic groundmass is partially replaced by a fine-grained mixture of quartz and sericite. Neither the Fillmore nor the Chance dike is highly mineralized compared to breccias in the surrounding rock. The distal portion of the dacite dike at the Fillmore mine located in the carbonate hanging wall of the Exchequer fault contains anomalous values of Au, Sb, Ag, and As. The dike adjacent to the Chance mine is strongly enriched in W and is strongly enriched in Sb, Ag, and Au (Figure 56).

$^{40}Ar/^{39}Ar$ geochronology of sericite from the altered dacite at the Fillmore mine yielded a complex step-heating spectrum with a total gas age of 39.85 ± 0.18 Ma. Within this spectrum, the three youngest steps have nearly overlapping ages between 37.97 and 37.31 Ma that constitute 25% of the total ^{39}Ar released (Figure 55).

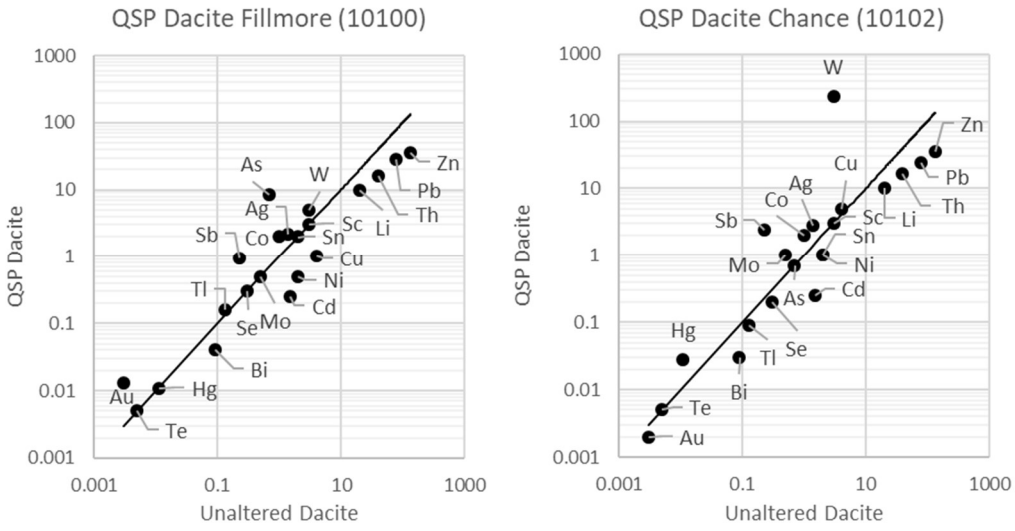

Figure 56. Isocon diagrams for phyllic-altered dacite at the Fillmore and Chance mines

TiCup-Chance Geochemistry

The mineralization characterized by the TiCup-Chance-Motherlode deposits is base-metal and Ag-rich, and are differentiated from the deeper veins primarily by their lack of gold (< 100 ppb; Figures 57). Mineralized veins and jasperoid breccias contain substantial enrichments in Pb, Zn, Ag, W, Cu, Mn, Ba, and Sb on the order of 100 ppm are common. Strong correlations exist between Cu, Ag, Pb, and Sb, which also correlate weakly to moderately with Sn, Bi, and As. Mo, Bi, and As have moderate positive mutual correlations, possibly indicating the presence of a higher-temperature mineralization phase. W has a weak positive correlation with Zn (ρ=0.20) and weak negative correlations with Au (ρ=-0.23) and Ag (ρ=-0.24). Au has moderate correlations with Ag (ρ=0.45), Cu (ρ=0.40), and Bi (ρ=0.40), and weak correlations with Pb (ρ=0.29), As (ρ=0.22), and Sb (ρ=0.22), although the statistics are somewhat complicated by its low concentrations (Table 10).

Table 10. Geochemical Statistics for TiCup-Chance Carbonate Replacements in ppm (N=52)

Contituent	Mean	Median	Minimum	Maximum	IQR
Au	0.04	0.04	0.01	0.20	0.05
Ag	189.87	45.90	0.39	1200.00	187.49
Sb	106.60	50.70	1.73	659.00	92.18
As	19.34	13.05	1.60	97.60	12.23
Cu	180.75	68.40	4.90	1235.00	150.58
Pb	646.23	171.00	9.10	11400.00	620.00
Zn	320.17	117.00	10.00	3210.00	229.50
W	163.01	30.20	0.40	1280.00	166.80
Te	0.20	0.07	0.05	1.10	0.18
Tl	0.21	0.15	0.03	1.18	0.13
Mn	168.94	100.00	31.00	1800.00	101.75
Ba	279.42	50.00	10.00	2480.00	110.00
Sn	0.70	0.35	0.20	5.30	0.60
Bi	1.14	0.06	0.01	46.50	0.08
Mo	3.51	1.64	0.18	23.30	4.33
S (%)	0.04	0.02	0.01	0.22	0.04

	Au	Ag	Cu	Pb	Zn	W	Sn	Bi	Mo	As	Sb	Ba	Mn	Tl
Au	1													
Ag	0.45	1												
Cu	0.40	0.78	1											
Pb	0.29	0.65	0.78	1										
Zn	0.13	0.49	0.68	0.69	1									
W	-0.23	-0.24	-0.09	-0.09	0.20	1								
Sn	0.06	0.41	0.56	0.42	0.37	-0.15	1							
Bi	0.40	0.28	0.49	0.53	0.32	-0.07	0.34	1						
Mo	0.12	-0.10	0.25	0.17	0.14	0.30	0.14	0.45	1					
As	0.22	0.24	0.49	0.59	0.58	0.16	0.32	0.62	0.51	1				
Sb	0.22	0.83	0.72	0.66	0.60	0.03	0.41	0.29	0.01	0.38	1			
Ba	-0.05	-0.21	-0.05	0.01	0.10	0.34	-0.18	0.35	0.25	0.34	-0.09	1		
Mn	-0.10	0.01	0.19	0.27	0.32	-0.17	0.07	0.24	-0.16	0.13	0.03	-0.11	1	
Tl	0.15	-0.08	0.14	0.15	0.27	0.35	0.03	0.35	0.52	0.55	0.12	0.50	-0.06	1

Figure 57. Elemental Spearman rank correlation matrix for TiCup-Chance carbonate breccia replacements (N=52)

Flint Canyon Au-Ag-Bearing Jasperoids

The Upper Cambrian carbonate rocks in Flint Spring Canyon on the west side of the central Cherry Creek Range host another series of stratiform and structurally-controlled jasperoids that differ considerably from the polymetallic features present in the TiCup area. At Flint Spring Canyon, several horizons of interbedded carbonate and shale strata have experienced intense silicification along 2 km of the Black Metal fault (Figure 19). The most profound development of jasperoid is focused along the Orr Limestone-Dunderberg Shale contact in the footwall of the Black Metal fault, and apart from the important distinction that it is about 1400 m shallower in terms of Eocene paleodepth, it is the stratigraphic and structural analogue to the Motherlode (Figure 16). The Flint Spring Canyon area is the first shallowly-formed (< 3.5 km) deposit described in this study.

Mineralization

Hydrothermal alteration at Flint Spring Canyon occurs in the Orr Limestone along its contact with overlying Dunderberg Shale. The dominant mode of hydrothermal alteration is silicification of limestone, resulting in a somewhat continuous 5-15-meter-thick sheet of jasperoid. Jasperoids along the Orr-Dunderberg contact are generally massive in texture and bulbous in shape. Some are highly fractured due to post-mineral faulting. Jasperoid breccias are also common and are usually healed with fine-grained quartz, although examples of calcite-cemented breccias and skeletonized breccias encrusted with late, drusy quartz can also be found (Figure 58). Others are merely fractured and host numerous quartz veinlets. Beneath this mineralized zone the footwall Orr Formation is variably fractured and silicified, and in places it hosts swarms of quartz or quartz and calcite veinlets. In some of the most heavily faulted zones, fractured Dunderberg shale has also experienced silicification.

The intensity of supergene oxidation is a distinctive factor of the Flint Canyon occurrences. It is especially evident in the siltstone beds of the Orr and Pogonip formations, which are ruddy and porous and have clearly been strongly affected by weathering of sulfides.

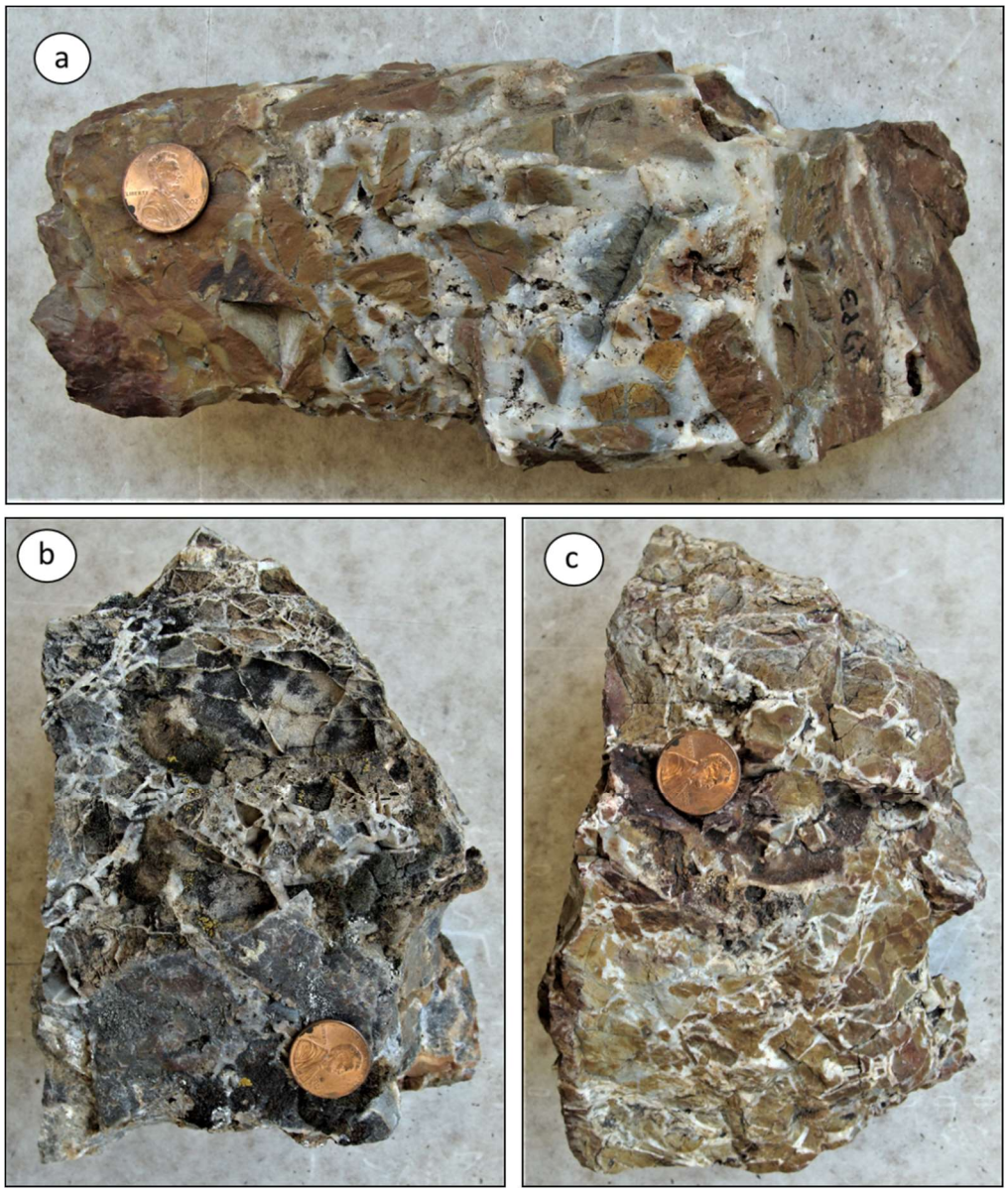

Figure 58. Jasperoid breccias from Flint Spring Canyon. Jasperoids containing brown clasts of finely-laminated and silicified Dunderberg Shale (a, c) are rare but were noted in several localities in association with high angle, northwest-trending faults in proximity to the Black Metal fault. More typical jasperoid breccias containing clasts of Orr Limestone (b) are widespread. Note the presence in (b) of skeletonized quartz matrix probably due to weathering following incomplete silicification

Some siltstone beds are extremely porous, friable, and contain vugs filled with crystalline calcite, suggesting that they served as conduits for hydrothermal fluids.

In Flint Canyon, argillic alteration typically forms in the lower Dunderberg Shale outboard the west-dipping, bedding-parallel jasperoid in the underlying Orr formation. Argillically-altered dikes are also commonly associated with jasperoid, in at least three cases having been found to lie directly above the jasperoid (Figure 59). Most of the argillically altered dikes are almost unrecognizable; in addition to the alteration they seem to be heavily faulted and deformed. Most seem to strike southeast and dip to the southwest. Away from the lithologic contacts and jasperoid bodies, the dacite dikes are strongly oxidized but

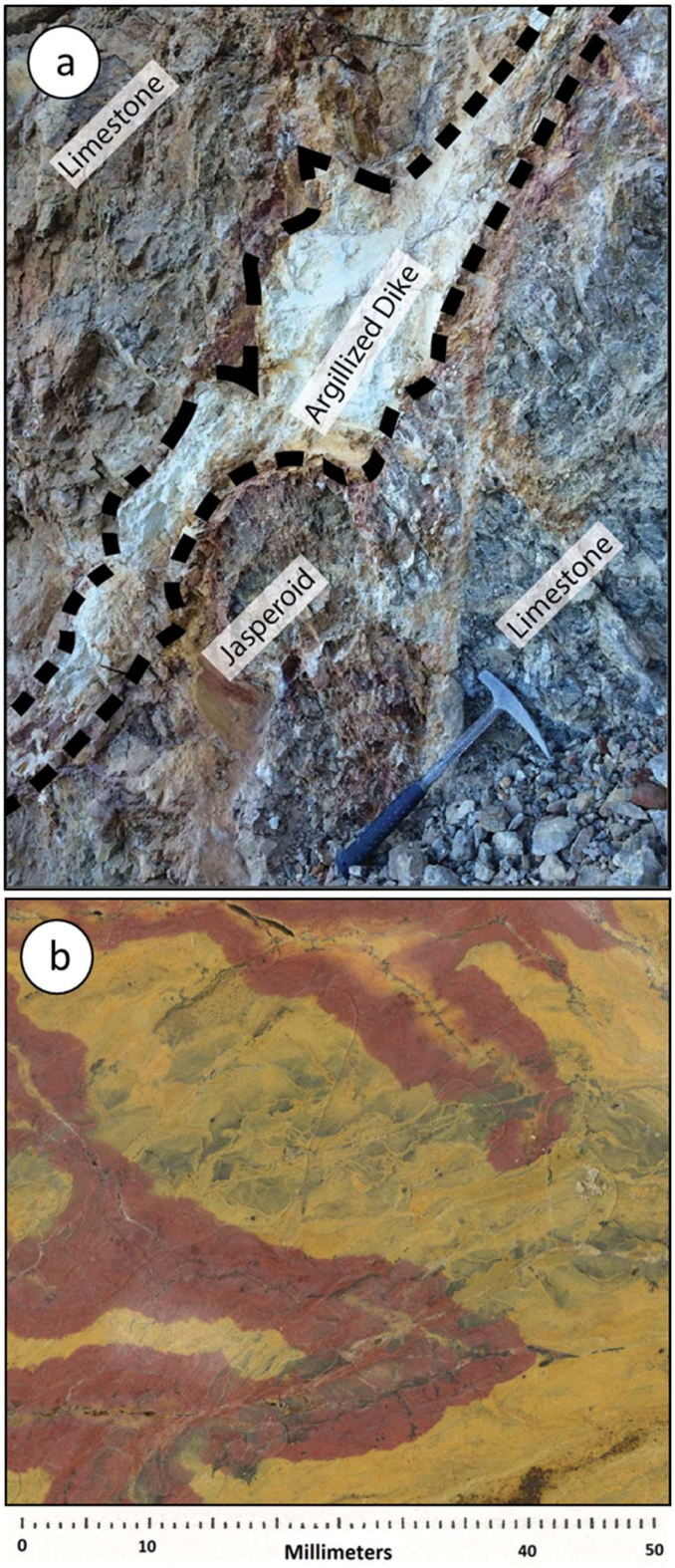

Figure 59. Field photo (a) and slab (b) of argillic-altered dike occurring along jasperoid in Flint Canyon

clearly significantly less affected by argillic alteration. They exhibit a spotty texture of iron oxides that appear to be weathered pyrite sites. SWIR spectroscopy of these altered dikes indicates the presence of illite and hematite, with minor amounts of montmorillonite. Four of five analyzed dikes had Au assays greater than 50 ppb, including one with 126 ppb and one with 249 ppb. An argillic dike intercepted by drilling contained over 4 ppm Au, which was the highest gold assay in the Flint Canyon area. In addition to gold, the altered dikes are also highly enriched in As, Sb, Tl, Mo, and Ag. Thus, it is likely that most dikes were subjected to similar hydrothermal conditions as the other mineralized rocks in Flint Canyon. Some of the more weakly altered have spherulitic textures, suggesting that they were devitrified.

The two altered dikes selected from the Flint Canyon area for $^{40}Ar/^{39}Ar$ dating of sericite yielded poor, crankshaft-shaped step-heating profiles that rendered Eocene ages but preclude more precise interpretation. The total gas age of sample 10129 is 49.89 ± 0.52 Ma, and the total gas age of sample 10265 is 41.81 ± 0.08 Ma (Figure 60).

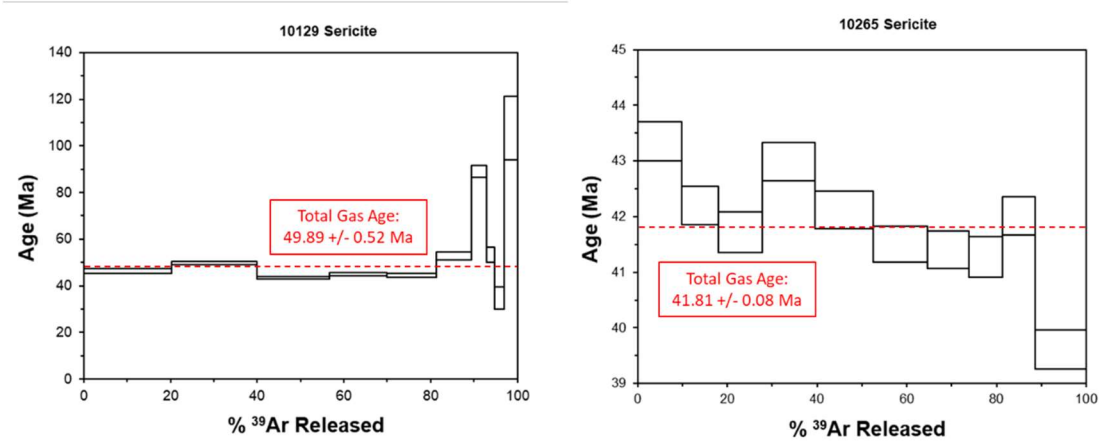

Figure 60. Ar-Ar step heating analyses for sericite of altered dikes 10129 and 10265

Structural and Lithological Controls on Mineralization

The Flint Spring Canyon occurrence is localized to a series of discrete, bedding-parallel mineralized zones within a succession of shale, siltstone, limestone, and dolomite in Upper Cambrian and Lower Ordovician strata. The relevant units are: 1) the Orr Formation, 2) the Dunderberg Shale, 3) the Notch Peak Formation, and 4) the Pogonip Formation. The most profound development of mineralization is manifested along the Orr-Dunderberg contact: a thick-bedded limestone under shale contact that is reminiscent of the TiCup. Other zones of less pervasive mineralization are found at siltstone-limestone horizons in the Orr formation.

The north side of the Flint Spring Canyon area is delineated by the Black Metal fault, which is oriented N75E with a sub vertical dip. In this interval, the Black Metal fault juxtaposes undivided Ordovician and Silurian limestones and dolomites on the north against the Cambrian Orr formation, Dunderberg Shale, and Notch Peak formation on the south. In Flint Spring Canyon, the Black Metal fault is associated with a number of high-angle, northwest and northeast-trending faults with offsets of less than 25 meters, which define a strongly deformed 1 by 2-kilometer zone that extends northeast along the Black Metal fault. The style, orientation, and displacement of these subsidiary faults are reminiscent to those that peripherally control mineralization at the TiCup occurrence, and the two fault zones may in fact be continuous. The most important structural feature is the moderately west to northwest-dipping, bedding-parallel zone that marks the contact between the lower Dunderberg Shale and the upper Orr limestone.

Geochemistry

Mineralization of selected trace elements at the Flint Spring Canyon occurrence is the lowest in terms of median values and range, signifying that elemental enrichment in Flint Canyon was less intense than that at the other deposits considered in this study. All

sedimentary-hosted Au values in Flint Spring Canyon >50 ppb were taken from strongly silicified rock. Of these, gold values were on the order of 100ppb, with values up to 700 ppb. Weakly mineralized limestone breccias below the contact have 10s of ppb Au. High-angle breccia zones that cut the lithologic contact contain jasperoid clasts in quartz and calcite matrix are also anomalous, up to a few hundred ppb Au. The highest grade of jasperoid in the Flint Spring Canyon area is 2 ppm Au. Notable trace elements ranges in the Flint Canyon area include Mn, As, Ba, and Zn, and the range and median values of Mo in Flint Spring Canyon is 2 to 4 times above the other area groups discussed above including the MCPV. One distinctive feature of the Flint Canyon jasperoid geochemistry is the lack of strongly elevated Cu, Pb, and Zn values (Table 11). This contrasts strongly with the patterns observed at the same lithologic contact in the structurally lower Motherlode area (Figure 53), where base metals and silver constituted a much larger portion of the enrichment. In the Flint Spring Canyon area, Au in jasperoid correlates strongly only with As (ρ=0.65). Weaker correlations exist between Au and W (ρ=0.42), Mo (ρ=0.41), Sb (ρ=0.34) and Ag (ρ=0.33). In addition to the above elements, As also correlates with Tl (ρ=0.55) and weakly with Cu (ρ=0.38), Zn (ρ=0.36), and Ba (ρ=0.36).

Table 11. Summary statistics for Flint Canyon Jasperoids in ppm (N=87)

Contituent	Mean	Median	Minimum	Maximum	IQR
Au	0.11	0.05	0.01	1.16	0.09
Ag	7.57	4.20	0.20	64.00	5.65
Sb	25.56	22.90	9.70	81.00	12.05
As	50.51	32.60	7.10	347.00	41.30
Cu	6.83	4.90	1.80	50.10	3.30
Pb	22.36	13.60	2.20	134.50	16.00
Zn	45.03	25.00	2.00	604.00	40.00
W	1.74	1.60	0.40	6.80	1.20
Te	0.12	0.12	0.07	0.16	0.09
Tl	0.25	0.18	0.08	4.95	0.15
Mn	130.67	105.00	38.00	604.00	91.00
Ba	202.64	70.00	20.00	6380.00	40.00
Sn	0.36	0.30	0.20	1.30	0.20
Bi	0.05	0.05	0.01	0.20	0.03
Mo	8.74	6.21	0.71	61.90	5.60
S (%)	0.02	0.01	0.01	0.17	0.01

	Au	Ag	Cu	Pb	Zn	W	Sn	Bi	Mo	As	Sb	Ba	Mn	Tl
Au	1													
Ag	0.33	1												
Cu	0.19	0.75	1											
Pb	0.13	0.34	0.45	1										
Zn	0.08	0.10	0.28	0.48	1									
W	0.42	0.36	0.44	0.18	0.16	1								
Sn	0.00	0.37	0.48	0.33	0.14	0.56	1							
Bi	0.07	0.36	0.51	0.30	0.09	0.56	0.55	1						
Mo	0.41	0.12	-0.06	0.04	0.09	-0.01	-0.21	-0.11	1					
As	0.65	0.30	0.38	0.24	0.36	0.54	0.29	0.30	0.43	1				
Sb	0.34	0.62	0.61	0.43	0.20	0.39	0.30	0.37	-0.10	0.34	1			
Ba	0.26	0.13	0.17	0.20	0.21	0.18	0.05	0.08	0.13	0.36	0.06	1		
Mn	-0.04	-0.24	-0.05	0.00	0.34	0.00	-0.02	-0.09	-0.01	0.19	-0.08	0.20	1	
Tl	0.27	0.34	0.41	0.26	0.29	0.45	0.47	0.27	0.11	0.55	0.28	0.33	0.15	1

Figure 61. Elemental Spearman rank correlation matrix for Flint Canyon jasperoids (N=87)

Discussion

Intrusive History of Cherry Creek

Fifteen new U/Pb dates on zircon constrain the magmatism of Cherry Creek to the late Eocene between 41.1 and 34.7 Ma. The 10 km^2 northern lobe of the phaneritic-porphyritic Cherry Creek pluton (CCP) was assembled between 38 and 36 Ma. The oldest ages obtained from the CCP are 37.89 ± 0.28 Ma, 37.76 ± 0.3 Ma, and 37.67 ± 0.3 Ma, from quartz monzonite and minor granodiorite that occur in the northwestern corner of the pluton and within ~ 350 m of its roof. In Cherry Creek Canyon, the CCP contains small lobes of granite, granodiorite, and aplitic quartz monzonite with ages 37.67, 37.23, and 36.72 Ma that overlap in 2σ uncertainties. To the south of Cherry Creek Canyon, two samples of porphyritic quartz monzonite are 36.62 and 36.18 Ma. The tonalite stock at Silver Canyon is separated spatially from the rest of the CCP but is indistinguishable in age at 37.33 ± 0.34 Ma, although a diorite enclave within it yields an age of about 41.1 Ma. The entire CCP was emplaced into the McCoy Creek Group at an estimated paleodepth of 7-8 km based on restored strata thickness.

These results show that the northern lobe of the Cherry Creek pluton, which is dominantly quartz monzonite with lesser granite, granodiorite, and quartz monzodiorite, was the first to crystallize and did so in the relatively short span of about 1.5 million years. The lack of overlap in 2σ uncertainties precludes a single emplacement and crystallization event, and demonstrates progressive younging away from the intrusive contact, consistent with conventional models for pluton assembly (e.g. Glazner et al., 2004). Furthermore, these data suggest that the north lobe of the Cherry Creek pluton may have assembled in two main pulses, one from ~37.9-37.7 Ma and another from ~36.7 to 36.2 Ma. The only evidence of a

substantially older phase of magmatism at Cherry Creek is the small, 15m^2 dioritic enclave located in the southeast corner of the Silver Canyon stock and dated at 40.16 ± 0.93 Ma. This is an outlier from the other plutonic ages at Cherry Creek and most likely represents an enclave of scavenged or inherited magmatic material at depth. Similar mafic enclaves are scattered through the margins of the CCP. The varied textures of the Cherry Creek pluton, which range from porphyritic-phaneritic to porphyritic-aphanitic and aplitic, signify diverse conditions during the pluton's emplacement and may point to discrete events of hydrothermal fluid release (Seedorff et al., 2008).

The ages of aphanitic-porphyritic dikes in the Cherry Creek district reflect at least two discrete periods of magmatism. One of the Exchequer fault-controlled porphyritic dacite dikes is 38.2 ± 0.5 Ma: indistinguishable from the earliest pulse of quartz monzonite plutonism. This date signifies that the Exchequer fault was established prior to or during the emplacement of magma in the late Eocene, and that some of the intrusive activity occurred as shallow as ~5 km paleodepth, or 1.5 km above the roof of the pluton. Other porphyritic dikes in Cherry Creek are significantly younger than the CCP but indistinguishable from the ages of volcanic rocks overlying the Eocene unconformity. Four rhyolite dikes that cut the CCP south of Cherry Creek Canyon yield ages between 35.98 and 34.89 Ma, and one strongly altered dacite dike from the mouth of Flint Spring Canyon in the northwest part of the study area yielded an age of 35.44 ± 0.41 despite it being ~3.5 km above the pluton's roof at an estimated paleodepth of ~3.5km. Biotite K-Ar ages on porphyritic rhyolite in Johnson Spring Basin (34.6 ± 1.9 Ma) on the west flank of the Cherry Creek Range, in the Butte Mountains (35.5 ± 1.4 Ma), and in the north Egan Range (35.1 ± 1.4 Ma: McKee, Silberman, Marvin, and Obradovich, 1973), overlap in age and are mineralogically similar to the younger pulse of intrusion at Cherry Creek. It is possible that the

slightly younger andesites in the Egan Range and Butte Mountains, which have K-Ar ages of 34.1 ± 0.2 Ma (Macdonald et al., 1992) and 32.9 ± 0.7 Ma (McKee et al., 1973), could be correlative to the young andesite dikes at Cherry Creek but not dated by this study.

Significance of Cherry Creek Magmatism in Eocene Nevada

The Cherry Creek pluton offers an important perspective on the igneous geology of eastern Nevada. Numerous other plutons exist at various Eocene structural levels in the vicinity. In the Egan Range to the south of Cherry Creek, 6-7-km-long exposures of quartz-monzonite and porphyritic latite on the east flank of Cocomongo Mountain (Adair, 1961) almost certainly represent the southerly extension of the CCP itself, albeit occupying a structural position slightly deeper than the north lobe of the pluton exposed at Cherry Creek. Approximately 30 km to the south of Cherry Creek, the substantial 20 km^2 Warm Springs pluton again intrudes McCoy Creek rocks, although much of its context is obscured by low-angle faulting (Fritz, 1968). Biotite in the Warm Springs pluton was dated at 38 ± 1 Ma (Armstrong, 1966) and 36.2 ± 0.7 Ma (Armstrong, 1970). About 55 km south of Cherry Creek, the Heusser Mountain pluton also intrudes phyllite and quartzite of the MCG (Whitney, 1972), and biotite from the pluton was dated 33.6 ± 0.7 Ma by K-Ar (Armstrong, 1970). The similar ages, structural relationships, and compositions of these features likely indicate a major pulse of Eocene intrusive activity from ~38 to 34 Ma resulting in the emplacement of this group of plutons. Similarly, a large 75 x 30 km magnetic anomaly in Steptoe Valley could represent a continuous, batholith-scale igneous body related to the exposed intrusions (Adair, 2005). To the east in the Schell Creek Range, another small intrusion is exposed in contact with the deepest McCoy Creek rocks at Black Mountain near Indian Springs (Hose et al., 1976). A small, undated granite porphyry stock is present in the Aurum District

near the northern end of the Schell Creek Range along with several syenite dikes that reach into the Lower Cambrian Pole Canyon Limestone (Hill, 1916; Hose et al., 1976). Granodiorite at the Kinsley Mine near the Elko-White Pine county line intrudes Middle Cambrian stratigraphy and is about 40 Ma, and is cut by dikes ranging from 40-35.5 Ma (Hill, 2016). The well-studied Harrison Pass pluton in the southern Ruby Mountains was emplaced over 1.5 Ma between 38.1 and 36.5 Ma (Barnes et al., 2001; Colgan et al., 2010), and is a good analogue for the composite pluton Cherry Creek pluton which was assembled over a similar timeframe.

The northern CCP occupies a sort of structural apex above the typical level of the Eocene plutonic rocks in the area. At Cherry Creek, this apex is as much as 750 m stratigraphically above the more typical level of the intrusive roof in the McCoy Creek Group. It is important to note that this apex occurs in the footwall block of the Exchequer fault (and, in turn, also of the Black Metal fault). The fact that these faults displace the Prospect Mountain Quartzite to the east, or down-section, is especially interesting because of the very apparent control this unit has on roof of the Cherry Creek pluton. As this study demonstrates, the same structures that define the apex are also the same that control hydrothermal mineralization in the overlying crust, even over 8 km of stratigraphy.

Hydrothermal History of Cherry Creek

One of the primary goals of this study has been to determine the relationships between igneous and hydrothermal geology. Hydrothermal alteration in the CCP is typically located along faulted margins of the intrusion. The phyllic alteration associated with the mineralized Maryanne fault, and phyllic and greisen alteration and quartz veins associated with the mineralized Salvi fault zone (SFZ) are examples. Pre-mineral dikes are commonly sericite-

chlorite-carbonate-pyrite-altered in the McCoy Creek Group, weakly quartz-sericite-pyrite-altered in mineralized Middle Cambrian rocks, and argillically altered in the Upper Cambrian rocks and above.

Ages of intrusion-proximal hydrothermal deposits from the deepest structural levels of the Cherry Creek Range closely correspond to the timing of emplacement for the first phases of the Cherry Creek pluton. The Maryanne system, which represents the best example of pluton-hosted quartz-sericite-pyrite alteration, was dated with one molybdenite Re-Os age and two sericite $^{40}Ar/^{39}Ar$ ages. The molybdenite yielded an age of 38.3 ± 0.2 Ma. Muscovite separated from the same specimen as the molybdenite yielded a $^{40}Ar/^{39}Ar$ total gas age of 38.05 ± 0.08 Ma. One sample of illite collected from a weakly sericite-chlorite-carbonate-altered segment of the Maryanne fault yielded a $^{40}Ar/^{39}Ar$ total gas age of 38.89 ± 0.06 Ma. Six dikes associated with polymetallic vein mineralization in the McCoy Creek Group exhibit moderate to intense sericite-chlorite-carbonate-pyrite alteration and a few are brecciated and mineralized with Ag-Au-Sb-Bi-Cu-Sn-W-(Pb-Mo-Te-Tl-Zn). Illite and muscovite separated from a mineralized dike at the Victoria mine yielded a total gas age of 38.87 ± 0.10 Ma, including 5 steps with overlapping ages between 38.16 and 37.81 Ma, totaling 50.1% of the total ^{39}Ar released. The profiles of all samples from intrusion-proximal deposits have between 3 and 6 steps representing as much as 60% of the total ^{39}Ar released that have overlapping errors but lack the criteria of consecutive overlapping steps required for true plateau ages. The $^{40}/Ar^{39}Ar$ total gas age of these samples nearly approximates the age of these overlapping steps, and is therefore likely a good approximation of the age.

The fact that sericite and molybdenite from intensely phyllic-altered rock at the Maryanne yield identical ages signifies that high-temperature polymetallic mineralization

occurred ~ 38.1 Ma in a small area on the northwest margin of the CCP. Although the sample from lower on the Maryanne structure yields 5 (out of 10) steps overlapping with errors of the molybdenite age, it also exhibits slightly more scattered step-heating behavior, probably resulting from recoil effects owing to less crystalline illite, and thus is considered less meaningful. It is interesting to note that the ^{39}Ar total gas age of sample 10081 is indistinguishable from that of sample 10264, which occurs about 3.5 km to the northeast in a MCPV-style mineralized dike, although the step-heating profiles are different. Due to the similar character of phyllic alteration, structural context, and geochemistry between the Maryanne (samples 10081, 10088) and the Victoria (sample 10264) occurrences, there is good evidence to suggest that they formed under similar conditions. Regardless of the small age discrepancies in the four age dates of these deep hydrothermal features, it is reasonable to conclude that this structurally deep mode of mineralization coincided broadly with the earliest known phases of the phaneritic Cherry Creek pluton.

The three sericite samples from intermediate and shallow depths presented significant problems with their $^{40}Ar/^{39}Ar$ profiles. One sample was collected from the Fillmore mine on the Exchequer fault zone, and two were collected from the Flint Canyon area. The three samples yielded widespread ages and have strongly developed saddle- or “crankshaft”-shaped step-heating profiles, possibly owing to excess non-radiogenic argon, argon released from multiple mineral phases, and/or ^{39}Ar recoil (Kelley, 2002). These results are not surprising, as the high partition coefficient of argon in hydrothermal fluids suggests that argon with a skewed, hydrothermal composition can interact with illite, especially in hydrothermal systems associated with felsic intrusions (Kelley, 2002). Especially in the case of mutual overprinting hydrothermal systems or ongoing hydrothermal activity that waxes and wanes, non-radiogenic argon is almost

certainly a component of the Cherry Creek system. It is likely for this reason that the deepest, highest temperature, and most intensely altered samples yield the best age results. The two dikes from the shallow Flint Canyon zone are strongly oxidized, likely indicating that they experienced supergene alteration by meteoric fluids. While hyperspectral analyses of all three samples yield profiles consistent with illite (Appendix B) and thus were selected for analysis, the oxidized samples may have also contained small amounts of kaolinite or smectite that could have affected their step-heating profiles. Despite poor spectra, the $^{40}Ar/^{39}Ar$ results of sericite in the Cherry Creek study area yield unanimously Eocene ages that approximate the timing of mineralization as synchronous or shortly following intrusion. Although no samples yielded valid isochrons or plateaus, results yield consistent and reasonable albeit scattered step heating ages that are best approximated by the Eocene total gas ages.

Hydrothermal Zonation in Cherry Creek

The zonation of mineral deposits in Cherry Creek illustrates the importance of paleodepth and proximity to the structural level of its Eocene pluton. Similarities in alteration and geochemistry between the deposits in the uppermost 3.5 km of exposed strata in the central Cherry Creek Range and jasperoidal Carlin-type Au deposits elsewhere in Nevada suggests that similar, intrusion-distal hydrothermal systems prevailed in the shallow Eocene crust in both cases. The nature of the highest temperature and structurally deepest mineralization in the district and its relationship to the CCP is also an interesting question. Ultimately, this question bears on the connection between magmatic-hydrothermal and distal conditions at the district scale. Several well-studied but highly variable types of Eocene magmatic-hydrothermal systems in the Great Basin (e.g. Copper Canyon, Mount Hope, Bingham,

Cove-McCoy) represent productive districts attributable to high-temperature mineralization that are contemporaneous with Cherry Creek. In many ways, it is appealing to consider Cherry Creek in terms of one of the types of Eocene porphyries exemplified by these districts, however the findings of this study demonstrate that Cherry Creek is substantially different.

The lack of classical porphyry alteration and metal zonation at Cherry Creek suggests the absence of porphyry-type mineralization anywhere in the vicinity. Although intense hydrothermal alteration is developed in the Cherry Creek pluton, it is largely localized along structurally-controlled fractures along the edges of the intrusion and accompanied by quartz flooding and intense hydrolytic alteration. The mineralized Salvi fault zone (SFZ) is characterized by quartz veins with greisen-style muscovite and quartz-sericite-chlorite-carbonate-pyrite alteration selvages, and associated with a W, Sn, Bi, Sb, Au, As, Te, Mo, and Ag geochemical signature. A similar geochemical signature occurs in late, west-trending fractures that control phyllic alteration and track towards isolated Sn-W-Mo skarn mineralization outboard of the pluton along the western side of the pluton near Cherry Hill, and in the Maryanne in the northwest corner of the CCP, where intense phyllic alteration of quartz monzonite is continuous up-structure with northeast-striking veins at the Flagstaff occurrence. The polymetallic veins that flank the pluton in the MCG have strong associations between Au, Ag, Cu, Zn, Pb, Sb, Te, and As, along with a separate Bi, Mo, Ba, Tl signature that may represent a discrete event. Porphyritic dacite dikes have experienced additions of these elements as well. Based on stratigraphic relationships, this mineralization in the pluton and MCG occurred at depths exceeding 7.5 km.

These deep mineralization styles at Cherry Creek are inconsistent with those of the typical porphyry environment, as it lacks the relationships between late porphyry intrusions and

disseminated potassic alteration of a crystalline carapace (e.g. Sillitoe, 2010). Although igneous-hosted alteration is intense in Cherry Creek, it is largely localized to vein selvages and not demonstrably related to any discrete magmatic phase. While small aplitic and pegmatitic dikes do exist in the CCP and probably signify a class of late-stage, magmatic-hydrothermal fluid features, their relationships seem to be more associated with sodic-calcic metasomatism at the pluton's core than the precious- and base-metal-bearing hydrolytic phyllic and greisen alteration along its margins. The paleodepth of igneous-hosted mineralization at Cherry Creek based on overlying Paleozoic strata is also greater than typical porphyry depths (7.5-8.5 km vs 1-6 km), and the strong degree of structural control is another difference. In parts of the Basin and Range province where high-magnitude extension has exhumed the deep zones of porphyry districts (e.g. Yerington, Sierrita-Esperanza, Rey, Miami-Inspiration), many features of the porphyry systems beneath the epizonal or shallow mesozonal orebodies are reminiscent of those at Cherry Creek (Seedorff et al., 2008). The root zones of porphyry intrusions themselves vary considerably as a function of depth, with groundmass textures coarsening downward to become seriate, phaneritic-porphyritic, and granitic (Seedorff et al., 2008). These are the same textures present in the phaneritic igneous rocks of Cherry Creek. The alteration patterns of these root zones are also similar to those of Cherry Creek. Quartz-muscovite greisen is present at paleodepths of 6-7 km at Luhr Hill in the Yerington district, forming a distinct alteration phase that occurs in the absence of potassic, phyllic, and advanced argillic alteration found in the shallow porphyry environment (Runyon et al., 2017). With the absence of an intrusive cupola zone extending to shallower depths, and with the apparent limitations on pluton emplacement depth imposed by quartzites of the McCoy Creek Group and Prospect Mountain Quartzite, the

setting of the Cherry Creek pluton and the magmatic-hydrothermal alteration it hosts seems to be exclusively at depths greater than 7.5 km.

The deep (> 5 km) environment of intrusion-related deposits (Thompson et al., 1999; Baker, 2002) is the best analogue to the conditions of pluton-hosted mineralization at Cherry Creek, although the conditions likely overlap with those of the porphyry root environment. Under the high lithostatic pressure prevailing at the depths of the Cherry Creek pluton, the phyllic, greisen, and sericite-chlorite alteration that occur along faults within the pluton and in the surrounding rocks might be the result of mainly passive, much less focused release of a magmatic-hydrothermal fluid (Harris and Golding, 2002; Pirajno and Bentley, 1985; Thompson et al., 1999), yielding an intrusion-related elemental signature in the surrounding veins and alteration. These processes are evident in the intrusion-related deposits of the Pine Creek tungsten district in the Sierra Nevada batholith of California which contains quartz monzonite with myrmekite and anastomosing granoblastic quartz interpreted as the gradual, nonexplosive release of magmatic fluids that in a shallower porphyry Cu environment might result in stockwork quartz veining, brecciation, and mineralization (Newberry, 1982; Meinert, 1997). The foliated and cataclastic nature of quartz veins and phyllic alteration along the Salvi fault that carry spotty Au values are similar to those described in the ore zones of the Fairbanks district (McCoy et al., 1997), suggesting that deformation and mineralization processes in the deepest levels of Cherry Creek were similar to those of intrusion-related Au deposits.

In terms of geochemistry, intrusion-related systems are characterized by low-sulfide, Bi-W-As-Mo-Te-Sb ± Sn geochemical signatures and restricted or weak alteration footprints at depth associated with carbonic hydrothermal fluids (Lang and Baker, 2001). Zonation in the intrusion-related deposits is pronounced, with W, Mo, Sn, Bi, Au occurring in the intrusive

center, zoned outward to peripheral Au, As, Sb, and distal Zn, Pb, and Ag at 2-5 km from the intrusion (Thompson and Newberry, 2000). Some intrusion-related deposits in the Tombstone Belt, Yukon (eg. Brewery Creek and True North) have distal-disseminated Au deposits sharing alteration and geochemical characteristics of Carlin-type deposits (Thompson et al., 1999). Bi is commonly closely associated with Au in the plutonic and pluton-proximal (<1 km) environment in intrusion-related systems and often occurs with molybdenite and scheelite (e.g. Dublin Gulch), although spotty Bi values (>10ppm) can locally occur in the distal environment. There is commonly a close contemporaneity between intrusions and mineralization in intrusion-related deposits (Thompson and Newberry, 2000). These geochemical characteristics are widespread in the deepest deposits at Cherry Creek, which are distinguished by greisen, phyllic, and sericite-chlorite-carbonate alteration assemblages that have been dated by this study to closely approximate the early stages of the CCP. The intrusion-hosted mineralization signature at Cherry Creek includes Ag, Bi, Pb, Mo, Sn, Sb, Au, As, and Te, although the distribution of these enrichments is spotty and not well constrained. It is likely that while some of these phases strongly resemble intrusion-related Au deposits (e.g. Fairbanks Alaska, McCoy et al., 1997; Lang and Baker, 2001), other processes were also at play.

Outboard of the pluton but at the same structural depth are the quartzite and minor phyllite-hosted veins of the McCoy Creek polymetallic veins (MCPV), which flank the CCP to the northeast and southwest at an inferred paleodepth of 7-8 km. The coarse-grained nature of the MCPV, their “intrusion-related” geochemical signature of Au-Ag-As-Bi-Mo-Pb-Sb-Sn-Te, and their persistence along strike and down-dip within their preferred quartzite host suggests that they were emplaced lateral to and by similar hydrothermal fluids to those that affected alteration in the CCP. The spatial and temporal relationships evidenced by the ~38 Ma MCPV-

mineralized dikes and the continuity of ~38 Ma mineralization between the quartz monzonite-hosted Maryanne deposit and the quartzite-hosted Flagstaff deposit are further evidence of their magmatic-hydrothermal origin.

Much in the same way that the massive Prospect Mountain Quartzite (PMQ) impeded the ascent of the Cherry Creek pluton, the thick, impermeable quartzite was also an effective barrier to hydrothermal fluids. Localized zones of secondary permeability, such as those found along the Exchequer fault zone that cut the brittle quartzite, were critical for channeling hydrothermal fluids through fractures and in some cases, along dike margins between paleodepths of 6-7 km. Dilatant movement along the Exchequer fault is evident in the dike-filled strands that are found in Exchequer Canyon and at the Geneva mine in upper El Rey Canyon, and demonstrates that the Exchequer fault was open and likely active during Eocene magmatism around 38 Ma. The same strands were obviously also active after dike emplacement, based on the widespread fracturing and faulting observed in the dikes and surrounding quartzite, and allowed for alteration and mineralization by hydrothermal fluids that enriched the rock in Ag-Au-Pb-Zn-Cu-As-Sb-Mo at least over a 1250 m interval between the Exchequer and Geneva deposits (Figure 46). Much of the intrusion-related signature is retained, especially in As-Sb-Pb, although the Exchequer mineralization is differentiated from the MCPV in its lower sulfide contents and sporadic and generally sub-ppm values of Bi-Sn-Te.

In the stratiform carbonate replacement deposits that abut the Exchequer and Black Metal faults at paleodepths of ~4-5 km, the associations between igneous rocks and hydrothermal mineralization are less pronounced. Although the deposits occur with small sericite-chlorite-pyrite altered 38.2 Ma dikes in areas of dense fracturing there is no demonstrable zonation around the dikes. Instead, the characteristics of these deposits are

indicative of distal hydrothermal mineralization, as they are overwhelmingly siliceous, contain relatively little copper, and are structurally controlled but lack strong zonation. Most likely, these bodies are the distal expressions of a Zn-Pb-Ag system related to the mineralization on the Exchequer fault. The few breccia bodies that do exist in the carbonate replacement deposits at Cherry Creek do not bear many similarities to the explosive breccia pipes detailed in the upper porphyry environment (Megaw et al., 1998; Meinert, 1982). Instead, the breccias seem to be nearly flat structural intersections (in terms of their pre-tilt orientation) that may have had increased porosity and permeability and allowed for more fluid circulation along the stratiform horizon. The breccias are mostly quartz-matrix mosaics, and the dominance of jasperoid suggests that hydrothermal fluids that cooled below ~300˚ were responsible for the dissolution of the Swasey Limestone beneath the lithologic contact due to the opposing solubilities between quartz and calcite (Barton et al., 2000). The clasts of retrograde skarn that occur in the breccias may also be related to the silicification, but the relict pyroxene amid retrograde chlorite and amphibole alteration signifies temperature conditions of 400˚ or more during mineralization (Meinert, 1997). Whether the skarn reactions represent a separate pulse of fluid is unknown, although further investigation focused on identifying zones of high-temperature alteration and high-angle structural intersections could provide information on the nature and architecture of any unexposed high-temperature mineralization. The carbonate replacement deposits bear some geochemical similarities to the Exchequer veins, as they are characterized by Ag-Pb-Zn-W-Cu-Mn-Ba-Sb-As and inconsistent Mo-Bi enrichments, but are differentiated by their lack of Au and abundance of W. This change in geochemistry is likely due to the different depositional mechanisms, with neutralization and cooling of the hydrothermal fluid leading to chloride-

complex destabilization acting as the dominant driver for deposition in the carbonate-hosted deposits.

The structural and lithologic relationships at the TiCup-Exchequer zone are echoed in the hanging wall of the Black Metal fault, where the same general geologic setting exists at its intersection with the Dunderberg Shale – Orr Limestone brought nearly into line with the stratigraphically deeper Wheeler Shale – Swasey Limestone contact by the motion of the Black Metal fault. In this way, the Dunderberg – Orr contact inhabits two structural levels in the Cherry Creek study area and provides an opportunity to test the influence of stratigraphic position versus structural depth as an agent of hydrothermal control. The Dunderberg-Orr contact on the north side of the Black Metal fault is roughly in line with the TiCup horizon, with an inferred paleodepth of 4 – 5 km, and is known as the Motherlode zone. The Dunderberg-Orr contact on the south side of the Black Metal fault is stratigraphically 1500 m above the TiCup, with an inferred paleodepth of 2.5 – 3.5 km, and is referred to as the Flint Canyon zone. The mode of mineralization in both cases is controlled largely by bedding-parallel geometries with subsidiary control provided by steep, NW-trending cross faults. Both are marked by the presence of jasperoid and polyphase jasperoid breccias, and both are controlled by the Black Metal fault. Despite these similarities, a few differences also exist. In the field, the most striking of these differences is the presence of argillic alteration in the Flint Spring Canyon zone. Argillic alteration is widespread but typically most intense in the immediate vicinity of jasperoids, particularly along the base of the Dunderberg Shale that is also marked by jasperoidal alteration of the underlying Orr Limestone. Argillization affected the Dunderberg as well as northwest-striking felsic to intermediate dikes, most of which have also experienced faulting and strong oxidation. In contrast, the Motherlode zone is essentially devoid of argillic alteration. Within

the Motherlode zone, the Dunderberg Shale is poorly exposed but unaltered, and the few dacite dikes that exist in the area are partially altered to sericite and pyrite. The other substantial difference concerns the geochemistry of the two areas. In terms of metals, the Motherlode horizon has much of the same base-metal-rich signature as the TiCup horizon. The jasperoids at Flint Spring Canyon share enrichments in Mn, Ba, As, Li, Sb, and Ag with those in the same strata at the Motherlode, but Flint Canyon jasperoids contain a much higher Au:Ag ratio and significantly less base metals, of which Zn is the most abundant. These effects are likely the result of hydrothermal zonation reflecting the 1500 m difference in paleo-depth between the two deposits formed in the same strata at 4 - 5 km and 2.5 - 3.5 km but on opposite sides of the Black Metal fault.

Comparable zonation could exist between mineralization in the Cherry Creek district and in the Limousine Butte gold deposits to its immediate southwest in the southern Cherry Creek Range. Limousine Butte is a previously explored Carlin-type district, with a historical production of 84,000 oz Au (60,000 oz recovered) at the Golden Butte mine in the 1980s (Wilson et al., 1994) and an additional inventory of 670,000 oz Au in at least six deposits spanning 65 mi^2 (Everson et al., 2005). The Limousine Butte deposits are characterized by the abundance of Au-bearing jasperoid, as well the presence of rocks affected by widespread dolomitization, argillization, and decalcification that have experienced enrichments in Au, As, Sb, Tl, and Hg. The jasperoids have fault and stratigraphic controls and occur mainly along certain lithologic contacts in Devonian and Mississippian rocks that follow south and southwest trends.

About 10 km to the south of the Golden Butte mine, the Butte Valley Cu-Mo porphyry intrudes Pennsylvanian rocks beneath ~500 m of Tertiary cover and is interpreted to be Mesozoic in age (Branham and Brown, 2001), however the presence of mineralized Eocene

dikes in the Limousine Butte area precludes the possibility that Carlin-type mineralization is related to the Mesozoic intrusive activity (Everson et al., 2005). Many similarities exist between the Limousine Butte deposits and the Flint Spring Canyon occurrence described in this study. In addition to the structural controls and auriferous jasperoid and argillic alteration that are characteristic of both, a similar signature of Au, Ag, As, Sb, Tl, and Hg is also present. Spotty jasperoid and dolomite alteration exists between Flint Springs Canyon to Cherry Creek Canyon, and it is likely that such mineralization is continuous between the two areas. If the deposits of the Limousine Butte area formed contemporaneously with the deposits elsewhere in the Cherry Creek area, they represent the shallowest mineralized Eocene structural levels at Cherry Creek. Based on stratigraphic relationships, the Limousine Butte deposits are hypothesized to have formed at depths of less than 2.5 km, and possibly as shallow as 500 m in the case of the Golden Butte orebody. These conditions mirror those of other Carlin-type deposits in eastern Nevada, such as those at Alligator Ridge in the southern Ruby Mountains (Nutt and Hofstra, 2003).

Implications for Carlin-Type Deposits

The Limousine Butte deposits and to some extent the Flint Canyon occurrence described in this paper have some characteristics consistent with Carlin-type deposits elsewhere in Nevada. Their relationship to igneous rocks at Cherry Creek is clearly distal, as evidenced by the 5-8 km of intervening strata that reflect the differences in paleodepth between the Cherry Creek pluton and the overlying disseminated Au deposits. In the classic Carlin-type districts, a spatial and temporal link between ore formation and Eocene plutonism has been hypothesized (Ressel and Henry, 2006) but not conclusively proven. Aeromagnetic anomalies within the districts and the occurrence of rhyolite dikes in many Carlin-type deposits (e.g. Beast, Ressel et al., 2000)

generally preclude the tops of plutons from being deeper than ~8-10 km paleodepth, although exhumation and erosion have not yet revealed these deep crustal levels in those districts. The fact that many Carlin-type deposits yield ages contemporaneous with magmatism (Hall et al., 2000; Muntean et al., 2011) is further evidence that the intrusions coincided with regional thermal anomalies that drove circulation of hydrothermal fluids. Some deep-magmatic models suggest that the ore fluids themselves may have been sourced from the intrusions, although a lack of evidence exists for fluid cooling or zonation at the km-scale in the conduits explored beneath the Carlin-type deposits (Cline et al., 2005). These fluids are hypothesized to have been sourced from ~10-km-deep reservoirs at the tops of plutons that had docked at the brittle ductile-transition by ascending along extensional Eocene faults from depths, well below those of typical porphyry systems (Muntean et al., 2011).

If the Exchequer and Black Metal faults of the central Cherry Creek Range are the structures controlling Carlin-type mineralization in the Limousine Butte district, as it has been hypothesized (Everson et al., 2005), then the high-temperature quartz veins, skarns, and polymetallic jasperoid deposits that lie along them likely represent the roots of the Carlin-type system that formed in the epizonal Eocene environment of the Cherry Creek Range. These faults were clearly active in the Eocene, signifying that localized faulting was active during the emplacement of the extensive Cherry Creek pluton.

Conclusions

The geology of the Cherry Creek district is characterized by a west-dipping monocline composed of more than 8 km of strata, including a deep-seated pluton that intrudes Precambrian phyllites and quartzites on its east side, thick basal Cambrian quartzites overlain by Cambrian through Permian shales, carbonates, and dolomites in the center, and volcanic rocks that lie conformably atop a Pennsylvanian-Permian paleosurface on its west side. ^{238}U-^{206}Pb zircon geochronology in this study constrains igneous activity in the Cherry Creek district to the late Eocene, with major granitic plutonism and minor dike emplacement taking place between 38.2 Ma and 35.9 Ma and a late episode of dike emplacement taking place contemporaneously with local rhyolite volcanism (McKee et al., 1973) between 35.9 Ma and 34.7 Ma.

The ore deposits of Cherry Creek are zoned with respect to their proximity to the Cherry Creek pluton and with respect to their inferred paleodepth or Eocene structural level. Fault-controlled hydrothermal activity taking place along a dominant southeast-dipping axis at the margins of the pluton resulted in Sn-Bi-Sb-As-(Au-Ag-Mo-W)-bearing quartz veins accompanied by phyllic and greisen alteration, at least some of which occurred during the earliest phases of plutonism around 38.1 Ma based on ^{187}Re - ^{187}Os analyses of molybdenite and ^{40}Ar - ^{39}Ar analyses of sericite. Quartzite-hosted polymetallic quartz veins occurring outboard of the pluton but at the same 7-8 km structural level localize Au-Ag-Pb-Zn-Cu-As-Sb-(Sn-Bi-Mo-W) mineralization that occur in small, discontinuous faults and along dike margins, many of which have experienced sericite-chlorite-pyrite alteration that has been dated to the late Eocene and may have occurred as late as 37.8 Ma based on ^{40}Ar - ^{39}Ar sericite geochronology. At structural levels of 6 - 7 km paleodepth and above the roof of the pluton, the range-scale, high-displacement Exchequer fault hosts lensoidal dikes and breccia bodies with Ag-Au-Pb-Zn-Cu-As-

Sb quartz mineralization. Intersections between the Exchequer fault and lithologic contacts in Middle Cambrian carbonate and shale strata are brecciated and strongly silicified, with traces of sulfide-bearing chlorite-amphibole-pyroxene skarn and sphalerite-galena massive sulfide occurring as clasts in the breccia. Quartz veins and siliceous breccia fill bearing Ag-Pb-Zn-W-Cu-Sb-(As-Mo) bleed out into jasperoid alteration from the structural intersections, forming a series of stratiform ore bodies at paleodepths of 4-5 km. Along the western edge of the central Cherry Creek Range, jasperoid formation is widespread and accompanied by localized base-metal and sulfide-poor Au-Ag-As-(Sb-Mo-Tl-W) mineralization, argillic alteration, and strong oxidation along lithologic contacts in Upper Cambrian carbonate and shale strata at paleodepths of 3-3.5 km. In the uppermost 2.5 km of strata, Carlin-type deposits of the Limousine Butte group manifest in Mississippian, Devonian, and Pennsylvanian rocks as stratigraphically controlled jasperoid and zones of decalcification and argillic alteration associated with Au-Ag-As-Sb-Tl-Hg (Everson et al., 2005).

The geochronological, geochemical, petrographic, and field data presented in this thesis define the central Cherry Creek Range as a district of varied Eocene magmatism and hydrothermal mineralization that occurred under a range of conditions. The deep-seated plutonism and intrusion-related mineralization evidenced by this work signify that hydrothermal activity was widespread at deep structural levels during at least the early stages of emplacement of the Cherry Creek pluton. Evidence of the transmission of these fluids into overlying rocks is recorded in the mesothermal vein and replacement deposits at intermediate structural levels, which occur along range-scale faults. The epizonal portion of the Cherry Creek system carries the signature of a distal environment, in which the same conduits localizing mineralization at depth are associated with jasperoidal deposits that verge on Carlin-type in vicinity of the

paleosurface. This study on the central Cherry Creek Range demonstrates the continuum of zoned magmatic-hydrothermal deposits that have been hypothesized in previous discussions of Eocene Nevada, particularly in relation to the enigmatic class of Carlin-type deposits but lends refinement from previous studies in better defining the batholithic nature of Eocene plutons that drove hydrothermal circulation and the types of deposits that occur above deep-seated intrusions. Although the characteristics of the central Cherry Creek Range are in many ways unique relative to other districts, the implications of the Cherry Creek system in the scope of Nevada geology are more broadly significant

References

Adair, D.H., 1961, Geology and Ore Deposits of the Cherry Creek Mining District, White Pine County, NV: University of Utah, 133 p.

Adair, D.H., 2005, Oligocene batholith in east-central Nevada, *in* Abstracts with Programs-Geological Society of America, p. 419–419.

Adair, D.H., 1983, Silver Prospects on the TiCup and Fillmore Mines Property, Cherry Creek, Nevada.

Armstrong, R.L., 1970, Geochronology of Tertiary igneous rocks, eastern Basin and Range Province, western Utah, eastern Nevada, and vicinity, U.S.A.: Geochimica et Cosmochimica Acta, v. 34, p. 203–232.

Armstrong, R.L., 1966, K-Ar dating using neutron activation for Ar analysis: granitic plutons of the eastern Great Basin, Nevada and Utah: Geochimica et Cosmochimica Acta, v. 30, p. 565–600.

Armstrong, R.L., 1968, Sevier orogenic belt in Nevada and Utah: Bulletin of the Geological Society of America, v. 79, p. 429–458.

Axen, G.J., Taylor, W.J., and Bartley, J.M., 1993, Space-time patterns and tectonic controls of Tertiary extension and magmatism in the Great Basin of the western United States: Geological Society of America Bulletin, v. 105, p. 56–76.

Baker, T., 2002, Emplacement depth and carbon dioxide-rich fluid inclusions in intrusion-related gold deposits: Economic Geology, v. 97, p. 1111–1117.

Barnes, C.G., Burton, B.R., Burling, T.C., Wright, J.E., and Karlsson, H.R., 2001, Petrology and Geochemistry of the Late Eocene Harrison Pass Pluton, Ruby Mountains Core Complex, Northeastern Nevada: Journal of Petrology, v. 42, p. 901–929.

Barton, M.D., Dilles, J.H., Einaudi, M.T., and Johnson, D.A., 2000, Contrasting Styles of Intrusion-Associated Hydrothermal Systems: Society of Economic Geologists Guidebook Series, v. 32.

Best, M.G., and Christiansen, E.H., 1991a, Limited extension during peak Tertiary volcanism, Great Basin of Nevada and Utah: Journal of Geophysical Research: Solid Earth, v. 96, p. 13509–13528.

Best, M.G., and Christiansen, E.H., 1991b, Limited extension during peak Tertiary volcanism, Great Basin of Nevada and Utah: Journal of Geophysical Research, v. 96, p. 13509.

Branham, A.D., and Brown, S., 2001, Tertiary Slideblocks: Butte Valley Copper Gold Porphyry, Cherry Creek Range, White Pine Co., Nevada.: Geological Society of Nevada Special Publication, v. 33, p. 335–340.

Cline, J.S., Hofstra, A.H., Muntean, J.L., Tosdal, R.M., and Hickey, K. a., 2005, Carlin-Type Gold Deposits in Nevada: Critical Geologic Characteristics and Viable Models: Economic Geology, v. 100th Anni, p. 451–484.

Colgan, J.P., Howard, K.A., Fleck, R.J., and Wooden, J.L., 2010, Rapid middle Miocene extension

and unroofing of the southern Ruby Mountains, Nevada: Tectonics, v. 29.

Dickinson, W.R., 2006, Geotectonic evolution of the Great Basin: Geosphere, v. 2, p. 353–368.

Druschke, P., Hanson, a. D., and Wells, M.L., 2009, Structural, stratigraphic, and geochronologic evidence for extension predating Palaeogene volcanism in the Sevier hinterland, east-central Nevada: International Geology Review, v. 51, p. 743–775.

Everson, C., Brown, S., Caldwell, D., Hibdon, Z., and Branham, A., 2005, Geology and mineralization of the Limousine Butte gold deposits , White Pine County , Nevada: , p. 419–430.

Fritz, W.H., 1968, Geologic Map and Sections of the Southern Cherry Creek and Northern Egan Ranges, White Pine County, NV.

Fritz, W.H., 1960, Structure and Stratigraphy of the Northern Egan Range, White Pine County, Nevada: University of Washington, 147 p.

Glazner, A.F., Bartley, J.M., Coleman, D.S., Gray, W., and Taylor, R.Z., 2004, Are plutons assembled over millions of years by amalgamation from small magma chambers? Gsa Today, v. 5173, p. 4–10.

Grant, J.A., 1986, The isocon diagram-a simple solution to Gresens' equation for metasomatic alteration.: Economic Geology, v. 81, p. 1976–1982.

Groves, W.D., 1982, Report on Silver-Gold Properties of Cherry Creek, NV. Internal Report, Goldera Resources Group.

Hall, C.M., Kesler, S.E., Simon, G., and Fortuna, J., 2000, Overlapping Cretaceous and Eocene Alteration, Twin Creeks Carlin-Type Deposit, Nevada: Economic Geology, v. 95, p. 1739–1752.

Harris, A.C., and Golding, S.D., 2002, genesis of porphyry Cu deposits New evidence of magmatic-fluid – related phyllic alteration : Implications for the genesis of porphyry Cu deposits: , p. 335–338.

Heard, A., 1881, Report on Tikup and Geneva Mines.Internal Report, The Tikup and Geneva Mining Companies.

Hill, J.M., 1916, Notes on some mining districts in eastern Nevada: U.S. Geological Survey Bulletin 648, 212 p.

Hill, T.J., 2016, Time-Space Relationships between Sediment-Hosted Gold Mineralization and Intrusion-Related Polymetallic Mineralization at Kinsley Mountain, NV.

Hofstra, A.H., and Cline, J.S., 2000, Characteristics and models for carlin-type gold deposits: Reviews in Economic Geology, v. 13, p. 163–220.

Holmes, G.H., 1950, Investigation of the Cherry Creek Tungsten District, White Pine County, Nevada.

Hose, R.K., Blake, M.C., and Smith, R.M., 1976, Geology and Mineral Rescources of White Pine County, Nevada: Nevada Bureau of Mines and Geology Bulletin, v. 85, p. 105.

Kelley, S., 2002, K-Ar and Ar-Ar Dating: Reviews in Mineralogy and Geochemistry, v. 47, p. 785–818.

Lang, J.R., and Baker, T., 2001, Intrusion-related gold systems: The present level of understanding: Mineralium Deposita, v. 36, p. 477–489.

Long, S.P., and Soignard, E., 2016, Shallow-crustal metamorphism during Late Cretaceous anatexis in the Sevier hinterland plateau: Peak temperature conditions from the Grant Range, eastern Nevada, U.S.A.: Lithosphere, v. c, p. L501.1.

Macdonald, W.D., Palmer, H.C., and Hayatsu, A., 1992, Egan Range Volcanic Complex, Nevada: geochronology, paleomagnetism, and magnetic fabrics: Physics of the Earth and Planetary Interiors, v. 74, p. 109–126.

McCoy, D., Newberry, R.J., Layer, P., DiMarchi, J.J., Bakke, A., Masterman, S.J., and Minehane, D.L., 1997, Plutonic-related gold deposits of interior Alaska: Economic Geology Monograph, v. 9, p. 191–241.

Mckee, E.H., and Moring, B.C., 1996, Chapter 6 Cenozoic Mineral Deposits and Cenozoic Igneous Rocks of Nevada.

McKee, E.H., Silberman, M.L., Marvin, R.E., and Obradovich, J.D., 1973, A summary of radiometric ages of Tertiary volcanic rocks in Nevada and eastern California. Part I: Central Nevada.

Megaw, P.K.M., Ruiz, J., and Titley, S.R., 1998, High-temperture, carbonate-hosted Ag-Pb-Zn-(Cu) deposits of northern Mexico: Economic Geology, v. 83, p. 1856–1885.

Meinert, L.D., 1997, Application of skarn deposit zonation models to mineral exploration: Exploration and Mining Geology, v. 6, p. 185–208.

Meinert, L.D., 1982, Skarn, manto, and breccia pipe formation in sedimentary rocks of the Cananea mining district, Sonora, Mexico.: Economic Geology, v. 77, p. 919–949.

Miller, E.L., and Gans, P.B., 1989, Cretaceous crustal structure and metamorphism in the hinterland of the Sevier thrust belt, western US Cordillera: Geology, v. 17, p. 59–62.

Misch, P., and Hazzard, J.C., 1962, Stratigraphy and metamorphism of Late Precambrian rocks in central northeastern Nevada and adjacent Utah: AAPG Bulletin, v. 46, p. 289–343.

Morabbi, M., 1980, The Geology and Ore Deposits of Cherry Creek Pluton, White Pine County, Nevada: Idaho State University, 110 p.

Muntean, J.L., Cline, J.S., Simon, A.C., and Longo, A. a., 2011, Magmatic–hydrothermal origin of Nevada's Carlin-type gold deposits: Nature Geoscience, v. 4, p. 122–127.

Muntean, J.L., and Einaudi, M.T., 2001, Porphyry-epithermal transition: Maricunga belt, Nothern Chile: Economic Geology, v. 96, p. 743–772.

Newberry, R.J., 1982, Tungsten-bearing skarns of the Sierra Nevada. I. The Pine Creek mine, California.: Economic Geology, v. 77, p. 823–844.

Nutt, C.J., and Hofstra, A.H., 2003, Alligator ridge district, East-Central Nevada: Carlin-type gold

mineralization at shallow depths: Economic Geology, v. 98, p. 1225–1241.

Park, C.F., 1957, The problem of vertical zoning: Economic Geology, v. 52, p. 477–481.

Pirajno, F., and Bentley, P., 1985, Greisen-related scheelite, gold and sulphide mineralisation at Kirwans Hili and Bateman Creek, Reefton district, Westland, New Zealand: New Zealand journal of geology and …, v. 28, p. 97–109.

Poole, F.G., Stewart, J.H., Palmer, A.R., Sandberg, C.A., Madrid, R.J., Ross, R.J., Hintze, L.F., Miller, M.M., and Wrucke, C.T., 1993, , Latest Precambrian to latest Devonian time: Development of a continental margin: Geological Society of America Bulletin, v. The Cordil, p. 9–56.

Ressel, M.W., and Henry, C.D., 2006, Igneous Geology of the Carlin Trend , Nevada : Development of the Eocene Plutonic Complex and Significance for Carlin-Type Gold Deposits: Economic Geology, v. 101, p. 347–383.

Ressel, M.W., Noble, D.C., Henry, C.D., and Trudel, W.S., 2000, Dike-hosted ores of the beast deposit and the importance of the Eocene magmatism in gold mineralization of the Carlin trend, Nevada: Economic Geology, v. 95, p. 1417–1444.

Runyon, S.E., Steele-MacInnis, M., Seedorff, E., Lecumberri-Sanchez, P., and Mazdab, F.K., 2017, Coarse muscovite veins and alteration deep in the Yerington batholith, Nevada: insights into fluid exsolution in the roots of porphyry copper systems: Mineralium Deposita, v. 52, p. 463–470.

Schrader, F.C., 1931, Spruce Mountain and Cherry Creek Districts. University of Nevada Bulletin v. 25 No. 1.

Seedorff, E., Barton, M.D., Stavast, W.J.A., and Maher, D.J., 2008, Root zones of porphyry systems: Extending the porphyry model to depth: Economic Geology, v. 103, p. 939–956.

Thompson, J.F.H., and Newberry, R.J., 2000, Gold Deposits Related to Reduced Granitic Intrusions: , p. 377–400.

Thompson, J.F.H., Sillitoe, R.H., Baker, T., Lang, J.R., and Mortensen, J.K., 1999, Intrusion-related gold deposits associated with tungsten-tin provinces: Mineralium Deposita, v. 34, p. 323–334.

Thorman, C.H., and Peterson, F., 2004, The Middle Jurassic Elko Orogeny - A Major Tectonic Event in Nevada-Utah: Search and Discovery.

Whitney, J.W., 1972, Geology of the Heusser Mountain Pluton, White Pine County, Nevada: University of Nebraska at Lincoln.

Wilson, D.J., Christiansen, E.H., and Tingey, D.G., 1994, Geology and Geochemistry of the Golden Butte Mine -- A Small Carlin-Type Gold Deposit in Eastern Nevada: BYU Geology Studies, v. 40.

Woodward, L.E., 1967, Stratigraphy and Correlation of Late Precambrian Rocks of Pilot Range, Elko County, Nevada and Box Elder County, Utah.

Zoback, M.L., McKee, E.H., Blakely, R.J., and Thompson, G.A., 1994, The northern Nevada rift: regional tectono-magmatic relations and Middle Miocene stress direction: Geological Society of America Bulletin, v. 106, p. 371–382.

Appendices

Appendix A. Concordia and Weighted Mean Diagrams

Sample	Unit	206Pb/238U Age	UTM E	UTM N
10107	quartz monzonite	37.89 +- 0.28	678259	4419595
10084	quartz monzonite	37.76 +- 0.30	677777	4417782
10111	quartz monzonite	37.67 +- 0.30	677788	4417783
10125	quartz monzonite	37.23 +- 0.35	679678	4419830
10060	quartz monzonite	36.72 +- 0.30	677922	4417551
10093	quartz monzonite	36.62 +- 0.26	678491	4417561
10059	quartz monzonite	36.18 +- 0.31	677928	4417902
10102	dacite	38.20 +- 0.50	679107	4422704
10079	dacite	35.59 +- 0.28	680584	4420534
10080	dacite	35.44 +- 0.41	680558	4420545
10129	rhyolite	35.44 +- 0.36	676322	4422858
10108	rhyolite	35.07 +- 0.34	677963	4417623
10091	rhyolite	35.26 +- 0.37	678692	4417148
10053	tonalite	37.33 +- 0.34	682857	4424499
10075	monzodiorite	40.16 +- 0.93	682700	4423999

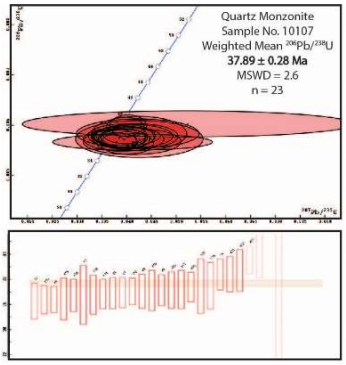
Quartz Monzonite
Sample No. 10107
Weighted Mean $^{206}Pb/^{238}U$
37.89 ± 0.28 Ma
MSWD = 2.6
n = 23

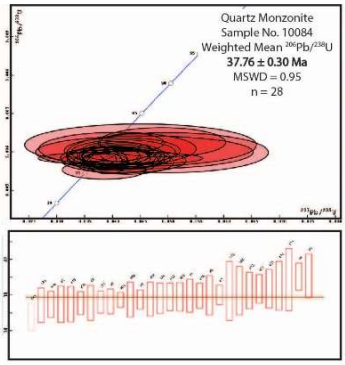
Quartz Monzonite
Sample No. 10084
Weighted Mean $^{206}Pb/^{238}U$
37.76 ± 0.30 Ma
MSWD = 0.95
n = 28

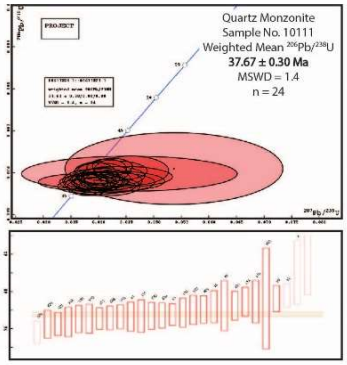
Quartz Monzonite
Sample No. 10111
Weighted Mean $^{206}Pb/^{238}U$
37.67 ± 0.30 Ma
MSWD = 1.4
n = 24

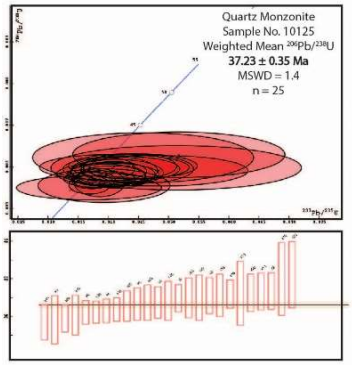
Quartz Monzonite
Sample No. 10125
Weighted Mean $^{206}Pb/^{238}U$
37.23 ± 0.35 Ma
MSWD = 1.4
n = 25

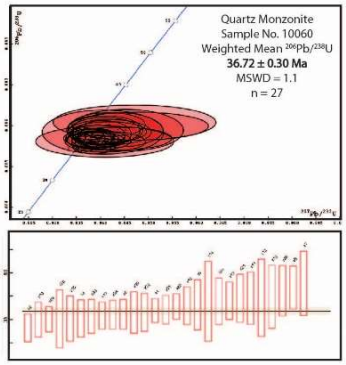
Quartz Monzonite
Sample No. 10060
Weighted Mean $^{206}Pb/^{238}U$
36.72 ± 0.30 Ma
MSWD = 1.1
n = 27

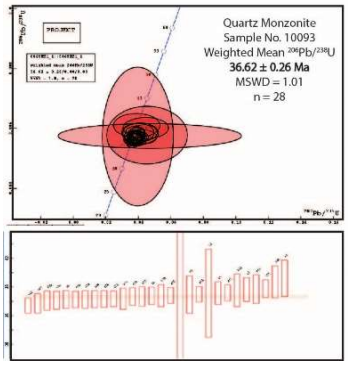
Quartz Monzonite
Sample No. 10093
Weighted Mean $^{206}Pb/^{238}U$
36.62 ± 0.26 Ma
MSWD = 1.01
n = 28

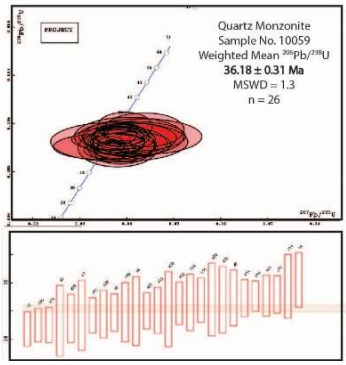
Quartz Monzonite
Sample No. 10059
Weighted Mean $^{206}Pb/^{238}U$
36.18 ± 0.31 Ma
MSWD = 1.3
n = 26

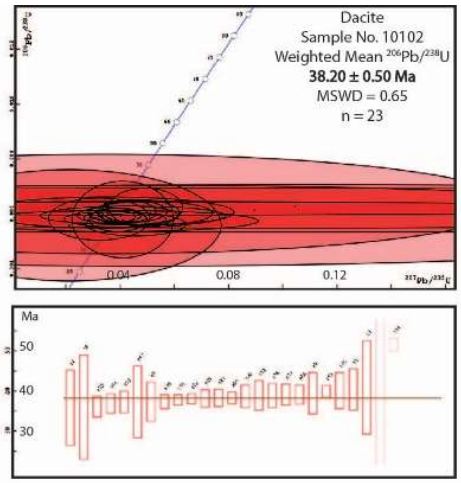
Dacite
Sample No. 10102
Weighted Mean $^{206}Pb/^{238}U$
38.20 ± 0.50 Ma
MSWD = 0.65
n = 23
Ma

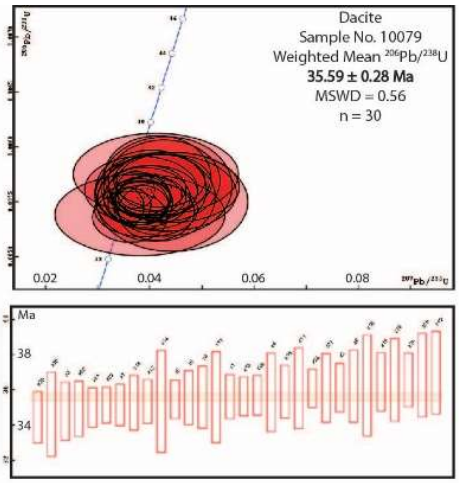
Dacite
Sample No. 10079
Weighted Mean $^{206}Pb/^{238}U$
35.59 ± 0.28 Ma
MSWD = 0.56
n = 30
Ma

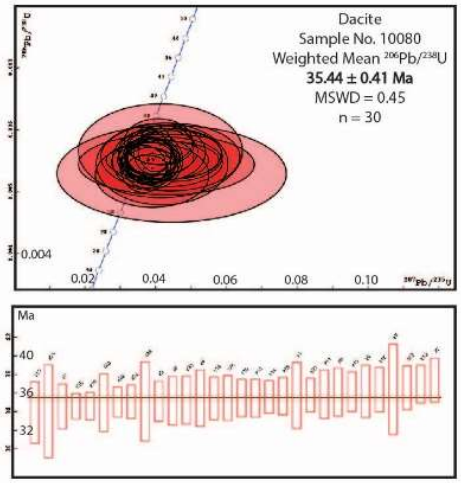
Dacite
Sample No. 10080
Weighted Mean $^{206}Pb/^{238}U$
35.44 ± 0.41 Ma
MSWD = 0.45
n = 30
Ma

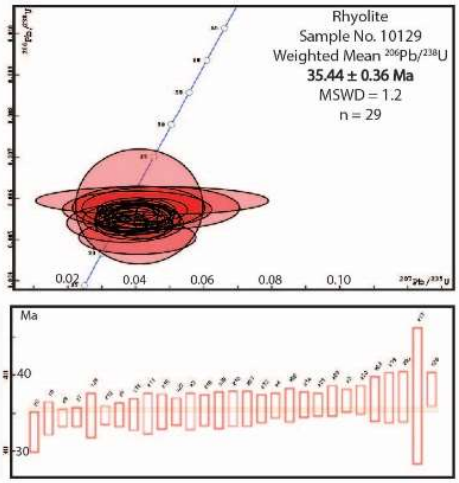
Rhyolite
Sample No. 10129
Weighted Mean $^{206}Pb/^{238}U$
35.44 ± 0.36 Ma
MSWD = 1.2
n = 29
Ma

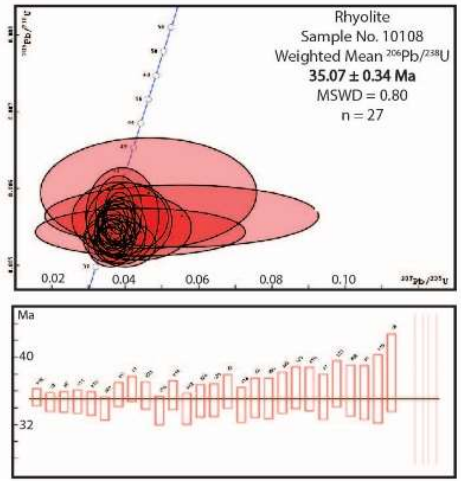
Rhyolite
Sample No. 10108
Weighted Mean $^{206}Pb/^{238}U$
35.07 ± 0.34 Ma
MSWD = 0.80
n = 27
Ma

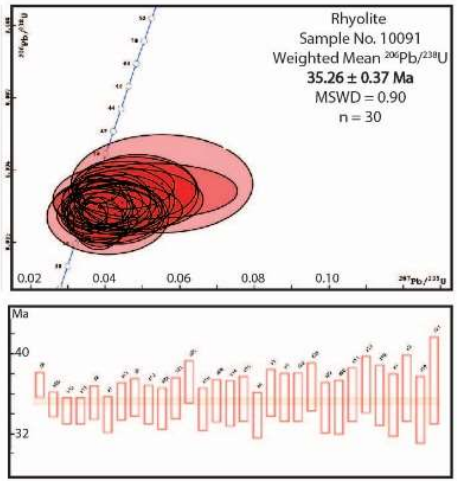
Rhyolite
Sample No. 10091
Weighted Mean $^{206}Pb/^{238}U$
35.26 ± 0.37 Ma
MSWD = 0.90
n = 30
Ma

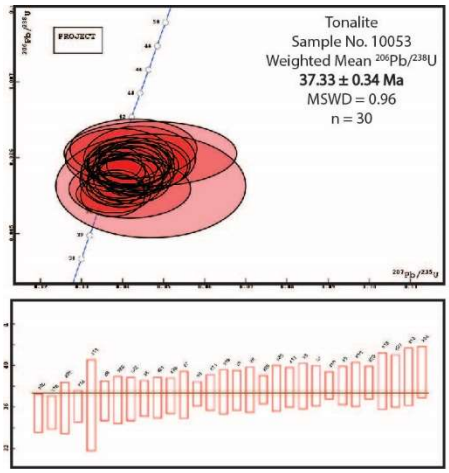
PROJECT
Tonalite
Sample No. 10053
Weighted Mean $^{206}Pb/^{238}U$
37.33 ± 0.34 Ma
MSWD = 0.96
n = 30

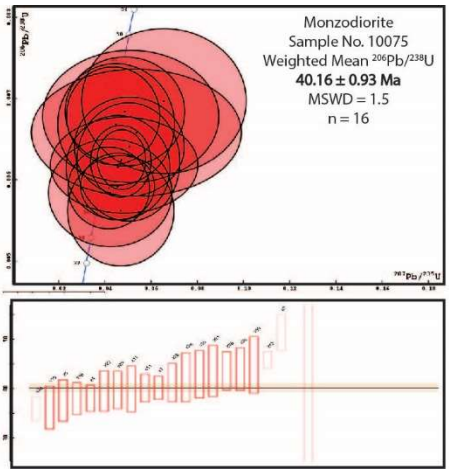
Monzodiorite
Sample No. 10075
Weighted Mean $^{206}Pb/^{238}U$
40.16 ± 0.93 Ma
MSWD = 1.5
n = 16

Mineral	Zrn																		
Sample Name	#10059																		
	Uranium and Thorium			Concordant Scans: Isotopic Ratios							Concordant Scans: Ages								
Analysis Name	U (ppm)	Th (ppm)	U/Th	207Pb/235U	2 sigma	206Pb/238U	2 sigma	207Pb/206Pb	2 sigma	Error Correlation	207Pb/235U	2- sigma	2+ sigma	206Pb/238U	2- sigma	2+ sigma	207Pb/206Pb	2- sigma	2+ sigma
0862AZ1_1	452	138	3.27	0.03869	0.00717	0.00555	0.00039	0.05055	0.00965	0.11	38.55	7.02	7.00	35.69	2.48	2.47	220.57	441.14	413.90
0862AZ1_2	379	384	0.99	0.03804	0.00844	0.00549	0.00039	0.05024	0.01135	0.10	37.91	8.27	8.24	35.30	2.50	2.50	206.30	412.60	485.88
0862AZ1_3	643	458	1.40	0.03926	0.00695	0.00560	0.00038	0.05086	0.00921	0.13	39.10	6.80	6.77	35.99	2.45	2.45	234.33	446.94	392.92
0862AZ1_4	912	359	2.54	0.03963	0.00580	0.00594	0.00030	0.04837	0.00724	0.10	39.46	5.67	5.65	38.19	1.93	1.93	117.17	234.35	335.35
0862AZ1_5	737	594	1.24	0.03783	0.00592	0.00558	0.00021	0.04916	0.00783	0.04	37.71	5.80	5.79	35.88	1.33	1.33	155.53	311.05	353.05
0862AZ1_6	93	49	1.89	4.18722	0.25572	0.27927	0.00967	0.10874	0.00687	0.21	1671.52	50.68	49.45	1587.69	48.80	48.61	1778.45	117.54	113.08
0862AZ1_7	1880	778	2.42	0.03657	0.00339	0.00540	0.00019	0.04910	0.00466	0.12	36.47	3.32	3.32	34.73	1.23	1.23	152.57	230.36	215.20
0862AZ1_8	271	445	0.61	0.04113	0.01138	0.00574	0.00031	0.05195	0.01461	0.01	40.93	11.13	11.07	36.91	1.97	1.97	283.25	566.50	586.36
0862AZ1_9	325	55	5.95	0.35679	0.04187	0.04599	0.00198	0.05626	0.00675	0.12	309.82	31.58	31.10	289.88	12.20	12.19	462.72	277.58	255.45
0862AZ1_10	1819	575	3.16	0.03887	0.00317	0.00576	0.00017	0.04892	0.00407	0.11	38.72	3.10	3.09	37.04	1.07	1.07	144.17	201.44	189.76
0862AZ1_11	433	326	1.33	0.04369	0.00856	0.00587	0.00035	0.05396	0.01097	0.03	43.42	8.35	8.31	37.74	2.25	2.25	369.48	493.50	427.93
0862AZ1_12	2608	724	3.60	0.03861	0.00351	0.00578	0.00021	0.04842	0.00445	0.16	38.47	3.43	3.42	37.18	1.33	1.33	119.67	223.87	209.56
0862AZ1_13	39	25	1.53	2.04777	0.23248	0.18417	0.00824	0.08064	0.00915	0.19	1131.55	78.97	76.01	1089.70	44.91	44.76	1212.76	231.91	215.59
0862AZ1_14	985	306	3.22	0.03832	0.00522	0.00574	0.00021	0.04840	0.00667	0.08	38.18	5.12	5.10	36.91	1.32	1.32	118.65	237.30	309.93
0862AZ1_15	695	291	2.39	0.03862	0.00606	0.00572	0.00025	0.04894	0.00776	0.09	38.47	5.93	5.91	36.78	1.57	1.58	145.15	290.31	352.36
0862AZ1_16	1668	480	3.48	0.03694	0.00341	0.00545	0.00020	0.04920	0.00461	0.15	36.83	3.34	3.34	35.01	1.26	1.26	157.31	226.92	212.19
0862AZ1_17	2943	582	5.06	0.03661	0.00291	0.00555	0.00019	0.04783	0.00375	0.24	36.51	2.85	2.84	35.69	1.23	1.23	90.94	181.88	180.80
0862AZ1_18	365	93	3.94	0.03981	0.00878	0.00559	0.00033	0.05169	0.01163	0.06	39.64	8.59	8.56	35.91	2.10	2.10	271.58	543.16	478.36
0862AZ1_19	935	581	1.61	0.03829	0.00559	0.00561	0.00026	0.04954	0.00736	0.10	38.15	5.47	5.45	36.04	1.65	1.65	173.47	346.94	329.34
0862AZ1_20	269	153	1.75	0.04050	0.01165	0.00573	0.00040	0.05130	0.01511	0.02	40.31	11.40	11.34	36.80	2.58	2.59	254.13	508.26	615.01
0862AZ1_21	990	684	1.45	0.03878	0.00561	0.00577	0.00023	0.04877	0.00715	0.08	38.64	5.49	5.47	37.07	1.45	1.44	137.03	274.05	327.33
0862AZ1_22	451	149	3.03	0.03715	0.00893	0.00568	0.00023	0.04741	0.01151	0.02	37.04	8.76	8.72	36.53	1.50	1.50	70.03	140.06	531.61
0862AZ1_23	181	123	1.47	0.03841	0.01457	0.00562	0.00041	0.04957	0.01905	0.03	38.27	14.30	14.20	36.13	2.65	2.65	174.75	349.51	791.38
0862AZ1_24	338	256	1.32	0.04071	0.00986	0.00570	0.00031	0.05184	0.01281	0.02	40.51	9.64	9.60	36.61	2.01	2.01	278.43	556.86	521.15
0862AZ1_25	412	301	1.37	0.04097	0.00841	0.00557	0.00026	0.05337	0.01119	0.02	40.77	8.22	8.19	35.79	1.69	1.69	344.51	512.92	442.55
0862AZ1_26	227	99	2.29	0.04327	0.01275	0.00573	0.00037	0.05482	0.01648	0.01	43.02	12.45	12.37	36.80	2.36	2.35	404.77	754.53	610.89
0862AZ1_27	809	221	3.66	0.03828	0.00542	0.00560	0.00020	0.04960	0.00717	0.04	38.15	5.31	5.30	35.99	1.29	1.29	176.13	352.06	320.63
0862AZ1_28	335	135	2.48	0.03527	0.01090	0.00552	0.00027	0.04637	0.01447	0.01	35.20	10.72	10.66	35.47	1.71	1.70	16.64	33.29	675.29
0862AZ1_29	428	32	13.41	0.40580	0.03584	0.05079	0.00209	0.05795	0.00508	0.25	345.85	26.06	25.73	319.35	12.84	12.82	527.95	198.18	186.60
0862AZ1_30	744	326	2.28	0.03713	0.00620	0.00544	0.00018	0.04948	0.00837	0.03	37.02	6.08	6.06	34.99	1.18	1.18	170.71	341.42	372.63

Mineral	Zrn																		
Sample Name	#10060																		
	Uranium and Thorium			Concordant Scans: Isotopic Ratios							Concordant Scans: Ages								
Analysis Name	U (ppm)	Th (ppm)	U/Th	207Pb/235U	2 sigma	206Pb/238U	2 sigma	207Pb/206Pb	2 sigma	Error Correlation	207Pb/235U	2- sigma	2+ sigma	206Pb/238U	2- sigma	2+ sigma	207Pb/206Pb	2- sigma	2+ sigma
0863AZ1_1	1076	209	5.15	0.04019	0.00499	0.00572	0.00016	0.05096	0.00642	0.04	40.01	4.88	4.86	36.77	1.03	1.03	238.87	304.10	278.09
0863AZ1_2	1310	628	2.09	0.03865	0.00445	0.00549	0.00018	0.05106	0.00601	0.06	38.50	4.35	4.34	35.29	1.18	1.18	243.71	283.13	260.44
0863AZ1_3	563	308	1.83	0.04101	0.00838	0.00561	0.00025	0.05299	0.01103	0.02	40.81	8.19	8.15	36.09	1.59	1.59	328.27	510.35	440.70
0863AZ1_4	1123	189	5.94	0.14437	0.04855	0.01648	0.00188	0.06352	0.02182	0.10	136.93	43.54	42.63	105.40	11.94	11.93	725.57	827.43	654.98
0863AZ1_5	1414	789	1.79	0.03811	0.00417	0.00567	0.00020	0.04875	0.00544	0.09	37.98	4.09	4.08	36.45	1.27	1.28	135.60	270.99	252.34
0863AZ1_6	432	120	3.60	0.00000	0.00000	0.00000	0.00000	0.00000	0.00000	0.00	0.00	0.00	0.00	0.00	0.00	0.00	0.00	0.00	0.00
0863AZ1_7	210	133	1.58	0.04711	0.01699	0.00608	0.00043	0.05615	0.02060	0.01	46.74	16.55	16.41	39.10	2.76	2.76	458.39	916.78	724.37
0863AZ1_8	545	261	2.09	0.04176	0.00766	0.00603	0.00029	0.05023	0.00946	0.02	41.54	7.48	7.46	38.75	1.84	1.84	205.62	411.25	410.05
0863AZ1_9	741	272	2.72	0.04058	0.00588	0.00580	0.00033	0.05077	0.00773	0.07	40.39	5.75	5.73	37.26	2.14	2.14	230.19	371.84	333.69
0863AZ1_10	4840	1161	4.17	0.03709	0.00237	0.00560	0.00023	0.04805	0.00319	0.26	36.98	2.32	2.32	35.99	1.50	1.50	101.92	160.97	153.45
0863AZ1_11	456	493	0.93	0.04091	0.00795	0.00589	0.00035	0.05041	0.01016	0.03	40.71	7.77	7.74	37.83	2.24	2.24	213.92	427.84	435.99
0863AZ1_12	282	144	1.96	0.04528	0.01208	0.00589	0.00051	0.05574	0.01516	0.10	44.97	11.76	11.70	37.87	3.30	3.30	441.90	669.92	554.03
0863AZ1_13	394	127	3.10	0.04363	0.00941	0.00590	0.00042	0.05361	0.01186	0.09	43.36	9.17	9.13	37.94	2.70	2.70	354.58	542.44	464.30
0863AZ1_14	197	75	2.64	0.04055	0.01268	0.00584	0.00054	0.05033	0.01608	0.07	40.36	12.41	12.34	37.56	3.43	3.43	210.05	420.10	666.75
0863AZ1_15	1575	1813	0.87	0.03842	0.00444	0.00561	0.00030	0.04966	0.00589	0.17	38.28	4.34	4.33	36.07	1.95	1.95	179.02	289.05	265.54
0863AZ1_16	733	289	2.54	0.03945	0.00584	0.00578	0.00025	0.04948	0.00755	0.04	39.29	5.71	5.70	37.17	1.61	1.61	170.83	341.65	337.87
0863AZ1_17	1369	546	2.51	0.03941	0.00453	0.00565	0.00018	0.05058	0.00593	0.06	39.25	4.43	4.42	36.33	1.16	1.16	221.77	283.03	260.39
0863AZ1_18	428	137	3.13	0.17793	0.09817	0.02150	0.00364	0.06002	0.03425	0.04	166.28	86.44	82.91	137.13	23.00	22.97	604.34	1208.69	1041.26
0863AZ1_19	452	194	2.33	0.04182	0.00778	0.00585	0.00025	0.05183	0.00984	0.02	41.60	7.59	7.56	37.61	1.61	1.61	277.93	466.73	407.97
0863AZ1_20	1091	565	1.93	0.03858	0.00446	0.00577	0.00017	0.04846	0.00572	0.03	38.43	4.36	4.35	37.11	1.09	1.09	121.94	243.87	267.08
0863AZ1_21	403	376	1.07	0.04190	0.00873	0.00584	0.00031	0.05200	0.01115	0.01	41.68	8.52	8.49	37.56	2.00	2.01	285.51	531.22	456.36
0863AZ1_22	1266	486	2.60	0.03690	0.00408	0.00570	0.00025	0.04698	0.00538	0.11	36.79	4.00	3.99	36.62	1.63	1.63	48.14	96.27	262.88
0863AZ1_23	743	517	1.44	0.03976	0.00663	0.00564	0.00023	0.05109	0.00871	0.02	39.59	6.48	6.46	36.28	1.45	1.45	244.97	418.47	370.72
0863AZ1_24	888	476	1.87	0.03890	0.00608	0.00566	0.00019	0.04981	0.00791	0.03	38.75	5.95	5.94	36.41	1.24	1.24	186.22	372.44	350.09
0863AZ1_25	191	96	1.98	0.04090	0.01441	0.00561	0.00038	0.05290	0.01896	0.01	40.71	14.11	14.01	36.05	2.47	2.47	324.33	648.66	725.53
0863AZ1_26	1200	575	2.09	0.03885	0.00487	0.00560	0.00017	0.05029	0.00642	0.04	38.70	4.77	4.76	36.02	1.07	1.07	208.30	310.08	283.13
0863AZ1_27	1898	689	2.76	0.03882	0.00407	0.00573	0.00019	0.04911	0.00509	0.19	38.67	3.99	3.98	36.86	1.22	1.22	152.86	252.43	234.34
0863AZ1_28	220	75	2.92	0.04796	0.01458	0.00599	0.00034	0.05811	0.01792	0.01	47.57	14.17	14.08	38.48	2.15	2.15	533.89	757.93	612.13
0863AZ1_29	541	232	2.33	0.04087	0.00742	0.00588	0.00032	0.05038	0.00949	0.02	40.67	7.25	7.23	37.81	2.05	2.05	212.73	425.46	409.35
0863AZ1_30	294	167	1.75	0.04360	0.01131	0.00569	0.00028	0.05555	0.01463	0.01	43.33	11.04	10.98	36.59	1.78	1.78	434.33	647.39	538.59

Mineral	Zrn																		
Sample Name	#10079																		
	Uranium and Thorium			Concordant Scans: Isotopic Ratios							Concordant Scans: Ages								
Analysis Name	U (ppm)	Th (ppm)	U/Th	207Pb/235U	2 sigma	206Pb/238U	2 sigma	207Pb/206Pb	2 sigma	Error Correlation	207Pb/235U	2- sigma	2+ sigma	206Pb/238U	2- sigma	2+ sigma	207Pb/206Pb	2- sigma	2+ sigma
0865AZ1_1	522	1038	0.50	0.04037	0.00651	0.00554	0.00019	0.05284	0.00868	0.02	40.18	6.37	6.35	35.62	1.25	1.24	321.85	396.34	353.04
0865AZ1_2	509	575	0.89	0.03955	0.00736	0.00562	0.00021	0.05104	0.00966	0.02	39.39	7.20	7.18	36.13	1.38	1.38	242.65	467.99	409.06
0865AZ1_3	641	343	1.87	0.04124	0.00728	0.00541	0.00026	0.05529	0.01004	0.03	41.04	7.11	7.09	34.78	1.67	1.67	423.91	432.95	381.49
0865AZ1_4	255	258	0.99	0.04301	0.01363	0.00558	0.00035	0.05593	0.01801	0.01	42.76	13.31	13.22	35.85	2.23	2.23	449.41	808.32	645.26
0865AZ1_5	1056	1246	0.85	0.03870	0.00525	0.00552	0.00017	0.05088	0.00704	0.03	38.55	5.14	5.13	35.46	1.11	1.11	235.54	335.84	304.40
0865AZ1_6	716	629	1.14	0.03762	0.00647	0.00553	0.00024	0.04933	0.00867	0.03	37.50	6.34	6.32	35.56	1.52	1.53	163.62	327.24	387.12
0865AZ1_7	1011	1071	0.94	0.03832	0.00524	0.00547	0.00018	0.05082	0.00705	0.06	38.18	5.13	5.12	35.15	1.17	1.17	232.75	337.05	305.39
0865AZ1_8	307	431	0.71	0.04414	0.01299	0.00563	0.00032	0.05684	0.01699	0.01	43.86	12.67	12.59	36.21	2.05	2.05	485.17	738.32	599.64
0865AZ1_9	362	308	1.17	0.03886	0.00891	0.00554	0.00027	0.05091	0.01191	0.01	38.71	8.73	8.69	35.59	1.76	1.76	236.74	473.48	498.91
0865AZ1_10	978	917	1.07	0.03821	0.00562	0.00554	0.00017	0.05001	0.00746	0.03	38.07	5.50	5.49	35.63	1.11	1.10	195.33	366.71	329.63
0865AZ1_11	262	318	0.83	0.04024	0.01065	0.00561	0.00036	0.05200	0.01411	0.01	40.06	10.42	10.36	36.08	2.29	2.29	285.58	571.16	567.52
0865AZ1_12	892	269	3.32	0.03828	0.00524	0.00550	0.00019	0.05051	0.00708	0.03	38.14	5.13	5.12	35.34	1.24	1.24	218.38	341.49	309.06
0865AZ1_13	203	131	1.56	0.04117	0.01583	0.00575	0.00037	0.05192	0.02021	0.01	40.96	15.50	15.38	36.97	2.35	2.35	281.79	563.58	786.15
0865AZ1_14	173	122	1.42	0.04429	0.01448	0.00550	0.00045	0.05844	0.01967	0.01	44.00	14.13	14.03	35.34	2.90	2.90	546.18	835.14	661.35
0865AZ1_15	708	155	4.56	0.03885	0.00546	0.00549	0.00024	0.05136	0.00750	0.03	38.70	5.34	5.33	35.27	1.55	1.55	257.14	353.93	319.14
0865AZ1_16	224	90	2.50	0.04317	0.01254	0.00564	0.00045	0.05552	0.01668	0.01	42.92	12.24	12.16	36.25	2.86	2.86	433.27	749.52	607.40
0865AZ1_17	195	111	1.76	0.04100	0.01150	0.00554	0.00040	0.05371	0.01553	0.01	40.80	11.25	11.19	35.59	2.57	2.57	358.72	717.44	593.97
0865AZ1_18	550	273	2.01	0.04041	0.00864	0.00559	0.00024	0.05247	0.01140	0.02	40.22	8.45	8.42	35.90	1.51	1.51	305.95	536.84	460.41
0865AZ1_19	377	296	1.27	0.04275	0.00914	0.00567	0.00026	0.05467	0.01192	0.01	42.51	8.92	8.88	36.46	1.65	1.65	398.60	529.53	454.63
0865AZ1_20	469	224	2.09	0.03624	0.00716	0.00536	0.00023	0.04905	0.00988	0.02	36.15	7.03	7.01	34.45	1.47	1.47	150.32	300.64	440.73
0865AZ1_21	2394	606	3.95	0.03597	0.00288	0.00545	0.00017	0.04790	0.00385	0.18	35.88	2.82	2.82	35.01	1.12	1.12	94.25	188.49	185.22
0865AZ1_22	452	171	2.64	0.03932	0.00989	0.00543	0.00025	0.05249	0.01336	0.02	39.16	9.68	9.64	34.93	1.57	1.57	306.66	613.32	533.15
0865AZ1_23	1622	632	2.56	0.03612	0.00414	0.00547	0.00016	0.04793	0.00561	0.04	36.03	4.07	4.06	35.14	1.02	1.02	95.87	191.74	265.92
0865AZ1_24	2047	218	9.38	0.03729	0.00364	0.00561	0.00017	0.04819	0.00470	0.16	37.17	3.57	3.56	36.08	1.08	1.08	108.53	217.06	222.48
0865AZ1_25	230	125	1.84	0.04150	0.01019	0.00573	0.00037	0.05253	0.01329	0.01	41.29	9.96	9.91	36.83	2.36	2.36	308.65	617.30	530.04
0865AZ1_26	218	278	0.78	0.04277	0.01071	0.00569	0.00037	0.05454	0.01407	0.01	42.52	10.46	10.40	36.56	2.34	2.34	393.35	637.53	531.99
0865AZ1_27	250	214	1.17	0.03837	0.01082	0.00561	0.00030	0.04957	0.01421	0.01	38.23	10.61	10.55	36.09	1.95	1.95	174.94	349.87	608.10
0865AZ1_28	641	478	1.34	0.03944	0.00675	0.00555	0.00018	0.05153	0.00892	0.03	39.28	6.60	6.58	35.69	1.12	1.12	264.55	423.69	374.75
0865AZ1_29	397	380	1.04	0.04186	0.00873	0.00569	0.00024	0.05339	0.01132	0.01	41.64	8.53	8.49	36.56	1.52	1.52	345.36	519.09	447.14
0865AZ1_30	171	223	0.77	0.03812	0.01627	0.00538	0.00037	0.05137	0.02219	0.00	37.99	15.98	15.85	34.60	2.40	2.40	257.34	514.69	865.38

Mineral	Zrn																		
Sample Name	#10075																		
	Uranium and Thorium			Concordant Scans: Isotopic Ratios							Concordant Scans: Ages								
Analysis Name	U (ppm)	Th (ppm)	U/Th	207Pb/235U	2 sigma	206Pb/238U	2 sigma	207Pb/206Pb	2 sigma	Error Correlation	207Pb/235U	2- sigma	2+ sigma	206Pb/238U	2- sigma	2+ sigma	207Pb/206Pb	2- sigma	2+ sigma
0864AZ1_1	370	37	10.05	0.05731	0.01200	0.00799	0.00058	0.05202	0.01112	0.11	56.59	11.55	11.49	51.31	3.69	3.69	286.16	529.44	455.04
0864AZ1_2	4	2	2.50	0.61509	0.57120	0.01757	0.00593	0.25396	0.25054	0.00	486.76	395.18	330.66	112.25	37.62	37.51	3209.62	2258.91	1238.15
0864AZ1_3	744	37	20.28	0.14320	0.01155	0.02107	0.00085	0.04930	0.00401	0.23	135.89	10.28	10.23	134.40	5.40	5.40	162.04	196.21	185.10
0864AZ1_4	174	97	1.79	0.04558	0.01595	0.00592	0.00041	0.05584	0.01988	0.01	45.26	15.55	15.43	38.05	2.63	2.63	445.88	891.77	706.90
0864AZ1_5	72	33	2.21	0.04237	0.02676	0.00584	0.00066	0.05261	0.03374	0.00	42.13	26.24	25.90	37.54	4.22	4.22	311.93	623.86	1202.11
0864AZ1_6	106	7	14.27	0.56279	0.16175	0.05764	0.00474	0.07081	0.02077	0.07	453.34	107.91	102.46	361.28	28.91	28.84	951.92	666.14	548.42
0864AZ1_7	295	383	0.77	0.04725	0.01042	0.00625	0.00037	0.05483	0.01240	0.04	46.88	10.13	10.08	40.16	2.38	2.38	405.50	550.35	469.85
0864AZ1_8	0	2	0.21	12.26697	9.46462	0.22095	0.08434	0.40267	0.33533	0.08	2625.05	895.86	619.49	1286.88	453.17	437.78	3919.07	1665.28	1030.22
0864AZ1_9	113	30	3.76	1.13638	0.09040	0.11969	0.00424	0.06886	0.00566	0.14	770.79	43.43	42.52	728.76	24.42	24.37	894.59	174.59	165.34
0864AZ1_10	74	24	3.06	0.04486	0.02522	0.00668	0.00075	0.04872	0.02771	0.04	44.56	24.66	24.36	42.91	4.80	4.80	134.35	268.69	1118.88
0864AZ1_11	242	158	1.53	0.04687	0.01313	0.00623	0.00044	0.05454	0.01566	0.02	46.51	12.78	12.70	40.06	2.82	2.82	393.42	718.01	586.83
0864AZ1_12	497	86	5.76	0.14328	0.01376	0.02040	0.00120	0.05094	0.00503	0.26	135.96	12.26	12.18	130.18	7.60	7.60	238.29	236.08	220.10
0864AZ1_13	85	13	6.37	0.04690	0.02311	0.00562	0.00068	0.06048	0.03048	0.03	46.54	22.54	22.29	36.16	4.39	4.38	620.75	1241.51	933.67
0864AZ1_14	61	25	2.47	2.54157	0.15628	0.21794	0.00822	0.08458	0.00542	0.23	1284.02	45.31	44.32	1270.97	43.58	43.43	1305.94	126.93	121.86
0864AZ1_15	58	18	3.20	2.54091	0.18225	0.21482	0.01125	0.08579	0.00614	0.36	1283.83	52.95	51.60	1254.43	59.81	59.54	1333.38	141.80	135.49
0864AZ1_16	714	86	8.29	0.09374	0.01176	0.01362	0.00081	0.04991	0.00643	0.18	90.99	10.95	10.89	87.23	5.15	5.15	190.71	314.45	286.80
0864AZ1_17	87	106	0.82	0.05023	0.02231	0.00622	0.00073	0.05860	0.02660	0.05	49.76	21.68	21.45	39.95	4.67	4.67	552.40	1104.80	861.68
0864AZ1_18	153	106	1.45	0.04168	0.01769	0.00590	0.00050	0.05122	0.02213	0.01	41.46	17.32	17.17	37.93	3.23	3.23	250.94	501.88	866.30
0864AZ1_19	1911	650	2.94	0.04767	0.00419	0.00712	0.00027	0.04853	0.00424	0.22	47.29	4.06	4.05	45.77	1.71	1.70	125.15	212.17	199.27
0864AZ1_20	3	1	4.29	0.49797	0.49691	0.01626	0.01375	0.22218	0.27724	0.09	410.33	368.29	311.64	103.95	87.50	86.91	2996.56	3428.41	1513.33
0864AZ1_21	61	53	1.16	0.05114	0.03815	0.00678	0.00081	0.05468	0.04125	0.01	50.64	37.19	36.52	43.58	5.21	5.21	399.28	798.56	1354.96
0864AZ1_22	91	100	0.91	0.04579	0.02249	0.00615	0.00064	0.05401	0.02709	0.00	45.47	21.96	21.72	39.52	4.12	4.12	371.31	742.63	967.04
0864AZ1_23	131	120	1.09	0.03778	0.02073	0.00560	0.00038	0.04897	0.02704	0.01	37.66	20.39	20.19	35.97	2.42	2.43	146.56	293.12	1089.12
0864AZ1_24	56	50	1.12	0.05358	0.04543	0.00658	0.00078	0.05906	0.05054	0.00	53.00	44.26	43.31	42.28	5.00	5.00	569.45	1138.91	1461.66
0864AZ1_25	98	103	0.95	0.05059	0.02374	0.00641	0.00061	0.05725	0.02738	0.01	50.11	23.07	22.81	41.18	3.93	3.93	501.31	1002.62	908.93
0864AZ1_26	95	94	1.01	0.04870	0.02582	0.00684	0.00067	0.05164	0.02781	0.01	48.28	25.16	24.85	43.94	4.32	4.31	269.48	538.96	1044.86
0864AZ1_27	58	35	1.65	9.49775	0.74519	0.40863	0.02426	0.16857	0.01382	0.31	2387.33	73.39	70.83	2208.64	111.51	110.55	2543.54	140.82	134.25
0864AZ1_28	93	81	1.15	0.04362	0.02025	0.00679	0.00060	0.04661	0.02200	0.01	43.35	19.80	19.61	43.61	3.87	3.87	29.19	58.37	971.32
0864AZ1_29	84	92	0.92	0.04841	0.03192	0.00618	0.00059	0.05684	0.03783	0.01	48.00	31.16	30.69	39.70	3.79	3.79	485.14	970.28	1206.65
0864AZ1_30	78	71	1.09	0.06557	0.03556	0.00697	0.00089	0.06819	0.03788	0.01	64.48	34.18	33.61	44.80	5.72	5.72	874.22	1429.14	978.06

Mineral	Zrn																		
Sample Name	#10080																		
	Uranium and Thorium			Concordant Scans: Isotopic Ratios							Concordant Scans: Ages								
Analysis Name	U (ppm)	Th (ppm)	U/Th	207Pb/235U	2 sigma	206Pb/238U	2 sigma	207Pb/206Pb	2 sigma	Error Correlation	207Pb/235U	2- sigma	2+ sigma	206Pb/238U	2- sigma	2+ sigma	207Pb/206Pb	2- sigma	2+ sigma
0866AZ1_1	135	67	2.02	0.04410	0.01968	0.00556	0.00055	0.05754	0.02616	0.03	43.82	19.23	19.05	35.73	3.56	3.56	512.22	1024.44	868.19
0866AZ1_2	381	301	1.27	0.04073	0.00969	0.00581	0.00037	0.05081	0.01226	0.08	40.54	9.47	9.43	37.37	2.39	2.39	232.13	464.27	513.82
0866AZ1_3	589	67	8.80	0.03869	0.00693	0.00546	0.00034	0.05137	0.00933	0.13	38.55	6.79	6.77	35.12	2.17	2.17	257.42	446.67	392.63
0866AZ1_4	273	236	1.16	0.03770	0.00992	0.00551	0.00048	0.04962	0.01341	0.08	37.58	9.73	9.68	35.42	3.06	3.06	177.33	354.66	575.96
0866AZ1_5	90	76	1.18	0.04134	0.02315	0.00566	0.00076	0.05294	0.03023	0.04	41.13	22.70	22.45	36.40	4.86	4.85	326.29	652.59	1088.02
0866AZ1_6	238	120	1.97	0.04286	0.01123	0.00563	0.00044	0.05523	0.01470	0.09	42.61	10.96	10.91	36.18	2.82	2.82	421.42	656.46	544.93
0866AZ1_7	637	368	1.73	0.03661	0.00646	0.00537	0.00038	0.04944	0.00876	0.19	36.51	6.34	6.32	34.53	2.42	2.42	168.88	337.76	389.34
0866AZ1_8	519	278	1.87	0.03782	0.00759	0.00547	0.00041	0.05013	0.01013	0.17	37.69	7.44	7.41	35.17	2.62	2.62	201.02	402.03	438.12
0866AZ1_9	188	115	1.64	0.04406	0.01457	0.00561	0.00041	0.05693	0.01922	0.01	43.78	14.22	14.12	36.09	2.61	2.61	488.83	846.80	669.15
0866AZ1_10	186	229	0.81	0.04196	0.01591	0.00551	0.00031	0.05521	0.02114	0.01	41.73	15.56	15.44	35.44	2.01	2.01	420.55	841.10	757.31
0866AZ1_11	226	180	1.26	0.04527	0.01366	0.00558	0.00041	0.05887	0.01826	0.01	44.96	13.32	13.23	35.86	2.64	2.64	562.12	759.06	612.66
0866AZ1_12	229	154	1.48	0.04197	0.01288	0.00551	0.00032	0.05522	0.01721	0.01	41.75	12.59	12.51	35.44	2.03	2.03	421.30	782.99	629.26
0866AZ1_13	310	430	0.72	0.04134	0.00937	0.00575	0.00032	0.05219	0.01214	0.01	41.14	9.16	9.12	36.93	2.04	2.04	293.94	579.85	491.73
0866AZ1_14	524	365	1.44	0.03901	0.00768	0.00553	0.00027	0.05116	0.01035	0.01	38.85	7.52	7.50	35.55	1.75	1.75	248.18	496.36	434.97
0866AZ1_15	273	339	0.81	0.04059	0.01124	0.00565	0.00037	0.05209	0.01479	0.01	40.40	11.00	10.94	36.33	2.38	2.38	289.15	578.29	591.25
0866AZ1_16	628	419	1.50	0.03899	0.00732	0.00538	0.00023	0.05258	0.01009	0.02	38.84	7.17	7.14	34.58	1.49	1.49	310.64	468.83	409.46
0866AZ1_17	197	306	0.64	0.03896	0.01611	0.00527	0.00052	0.05361	0.02238	0.08	38.81	15.81	15.68	33.88	3.33	3.33	354.83	709.66	826.11
0866AZ1_18	606	352	1.72	0.03936	0.00770	0.00551	0.00036	0.05181	0.01036	0.10	39.20	7.54	7.51	35.42	2.29	2.29	277.23	493.40	428.21
0866AZ1_19	1236	909	1.36	0.03914	0.00516	0.00562	0.00034	0.05051	0.00691	0.14	38.98	5.05	5.04	36.13	2.16	2.16	218.43	333.02	302.11
0866AZ1_20	113	53	2.13	0.04302	0.02484	0.00544	0.00049	0.05734	0.03340	0.02	42.77	24.33	24.04	34.98	3.12	3.13	504.67	1009.34	1075.83
0866AZ1_21	75	49	1.54	0.04448	0.03245	0.00529	0.00078	0.06095	0.04497	0.04	44.19	31.79	31.30	34.03	4.99	4.99	637.35	1274.70	1283.94
0866AZ1_22	608	1101	0.55	0.03696	0.00732	0.00545	0.00028	0.04915	0.00984	0.09	36.85	7.18	7.16	35.07	1.81	1.81	154.89	309.77	437.94
0866AZ1_23	1318	1850	0.71	0.03988	0.00489	0.00569	0.00037	0.05087	0.00618	0.28	39.71	4.78	4.77	36.55	2.37	2.37	234.76	293.11	268.88
0866AZ1_24	106	123	0.86	0.04180	0.01862	0.00545	0.00066	0.05558	0.02546	0.03	41.58	18.23	18.07	35.07	4.25	4.25	435.74	871.48	884.78
0866AZ1_25	482	584	0.83	0.03806	0.00759	0.00551	0.00038	0.05009	0.01036	0.06	37.93	7.44	7.41	35.43	2.42	2.42	199.22	398.43	447.81
0866AZ1_26	910	640	1.42	0.03752	0.00592	0.00538	0.00021	0.05061	0.00807	0.08	37.40	5.80	5.78	34.57	1.38	1.38	222.98	391.52	349.47
0866AZ1_27	340	204	1.66	0.04094	0.00970	0.00556	0.00029	0.05337	0.01286	0.03	40.74	9.49	9.44	35.76	1.83	1.83	344.38	596.72	503.54
0866AZ1_28	538	374	1.44	0.03841	0.00719	0.00545	0.00026	0.05114	0.00981	0.02	38.27	7.04	7.01	35.02	1.64	1.64	247.15	474.44	413.96
0866AZ1_29	517	381	1.36	0.03778	0.00823	0.00555	0.00031	0.04938	0.01095	0.06	37.66	8.07	8.03	35.67	2.01	2.01	165.98	331.95	480.63
0866AZ1_30	178	85	2.09	0.04316	0.01569	0.00548	0.00040	0.05711	0.02113	0.01	42.91	15.33	15.21	35.24	2.59	2.59	495.70	939.72	725.69

Mineral	Zrn																		
Sample Name	#10084																		
	Uranium and Thorium			Concordant Scans: Isotopic Ratios							Concordant Scans: Ages								
Analysis Name	U (ppm)	Th (ppm)	U/Th	207Pb/235U	2 sigma	206Pb/238U	2 sigma	207Pb/206Pb	2 sigma	Error Correlation	207Pb/235U	2- sigma	2+ sigma	206Pb/238U	2- sigma	2+ sigma	207Pb/206Pb	2- sigma	2+ sigma
0867AZ1_1	2582	922	2.80	0.04134	0.00347	0.00592	0.00017	0.05068	0.00431	0.13	41.13	3.38	3.38	38.02	1.10	1.10	226.50	202.49	190.63
0867AZ1_2	605	495	1.22	0.04204	0.00737	0.00580	0.00022	0.05257	0.00938	0.03	41.81	7.20	7.17	37.28	1.40	1.41	310.35	433.67	382.39
0867AZ1_3	322	149	2.17	0.04203	0.01120	0.00577	0.00031	0.05279	0.01432	0.01	41.81	10.95	10.89	37.12	1.97	1.97	319.75	639.50	564.12
0867AZ1_4	784	429	1.83	0.04349	0.00576	0.00624	0.00024	0.05058	0.00690	0.04	43.22	5.62	5.60	40.07	1.53	1.53	221.81	331.75	301.06
0867AZ1_5	1016	1134	0.90	0.04144	0.01476	0.00583	0.00017	0.05155	0.01839	0.02	41.23	14.44	14.34	37.48	1.08	1.08	265.35	530.70	729.45
0867AZ1_6	2484	503	4.94	0.03917	0.00362	0.00575	0.00032	0.04940	0.00432	0.38	39.01	3.54	3.53	36.96	2.06	2.06	167.01	211.04	198.23
0867AZ1_7	617	413	1.49	0.04165	0.00703	0.00590	0.00029	0.05120	0.00882	0.07	41.43	6.87	6.84	37.92	1.85	1.85	249.80	422.82	374.11
0867AZ1_8	564	231	2.44	0.04174	0.00764	0.00590	0.00034	0.05128	0.00960	0.09	41.52	7.46	7.43	37.95	2.21	2.21	253.41	461.44	404.01
0867AZ1_9	323	106	3.05	0.04888	0.01142	0.00625	0.00038	0.05671	0.01362	0.02	48.46	11.09	11.03	40.17	2.43	2.43	480.18	579.99	490.91
0867AZ1_10	139	35	3.93	0.83942	0.10561	0.08997	0.00335	0.06767	0.00873	0.06	618.82	59.15	57.47	555.37	19.81	19.77	858.34	279.87	256.87
0867AZ1_11	104	64	1.61	0.04506	0.02082	0.00618	0.00055	0.05286	0.02485	0.00	44.75	20.34	20.13	39.73	3.51	3.51	322.58	645.16	921.75
0867AZ1_12	1028	297	3.46	0.03974	0.00528	0.00588	0.00024	0.04903	0.00673	0.04	39.57	5.17	5.15	37.78	1.54	1.54	149.42	298.83	306.94
0867AZ1_13	350	186	1.88	0.04195	0.00936	0.00599	0.00032	0.05081	0.01161	0.02	41.73	9.14	9.10	38.49	2.06	2.06	232.04	464.08	488.73
0867AZ1_14	375	378	0.99	0.04058	0.00990	0.00584	0.00030	0.05039	0.01252	0.01	40.39	9.68	9.63	37.54	1.91	1.91	213.16	426.32	529.82
0867AZ1_15	508	294	1.73	0.04071	0.00766	0.00575	0.00031	0.05134	0.00999	0.02	40.51	7.49	7.46	36.96	1.97	1.97	256.05	480.87	418.82
0867AZ1_16	660	276	2.39	0.04018	0.00657	0.00590	0.00022	0.04939	0.00822	0.03	40.00	6.42	6.40	37.92	1.42	1.42	166.23	332.46	367.37
0867AZ1_17	1555	583	2.67	0.03813	0.00352	0.00579	0.00020	0.04778	0.00449	0.13	37.99	3.44	3.44	37.20	1.26	1.26	88.41	176.81	215.55
0867AZ1_18	192	187	1.03	0.04093	0.01412	0.00608	0.00043	0.04886	0.01718	0.01	40.73	13.82	13.73	39.05	2.75	2.75	140.93	281.86	735.47
0867AZ1_19	2048	1567	1.31	0.03846	0.00344	0.00575	0.00023	0.04853	0.00436	0.21	38.32	3.37	3.36	36.94	1.47	1.47	125.32	218.57	204.90
0867AZ1_20	649	548	1.18	0.03932	0.00748	0.00583	0.00030	0.04892	0.00949	0.07	39.16	7.32	7.30	37.47	1.95	1.95	144.01	288.02	425.85
0867AZ1_21	327	165	1.98	0.04176	0.01042	0.00603	0.00034	0.05026	0.01282	0.01	41.54	10.19	10.14	38.73	2.18	2.18	207.04	414.07	543.49
0867AZ1_22	119	36	3.31	0.04993	0.01810	0.00598	0.00052	0.06052	0.02252	0.01	49.47	17.59	17.43	38.46	3.31	3.31	622.09	924.24	715.14
0867AZ1_23	5525	2026	2.73	0.03832	0.00240	0.00582	0.00013	0.04771	0.00298	0.17	38.18	2.35	2.35	37.44	0.83	0.83	85.11	151.66	144.97
0867AZ1_24	471	181	2.60	0.03994	0.00786	0.00586	0.00027	0.04946	0.00997	0.01	39.77	7.69	7.66	37.64	1.74	1.74	169.83	339.67	439.59
0867AZ1_25	140	171	0.82	0.04571	0.01953	0.00599	0.00043	0.05538	0.02397	0.00	45.38	19.05	18.87	38.47	2.74	2.74	427.75	855.50	842.83
0867AZ1_26	2036	785	2.59	0.03865	0.00402	0.00577	0.00020	0.04856	0.00509	0.14	38.51	3.93	3.92	37.11	1.29	1.29	126.58	252.97	237.68
0867AZ1_27	658	352	1.87	0.04081	0.00647	0.00602	0.00025	0.04915	0.00799	0.03	40.61	6.32	6.30	38.70	1.62	1.62	154.93	309.87	359.90
0867AZ1_28	478	245	1.95	0.03902	0.00730	0.00588	0.00025	0.04812	0.00919	0.02	38.86	7.15	7.12	37.80	1.59	1.59	105.23	210.46	422.92
0867AZ1_29	323	352	0.92	0.04264	0.00838	0.00573	0.00031	0.05394	0.01094	0.01	42.39	8.17	8.14	36.85	1.96	1.96	368.39	492.83	427.43
0867AZ1_30	539	345	1.56	0.03851	0.00750	0.00553	0.00024	0.05052	0.01004	0.01	38.37	7.34	7.32	35.54	1.54	1.53	219.09	438.19	429.96

Mineral	Zrn																		
Sample Name	#10091																		
	Uranium and Thorium			Concordant Scans: Isotopic Ratios							Concordant Scans: Ages								
Analysis Name	U (ppm)	Th (ppm)	U/Th	207Pb/235U	2 sigma	206Pb/238U	2 sigma	207Pb/206Pb	2 sigma	Error Correlation	207Pb/235U	2- sigma	2+ sigma	206Pb/238U	2- sigma	2+ sigma	207Pb/206Pb	2- sigma	2+ sigma
0868AZ1_1	385	315	1.22	0.03868	0.00880	0.00543	0.00049	0.05170	0.01210	0.12	38.54	8.62	8.58	34.88	3.13	3.13	272.37	544.73	496.37
0868AZ1_2	194	257	0.75	0.04876	0.01623	0.00569	0.00052	0.06219	0.02099	0.09	48.34	15.78	15.66	36.55	3.33	3.33	680.72	817.34	649.03
0868AZ1_3	301	254	1.19	0.04190	0.01026	0.00561	0.00037	0.05414	0.01351	0.06	41.67	10.03	9.98	36.08	2.36	2.36	376.93	616.18	517.14
0868AZ1_4	522	400	1.31	0.03829	0.00679	0.00526	0.00036	0.05275	0.00960	0.12	38.15	6.65	6.63	33.85	2.28	2.28	318.01	442.52	389.23
0868AZ1_5	407	400	1.02	0.04272	0.00951	0.00554	0.00038	0.05592	0.01262	0.11	42.48	9.28	9.24	35.62	2.42	2.42	449.22	544.78	465.60
0868AZ1_6	910	489	1.86	0.03853	0.00559	0.00574	0.00019	0.04869	0.00720	0.02	38.39	5.47	5.46	36.89	1.24	1.24	132.91	265.82	330.47
0868AZ1_7	458	337	1.36	0.03805	0.00817	0.00527	0.00028	0.05232	0.01154	0.01	37.92	8.01	7.98	33.92	1.80	1.80	299.49	546.55	467.56
0868AZ1_8	332	315	1.05	0.03817	0.01191	0.00554	0.00030	0.04995	0.01578	0.01	38.03	11.68	11.61	35.63	1.90	1.90	192.62	385.23	662.08
0868AZ1_9	627	368	1.70	0.03864	0.00811	0.00547	0.00027	0.05128	0.01098	0.03	38.50	7.95	7.92	35.13	1.70	1.70	253.41	506.81	458.20
0868AZ1_10	270	242	1.12	0.03895	0.00994	0.00536	0.00033	0.05271	0.01379	0.01	38.80	9.73	9.69	34.46	2.12	2.12	316.22	632.44	545.97
0868AZ1_11	227	182	1.25	0.04745	0.01891	0.00559	0.00042	0.06160	0.02491	0.02	47.08	18.42	18.25	35.91	2.69	2.69	660.41	1011.01	765.44
0868AZ1_12	454	351	1.29	0.04375	0.01063	0.00543	0.00030	0.05842	0.01439	0.05	43.48	10.37	10.32	34.92	1.92	1.92	545.48	589.08	497.08
0868AZ1_13	582	606	0.96	0.03818	0.00951	0.00548	0.00029	0.05054	0.01280	0.02	38.04	9.32	9.28	35.22	1.84	1.84	219.92	439.83	538.50
0868AZ1_14	200	189	1.06	0.04481	0.01592	0.00545	0.00035	0.05964	0.02148	0.01	44.51	15.53	15.42	35.03	2.26	2.26	590.38	895.23	697.99
0868AZ1_15	288	284	1.01	0.03718	0.00885	0.00552	0.00035	0.04888	0.01201	0.01	37.06	8.68	8.65	35.46	2.26	2.26	141.94	283.87	530.92
0868AZ1_16	215	332	0.65	0.04227	0.01627	0.00558	0.00047	0.05497	0.02162	0.01	42.04	15.92	15.79	35.85	3.04	3.04	410.95	821.91	776.69
0868AZ1_17	728	123	5.94	0.03540	0.00531	0.00533	0.00021	0.04816	0.00737	0.04	35.32	5.21	5.20	34.28	1.33	1.33	107.20	214.39	343.04
0868AZ1_18	199	107	1.86	0.04069	0.01630	0.00535	0.00052	0.05513	0.02261	0.02	40.49	15.96	15.84	34.41	3.34	3.34	417.59	835.17	805.08
0868AZ1_19	2251	1403	1.60	0.03693	0.00347	0.00534	0.00021	0.05019	0.00479	0.16	36.82	3.40	3.39	34.31	1.32	1.32	203.79	229.30	214.23
0868AZ1_20	2240	832	2.69	0.03735	0.00344	0.00544	0.00019	0.04982	0.00451	0.23	37.23	3.37	3.36	34.95	1.25	1.25	186.57	217.88	204.24
0868AZ1_21	275	279	0.99	0.05530	0.02432	0.00581	0.00068	0.06903	0.03132	0.01	54.66	23.54	23.27	37.35	4.34	4.33	899.64	1110.30	817.71
0868AZ1_22	292	260	1.12	0.04466	0.01271	0.00555	0.00038	0.05837	0.01703	0.01	44.36	12.39	12.32	35.67	2.43	2.42	543.57	710.86	581.03
0868AZ1_23	426	272	1.57	0.04190	0.01179	0.00553	0.00032	0.05496	0.01572	0.02	41.67	11.52	11.45	35.55	2.07	2.07	410.40	712.63	583.12
0868AZ1_24	316	203	1.56	0.04026	0.01210	0.00537	0.00032	0.05435	0.01660	0.02	40.07	11.85	11.78	34.54	2.06	2.06	385.57	770.89	621.72
0868AZ1_25	231	199	1.16	0.05284	0.02258	0.00571	0.00038	0.06715	0.02899	0.01	52.28	21.89	21.66	36.68	2.43	2.43	842.37	1057.15	789.29
0868AZ1_26	474	441	1.07	0.04512	0.01346	0.00579	0.00033	0.05654	0.01711	0.02	44.81	13.12	13.03	37.21	2.11	2.11	473.51	750.35	607.64
0868AZ1_27	203	174	1.16	0.04784	0.01662	0.00574	0.00044	0.06040	0.02143	0.01	47.45	16.17	16.04	36.92	2.84	2.84	617.97	875.13	685.47
0868AZ1_28	337	238	1.42	0.04354	0.01173	0.00549	0.00033	0.05751	0.01577	0.03	43.27	11.45	11.38	35.30	2.12	2.12	511.21	667.34	551.84
0868AZ1_29	228	184	1.24	0.04115	0.01407	0.00538	0.00039	0.05547	0.01934	0.01	40.95	13.76	13.67	34.59	2.51	2.51	431.21	862.43	695.45
0868AZ1_30	197	128	1.54	0.04271	0.01338	0.00539	0.00042	0.05746	0.01849	0.01	42.46	13.07	12.99	34.65	2.67	2.67	509.40	798.64	638.58

Mineral	Zrn																		
Sample Name	#10093																		
	Uranium and Thorium			Concordant Scans: Isotopic Ratios							Concordant Scans: Ages								
Analysis Name	U (ppm)	Th (ppm)	U/Th	207Pb/235U	2 sigma	206Pb/238U	2 sigma	207Pb/206Pb	2 sigma	Error Correlation	207Pb/235U	2- sigma	2+ sigma	206Pb/238U	2- sigma	2+ sigma	207Pb/206Pb	2- sigma	2+ sigma
0869AZ1_1	1030	326	3.16	0.03889	0.00555	0.00578	0.00025	0.04882	0.00717	0.04	38.74	5.43	5.42	37.14	1.57	1.57	139.02	278.05	327.80
0869AZ1_2	195	172	1.14	0.04537	0.02485	0.00578	0.00096	0.05697	0.03259	0.00	45.06	24.28	23.99	37.13	6.16	6.15	490.47	980.94	1061.74
0869AZ1_3	1435	891	1.61	0.04367	0.00804	0.00586	0.00026	0.05405	0.01002	0.09	43.40	7.83	7.80	37.66	1.65	1.65	373.30	446.55	392.17
0869AZ1_4	285	197	1.45	0.03892	0.01432	0.00610	0.00040	0.04629	0.01726	0.01	38.77	14.05	13.95	39.20	2.54	2.54	12.54	25.07	792.69
0869AZ1_5	323	112	2.89	0.04704	0.05633	0.00575	0.00041	0.05933	0.07116	0.00	46.67	55.37	53.90	36.96	2.61	2.61	579.15	1158.30	1894.20
0869AZ1_6	1668	903	1.85	0.03664	0.00572	0.00564	0.00019	0.04716	0.00741	0.08	36.54	5.61	5.60	36.23	1.25	1.25	57.38	114.76	354.58
0869AZ1_7	318	323	0.98	0.03962	0.02186	0.00573	0.00231	0.05017	0.03425	0.00	39.46	21.47	21.24	36.82	14.78	14.77	203.09	406.19	1288.06
0869AZ1_8	180	93	1.93	10.57480	1.96871	0.38717	0.05769	0.19809	0.03252	0.54	2486.50	180.49	165.75	2109.69	270.91	265.34	2810.55	281.80	256.42
0869AZ1_9	1131	342	3.31	0.03951	0.00657	0.00572	0.00019	0.05009	0.00845	0.02	39.34	6.43	6.41	36.77	1.19	1.19	199.10	398.20	369.74
0869AZ1_10	1870	1023	1.83	0.03879	0.00562	0.00564	0.00018	0.04989	0.00724	0.10	38.64	5.50	5.49	36.25	1.15	1.15	189.85	356.21	321.14
0869AZ1_11	843	336	2.51	0.03819	0.00603	0.00588	0.00019	0.04712	0.00756	0.03	38.05	5.91	5.89	37.78	1.24	1.24	55.10	110.20	361.82
0869AZ1_12	1898	817	2.32	0.03811	0.00378	0.00564	0.00019	0.04900	0.00490	0.15	37.97	3.70	3.70	36.26	1.24	1.24	147.70	243.28	226.44
0869AZ1_13	941	341	2.76	0.03990	0.00509	0.00566	0.00023	0.05116	0.00675	0.04	39.72	4.97	4.96	36.35	1.47	1.47	248.19	318.85	290.36
0869AZ1_14	334	232	1.44	0.03967	0.00987	0.00586	0.00031	0.04907	0.01240	0.03	39.50	9.67	9.62	37.69	1.98	1.98	150.98	301.96	544.10
0869AZ1_15	100	35	2.85	4.46282	0.20286	0.28983	0.00597	0.11168	0.00514	0.18	1724.09	38.06	37.36	1640.67	29.87	29.80	1826.90	84.63	82.29
0869AZ1_16	2232	1006	2.22	0.03835	0.00340	0.00573	0.00018	0.04857	0.00427	0.19	38.21	3.32	3.32	36.81	1.12	1.12	127.05	213.72	200.63
0869AZ1_17	1385	815	1.70	0.03919	0.00426	0.00578	0.00017	0.04915	0.00541	0.09	39.03	4.17	4.16	37.17	1.12	1.12	155.06	268.27	247.93
0869AZ1_18	1241	651	1.91	0.03879	0.00534	0.00576	0.00017	0.04888	0.00678	0.07	38.64	5.23	5.21	37.00	1.08	1.08	141.89	283.78	310.28
0869AZ1_19	358	419	0.86	0.04130	0.01015	0.00572	0.00025	0.05233	0.01302	0.01	41.10	9.92	9.87	36.80	1.57	1.57	299.68	599.35	522.77
0869AZ1_20	294	236	1.25	0.04453	0.01398	0.00602	0.00035	0.05361	0.01710	0.01	44.23	13.64	13.55	38.71	2.27	2.27	354.82	709.64	649.86
0869AZ1_21	1458	1286	1.13	0.03902	0.00407	0.00570	0.00021	0.04961	0.00533	0.09	38.87	3.98	3.97	36.67	1.35	1.36	176.83	260.49	241.24
0869AZ1_22	2468	901	2.74	0.03785	0.00332	0.00565	0.00017	0.04856	0.00430	0.14	37.72	3.25	3.25	36.34	1.10	1.10	126.56	215.41	202.12
0869AZ1_23	260	100	2.59	0.04128	0.01097	0.00584	0.00035	0.05125	0.01393	0.01	41.07	10.73	10.67	37.54	2.28	2.27	252.30	504.60	571.50
0869AZ1_24	1654	728	2.27	0.03911	0.00376	0.00565	0.00019	0.05024	0.00489	0.13	38.95	3.68	3.67	36.29	1.19	1.19	206.29	234.15	218.45
0869AZ1_25	1523	866	1.76	0.03812	0.00403	0.00570	0.00019	0.04849	0.00515	0.14	37.98	3.95	3.94	36.65	1.21	1.21	123.09	246.18	241.28
0869AZ1_26	2095	959	2.19	0.03660	0.00337	0.00551	0.00016	0.04820	0.00446	0.14	36.50	3.31	3.30	35.41	1.03	1.03	109.17	218.35	211.39
0869AZ1_27	2385	1218	1.96	0.03563	0.00328	0.00556	0.00021	0.04649	0.00433	0.17	35.55	3.21	3.21	35.73	1.35	1.34	22.95	45.90	216.47
0869AZ1_28	2446	741	3.30	0.03872	0.00320	0.00565	0.00018	0.04969	0.00408	0.21	38.58	3.13	3.13	36.33	1.16	1.16	180.63	197.20	185.96
0869AZ1_29	1455	1366	1.07	0.03834	0.00523	0.00562	0.00020	0.04947	0.00683	0.08	38.20	5.12	5.11	36.13	1.26	1.26	170.12	339.27	307.34
0869AZ1_30	1135	472	2.40	0.03680	0.00519	0.00562	0.00021	0.04751	0.00682	0.05	36.69	5.09	5.08	36.11	1.32	1.32	75.10	150.19	324.67

Mineral	Zrn																		
Sample Name	#10102																		
	Uranium and Thorium			Concordant Scans: Isotopic Ratios							Concordant Scans: Ages								
Analysis Name	U (ppm)	Th (ppm)	U/Th	207Pb/235U	2 sigma	206Pb/238U	2 sigma	207Pb/206Pb	2 sigma	Error Correlation	207Pb/235U	2- sigma	2+ sigma	206Pb/238U	2- sigma	2+ sigma	207Pb/206Pb	2- sigma	2+ sigma
08610AZ1_1	0	0	0.00	0.00000	0.00000	0.00000	0.00000	0.00000	0.00000	0.00	0.00	0.00	0.00	0.00	0.00	0.00	0.00	0.00	0.00
08610AZ1_2	241	338	0.71	0.17949	0.53025	0.00703	0.00874	0.18527	0.59370	0.00	167.62	335.25	411.76	45.14	56.05	55.80	2700.60	5401.20	2973.70
08610AZ1_3	322	316	1.02	0.10447	0.26456	0.00628	0.00080	0.12060	0.30578	0.00	100.89	201.78	229.72	40.37	5.13	5.13	1965.15	3930.30	2722.02
08610AZ1_4	219	246	0.89	0.04787	0.23410	0.00557	0.00147	0.06238	0.30547	0.00	47.48	94.97	215.04	35.78	9.43	9.43	687.26	1374.52	4514.52
08610AZ1_5	580	1083	0.54	0.03220	0.01864	0.00581	0.00077	0.04021	0.02383	0.01	32.18	18.42	18.25	37.33	4.95	4.95	0.00	0.00	581.44
08610AZ1_6	152	152	1.00	0.02126	0.05597	0.00559	0.00203	0.02757	0.07325	0.00	21.36	42.71	54.90	35.95	13.01	12.99	0.00	0.00	1495.96
08610AZ1_7	153	144	1.06	0.03444	0.15006	0.00636	0.00181	0.03926	0.17141	0.00	34.38	68.77	142.20	40.88	11.63	11.62	0.00	0.00	4056.74
08610AZ1_8	0	0	0.00	0.00000	0.00000	0.00000	0.00000	0.00000	0.00000	0.00	0.00	0.00	0.00	0.00	0.00	0.00	0.00	0.00	0.00
08610AZ1_9	108	85	1.26	0.08962	0.70846	0.00614	0.00080	0.10581	0.83656	0.00	87.15	174.30	571.63	39.48	5.16	5.16	1728.45	3456.91	5163.98
08610AZ1_10	1026	2215	0.46	0.03806	0.01145	0.00587	0.00021	0.04703	0.01421	0.01	37.93	11.23	11.17	37.73	1.32	1.32	50.94	101.87	651.79
08610AZ1_11	185	209	0.88	0.03801	0.05302	0.00574	0.00038	0.04804	0.06708	0.00	37.88	52.54	51.21	36.89	2.45	2.45	101.20	202.39	2268.38
08610AZ1_12	395	284	1.39	0.03534	0.04675	0.00605	0.00057	0.04239	0.05621	0.00	35.27	46.38	45.34	38.86	3.68	3.68	0.00	0.00	1885.38
08610AZ1_13	517	264	1.95	0.05324	0.18413	0.00620	0.00025	0.06227	0.21538	0.00	52.66	105.33	170.18	39.85	1.57	1.57	683.28	1366.55	3747.87
08610AZ1_14	548	101	5.43	0.05342	0.01239	0.00804	0.00025	0.04821	0.01125	0.02	52.84	11.98	11.91	51.59	1.59	1.59	109.77	219.53	509.16
08610AZ1_15	409	321	1.27	0.03815	0.01890	0.00581	0.00027	0.04765	0.02369	0.01	38.02	18.57	18.40	37.33	1.74	1.73	81.81	163.61	1006.76
08610AZ1_16	230	63	3.64	0.04693	0.01478	0.00605	0.00047	0.05628	0.01821	0.01	46.57	14.38	14.28	38.87	3.04	3.04	463.32	810.76	646.69
08610AZ1_17	172	287	0.60	0.04099	0.01866	0.00580	0.00140	0.05128	0.02639	0.00	40.79	18.28	18.12	37.27	8.97	8.96	253.28	506.56	1007.72
08610AZ1_18	349	648	0.54	0.03928	0.01052	0.00579	0.00043	0.04919	0.01359	0.02	39.12	10.31	10.26	37.23	2.73	2.73	157.11	314.22	589.82
08610AZ1_19	366	224	1.63	0.04232	0.01083	0.00608	0.00042	0.05046	0.01333	0.01	42.09	10.58	10.52	39.09	2.67	2.67	216.10	432.20	560.11
08610AZ1_20	70	23	3.04	2.22905	0.18502	0.19900	0.00563	0.08124	0.00684	0.12	1190.22	59.03	57.36	1169.96	30.28	30.21	1227.21	169.89	160.96
08610AZ1_21	817	291	2.80	0.03869	0.00941	0.00596	0.00023	0.04712	0.01153	0.04	38.55	9.22	9.17	38.28	1.50	1.49	55.07	110.15	537.28
08610AZ1_22	998	326	3.06	0.04029	0.00524	0.00591	0.00020	0.04941	0.00652	0.06	40.11	5.12	5.10	38.01	1.26	1.26	167.41	323.68	294.50
08610AZ1_23	184	271	0.68	0.04583	0.01839	0.00562	0.00041	0.05917	0.02409	0.01	45.50	17.93	17.78	36.11	2.60	2.60	573.39	1035.42	780.38
08610AZ1_24	370	17	21.24	0.30728	0.13365	0.02970	0.00495	0.07504	0.03433	0.05	272.07	106.55	101.24	188.66	31.03	30.95	1069.68	1088.99	804.02
08610AZ1_25	221	124	1.78	0.04941	0.01361	0.00624	0.00070	0.05739	0.01689	0.03	48.97	13.21	13.12	40.12	4.47	4.47	506.74	722.55	589.06
08610AZ1_26	329	299	1.10	0.04525	0.01210	0.00609	0.00038	0.05388	0.01473	0.02	44.93	11.79	11.72	39.14	2.43	2.43	366.16	683.00	563.44
08610AZ1_27	343	392	0.87	0.04268	0.01854	0.00595	0.00034	0.05204	0.02272	0.03	42.44	18.13	17.97	38.24	2.19	2.19	287.12	574.24	868.94
08610AZ1_28	41	13	3.03	4.85060	0.29699	0.31412	0.01323	0.11199	0.00675	0.36	1793.72	52.21	50.90	1760.97	65.06	64.73	1832.02	111.33	107.30
08610AZ1_29	186	185	1.00	0.04479	0.03417	0.00594	0.00034	0.05472	0.04186	0.00	44.49	33.48	32.94	38.16	2.21	2.21	400.63	801.26	1370.10
08610AZ1_30	163	148	1.11	0.05106	0.02289	0.00602	0.00044	0.06148	0.02790	0.00	50.57	22.23	21.99	38.71	2.84	2.84	656.20	1160.35	847.87

Mineral	Zrn																		
Sample Name	#10107																		
	Uranium and Thorium			Concordant Scans: Isotopic Ratios							Concordant Scans: Ages								
Analysis Name	U (ppm)	Th (ppm)	U/Th	207Pb/235U	2 sigma	206Pb/238U	2 sigma	207Pb/206Pb	2 sigma	Error Correlation	207Pb/235U	2- sigma	2+ sigma	206Pb/238U	2- sigma	2+ sigma	207Pb/206Pb	2- sigma	2+ sigma
08611AZ1_1	279	166	1.69	0.04256	0.01287	0.00572	0.00037	0.05399	0.01666	0.01	42.32	12.58	12.50	36.76	2.35	2.35	370.43	740.87	629.04
08611AZ1_2	79	212	0.37	0.17852	0.31904	0.00972	0.00694	0.13315	0.25589	0.00	166.78	295.35	257.80	62.38	44.41	44.26	2139.86	4279.72	2226.88
08611AZ1_3	1347	1057	1.27	0.03906	0.00476	0.00574	0.00019	0.04931	0.00608	0.08	38.90	4.65	4.64	36.93	1.20	1.20	162.60	301.57	276.09
08611AZ1_4	1693	889	1.91	0.04121	0.01609	0.00566	0.00016	0.05278	0.02063	0.03	41.00	15.76	15.63	36.40	1.04	1.04	319.35	638.69	784.00
08611AZ1_5	3124	778	4.02	0.03979	0.00700	0.00578	0.00019	0.04996	0.00882	0.07	39.62	6.85	6.82	37.13	1.24	1.24	193.03	386.07	386.74
08611AZ1_6	1409	688	2.05	0.04022	0.00533	0.00576	0.00021	0.05063	0.00684	0.06	40.04	5.21	5.20	37.04	1.35	1.35	223.82	328.19	298.12
08611AZ1_7	1180	1059	1.11	0.04007	0.00538	0.00564	0.00022	0.05152	0.00696	0.12	39.90	5.26	5.25	36.27	1.42	1.42	264.15	326.03	296.27
08611AZ1_8	910	489	1.86	0.03853	0.00559	0.00574	0.00019	0.04869	0.00720	0.02	38.39	5.47	5.46	36.89	1.24	1.24	132.91	265.82	330.47
08611AZ1_9	1917	657	2.92	0.03966	0.00374	0.00597	0.00019	0.04814	0.00455	0.16	39.49	3.66	3.65	38.40	1.23	1.23	106.34	212.68	216.03
08611AZ1_10	1731	821	2.11	0.03800	0.00416	0.00566	0.00018	0.04871	0.00537	0.11	37.87	4.08	4.07	36.37	1.13	1.13	133.74	267.28	249.36
08611AZ1_11	90	41	2.18	3.17406	0.17397	0.23800	0.00570	0.09672	0.00542	0.15	1450.87	42.77	41.89	1376.29	29.73	29.66	1561.88	106.98	103.31
08611AZ1_12	135	31	4.34	1.30744	0.06913	0.13615	0.00359	0.06965	0.00385	0.14	849.00	30.65	30.19	822.86	20.37	20.34	917.95	115.92	111.76
08611AZ1_13	341	344	0.99	0.04225	0.01235	0.00583	0.00029	0.05254	0.01555	0.01	42.02	12.06	11.99	37.49	1.87	1.87	309.15	618.30	611.61
08611AZ1_14	1263	785	1.61	0.06539	0.00736	0.00873	0.00025	0.05435	0.00616	0.09	64.32	7.03	7.00	56.01	1.58	1.58	385.49	265.41	245.20
08611AZ1_15	354	137	2.58	0.04111	0.00987	0.00567	0.00026	0.05260	0.01282	0.01	40.91	9.65	9.60	36.44	1.67	1.67	311.46	608.18	511.85
08611AZ1_16	594	465	1.28	0.04211	0.00824	0.00578	0.00025	0.05288	0.01055	0.02	41.88	8.04	8.01	37.12	1.61	1.61	323.74	487.98	423.95
08611AZ1_17	711	578	1.23	0.03901	0.00676	0.00578	0.00024	0.04891	0.00866	0.02	38.85	6.61	6.59	37.18	1.52	1.52	143.59	287.18	390.93
08611AZ1_18	2374	623	3.81	0.03841	0.00351	0.00573	0.00018	0.04865	0.00449	0.14	38.28	3.44	3.43	36.82	1.17	1.17	130.76	224.67	210.25
08611AZ1_19	1343	362	3.71	0.03870	0.00525	0.00576	0.00017	0.04872	0.00670	0.04	38.55	5.14	5.13	37.03	1.07	1.07	134.45	268.90	308.21
08611AZ1_20	518	521	0.99	0.04133	0.00800	0.00578	0.00023	0.05188	0.01021	0.01	41.12	7.82	7.79	37.14	1.46	1.46	280.23	484.88	421.77
08611AZ1_21	1047	590	1.77	0.04452	0.00658	0.00615	0.00017	0.05250	0.00784	0.04	44.23	6.41	6.39	39.53	1.11	1.11	307.28	359.26	323.36
08611AZ1_22	327	110	2.98	0.05232	0.03337	0.00602	0.00026	0.06303	0.04028	0.00	51.78	32.46	31.95	38.69	1.66	1.66	709.18	1418.35	1127.99
08611AZ1_23	193	87	2.21	0.05734	0.03419	0.00629	0.00036	0.06614	0.03958	0.01	56.61	33.10	32.57	40.41	2.28	2.28	810.75	1590.22	1051.74
08611AZ1_24	894	51	17.44	0.16635	0.01091	0.02367	0.00050	0.05097	0.00342	0.08	156.25	9.52	9.48	150.81	3.18	3.18	239.58	158.27	150.92
08611AZ1_25	959	486	1.97	0.03961	0.00505	0.00571	0.00020	0.05029	0.00659	0.03	39.44	4.94	4.92	36.72	1.29	1.29	208.51	318.95	290.51
08611AZ1_26	435	382	1.14	0.04253	0.00961	0.00583	0.00034	0.05293	0.01231	0.01	42.29	9.38	9.34	37.46	2.17	2.17	325.68	576.26	488.99
08611AZ1_27	2189	577	3.79	0.04031	0.00371	0.00598	0.00022	0.04891	0.00446	0.22	40.12	3.62	3.61	38.41	1.41	1.41	143.52	221.01	207.03
08611AZ1_28	1531	1085	1.41	0.03963	0.00435	0.00581	0.00018	0.04943	0.00544	0.13	39.46	4.25	4.24	37.38	1.17	1.17	168.15	267.61	247.35
08611AZ1_29	226	66	3.44	2.30234	0.43061	0.18997	0.01705	0.08790	0.01639	0.24	1213.01	136.91	128.26	1121.22	92.71	92.04	1380.25	381.28	338.72
08611AZ1_30	506	280	1.80	0.03939	0.00810	0.00572	0.00024	0.04995	0.01046	0.01	39.23	7.93	7.90	36.77	1.56	1.56	192.54	385.09	453.61

Mineral	Zrn																		
Sample Name	#10108																		
	Uranium and Thorium			Concordant Scans: Isotopic Ratios							Concordant Scans: Ages								
Analysis Name	U (ppm)	Th (ppm)	U/Th	207Pb/235U	2 sigma	206Pb/238U	2 sigma	207Pb/206Pb	2 sigma	Error Correlation	207Pb/235U	2- sigma	2+ sigma	206Pb/238U	2- sigma	2+ sigma	207Pb/206Pb	2- sigma	2+ sigma
08612AZ1_1	226	148	1.53	0.04110	0.01163	0.00557	0.00050	0.05349	0.01548	0.08	40.90	11.37	11.31	35.82	3.18	3.18	349.76	699.52	595.32
08612AZ1_2	4004	5056	0.79	0.03724	0.00346	0.00559	0.00031	0.04831	0.00455	0.27	37.12	3.39	3.38	35.94	1.98	1.98	114.57	228.95	215.11
08612AZ1_3	748	469	1.59	0.03913	0.00657	0.00548	0.00037	0.05181	0.00885	0.15	38.97	6.43	6.41	35.21	2.35	2.35	277.20	416.74	369.27
08612AZ1_4	2572	614	4.19	0.03843	0.00347	0.00564	0.00023	0.04940	0.00450	0.20	38.29	3.40	3.39	36.27	1.48	1.48	166.91	220.01	206.13
08612AZ1_5	697	217	3.21	0.42757	0.02028	0.05796	0.00124	0.05350	0.00257	0.18	361.45	14.48	14.37	363.23	7.53	7.53	350.08	110.44	106.78
08612AZ1_6	1634	1498	1.09	0.03734	0.00436	0.00540	0.00019	0.05016	0.00583	0.16	37.22	4.27	4.26	34.71	1.21	1.21	202.30	281.72	259.31
08612AZ1_7	219	100	2.20	0.04399	0.01400	0.00549	0.00042	0.05809	0.01886	0.03	43.71	13.66	13.57	35.31	2.67	2.67	533.09	803.27	641.34
08612AZ1_8	3378	1578	2.14	0.03561	0.00321	0.00539	0.00018	0.04790	0.00430	0.19	35.52	3.15	3.15	34.66	1.12	1.12	94.55	189.09	206.14
08612AZ1_9	88	49	1.82	0.04640	0.02947	0.00594	0.00072	0.05666	0.03650	0.02	46.05	28.80	28.40	38.17	4.60	4.60	478.39	956.78	1175.37
08612AZ1_10	946	687	1.38	0.03600	0.00603	0.00524	0.00026	0.04986	0.00858	0.06	35.91	5.92	5.91	33.66	1.70	1.70	188.70	377.39	377.74
08612AZ1_11	1768	1810	0.98	0.03640	0.00375	0.00540	0.00021	0.04885	0.00506	0.18	36.30	3.68	3.67	34.74	1.37	1.37	140.64	252.43	234.36
08612AZ1_12	488	271	1.80	0.03608	0.00696	0.00537	0.00022	0.04873	0.00954	0.03	35.99	6.83	6.81	34.53	1.39	1.39	134.99	269.98	430.37
08612AZ1_13	420	511	0.82	0.03702	0.00841	0.00534	0.00032	0.05029	0.01174	0.03	36.91	8.25	8.22	34.33	2.06	2.06	208.44	416.88	500.37
08612AZ1_14	935	705	1.33	0.03808	0.00599	0.00552	0.00027	0.05000	0.00788	0.15	37.94	5.87	5.85	35.50	1.75	1.75	195.10	388.39	347.05
08612AZ1_15	151	85	1.78	0.16169	0.72459	0.00724	0.00410	0.16202	0.73183	0.00	152.19	304.37	551.26	46.49	26.28	26.22	2476.87	4953.73	3688.61
08612AZ1_16	187	180	1.04	0.05536	0.03733	0.00564	0.00040	0.07125	0.04829	0.00	54.71	36.24	35.60	36.23	2.58	2.58	964.46	1820.39	1142.71
08612AZ1_17	905	516	1.76	0.03839	0.00591	0.00553	0.00022	0.05032	0.00795	0.02	38.25	5.79	5.77	35.57	1.41	1.41	209.82	388.36	346.99
08612AZ1_18	3646	2458	1.48	0.03649	0.00270	0.00548	0.00016	0.04825	0.00353	0.21	36.39	2.64	2.64	35.26	1.02	1.02	111.73	177.47	168.36
08612AZ1_19	527	113	4.65	0.03916	0.00993	0.00564	0.00063	0.05036	0.01293	0.19	39.00	9.72	9.68	36.25	4.06	4.05	211.83	423.66	546.07
08612AZ1_20	2089	342	6.11	0.03722	0.00333	0.00552	0.00026	0.04892	0.00451	0.20	37.10	3.26	3.26	35.47	1.64	1.64	144.21	223.72	209.41
08612AZ1_21	1053	1227	0.86	0.03588	0.00439	0.00527	0.00022	0.04934	0.00623	0.06	35.79	4.31	4.30	33.91	1.39	1.39	164.09	309.44	282.67
08612AZ1_22	363	615	0.59	0.03989	0.00844	0.00527	0.00029	0.05488	0.01194	0.02	39.71	8.26	8.23	33.89	1.84	1.84	407.49	527.49	453.09
08612AZ1_23	19	59	0.33	0.84359	0.86451	0.00967	0.01146	0.63299	0.90802	0.16	621.13	542.58	427.75	62.01	73.40	72.98	4560.00	3833.21	0.00
08612AZ1_24	1845	1158	1.59	0.03608	0.00454	0.00542	0.00030	0.04831	0.00609	0.22	35.99	4.46	4.45	34.83	1.92	1.92	114.30	228.60	284.54
08612AZ1_25	227	215	1.06	0.04413	0.02863	0.00543	0.00031	0.05893	0.03833	0.01	43.85	28.03	27.65	34.91	1.96	1.96	564.68	1129.36	1169.55
08612AZ1_26	2057	1222	1.68	0.03853	0.00418	0.00557	0.00038	0.05018	0.00529	0.36	38.38	4.09	4.09	35.80	2.45	2.45	203.40	254.32	235.92
08612AZ1_27	577	335	1.72	0.03826	0.00627	0.00573	0.00043	0.04840	0.00805	0.19	38.12	6.14	6.12	36.85	2.74	2.74	118.93	237.86	370.37
08612AZ1_28	198	157	1.27	0.03860	0.01313	0.00561	0.00047	0.04992	0.01718	0.08	38.46	12.88	12.80	36.06	3.03	3.03	191.12	382.25	715.34
08612AZ1_29	2125	1348	1.58	0.03844	0.00418	0.00566	0.00039	0.04927	0.00512	0.38	38.30	4.09	4.08	36.37	2.49	2.49	160.88	252.63	234.51
08612AZ1_30	991	1282	0.77	0.03728	0.00554	0.00546	0.00037	0.04949	0.00762	0.15	37.17	5.43	5.41	35.13	2.40	2.40	170.88	341.75	341.14

Mineral	Zrn																		
Sample Name	#10111																		
	Uranium and Thorium			Concordant Scans: Isotopic Ratios							Concordant Scans: Ages								
Analysis Name	U (ppm)	Th (ppm)	U/Th	207Pb/235U	2 sigma	206Pb/238U	2 sigma	207Pb/206Pb	2 sigma	Error Correlation	207Pb/235U	2- sigma	2+ sigma	206Pb/238U	2- sigma	2+ sigma	207Pb/206Pb	2- sigma	2+ sigma
08613AZ1_1	419	236	1.77	0.04287	0.00910	0.00580	0.00024	0.05358	0.01154	0.02	42.62	8.88	8.84	37.30	1.56	1.56	353.24	527.16	453.07
08613AZ1_2	2651	999	2.65	0.04249	0.00363	0.00615	0.00020	0.05008	0.00425	0.20	42.25	3.54	3.53	39.55	1.25	1.25	198.70	203.08	191.17
08613AZ1_3	1691	570	2.96	0.04010	0.00371	0.00584	0.00018	0.04981	0.00466	0.13	39.92	3.63	3.62	37.53	1.18	1.18	186.03	225.50	210.92
08613AZ1_4	127	163	0.78	0.04562	0.01954	0.00598	0.00042	0.05529	0.02396	0.01	45.30	19.07	18.89	38.46	2.68	2.67	424.07	848.14	844.37
08613AZ1_5	129	50	2.58	0.77627	0.15262	0.07981	0.00677	0.07054	0.01430	0.14	583.35	89.17	85.42	494.98	40.49	40.37	944.23	445.35	389.54
08613AZ1_6	39	40	0.97	0.28206	0.39476	0.01038	0.00421	0.19713	0.28576	0.02	252.29	339.50	290.79	66.55	26.92	26.86	2802.62	4841.93	1720.43
08613AZ1_7	60	15	4.02	0.00000	0.00000	0.00000	0.00000	0.00000	0.00000	0.00	0.00	0.00	0.00	0.00	0.00	0.00	0.00	0.00	0.00
08613AZ1_8	2098	636	3.30	0.04145	0.00357	0.00611	0.00022	0.04924	0.00428	0.18	41.24	3.48	3.48	39.24	1.40	1.40	159.23	209.90	197.23
08613AZ1_9	1972	503	3.92	0.03959	0.00371	0.00597	0.00027	0.04812	0.00458	0.21	39.42	3.63	3.63	38.36	1.74	1.74	105.00	210.01	217.48
08613AZ1_10	879	964	0.91	0.04047	0.00525	0.00587	0.00024	0.05001	0.00670	0.05	40.29	5.13	5.12	37.73	1.56	1.55	195.46	327.34	297.48
08613AZ1_11	752	636	1.18	0.03912	0.00561	0.00581	0.00028	0.04883	0.00728	0.04	38.97	5.49	5.48	37.35	1.77	1.77	139.86	279.71	332.69
08613AZ1_12	1803	818	2.20	0.04046	0.00391	0.00580	0.00020	0.05062	0.00498	0.13	40.28	3.82	3.81	37.27	1.29	1.29	223.53	235.62	219.71
08613AZ1_13	681	613	1.11	0.04157	0.00864	0.00577	0.00024	0.05228	0.01101	0.03	41.35	8.44	8.41	37.06	1.57	1.57	297.73	520.08	448.06
08613AZ1_14	1391	911	1.53	0.04226	0.00660	0.00605	0.00024	0.05066	0.00790	0.13	42.03	6.44	6.42	38.89	1.55	1.55	225.44	381.98	341.85
08613AZ1_15	1472	430	3.42	0.03806	0.00408	0.00571	0.00025	0.04833	0.00528	0.15	37.93	4.00	3.99	36.72	1.58	1.58	115.44	230.88	248.11
08613AZ1_16	108	168	0.65	0.00000	0.00000	0.00000	0.00000	0.00000	0.00000	0.00	0.00	0.00	0.00	0.00	0.00	0.00	0.00	0.00	0.00
08613AZ1_17	1223	460	2.66	0.03924	0.00407	0.00577	0.00018	0.04932	0.00526	0.06	39.08	3.99	3.98	37.09	1.16	1.16	163.20	259.15	240.11
08613AZ1_18	764	396	1.93	0.05543	0.01894	0.00654	0.00054	0.06145	0.02148	0.02	54.78	18.31	18.14	42.04	3.44	3.44	654.93	854.96	672.72
08613AZ1_19	3327	2098	1.59	0.04595	0.00677	0.00605	0.00035	0.05508	0.00820	0.17	45.62	6.58	6.56	38.89	2.26	2.27	415.40	351.09	316.50
08613AZ1_20	1128	488	2.31	0.03962	0.00483	0.00582	0.00021	0.04936	0.00614	0.08	39.46	4.73	4.72	37.42	1.35	1.35	164.84	304.47	278.51
08613AZ1_21	938	241	3.88	0.04039	0.00494	0.00599	0.00024	0.04894	0.00612	0.10	40.20	4.83	4.82	38.47	1.55	1.55	144.76	289.52	280.83
08613AZ1_22	835	568	1.47	0.03964	0.00706	0.00568	0.00019	0.05063	0.00913	0.03	39.48	6.91	6.88	36.51	1.24	1.24	223.99	445.76	392.03
08613AZ1_23	1263	352	3.59	0.05368	0.01975	0.00610	0.00085	0.06378	0.02388	0.14	53.10	19.12	18.94	39.23	5.42	5.42	734.31	911.77	706.55
08613AZ1_24	3437	757	4.54	0.03729	0.00293	0.00554	0.00019	0.04883	0.00377	0.26	37.17	2.87	2.87	35.61	1.21	1.21	139.66	186.29	176.26
08613AZ1_25	586	693	0.85	0.04098	0.00659	0.00568	0.00023	0.05236	0.00862	0.03	40.78	6.44	6.42	36.49	1.50	1.50	301.15	398.67	354.95
08613AZ1_26	1757	601	2.93	0.03860	0.00304	0.00576	0.00023	0.04859	0.00383	0.24	38.46	2.97	2.97	37.04	1.47	1.47	127.93	191.09	180.56
08613AZ1_27	498	301	1.65	0.04474	0.00862	0.00591	0.00024	0.05488	0.01076	0.02	44.44	8.39	8.36	38.00	1.57	1.57	407.50	471.30	411.01
08613AZ1_28	530	330	1.60	0.03726	0.00814	0.00578	0.00020	0.04675	0.01030	0.02	37.15	7.98	7.95	37.16	1.28	1.28	36.41	72.83	489.20
08613AZ1_29	1163	557	2.09	0.04260	0.00574	0.00592	0.00023	0.05217	0.00720	0.05	42.36	5.60	5.58	38.06	1.46	1.46	293.05	331.45	300.68
08613AZ1_30	1667	959	1.74	0.04266	0.00521	0.00582	0.00022	0.05321	0.00654	0.13	42.42	5.08	5.06	37.38	1.43	1.44	337.80	291.24	267.15

Mineral	Zrn																		
Sample Name	#10125																		
	Uranium and Thorium			Concordant Scans: Isotopic Ratios							Concordant Scans: Ages								
Analysis Name	U (ppm)	Th (ppm)	U/Th	207Pb/235U	2 sigma	206Pb/238U	2 sigma	207Pb/206Pb	2 sigma	Error Correlation	207Pb/235U	2- sigma	2+ sigma	206Pb/238U	2- sigma	2+ sigma	207Pb/206Pb	2- sigma	2+ sigma
08614AZ1_1	265	159	1.66	0.03927	0.01097	0.00555	0.00040	0.05135	0.01478	0.01	39.11	10.75	10.69	35.65	2.55	2.55	256.62	513.24	601.71
08614AZ1_2	512	165	3.11	0.03989	0.00847	0.00583	0.00026	0.04959	0.01069	0.03	39.72	8.29	8.26	37.50	1.68	1.68	176.04	352.08	467.48
08614AZ1_3	358	132	2.71	0.04410	0.01069	0.00602	0.00030	0.05312	0.01311	0.01	43.82	10.42	10.37	38.69	1.94	1.94	334.06	613.72	515.64
08614AZ1_4	2364	3025	0.78	0.03764	0.00354	0.00569	0.00020	0.04797	0.00449	0.19	37.51	3.47	3.47	36.58	1.26	1.26	97.60	195.19	214.56
08614AZ1_5	856	478	1.79	0.04088	0.00548	0.00590	0.00023	0.05024	0.00691	0.05	40.68	5.36	5.34	37.93	1.47	1.47	206.29	335.53	304.20
08614AZ1_6	2593	3069	0.84	0.03728	0.00336	0.00567	0.00020	0.04770	0.00422	0.23	37.17	3.29	3.28	36.43	1.27	1.27	84.62	169.25	203.52
08614AZ1_7	145	40	3.63	1.07204	0.09742	0.11079	0.00442	0.07018	0.00649	0.17	739.74	48.31	47.19	677.31	25.65	25.60	933.69	195.74	184.16
08614AZ1_8	597	582	1.03	0.03965	0.00648	0.00580	0.00027	0.04954	0.00828	0.06	39.49	6.34	6.32	37.31	1.72	1.72	173.66	347.32	368.36
08614AZ1_9	491	61	8.09	0.04216	0.00971	0.00595	0.00030	0.05143	0.01207	0.02	41.93	9.48	9.43	38.22	1.92	1.92	260.12	520.23	498.41
08614AZ1_10	60	39	1.54	1.62803	0.13255	0.16257	0.00629	0.07263	0.00589	0.24	981.10	51.87	50.58	971.06	34.92	34.82	1003.62	169.15	160.40
08614AZ1_11	465	400	1.16	0.04360	0.00778	0.00601	0.00030	0.05257	0.00951	0.09	43.33	7.59	7.56	38.65	1.95	1.95	310.48	440.37	387.59
08614AZ1_12	119	73	1.64	0.04578	0.01833	0.00622	0.00060	0.05336	0.02193	0.01	45.45	17.88	17.72	39.99	3.85	3.85	344.33	688.67	816.47
08614AZ1_13	160	82	1.95	0.05128	0.02080	0.00598	0.00053	0.06215	0.02575	0.01	50.78	20.19	19.99	38.46	3.39	3.39	679.42	1036.57	779.73
08614AZ1_14	140	42	3.30	1.36217	0.19692	0.12546	0.00636	0.07874	0.01159	0.12	872.80	86.46	82.93	761.93	36.51	36.40	1165.70	306.34	278.55
08614AZ1_15	1502	532	2.82	0.04065	0.00380	0.00597	0.00024	0.04937	0.00469	0.17	40.46	3.71	3.71	38.38	1.51	1.51	165.48	229.81	214.71
08614AZ1_16	862	238	3.62	0.03856	0.00594	0.00571	0.00020	0.04896	0.00764	0.05	38.42	5.81	5.80	36.72	1.26	1.26	146.15	292.30	346.69
08614AZ1_17	311	157	1.98	0.03678	0.01203	0.00550	0.00029	0.04848	0.01602	0.02	36.67	11.81	11.75	35.37	1.86	1.86	122.59	245.18	697.83
08614AZ1_18	406	257	1.58	0.04486	0.00932	0.00595	0.00035	0.05468	0.01173	0.02	44.56	9.08	9.04	38.24	2.24	2.24	399.32	520.42	447.90
08614AZ1_19	2082	745	2.79	0.03853	0.00418	0.00562	0.00033	0.04970	0.00523	0.32	38.39	4.09	4.09	36.14	2.12	2.12	181.22	255.04	236.56
08614AZ1_20	950	1134	0.84	0.04099	0.01244	0.00599	0.00031	0.04963	0.01518	0.04	40.79	12.17	12.10	38.50	1.98	1.98	177.50	355.01	644.55
08614AZ1_21	1066	15	70.32	0.11923	0.03799	0.01601	0.00225	0.05400	0.01833	0.07	114.37	34.76	34.17	102.41	14.26	14.24	371.11	742.23	685.51
08614AZ1_22	307	301	1.02	0.04850	0.01470	0.00591	0.00037	0.05949	0.01832	0.03	48.09	14.29	14.19	38.00	2.40	2.40	585.03	749.54	606.28
08614AZ1_23	505	328	1.54	0.04057	0.00717	0.00582	0.00029	0.05052	0.00923	0.02	40.38	7.01	6.99	37.44	1.88	1.88	218.94	437.88	397.45
08614AZ1_24	527	240	2.20	0.04099	0.00720	0.00591	0.00033	0.05031	0.00910	0.06	40.79	7.04	7.02	37.98	2.12	2.12	209.31	418.62	394.49
08614AZ1_25	148	60	2.46	0.05170	0.01760	0.00629	0.00055	0.05961	0.02077	0.04	51.18	17.07	16.92	40.42	3.50	3.50	589.51	861.58	677.40
08614AZ1_26	431	344	1.25	0.04137	0.00774	0.00586	0.00032	0.05120	0.00975	0.08	41.16	7.56	7.53	37.67	2.06	2.06	249.75	470.58	411.01
08614AZ1_27	811	379	2.14	0.04055	0.00574	0.00577	0.00025	0.05093	0.00745	0.04	40.36	5.61	5.59	37.12	1.62	1.62	237.73	356.01	320.87
08614AZ1_28	1173	278	4.23	0.04141	0.00478	0.00567	0.00018	0.05294	0.00616	0.11	41.20	4.67	4.66	36.46	1.17	1.17	326.36	275.61	253.96
08614AZ1_29	2055	996	2.06	0.03687	0.00343	0.00557	0.00022	0.04804	0.00442	0.24	36.76	3.36	3.36	35.78	1.44	1.43	101.42	202.85	210.43
08614AZ1_30	417	110	3.80	0.19554	0.05517	0.02247	0.00257	0.06313	0.01875	0.07	181.35	47.41	46.33	143.22	16.21	16.19	712.47	703.87	575.24

Mineral	Zrn																		
Sample Name	#10129																		
	Uranium and Thorium			Concordant Scans: Isotopic Ratios							Concordant Scans: Ages								
Analysis Name	U (ppm)	Th (ppm)	U/Th	207Pb/235U	2 sigma	206Pb/238U	2 sigma	207Pb/206Pb	2 sigma	Error Correlation	207Pb/235U	2- sigma	2+ sigma	206Pb/238U	2- sigma	2+ sigma	207Pb/206Pb	2- sigma	2+ sigma
08615AZ1_1	0	0	0.00	0.00000	0.00000	0.00000	0.00000	0.00000	0.00000	0.00	0.00	0.00	0.00	0.00	0.00	0.00	0.00	0.00	0.00
08615AZ1_2	194	173	1.12	0.03704	0.01248	0.00548	0.00038	0.04899	0.01681	0.01	36.93	12.25	12.18	35.25	2.41	2.41	147.45	294.91	718.69
08615AZ1_3	561	472	1.19	0.03841	0.00848	0.00570	0.00024	0.04885	0.01094	0.01	38.27	8.31	8.27	36.66	1.52	1.52	140.75	281.49	487.45
08615AZ1_4	578	136	4.24	0.04215	0.00799	0.00560	0.00026	0.05457	0.01057	0.03	41.92	7.79	7.77	36.01	1.66	1.66	394.57	466.30	407.24
08615AZ1_5	235	127	1.84	0.03955	0.01144	0.00534	0.00034	0.05374	0.01588	0.01	39.39	11.20	11.14	34.32	2.16	2.16	360.10	720.20	605.70
08615AZ1_6	141	115	1.23	0.04053	0.01722	0.00505	0.00041	0.05819	0.02514	0.00	40.34	16.87	16.74	32.49	2.63	2.63	536.87	1073.74	827.30
08615AZ1_7	459	636	0.72	0.03630	0.00688	0.00536	0.00020	0.04908	0.00944	0.01	36.20	6.75	6.73	34.48	1.27	1.26	151.82	303.65	422.06
08615AZ1_8	929	724	1.28	0.03501	0.00507	0.00535	0.00018	0.04750	0.00700	0.03	34.94	4.98	4.96	34.37	1.15	1.15	74.26	148.52	332.88
08615AZ1_9	720	979	0.74	0.03790	0.00603	0.00541	0.00024	0.05081	0.00836	0.02	37.78	5.91	5.89	34.78	1.56	1.56	232.38	403.52	358.97
08615AZ1_10	249	136	1.83	0.04069	0.01232	0.00553	0.00036	0.05334	0.01649	0.01	40.49	12.05	11.98	35.56	2.32	2.32	343.50	687.00	632.72
08615AZ1_11	330	255	1.30	0.04127	0.00957	0.00544	0.00042	0.05500	0.01339	0.01	41.06	9.36	9.31	34.98	2.69	2.69	412.35	596.09	502.74
08615AZ1_12	913	981	0.93	0.03756	0.00626	0.00540	0.00019	0.05040	0.00855	0.02	37.44	6.14	6.12	34.75	1.22	1.22	213.60	418.76	371.03
08615AZ1_13	358	313	1.15	0.04148	0.00860	0.00554	0.00029	0.05434	0.01156	0.02	41.27	8.40	8.37	35.59	1.85	1.84	385.09	516.93	445.37
08615AZ1_14	691	708	0.98	0.04228	0.00812	0.00562	0.00026	0.05457	0.01074	0.02	42.05	7.93	7.90	36.12	1.69	1.69	394.77	474.37	413.39
08615AZ1_15	373	252	1.48	0.03534	0.00737	0.00542	0.00032	0.04727	0.01020	0.02	35.26	7.24	7.21	34.86	2.07	2.07	63.03	126.07	477.30
08615AZ1_16	251	52	4.85	0.04055	0.01270	0.00548	0.00036	0.05371	0.01715	0.01	40.36	12.43	12.35	35.20	2.30	2.30	359.06	718.12	650.03
08615AZ1_17	172	287	0.60	0.04099	0.01866	0.00580	0.00140	0.05128	0.02639	0.00	40.79	18.28	18.12	37.27	8.97	8.96	253.28	506.56	1007.72
08615AZ1_18	351	85	4.14	0.03969	0.00869	0.00550	0.00031	0.05230	0.01178	0.01	39.52	8.50	8.47	35.38	2.01	2.01	298.65	559.24	476.81
08615AZ1_19	116	103	1.12	0.04735	0.02322	0.00576	0.00052	0.05962	0.02970	0.00	46.97	22.64	22.39	37.02	3.31	3.31	589.69	1179.37	928.94
08615AZ1_20	519	330	1.57	0.04518	0.00997	0.00572	0.00028	0.05727	0.01292	0.01	44.86	9.71	9.67	36.77	1.83	1.83	502.10	539.57	461.56
08615AZ1_21	540	588	0.92	0.03995	0.00678	0.00562	0.00024	0.05152	0.00895	0.02	39.78	6.63	6.61	36.15	1.52	1.52	264.30	425.19	375.92
08615AZ1_22	337	244	1.38	0.03828	0.00937	0.00548	0.00028	0.05068	0.01264	0.01	38.15	9.19	9.15	35.22	1.78	1.78	226.08	452.15	530.62
08615AZ1_23	281	234	1.20	0.04021	0.01150	0.00570	0.00031	0.05118	0.01486	0.01	40.03	11.25	11.19	36.63	2.00	1.99	248.92	497.84	607.57
08615AZ1_24	137	93	1.47	0.04036	0.02189	0.00573	0.00045	0.05105	0.02796	0.00	40.17	21.47	21.25	36.86	2.91	2.91	243.03	486.06	1064.38
08615AZ1_25	155	89	1.74	0.03687	0.01714	0.00540	0.00046	0.04948	0.02336	0.00	36.76	16.85	16.72	34.74	2.92	2.92	170.48	340.95	948.53
08615AZ1_26	291	216	1.34	0.04118	0.01017	0.00561	0.00034	0.05323	0.01351	0.01	40.97	9.94	9.89	36.06	2.21	2.21	338.63	632.47	528.78
08615AZ1_27	397	262	1.51	0.03723	0.00924	0.00553	0.00036	0.04880	0.01236	0.05	37.11	9.06	9.02	35.56	2.29	2.28	138.38	276.75	546.39
08615AZ1_28	289	202	1.43	0.04132	0.00935	0.00551	0.00037	0.05442	0.01271	0.04	41.11	9.14	9.10	35.40	2.39	2.39	388.43	571.84	485.50
08615AZ1_29	186	185	1.00	0.04479	0.03417	0.00594	0.00034	0.05472	0.04186	0.00	44.49	33.48	32.94	38.16	2.21	2.21	400.63	801.26	1370.10
08615AZ1_30	135	145	0.93	0.04086	0.01953	0.00578	0.00052	0.05123	0.02489	0.00	40.66	19.14	18.96	37.18	3.31	3.31	251.25	502.51	959.17

Appendix B. Ar-Ar Step Heating Data

Sample	Rock Type	Alteration	Total Gas Age	UTM E	UTM N
10081	quartz monzonite	phyllic	38.89 +- 0.03	678283	4419597
10088	quartz monzonite	phyllic	38.05 +- 0.04	678398	4420011
10129	dacite	argillic	49.89 +- 0.26	676322	4422858
10256	dacite	phyllic	39.85 +- 0.09	678163	4421724
10264	dacite	chloritic	38.87 +- 0.05	681535	4423332
10265	rhyolite	phyllic-argillic	41.81 +- 0.04	677994	4423513

10081, Sericite, 24.16 mg, J = 0.001796 ± 0.39%

4 amu discrimination = 1.0615 ± 0.06%, 40/39K = 0.0136 ± 12.80%, 36/37Ca = 0.000301 ± 0.80%, 39/37Ca = 0.000831 ± 0.44%

step	T (C)	t (min.)	36Ar	37Ar	38Ar	39Ar	40Ar	%40Ar*	% 39Ar rlsd	Ca/K	40Ar*/39ArK	Age (Ma)	1s.d.
1	510	12	0.613	0.153	1.144	69.438	1030.28	84.3	3.2	0.01311211	12.536103	40.17	0.17
2	550	12	0.356	0.186	1.164	81.577	1090.16	91.8	3.8	0.01356825	12.302622	39.43	0.16
3	590	12	0.391	0.335	1.956	145.707	1851.74	94.7	6.7	0.01368179	12.113068	38.83	0.16
4	620	12	0.376	0.358	2.372	176.505	2212.13	95.7	8.1	0.01206992	12.092256	38.76	0.16
5	650	12	0.504	0.293	2.810	211.179	2685.38	95.1	9.7	0.00825647	12.206733	39.12	0.16
6	680	12	0.848	0.270	3.421	249.600	3249.73	93.0	11.5	0.00643719	12.230389	39.20	0.16
7	710	12	0.349	0.274	3.990	304.544	3743.45	97.6	14.0	0.00535399	12.128205	38.88	0.16
8	740	12	0.205	0.271	4.474	338.992	4068.91	98.8	15.6	0.00475726	11.988206	38.43	0.16
9	770	12	0.129	0.189	3.628	276.566	3354.49	99.2	12.7	0.00406668	12.154380	38.96	0.16
10	810	12	0.122	0.140	2.429	183.542	2221.43	99.0	8.5	0.0045391	12.069868	38.69	0.15
11	860	12	0.159	0.107	1.125	86.452	1064.48	96.9	4.0	0.00736523	11.944069	38.29	0.15
12	1000	12	0.538	0.156	0.699	47.455	723.122	82.1	2.2	0.0195624	12.155957	38.96	0.18
							Cumulative %39Ar rlsd =		100.0		Total gas age =	38.89	0.03

note: isotope beams in mV, rlsd = released, error in age includes J error, all errors 1 sigma
(36Ar through 40Ar are measured beam intensities, corrected for decay for the age calculations)

No plateau
No isochron

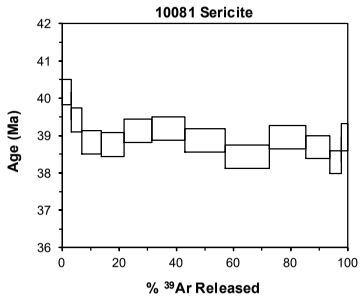

10088, Sericite, 13.83 mg, J = 0.001796 ± 0.37

4 amu discrimination = 0.9879 ± 0.08%, 40/39K = 0.0136 ± 12.80%, 36/37Ca = 0.000301 ± 0.80%, 39/37Ca = 0.000831 ± 0.44%

step	T (C)	t (min.)	36Ar	37Ar	38Ar	39Ar	40Ar	%40Ar*	% 39Ar rlsd	Ca/K	40Ar*/39ArK	Age (Ma)	1s.d.
1	510	12	0.521	0.181	1.074	61.716	925.58	83.9	5.0	0.01222866	12.431655	39.84	0.19
2	550	12	0.362	0.243	1.166	80.435	1092.61	90.8	6.5	0.01259678	12.194433	39.09	0.19
3	590	12	0.347	0.648	1.791	130.763	1667.58	94.2	10.6	0.02066282	11.912860	38.19	0.15
4	630	12	0.339	1.121	2.437	181.031	2238.66	95.8	14.7	0.0258198	11.759047	37.70	0.15
5	670	12	0.770	0.997	3.156	224.922	2934.25	92.4	18.3	0.01848257	11.972757	38.38	0.15
6	710	12	0.653	0.337	3.478	257.936	3260.97	94.2	20.9	0.00544772	11.835948	37.95	0.15
7	750	12	0.192	0.135	2.448	185.638	2210.43	97.8	15.1	0.00303224	11.550142	37.04	0.14
8	800	12	0.186	0.094	0.753	55.405	697.794	93.6	4.5	0.00707418	11.552347	37.05	0.15
9	900	12	0.272	0.112	0.488	33.795	490.602	85.5	2.7	0.0138186	12.079643	38.72	0.19
10	1000	12	0.286	0.099	0.325	19.855	327.861	78.6	1.6	0.02079049	12.138927	38.91	0.19
							Cumulative %39Ar rlsd =		100.0		Total gas age =	38.05	0.04

note: isotope beams in mV, rlsd = released, error in age includes J error, all errors 1 sigma
(36Ar through 40Ar are measured beam intensities, corrected for decay for the age calculations)

No plateau
No isochron

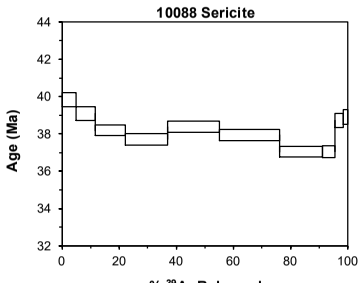

10129, Sericite, 11.34 mg, J = 0.001772 ± 0.42%

4 amu discrimination = 0.9929 ± 0.04%, 40/39K = 0.0136 ± 12.80%, 36/37Ca = 0.000301 ± 0.80%, 39/37Ca = 0.000831 ± 0.44%

step	T (C)	t (min.)	36Ar	37Ar	38Ar	39Ar	40Ar	%40Ar*	% 39Ar rlsd	Ca/K	40Ar*/39ArK	Age (Ma)	1s.d.
1	510	12	0.645	0.436	0.685	7.959	308.11	38.9	20.2	0.23178074	14.669285	46.30	0.50
2	550	12	0.269	0.426	0.365	7.758	201.501	63.3	19.7	0.23233213	15.735792	49.62	0.35
3	580	12	0.242	0.645	0.352	6.593	161.952	59.1	16.7	0.41395639	13.742827	43.41	0.28
4	610	12	0.198	0.632	0.345	5.230	132.543	60.0	13.3	0.51133864	14.218217	44.89	0.37
5	640	12	0.236	0.992	0.182	4.508	132.855	51.0	11.4	0.93129414	14.076489	44.45	0.38
6	670	12	0.960	0.621	0.253	3.174	337.956	16.0	8.1	0.82799474	16.749827	52.77	0.87
7	700	12	0.671	0.241	0.167	1.422	238.932	17.2	3.6	0.71720444	28.545830	89.02	1.32
8	730	12	0.177	0.130	0.048	0.702	63.602	20.7	1.8	0.78368618	16.911863	53.27	1.64
9	810	12	0.277	0.262	0.084	0.852	91.087	11.4	2.2	1.30160403	10.968192	34.73	2.31
10	1000	12	0.613	0.668	0.167	1.213	233.267	20.1	3.1	2.33181664	34.685048	107.61	6.78
							Cumulative %39Ar rlsd =		100.0		Total gas age =	49.89	0.26

note: isotope beams in mV, rlsd = released, error in age includes J error, all errors 1 sigma
(36Ar through 40Ar are measured beam intensities, corrected for decay for the age calculations)

No plateau
No isochron

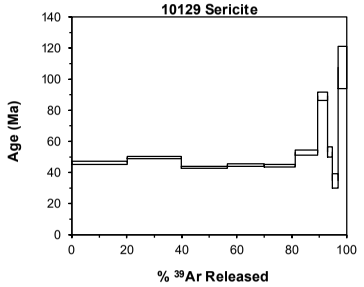

10256, Sericite, 16.14 mg, J = 0.001760 ± 0.42%

4 amu discrimination = 0.9929 ± 0.04%, 40/39K = 0.0136 ± 12.80%, 36/37Ca = 0.000301 ± 0.80%, 39/37Ca = 0.000831 ± 0.44%

step	T (C)	t (min.)	36Ar	37Ar	38Ar	39Ar	40Ar	%40Ar*	% 39Ar rlsd	Ca/K	40Ar*/39ArK	Age (Ma)	1s.d.
1	510	12	2.806	16.542	2.157	41.806	1382.56	40.0	12.5	1.78431229	13.142679	41.26	0.32
2	550	12	0.615	9.492	0.650	32.315	613.138	71.1	9.7	1.32435039	13.340561	41.87	0.25
3	580	12	0.530	13.855	0.680	35.668	587.022	74.3	10.7	1.75163702	12.084158	37.97	0.18
4	610	12	0.590	17.418	0.713	41.290	684.836	75.5	12.3	1.90236296	12.386580	38.91	0.20
5	640	12	0.827	18.686	0.761	42.266	801.564	68.5	12.6	1.99379044	12.881411	40.44	0.21
6	670	12	1.476	32.197	0.846	38.820	951.288	54.7	11.6	3.7427286	13.323155	41.82	0.43
7	700	12	1.204	31.415	0.704	32.767	764.860	54.3	9.8	4.32733424	12.567786	39.47	0.31
8	730	12	0.176	1.173	0.376	26.505	367.461	87.3	7.9	0.19945415	11.873200	37.31	0.21
9	810	12	0.265	1.616	0.373	24.121	368.074	80.0	7.2	0.30194998	11.937186	37.51	0.21
10	1000	12	0.600	1.899	0.397	19.153	429.985	59.1	5.7	0.44688919	12.989319	40.78	0.24
							Cumulative %39Ar rlsd =		100.0		Total gas age =	39.85	0.09

note: isotope beams in mV, rlsd = released, error in age includes J error, all errors 1 sigma
(36Ar through 40Ar are measured beam intensities, corrected for decay for the age calculations)

No plateau
No isochron

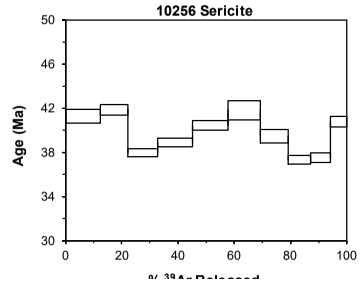

10264, Sericite, 7.79 mg, J = 0.001741 ± 0.39%

4 amu discrimination = 0.9929 ± 0.04%, 40/39K = 0.0136 ± 12.80%, 36/37Ca = 0.000301 ± 0.80%, 39/37Ca = 0.000831 ± 0.44%

step	T (C)	t (min.)	36Ar	37Ar	38Ar	39Ar	40Ar	%40Ar*	% 39Ar rlsd	Ca/K	40Ar*/39ArK	Age (Ma)	1s.d.
1	510	12	0.459	5.664	0.613	34.968	562.047	76.7	10.1	0.74248787	12.171492	37.83	0.16
2	550	12	0.378	7.995	0.765	53.009	782.411	86.5	15.3	0.69134965	12.635957	39.26	0.16
3	580	12	0.448	16.565	0.998	68.231	985.759	87.3	19.7	1.11302454	12.508094	38.87	0.16
4	610	12	0.579	27.462	1.050	72.009	1048.62	84.5	20.8	1.74879994	12.211484	37.95	0.16
5	640	12	0.655	32.035	0.888	55.021	865.856	78.7	15.9	2.67076421	12.277818	38.16	0.16
6	670	12	1.030	51.793	0.650	32.445	711.751	58.7	9.4	7.3348819	12.780120	39.70	0.18
7	700	12	0.976	59.694	0.413	14.813	502.070	44.8	4.3	18.591549	15.093508	46.80	0.32
8	730	12	0.250	0.847	0.150	5.870	145.785	51.4	1.7	0.66140809	12.220913	37.98	0.22
9	810	12	0.172	1.085	0.111	4.307	102.197	53.1	1.2	1.15493216	11.699922	36.38	0.72
10	1000	12	0.363	2.241	0.171	5.651	178.843	40.2	1.6	1.81853737	12.163363	37.81	0.87
							Cumulative %39Ar rlsd =		100.0		Total gas age =	38.87	0.05

note: isotope beams in mV, rlsd = released, error in age includes J error, all errors 1 sigma
(36Ar through 40Ar are measured beam intensities, corrected for decay for the age calculations)

No plateau
No isochron

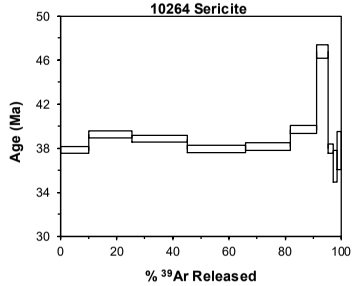

10265, Sericite, 11.23 mg, J = 0.001733 ± 0.38%

4 amu discrimination = 0.9929 ± 0.04%, 40/39K = 0.0136 ± 12.80%, 36/37Ca = 0.000301 ± 0.80%, 39/37Ca = 0.000831 ± 0.44%

step	T (C)	t (min.)	36Ar	37Ar	38Ar	39Ar	40Ar	%40Ar*	% 39Ar rlsd	Ca/K	40Ar*/39ArK	Age (Ma)	1s.d.
1	500	12	0.308	0.656	1.135	71.802	1101.75	92.2	9.9	0.04269159	14.033753	43.35	0.17
2	520	12	0.175	0.532	0.819	58.416	851.681	94.6	8.1	0.04255541	13.656117	42.20	0.17
3	540	12	0.189	0.676	0.996	71.246	1020.32	95.0	9.8	0.04433651	13.498322	41.72	0.18
4	560	12	0.166	0.814	1.133	84.628	1214.86	97.6	11.7	0.04494545	13.912542	42.98	0.17
5	580	12	0.165	0.912	1.265	93.799	1330.88	96.7	13.0	0.04543307	13.630252	42.12	0.17
6	600	12	0.172	0.838	1.162	87.868	1234.33	96.3	12.1	0.04456445	13.430568	41.51	0.16
7	620	12	0.161	0.643	0.897	67.205	950.423	95.6	9.3	0.04470795	13.396531	41.41	0.17
8	640	12	0.197	0.485	0.729	53.310	772.130	93.1	7.4	0.04251166	13.353004	41.27	0.18
9	670	12	0.691	0.466	0.859	53.913	940.277	78.6	7.4	0.04038937	13.594893	42.01	0.17
10	1000	12	1.292	0.776	1.378	81.773	1437.430	73.5	11.3	0.0443432	12.810344	39.61	0.18
							Cumulative %39Ar rlsd =		100.0		Total gas age =	41.81	0.04

note: isotope beams in mV, rlsd = released, error in age includes J error, all errors 1 sigma
(36Ar through 40Ar are measured beam intensities, corrected for decay for the age calculations)

No plateau
No isochron

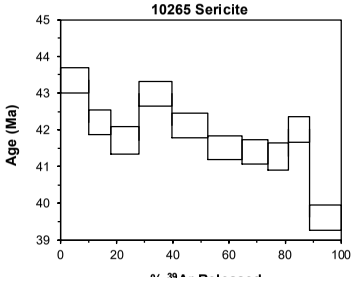

Appendix C. Shortwave Infrared Spectroscopy

Main groups of altered igneous rocks in the Cherry Creek District, organized by type.

Clockwise from upper left are: Type I: Stock-hosted greisen, Type II: Stock marginal silicic-phyllic alteration, Type III: Stock distal quartz-sericite-pyrite, Type IV: argillic

Group 1- Intrusion hosted

Sample: Egan G

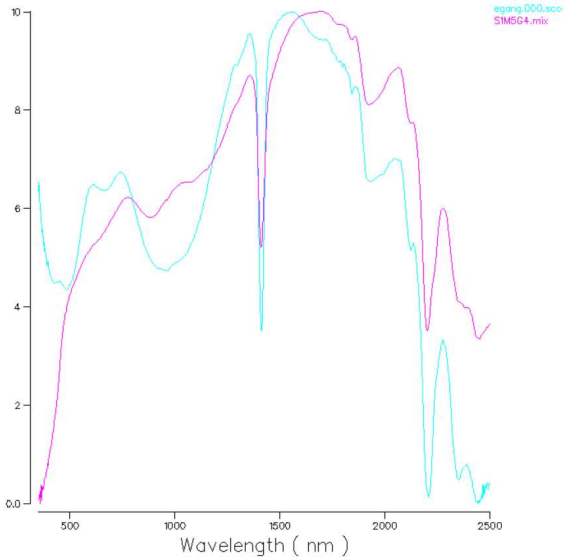

Quartz vein with selvedge of silver sheeted mineral (muscovite) and iron oxide in coarse grained granitic host. White to brown in color. Main iron oxide phase is goethite. Major absorption peaks 1413nm, 2207nm. Minor peak at 2121nm. 1900nm water feature is rounded, skewed right.

Composition: Muscovite, silica, goethite, minor illite (?)

Sample: 10269

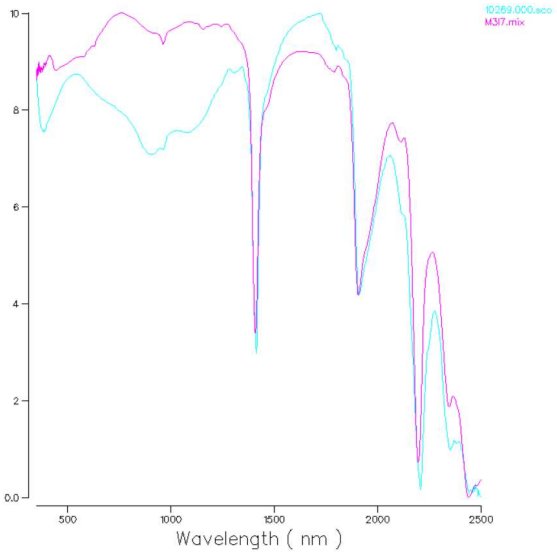

Clay-rich selvedge on quartz vein in altered granitic host. White to gray. Absorption peaks 1413nm, 2207nm, 1910nm. 1900nm water feature is moderately sharp and 80% intensity of major peaks. High wavelength features preserved. Hull from 1350nm-880nm parallels muscovite profile.

Composition: Illite, minor montmorillonite, minor muscovite (?)

Sample: 10106

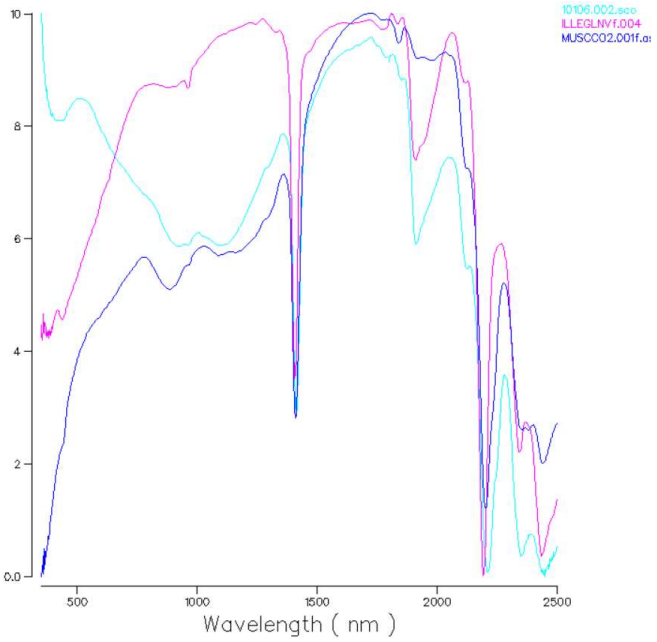

Silicified granite with 2% cubic iron oxides. Major absorption peaks 1409nm, 2210nm. 1913nm water feature moderately sharp but shallow. High wavelength 2351nm and 2441nm minor features present. Hull 880nm to 1350nm is parallel to muscovite.

Composition: Illite, minor muscovite (?), minor silica

Sample: 10121

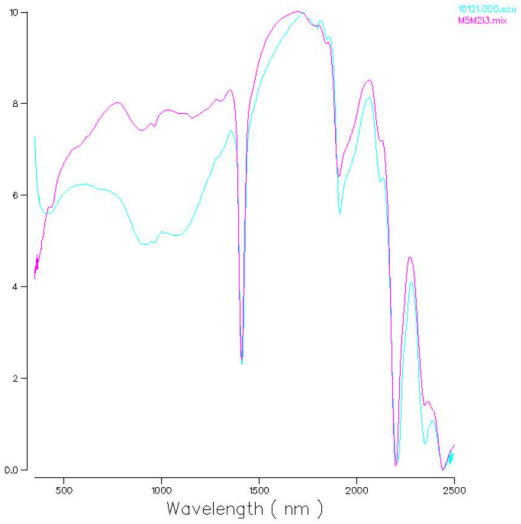

Silicified brecciated granite with quartz vein and iron oxide cement. Major absorption peaks 1409nm, 2210nm. 1913nm water feature is medium intensity, sharp, and inflected at 1968nm. High wavelength 2351nm and 2441nm minor features present. Hull 880nm to 1350nm is parallel to muscovite.

Composition: Illite, minor montmorillonite (?), minor muscovite (?)

Group 2- Intrusion margin <1/2km

Sample: 10088

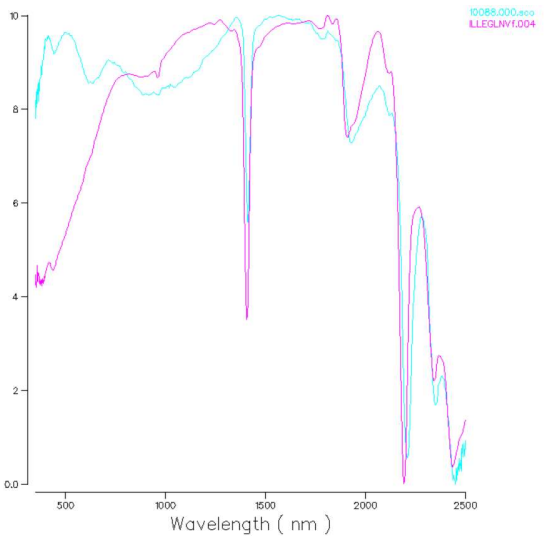

White to gray granular quartz-sericite-pyrite rock. Major absorption peaks 1413nm, 2211nm. Water feature minor, rounded, skewed right. High wavelength 2121nm, 2351nm, and 2441nm features present.

Composition: Illite, minor silica

Sample: 10081

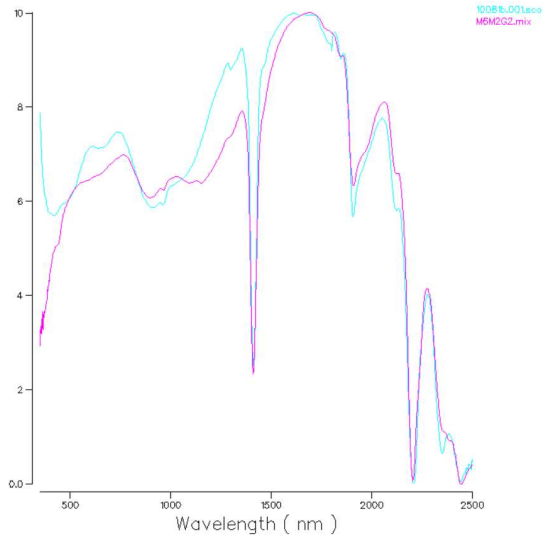

Iron-oxide veining in white to gray granitic protolith. Feldspars destroyed, sheared. Major absorption peaks 1413nm, 2211nm. 1910nm water feature moderate intensity, sharp, with inflection at 1968nm. High wavelength 2121nm, 2351nm, 2441nm features present. Iron oxide appears to be goethite. Hull 880nm to 1350nm is parallel to muscovite.

Composition: Illite, minor montmorillonite (?), minor muscovite (?)

Sample: 10087

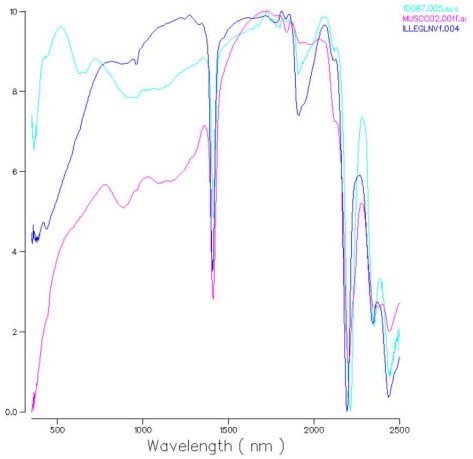

White to gray granular quartz-sericite-pyrite rock with minor quartz veining. Major absorption peaks 1413nm, 2211nm. 1911nm water feature minor, rounded. High wavelength 2121nm, 2351nm, 2441nm minor features present.

Composition: Muscovite, minor illite, minor silica

Group 3- Intrusion distal 1/2km to 3km

Sample: 10123

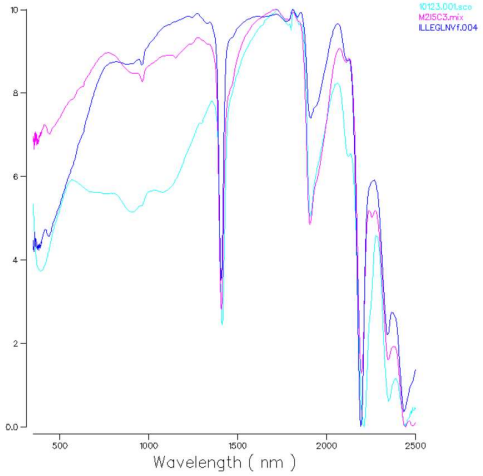

Green dacite porphyry dike with cubic iron oxides. Major absorption peaks 1413nm, 2211nm. 1911nm water feature medium intensity, sharp, inflected at 1968nm. Minor 2125nm, 2351nm, 2441nm features present. Hull 800nm-1350nm parallel to muscovite including minor 1297nm saddle, possibly due to chlorite.

Composition: Illite, minor muscovite (?), minor montmorillonite (?), minor chlorite (?)

Sample: 10285

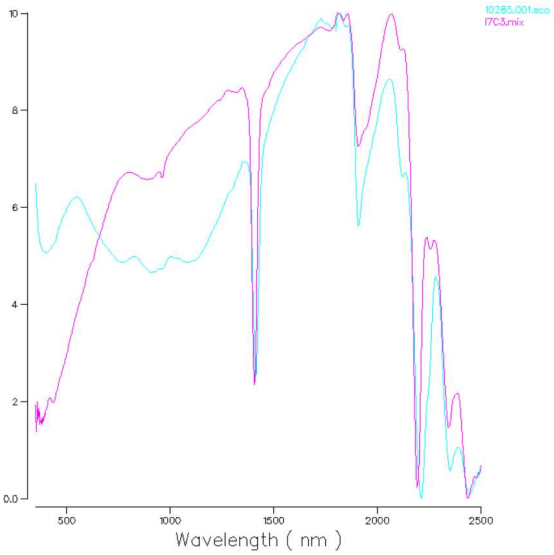

Green dacite porphyry with cubic iron oxides. Major absorption peaks 1413nm, 2211nm. 1911nm water feature sharp, medium intensity, inflected at 16968nm. High wavelength 2121nm, 2351nm, 2441nm features present. Upsloping hull parallel to muscovite in 800-1350nm, possibly chlorite?

Composition: Illite, minor montmorillonite, minor chlorite (?)

Sample: 10264

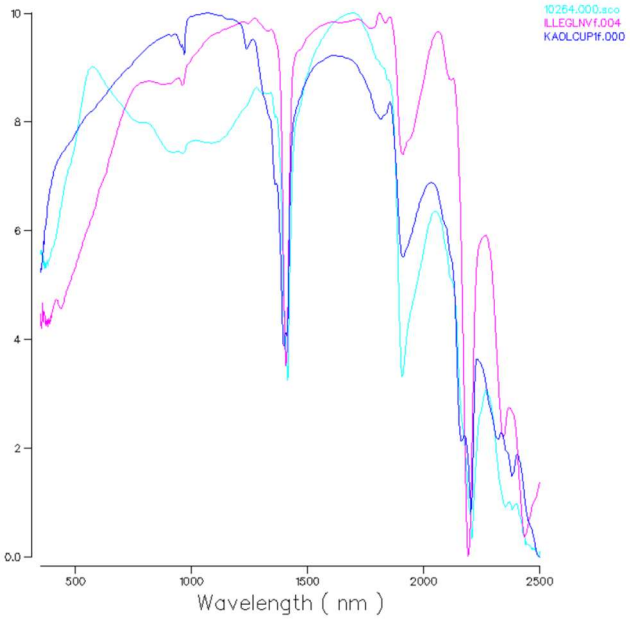

Brown-green porphyritic dacite dike. Major absorption peaks 1413nm, 2211nm. Water feature high intensity, sharp, inflected at 1968nm. Minor features abundant, include apparent doublet at 2351nm-2383nm, shoulder at 1359nm.

Composition: Illite, montmorillonite, minor kaolinite (?),

Group 4- Carlin zone

Sample: FC Dund

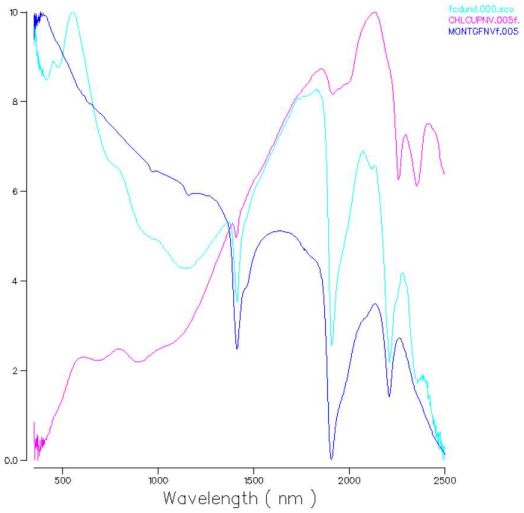

Green porphyry rhyolite dike with opaque white feldspar sites and quartz. Major absorption peaks 2211nm, 1910nm, 1413nm. Minor peaks 2359nm, 2117nm.

Composition: Chlorite, montmorillonite, minor illite.

Sample: 10129

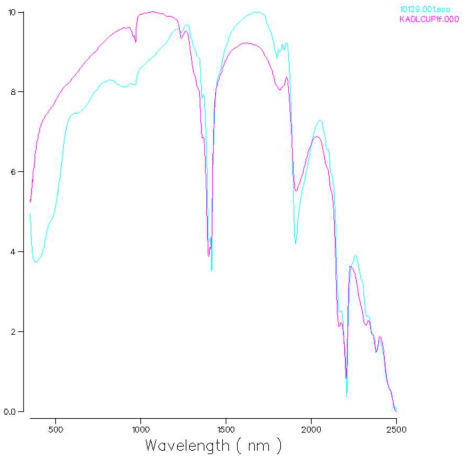

Buff-colored, argillically altered dacite dike. Absorption peaks at 2211nm, 1413nm. 1911nm water feature is high-intensity, sharp, inflected at 1968nm. Minor features, especially shoulders, abundant. Notable minor features include 2383nm peak, 2168nm shoulder, distinctive 1800nm skewed peak, 1362nm peak, subdued 1398nm-1413nm doublet.

Composition: Kaolinite, montmorillonite, minor illite (?)

Sample: FC 4

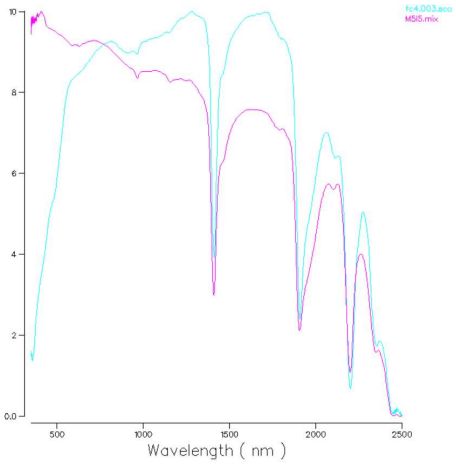

Buff-colored, argillically altered rhyolite dike. Absorption peaks at 1413nm, 2204nm. Major, sharp 1910nm water feature. 2351nm and 2445nm minor features present but subdued, shoulder at 1792nm.

Composition: Illite, montmorillonite

Sample: 10265

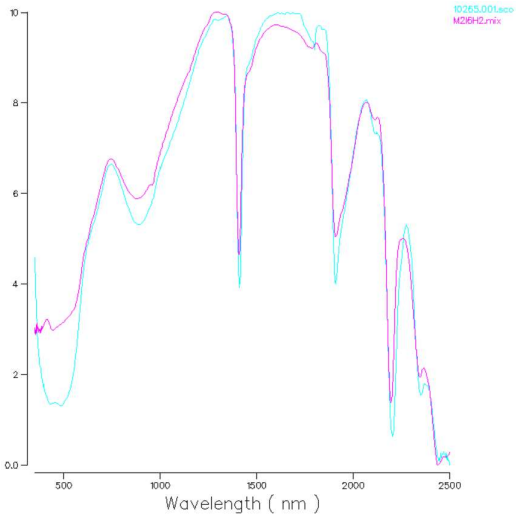

Red rhyolite porphyry dike. Cubic iron oxides. Minor calcite veining. Low wavelength feature below 1000nm indicates main iron oxide is hematite. Major absorption peaks 1413nm, 2203nm. Shoulders at 1468nm and 1968nm. Major water feature at 1910nm. High wavelength 2351nm and 2445nm subdued but present.

Composition: Illite, hematite, montmorillonite

Sample: 10290

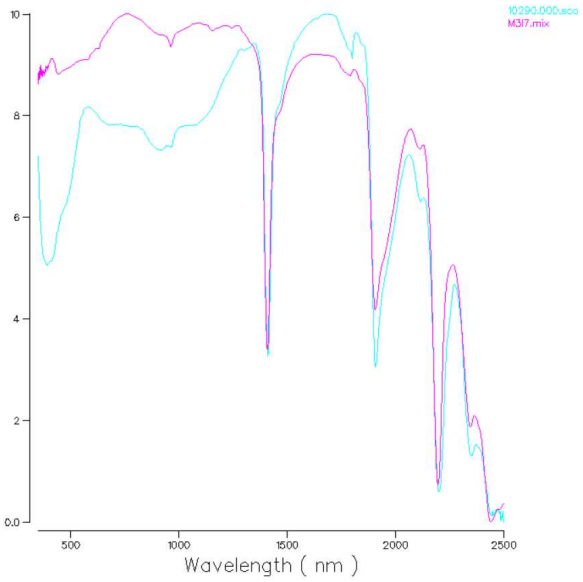

Pink-green finely porphyritic rhyolite dike. Minor cubic iron oxides. Absorption peaks at 1410nm, 2200nm. Water feature sharp, high intensity, inflected at 1967nm. Minor features at 2118nm, 2349nm, and 2447nm present, higher wavelengths are subdued.

Composition: Illite, montmorillonite

Discussion

Alteration of igneous rocks in the Cherry Creek district occurs in a number of places across the range. Kilometer-scale zonation from deep (intrusion-hosted) to shallow (<2km paleodepth) is reflected largely in the textures and alteration assemblages of the district's intrusive rocks, which provide an index and baseline for alteration despite variable host strata. Hyperspectral analyses, conducted with the ASD Terraspec, reveal the dominant products of alteration across four zones of increasing distance from the main Cherry Creek stock.

The deepest alteration phase (Group 1) is associated with quartz veining and feldspar-destructive hydrothermal activity up to 1km beneath the roof of the Cherry Creek stock. This alteration type is characterized by relatively little water-bearing mineralogy, limited mainly to quartz and minor amounts of montmorillonite. Illite and muscovite both appear to be present, the latter primarily associated with coarsely-crystalline quartz vein selvedge. Muscovite's hyperspectral signature is often best expressed in the 800nm-1350nm region with subdued 886nm and 963nm absorption peaks along a positive slope and single absorption low at 1362nm. These observations, along with the presence of major sharp features at 1409nm and 2200nm, subdued doublet at 2351nm and 2379nm, and a very minor 1900nm water feature, suggest that muscovite is a main phase. Other important phases in this zone include quartz and goethite. Montmorillonite, largely indicated by relatively sharp and exaggerated water features at 1900nm-1911nm with the characteristic inflected shape, may be related to surficial weathering rather than the primary hyrothermal alteration.

Alteration along the upper margin of the Cherry Creek stock (Group 2) is distinguished from the first group by its texture, which is characterized by near-complete destruction of igneous texture and disseminated silicification rather than quartz veining. Terraspec analyses of these samples indicate that their major mineralogical phases include illite, silica, and minor muscovite. The main hyperspectral distinction of this group is the general (2/3) absence of a characteristic muscovite-parallel hull between 800 and 1350nm. Instead, the low wavelength zone here retains a high pseudoreflectance that more closely mirrors the signature of illite, suggesting that illite rather than muscovite is the dominant phase. It is also possible that the low wavelength anomalies are attributable to a higher sulfide content in this group.

Beyond the margin of the stock, alteration occurs in porphyritic rhyolite and dacite dikes. For simplicity, the group selected here is from a discrete swarm between ½ and 3km from the uppermost exent of coarsely crystalline intrusive rocks (Group 3). Evidence of hydrothermal activity is most abundant in the main NE-trending structural corridor, which also hosts the highest abundance of dikes in stratigraphy above the stock. The alteration that characterizes this zone is mainly quartz-sericite-pyrite type with variable amounts of chlorite. Major hyperspectral features from this group are the major 1413nm and 2211nm absorption peaks, as well as the presence of a large amplitude sharp water feature at 1911nm. The shape of the profile in many ways parallels the first two groups, but is more likely here due to the presence of chlorite rather than muscovite due to the presence of a large and defined water feature and visual confirmation of chlorite.

Far removed from the mineralization of the previous three groups, the fourth group of altered igneous samples are from a $3km^2$ area over 6km from the nearest exposure of the igneous stock. This group is associated spatially with surface expression of jasperoid and Au-Ag-As-Sb-Tl mineralization within 2km of the paleosurface. Group 4 is characterized by hyperspectral profiles indicating sharp water features of equal of greater intensity than the other major peaks. Signatures of illite, especially in the higher wavelength range between 2350 and 2450nm indicate that this main clay constituent of the previous groups is present in the uppermost zone. However, relative intensity of the features indicate that montmorillonite is as important in this zone. Kaolinite is present in two of the most intensely argillized samples.

Appendix D Geochemistry

Appendix D1: Geochemistry of Igneous Rocks

		Sample No.	10082	10051	10054	10056	10057	10063	10066
		Rock Type	dacite	andesite	dacite	andesite	dacite	gabbro	gabbro
		Alteration							
		UTM E (NAD27)	677962	682689	682561	680088	679617	682932	682338
		UTM N (NAD27)	4418201	4425658	4424480	4418782	4418749	4423777	4423828
Method	Analysis	Unit							
ME-ICP06	SiO2	%	70.3	62.2	78.2	66.4	72.8	57.9	54.9
ME-ICP06	Al2O3	%	13.6	15.6	11.15	15.55	13.8	15.2	13.75
ME-ICP06	Fe2O3	%	2.52	2.67	2.32	6.31	2.23	6.02	7.13
ME-ICP06	CaO	%	1.48	4.47	0.1	0.73	1.5	5.52	6.25
ME-ICP06	MgO	%	0.51	1.12	0.48	1.73	0.39	4.28	7.03
ME-ICP06	Na2O	%	2.64	0.02	0.24	0.08	2.89	2.77	2.48
ME-ICP06	K2O	%	4.93	5	4.98	5.23	5.17	2.86	3.23
ME-ICP06	Cr2O3	%	<0.01	<0.01	0.01	<0.01	<0.01	0.03	0.07
ME-ICP06	TiO2	%	0.3	0.63	0.25	0.9	0.24	0.95	0.67
ME-ICP06	MnO	%	0.04	0.06	0.01	0.04	0.05	0.1	0.11
ME-ICP06	P2O5	%	0.17	0.2	0.02	0.34	0.07	0.31	0.24
ME-ICP06	SrO	%	0.03	<0.01	<0.01	0.01	0.02	0.08	0.06
ME-ICP06	BaO	%	0.12	0.06	0.1	0.13	0.11	0.19	0.21
ME-MS81	C	%	0.32	0.96	0.07	0.03	0.2	0.6	0.46
ME-MS81	S	%	0.01	<0.01	<0.01	0.01	0.02	<0.01	0.01
C-IR07	LOI	%	2.47	6.49	1.77	4.51	1.44	4.69	3.93
S-IR08	Total	%	99.11	98.52	99.63	101.96	100.71	100.9	100.06
ME-MS81	Ba	ppm	1180	540	874	1075	896	1625	1790
ME-MS81	Ce	ppm	128.5	114	33.1	107	101	101	61
ME-MS81	Cr	ppm	20	20	50	30	30	220	490
ME-MS81	Cs	ppm	4.5	7.24	3.03	7.94	3.58	1.16	0.6
ME-MS81	Dy	ppm	4.27	4.57	2.16	5.56	4.41	3.93	3.58
ME-MS81	Er	ppm	2.2	2.25	1.02	3.43	2.44	1.87	2.1
ME-MS81	Eu	ppm	1.22	1.53	0.61	1.47	0.98	1.64	1.3
ME-MS81	Ga	ppm	20.3	21.9	13.2	23.8	20	22	17.9
ME-MS81	Gd	ppm	5.5	5.58	1.81	6.9	5.08	5.47	4.55
ME-MS81	Ge	ppm	<5	<5	<5	<5	<5	<5	<5
ME-MS81	Hf	ppm	6.5	7.1	4.9	8.8	5.8	5.3	4.2
ME-MS81	Ho	ppm	0.84	0.86	0.38	1.11	0.82	0.78	0.76
ME-MS81	La	ppm	70.1	60.5	15.4	60.8	54.2	57	32.2
ME-MS81	Lu	ppm	0.36	0.33	0.2	0.55	0.39	0.26	0.31
ME-MS81	Nb	ppm	22.6	21.1	5.9	24.3	23.6	18.6	10.3
ME-MS81	Nd	ppm	47.6	45.4	11.6	47.7	38.2	40.8	27.9
ME-MS81	Pr	ppm	13.5	12.3	3.29	12.9	10.9	11.1	7.05
ME-MS81	Rb	ppm	222	266	147	282	233	82.6	89.3
ME-MS81	Sm	ppm	8.09	7.59	2.02	7.97	6.59	7.04	5.48
ME-MS81	Sn	ppm	4	2	1	5	13	1	1
ME-MS81	Sr	ppm	223	51.5	36.8	91.5	195.5	730	481
ME-MS81	Ta	ppm	1.8	1.1	0.4	1.3	2.1	1	0.4
ME-MS81	Tb	ppm	0.82	0.81	0.33	0.94	0.72	0.73	0.63
ME-MS81	Th	ppm	38.1	25.4	7.07	31.2	39	18.85	10.2
ME-MS81	Tm	ppm	0.34	0.33	0.2	0.46	0.31	0.3	0.28
ME-MS81	U	ppm	6.47	4.83	1.21	8.77	10.85	4.36	1.97
ME-MS81	V	ppm	23	44	26	128	17	116	145
ME-MS81	W	ppm	2	3	1	31	2	1	1
ME-MS81	Y	ppm	22.3	22.5	10.9	30.2	24.2	20.3	18.9
ME-MS42	Yb	ppm	2.16	2.21	1.21	3.45	2.47	1.86	2.26
ME-MS42	Zr	ppm	209	275	186	332	188	205	152
ME-MS42	As	ppm	3.2	2.8	0.6	6	1.7	1.3	1.1
ME-MS42	Bi	ppm	0.14	0.08	0.02	0.38	0.43	0.02	0.04
ME-MS42	Hg	ppm	0.02	0.009	0.008	0.068	0.013	<0.005	<0.005
ME-MS42	In	ppm	0.012	0.021	<0.005	0.077	0.067	0.022	0.017
ME-MS42	Re	ppm	<0.001	0.001	<0.001	0.001	0.001	<0.001	<0.001
ME-MS42	Sb	ppm	0.19	0.31	0.11	1.3	0.1	0.38	0.24
ME-MS42	Se	ppm	0.4	0.6	0.2	0.8	0.5	0.3	0.2
OA-GRA05	Te	ppm	<0.01	<0.01	<0.01	0.01	<0.01	<0.01	<0.01
TOT-ICP06	Tl	ppm	0.12	0.21	0.11	0.3	0.35	0.02	0.03
ME-4ACD81	Ag	ppm	<0.5	<0.5	0.8	<0.5	<0.5	1.4	0.6
ME-4ACD81	Cd	ppm	<0.5	<0.5	<0.5	<0.5	0.5	<0.5	<0.5
ME-4ACD81	Co	ppm	3	3	10	8	2	15	29
ME-4ACD81	Cu	ppm	2	5	1	69	5	3	46
ME-4ACD81	Li	ppm	20	10	20	60	30	40	10
ME-4ACD81	Mo	ppm	<1	<1	<1	8	1	<1	<1
ME-4ACD81	Ni	ppm	3	1	17	3	1	36	110
ME-4ACD81	Pb	ppm	26	21	15	18	49	20	18
ME-4ACD81	Sc	ppm	3	6	4	11	3	13	18
ME-4ACD81	Zn	ppm	45	46	17	91	114	79	69
Au-ICP21	Au	ppm	0.002	<0.001	<0.001	0.001	<0.001	0.011	0.006
Ag-OG62	Ag	ppm							
Pb-OG62	Pb	%							
Zn-OG62	Zn	%							

		Sample No.	10074	10084	10110	10111	10119	10122	10267
		Rock Type	tonalite	quartz monzonite	quartz monzonite	quartz monzodiorite	quartz monzonite	quartz monzonite	granodiorite
		Alteration							
		UTM E (NAD27)	682857	677777	677813	677788	680730	678911	680897
		UTM N (NAD27)	4424499	4417782	4417737	4417783	4420914	4417671	4421925
Method	Analysis	Unit							
ME-ICP06	SiO2	%	60.9	70.7	71.1	69.8	72.1	72.3	66.4
ME-ICP06	Al2O3	%	16.95	13.85	14.3	15.25	14.25	16.3	14.6
ME-ICP06	Fe2O3	%	5.82	3.14	3.03	3.33	2.79	1.15	4.56
ME-ICP06	CaO	%	4.76	2.39	1.74	2.69	1.16	1.89	1.03
ME-ICP06	MgO	%	2.76	0.67	0.78	0.81	0.5	0.25	1.43
ME-ICP06	Na2O	%	3.42	3.04	3.55	3.23	2.98	4.25	2.71
ME-ICP06	K2O	%	2.35	3.81	3.94	3.9	5.12	3.74	3.63
ME-ICP06	Cr2O3	%	0.01	<0.01	<0.01	<0.01	<0.01	<0.01	<0.01
ME-ICP06	TiO2	%	0.9	0.4	0.46	0.46	0.29	0.14	0.6
ME-ICP06	MnO	%	0.09	0.05	0.06	0.05	0.03	0.02	0.07
ME-ICP06	P2O5	%	0.22	0.16	0.15	0.2	0.1	0.04	0.19
ME-ICP06	SrO	%	0.06	0.04	0.05	0.05	0.02	0.13	0.03
ME-ICP06	BaO	%	0.11	0.11	0.13	0.13	0.11	0.38	0.11
ME-MS81	C	%	0.06	0.05	0.05	0.02	0.1	0.08	0.11
ME-MS81	S	%	<0.01	0.01	<0.01	<0.01	0.01	<0.01	0.02
C-IR07	LOI	%	2.26	0.68	1.31	0.6	1.35	0.8	3.49
S-IR08	Total	%	100.61	99.04	100.6	100.5	100.8	101.39	98.85
ME-MS81	Ba	ppm	971	1030	1180	1250	1055	3600	1015
ME-MS81	Ce	ppm	94.7	96.1	101.5	110	130.5	13.6	115
ME-MS81	Cr	ppm	50	20	20	20	20	20	20
ME-MS81	Cs	ppm	1.48	2.26	4.11	2.46	5.29	2.39	4.26
ME-MS81	Dy	ppm	4.63	3.86	3.63	3.95	3.9	0.65	4.24
ME-MS81	Er	ppm	2.51	1.97	1.84	1.75	2.15	0.41	2.44
ME-MS81	Eu	ppm	1.59	1.38	1.42	1.37	1.23	0.34	1.38
ME-MS81	Ga	ppm	22.4	22.3	21.5	22.9	20.8	20.2	21.2
ME-MS81	Gd	ppm	5.8	5.18	5.32	5.57	5.66	0.84	4.87
ME-MS81	Ge	ppm	<5	<5	<5	<5	<5	<5	<5
ME-MS81	Hf	ppm	5.8	5.6	6	6.5	6.6	2.9	7.4
ME-MS81	Ho	ppm	0.9	0.74	0.68	0.7	0.74	0.13	0.87
ME-MS81	La	ppm	50.6	53.4	56.4	61.2	72.9	7.9	55.1
ME-MS81	Lu	ppm	0.3	0.3	0.25	0.25	0.3	0.06	0.39
ME-MS81	Nb	ppm	17.2	21.3	21.2	21.5	22.7	9	19
ME-MS81	Nd	ppm	39.6	39.2	40.4	42.3	48.1	5.6	40.4
ME-MS81	Pr	ppm	10.3	10.45	10.9	11.8	13.65	1.49	11.6
ME-MS81	Rb	ppm	58.9	157.5	206	158	227	128	162
ME-MS81	Sm	ppm	6.97	6.73	7.37	7.38	8.42	1	6.42
ME-MS81	Sn	ppm	2	3	5	3	2	1	2
ME-MS81	Sr	ppm	566	348	443	416	224	1130	292
ME-MS81	Ta	ppm	1	2.1	1.7	2.1	2	0.5	1.3
ME-MS81	Tb	ppm	0.78	0.74	0.71	0.76	0.78	0.12	0.78
ME-MS81	Th	ppm	15.35	25.6	26.5	27.2	43.6	2.78	22.5
ME-MS81	Tm	ppm	0.33	0.29	0.26	0.25	0.31	0.06	0.32
ME-MS81	U	ppm	2.12	5.4	4.6	5.6	8.54	1.46	5.14
ME-MS81	V	ppm	114	37	37	40	22	10	87
ME-MS81	W	ppm	1	2	8	1	4	2	5
ME-MS81	Y	ppm	22.5	20.2	18	19.2	20.6	3.9	22.7
ME-MS42	Yb	ppm	2.27	1.93	1.57	1.74	2.04	0.37	2.44
ME-MS42	Zr	ppm	219	180	207	208	227	104	271
ME-MS42	As	ppm	1.4	1.3	0.5	0.4	4.5	0.5	3.9
ME-MS42	Bi	ppm	0.05	0.13	0.06	0.03	1.96	0.16	0.02
ME-MS42	Hg	ppm	<0.005	0.013	0.008	0.007	0.043	0.009	0.014
ME-MS42	In	ppm	0.018	0.029	0.014	0.032	0.01	0.009	0.027
ME-MS42	Re	ppm	<0.001	<0.001	<0.001	<0.001	<0.001	<0.001	<0.001
ME-MS42	Sb	ppm	0.15	0.15	0.23	0.08	0.46	0.11	0.34
ME-MS42	Se	ppm	0.5	0.3	0.3	0.2	0.6	0.2	<0.2
OA-GRA05	Te	ppm	<0.01	0.01	<0.01	<0.01	0.02	<0.01	0.01
TOT-ICP06	Tl	ppm	0.02	0.28	0.16	0.39	0.09	0.1	0.08
ME-4ACD81	Ag	ppm	<0.5	<0.5	<0.5	<0.5	<0.5	<0.5	<0.5
ME-4ACD81	Cd	ppm	<0.5	<0.5	<0.5	<0.5	<0.5	<0.5	<0.5
ME-4ACD81	Co	ppm	12	2	3	3	3	1	8
ME-4ACD81	Cu	ppm	5	17	2	1	11	2	3
ME-4ACD81	Li	ppm	20	20	20	30	20	10	30
ME-4ACD81	Mo	ppm	1	<1	<1	<1	<1	<1	1
ME-4ACD81	Ni	ppm	6	<1	<1	1	3	1	5
ME-4ACD81	Pb	ppm	20	23	16	22	46	35	17
ME-4ACD81	Sc	ppm	12	4	4	4	3	1	9
ME-4ACD81	Zn	ppm	79	51	44	67	30	20	67
Au-ICP21	Au	ppm	0.001	<0.001	0.001	0.001	0.002	<0.001	<0.001
Ag-OG62	Ag	ppm							
Pb-OG62	Pb	%							
Zn-OG62	Zn	%							

		Sample No.	10067	10072	10076	10079	10080	10085	10091
		Rock Type	gabbro	dacite	gabbro	monzonite	dacite	granite aplite	dacite
		Alteration							
		UTM E (NAD27)	682667	682577	682790	680584	680558	677437	678692
		UTM N (NAD27)	4423744	4424237	4423924	4420534	4420545	4418472	4417148
Method	Analysis	Unit							
ME-ICP06	SiO2	%	57.5	64.9	58.8	72.2	73.3	75.1	72.2
ME-ICP06	Al2O3	%	20.2	15.95	15.3	14.2	14.3	12.1	14.2
ME-ICP06	Fe2O3	%	7.32	4.07	6.03	2.46	2.41	1.98	2.87
ME-ICP06	CaO	%	0.22	2.31	5.49	1.03	0.85	1.01	1.4
ME-ICP06	MgO	%	2.75	1.06	4.26	0.44	0.48	0.3	0.34
ME-ICP06	Na2O	%	1.09	3.61	3.27	2.95	3.02	2.76	3.12
ME-ICP06	K2O	%	5.85	5.17	2.88	4.96	5.03	5.03	4.86
ME-ICP06	Cr2O3	%	0.02	<0.01	0.03	<0.01	<0.01	<0.01	<0.01
ME-ICP06	TiO2	%	0.81	0.6	0.96	0.29	0.29	0.19	0.26
ME-ICP06	MnO	%	0.04	0.06	0.09	0.04	0.04	0.03	0.09
ME-ICP06	P2O5	%	0.11	0.19	0.32	0.09	0.09	0.06	0.07
ME-ICP06	SrO	%	0.01	0.04	0.08	0.02	0.02	0.01	0.03
ME-ICP06	BaO	%	0.09	0.18	0.17	0.12	0.12	0.04	0.14
ME-MS81	C	%	0.02	0.28	0.5	0.22	0.18	0.03	0.27
ME-MS81	S	%	<0.01	<0.01	0.01	0.01	<0.01	0.01	<0.01
C-IR07	LOI	%	3.54	2.45	3.75	2.09	1.87	0.42	1.99
S-IR08	Total	%	99.55	100.59	101.43	100.89	101.82	99.03	101.57
ME-MS81	Ba	ppm	750	1535	1450	1050	963	425	1335
ME-MS81	Ce	ppm	117	127.5	105	129.5	117.5	36.7	143
ME-MS81	Cr	ppm	130	20	220	30	20	20	20
ME-MS81	Cs	ppm	6.97	1.56	0.82	3.59	3.79	1.76	5.29
ME-MS81	Dy	ppm	6.38	5.61	4.14	3.77	4.15	1.55	4.58
ME-MS81	Er	ppm	3.81	2.77	2.02	2.15	2.08	0.89	2.74
ME-MS81	Eu	ppm	1.55	1.56	1.76	1.05	0.96	0.63	1.39
ME-MS81	Ga	ppm	28.1	20.9	21.9	20.6	19.4	19.7	20.9
ME-MS81	Gd	ppm	6.96	6.64	5.7	5.25	5.11	1.63	5.81
ME-MS81	Ge	ppm	<5	<5	<5	<5	<5	<5	<5
ME-MS81	Hf	ppm	6.2	7.5	5.5	6.5	6.1	3.7	9.2
ME-MS81	Ho	ppm	1.29	0.96	0.79	0.72	0.76	0.31	0.94
ME-MS81	La	ppm	57.4	67.3	58.5	68.7	64.2	20.4	78.9
ME-MS81	Lu	ppm	0.56	0.41	0.3	0.28	0.3	0.19	0.41
ME-MS81	Nb	ppm	17.2	22.8	19.6	23.3	22.8	16	24.3
ME-MS81	Nd	ppm	50.6	50	43.1	44.4	43.8	13.5	50.5
ME-MS81	Pr	ppm	13.25	14	11.5	13.35	12.55	3.82	14.75
ME-MS81	Rb	ppm	186.5	176.5	93.5	209	208	192.5	212
ME-MS81	Sm	ppm	8.81	8.61	6.69	8.08	7.34	2.37	8.43
ME-MS81	Sn	ppm	4	3	2	3	3	1	2
ME-MS81	Sr	ppm	99.3	353	682	166.5	149.5	120	267
ME-MS81	Ta	ppm	1.1	1.4	1	1.7	1.8	1.4	1.9
ME-MS81	Tb	ppm	1.06	0.97	0.75	0.73	0.7	0.25	0.8
ME-MS81	Th	ppm	18.95	33.1	20.1	43.9	41.9	19.65	39.7
ME-MS81	Tm	ppm	0.52	0.41	0.29	0.33	0.31	0.14	0.39
ME-MS81	U	ppm	2.69	6.01	4.72	7.29	8.83	8.02	6.69
ME-MS81	V	ppm	115	56	120	23	21	22	12
ME-MS81	W	ppm	1	1	1	2	3	2	3
ME-MS81	Y	ppm	33.4	28.1	20.5	20.6	21.2	8.6	23.8
ME-MS42	Yb	ppm	3.77	2.65	1.89	2.23	2.04	1.07	2.61
ME-MS42	Zr	ppm	215	287	214	213	213	101	336
ME-MS42	As	ppm	0.4	1.3	0.9	1.3	0.7	0.7	0.7
ME-MS42	Bi	ppm	0.1	0.1	0.01	0.19	0.17	0.12	0.09
ME-MS42	Hg	ppm	<0.005	<0.005	<0.005	<0.005	<0.005	0.014	0.011
ME-MS42	In	ppm	0.013	0.028	0.015	0.015	0.013	0.017	0.009
ME-MS42	Re	ppm	<0.001	<0.001	<0.001	<0.001	<0.001	<0.001	<0.001
ME-MS42	Sb	ppm	0.11	0.84	0.31	0.23	0.06	0.1	0.23
ME-MS42	Se	ppm	0.4	0.6	0.4	0.4	0.3	0.2	0.3
OA-GRA05	Te	ppm	<0.01	<0.01	<0.01	0.01	<0.01	<0.01	<0.01
TOT-ICP06	Tl	ppm	0.11	0.05	0.02	0.13	0.13	0.12	0.13
ME-4ACD81	Ag	ppm	<0.5	2	<0.5	0.5	<0.5	<0.5	1.4
ME-4ACD81	Cd	ppm	<0.5	<0.5	<0.5	0.5	<0.5	<0.5	1.5
ME-4ACD81	Co	ppm	19	6	16	3	2	2	1
ME-4ACD81	Cu	ppm	6	6	2	5	3	27	4
ME-4ACD81	Li	ppm	30	20	20	20	20	<10	20
ME-4ACD81	Mo	ppm	<1	<1	<1	1	<1	4	<1
ME-4ACD81	Ni	ppm	50	1	37	3	1	1	2
ME-4ACD81	Pb	ppm	15	37	18	30	34	29	78
ME-4ACD81	Sc	ppm	13	7	13	3	3	3	3
ME-4ACD81	Zn	ppm	93	95	78	55	49	27	135
Au-ICP21	Au	ppm	0.002	0.006	0.001	<0.001	<0.001	0.001	0.003
Ag-OG62	Ag	ppm							
Pb-OG62	Pb	%							
Zn-OG62	Zn	%							

		Sample No.	10093	10096	10098	10105	10108	10109	10116
		Rock Type	quartz monzonite	virtric dacite	andesite	dacite	dacite	dacite	dacite
		Alteration	sodic-calcic						
		UTM E (NAD27)	678491	680193	680218	678965	677963	677983	678267
		UTM N (NAD27)	4417561	4422289	4422105	4417772	4417623	4417720	4416623
Method	Analysis	Unit							
ME-ICP06	SiO2	%	63.6	69	65.3	70.3	71.4	71	70.9
ME-ICP06	Al2O3	%	17.4	14.25	15.05	14.2	13.9	14.4	15.25
ME-ICP06	Fe2O3	%	2.49	3.08	4.53	3.16	2.48	2.83	2.84
ME-ICP06	CaO	%	3.26	1.99	2.83	1.08	1.71	0.99	0.24
ME-ICP06	MgO	%	1.01	0.54	1.36	0.35	0.49	0.39	0.63
ME-ICP06	Na2O	%	8.69	2.79	2.61	2.37	2.45	1.89	0.42
ME-ICP06	K2O	%	0.63	5.4	4.33	5.68	5.26	6.02	7.91
ME-ICP06	Cr2O3	%	<0.01	<0.01	<0.01	<0.01	<0.01	<0.01	<0.01
ME-ICP06	TiO2	%	0.55	0.35	0.63	0.26	0.3	0.27	0.38
ME-ICP06	MnO	%	0.09	0.06	0.06	0.09	0.05	0.03	0.02
ME-ICP06	P2O5	%	0.22	0.1	0.19	0.06	0.11	0.07	0.12
ME-ICP06	SrO	%	0.2	0.03	0.04	0.04	0.03	0.03	0.02
ME-ICP06	BaO	%	0.03	0.15	0.26	0.19	0.13	0.16	0.26
ME-MS81	C	%	0.3	0.65	0.34	0.16	0.36	0.24	0.03
ME-MS81	S	%	0.01	0.01	0.16	0.01	0.01	0.01	0.01
C-IR07	LOI	%	1.93	3.41	3.02	1.65	2.37	2.46	2.47
S-IR08	Total	%	100.1	101.15	100.21	99.43	100.68	100.54	101.46
ME-MS81	Ba	ppm	259	1395	2500	1735	1210	1500	2440
ME-MS81	Ce	ppm	114.5	138	108.5	140.5	132.5	139.5	129.5
ME-MS81	Cr	ppm	20	20	30	20	20	20	30
ME-MS81	Cs	ppm	0.53	5.51	5	4.58	6.52	7.84	17.45
ME-MS81	Dy	ppm	4.29	5.45	5.07	4.49	4.26	4.3	4.48
ME-MS81	Er	ppm	2.01	2.84	2.62	2.48	2.07	2.43	2.48
ME-MS81	Eu	ppm	1.63	1.49	1.54	1.43	1.21	1.32	1.29
ME-MS81	Ga	ppm	25.9	19.9	20.6	19.8	21.2	19.6	20.7
ME-MS81	Gd	ppm	5.94	6.78	5.93	6.09	5.85	5.65	5.99
ME-MS81	Ge	ppm	<5	<5	<5	<5	<5	<5	<5
ME-MS81	Hf	ppm	7	8.3	7.9	8.9	6.5	9.2	7.3
ME-MS81	Ho	ppm	0.75	1.07	1.02	0.91	0.78	0.89	0.83
ME-MS81	La	ppm	62.8	76.3	57.2	77.8	73.7	78.2	70.2
ME-MS81	Lu	ppm	0.29	0.45	0.37	0.38	0.31	0.38	0.34
ME-MS81	Nb	ppm	23.9	23.8	19.8	23.1	23.3	23.5	21.9
ME-MS81	Nd	ppm	45.6	50.5	43.6	50.2	46.9	50.4	48.8
ME-MS81	Pr	ppm	12.1	14.25	11.65	14.25	13.75	14.25	13.95
ME-MS81	Rb	ppm	23.3	209	168.5	269	314	285	341
ME-MS81	Sm	ppm	8.48	9.01	7.41	8.34	8.05	8.46	8.57
ME-MS81	Sn	ppm	14	4	5	3	2	3	4
ME-MS81	Sr	ppm	1645	248	321	297	206	239	169
ME-MS81	Ta	ppm	1.8	1.9	1.4	1.9	2	1.8	1.7
ME-MS81	Tb	ppm	0.8	0.99	0.86	0.83	0.78	0.8	0.84
ME-MS81	Th	ppm	26.9	37.9	23	36.6	43.1	38.1	36.1
ME-MS81	Tm	ppm	0.3	0.43	0.38	0.37	0.32	0.36	0.36
ME-MS81	U	ppm	6.29	8.13	5.89	6.75	6.38	7.07	7.8
ME-MS81	V	ppm	43	21	68	11	22	11	25
ME-MS81	W	ppm	9	2	1	11	9	8	10
ME-MS81	Y	ppm	20.5	27.5	25	24.2	21.1	23.1	23.4
ME-MS42	Yb	ppm	1.92	2.91	2.49	2.39	1.87	2.38	2.35
ME-MS42	Zr	ppm	244	297	289	319	224	344	260
ME-MS42	As	ppm	1	1.4	2.2	1.3	0.5	0.8	5.1
ME-MS42	Bi	ppm	0.06	0.3	0.17	0.88	0.09	0.1	0.8
ME-MS42	Hg	ppm	0.007	0.032	0.041	0.019	0.01	0.007	0.043
ME-MS42	In	ppm	0.091	0.027	0.026	0.079	0.006	0.015	0.037
ME-MS42	Re	ppm	<0.001	<0.001	<0.001	<0.001	<0.001	<0.001	<0.001
ME-MS42	Sb	ppm	0.19	0.44	0.72	0.45	0.14	0.14	0.37
ME-MS42	Se	ppm	0.2	0.3	0.3	0.3	0.3	0.5	0.5
OA-GRA05	Te	ppm	0.02	<0.01	0.04	0.01	<0.01	<0.01	<0.01
TOT-ICP06	Tl	ppm	0.02	0.11	0.21	0.15	0.24	0.28	0.88
ME-4ACD81	Ag	ppm	0.5	<0.5	5.1	0.6	<0.5	<0.5	2.2
ME-4ACD81	Cd	ppm	<0.5	<0.5	<0.5	2.3	1.6	0.7	1.1
ME-4ACD81	Co	ppm	1	1	7	3	2	2	3
ME-4ACD81	Cu	ppm	1	3	14	24	4	5	382
ME-4ACD81	Li	ppm	<10	10	20	30	20	30	30
ME-4ACD81	Mo	ppm	<1	2	2	<1	<1	<1	<1
ME-4ACD81	Ni	ppm	2	2	2	1	4	1	6
ME-4ACD81	Pb	ppm	3	28	24	181	22	40	245
ME-4ACD81	Sc	ppm	5	4	7	3	3	3	4
ME-4ACD81	Zn	ppm	23	61	51	572	82	107	2220
Au-ICP21	Au	ppm	0.004	0.001	0.036	0.057	0.013	0.006	0.002
Ag-OG62	Ag	ppm							
Pb-OG62	Pb	%							
Zn-OG62	Zn	%							

		Sample No.	10120	10253	10254	10273	10288	10290
		Rock Type	dacite	andesite	andesite	dacite	andesite	dacite
		Alteration						
		UTM E (NAD27)	678750	680193	680209	682790	681634	676826
		UTM N (NAD27)	4418681	4422124	4422112	4426558	4423396	4421589
Method	Analysis	Unit						
ME-ICP06	SiO2	%	73.2	63.5	63	73.1	64.6	73.8
ME-ICP06	Al2O3	%	13.8	15.15	15	13.85	16.65	13.7
ME-ICP06	Fe2O3	%	2.1	4.21	4.33	2.38	4.56	1.72
ME-ICP06	CaO	%	1.4	3.21	3.61	0.25	4.64	2.32
ME-ICP06	MgO	%	0.38	1.33	1.35	0.18	2.07	0.41
ME-ICP06	Na2O	%	3.24	2.6	2.76	2.97	3.1	0.02
ME-ICP06	K2O	%	5.02	4.5	4.23	5.35	2.79	3.86
ME-ICP06	Cr2O3	%	<0.01	<0.01	<0.01	<0.01	<0.01	<0.01
ME-ICP06	TiO2	%	0.23	0.59	0.6	0.21	0.7	0.23
ME-ICP06	MnO	%	0.04	0.07	0.07	0.05	0.08	0.03
ME-ICP06	P2O5	%	0.06	0.19	0.19	0.07	0.17	0.09
ME-ICP06	SrO	%	0.02	0.05	0.05	0.01	0.07	<0.01
ME-ICP06	BaO	%	0.09	0.15	0.14	0.09	0.15	0.16
ME-MS81	C	%	0.26	0.42	0.47	0.06	0.22	0.54
ME-MS81	S	%	<0.01	0.05	0.09	0.01	0.01	0.04
C-IR07	LOI	%	1.71	3.18	3.01	1.52	2.29	4.74
S-IR08	Total	%	101.29	98.73	98.34	100.03	101.87	101.08
ME-MS81	Ba	ppm	914	1415	1320	932	1405	1420
ME-MS81	Ce	ppm	108	120	117.5	150.5	96	63.4
ME-MS81	Cr	ppm	30	20	10	10	20	10
ME-MS81	Cs	ppm	4.5	5.83	4.07	3.48	3.69	8.35
ME-MS81	Dy	ppm	4.35	4.88	4.82	5.45	3.92	2.96
ME-MS81	Er	ppm	2.45	2.61	2.65	3.05	2.11	1.66
ME-MS81	Eu	ppm	1.09	1.51	1.44	1.15	1.62	0.82
ME-MS81	Ga	ppm	20.6	21.1	20.8	22.1	23.8	19.8
ME-MS81	Gd	ppm	5.92	5.93	5.69	7.45	5.31	3.15
ME-MS81	Ge	ppm	<5	<5	<5	<5	<5	<5
ME-MS81	Hf	ppm	6	7.5	6.8	6.8	5.6	4.5
ME-MS81	Ho	ppm	0.84	0.96	0.95	1.08	0.71	0.58
ME-MS81	La	ppm	58.8	61.3	61	79.2	49.8	33.8
ME-MS81	Lu	ppm	0.38	0.42	0.4	0.48	0.31	0.32
ME-MS81	Nb	ppm	23.8	20.9	20.2	26.7	17.1	18.9
ME-MS81	Nd	ppm	41	46	45.1	52.7	38.3	24.1
ME-MS81	Pr	ppm	11.4	12.9	12.85	15.55	10.5	6.69
ME-MS81	Rb	ppm	236	189.5	167.5	257	76.7	207
ME-MS81	Sm	ppm	6.86	7.66	7.98	9.05	6.78	3.91
ME-MS81	Sn	ppm	4	2	2	1	2	1
ME-MS81	Sr	ppm	197	426	426	110.5	692	28
ME-MS81	Ta	ppm	2.5	1.3	1.3	2.2	1	1.3
ME-MS81	Tb	ppm	0.83	0.83	0.89	1.01	0.74	0.53
ME-MS81	Th	ppm	38.3	24	22.9	42.2	13.85	16.7
ME-MS81	Tm	ppm	0.39	0.39	0.34	0.43	0.33	0.29
ME-MS81	U	ppm	11.05	5.57	5.24	8.76	2.94	4.53
ME-MS81	V	ppm	19	64	68	12	51	28
ME-MS81	W	ppm	5	3	2	2	1	3
ME-MS81	Y	ppm	24.4	26.3	26.9	31.4	21.5	17.6
ME-MS42	Yb	ppm	2.43	2.35	2.31	2.92	2.01	1.75
ME-MS42	Zr	ppm	192	282	273	237	215	153
ME-MS42	As	ppm	0.4	2.1	2	2.9	1.2	76.8
ME-MS42	Bi	ppm	0.42	0.05	0.04	0.15	0.09	0.04
ME-MS42	Hg	ppm	0.011	0.019	0.022	<0.005	0.011	0.024
ME-MS42	In	ppm	0.014	0.034	0.031	0.017	0.019	0.011
ME-MS42	Re	ppm	<0.001	0.001	<0.001	<0.001	<0.001	<0.001
ME-MS42	Sb	ppm	0.1	1.21	2.27	0.26	0.91	0.74
ME-MS42	Se	ppm	0.6	<0.2	0.2	<0.2	<0.2	0.3
OA-GRA05	Te	ppm	<0.01	<0.01	0.01	0.01	0.01	0.01
TOT-ICP06	Tl	ppm	0.12	0.19	0.16	0.09	0.18	0.24
ME-4ACD81	Ag	ppm	<0.5	0.6	0.7	<0.5	0.6	0.6
ME-4ACD81	Cd	ppm	<0.5	<0.5	<0.5	<0.5	<0.5	<0.5
ME-4ACD81	Co	ppm	2	8	7	2	7	2
ME-4ACD81	Cu	ppm	5	8	14	2	4	2
ME-4ACD81	Li	ppm	20	20	30	10	30	<10
ME-4ACD81	Mo	ppm	<1	2	1	1	2	1
ME-4ACD81	Ni	ppm	1	3	4	1	3	1
ME-4ACD81	Pb	ppm	39	37	39	36	20	83
ME-4ACD81	Sc	ppm	3	8	7	4	9	3
ME-4ACD81	Zn	ppm	53	79	80	44	91	41
Au-ICP21	Au	ppm	<0.001	0.004	0.008	<0.001	<0.001	0.011
Ag-OG62	Ag	ppm						
Pb-OG62	Pb	%						
Zn-OG62	Zn	%						

		Sample No.	10280	10282
		Rock Type	rhyolite	rhyolite
		Alteration		
		UTM E (NAD27)	670532	670592
		UTM N (NAD27)	4420569	4420293
Method	Analysis	Unit		
ME-ICP06	SiO2	%	72.9	67.4
ME-ICP06	Al2O3	%	13.25	14.6
ME-ICP06	Fe2O3	%	1.92	3.03
ME-ICP06	CaO	%	1.58	2.65
ME-ICP06	MgO	%	0.32	0.72
ME-ICP06	Na2O	%	2.81	2.95
ME-ICP06	K2O	%	5.42	4.74
ME-ICP06	Cr2O3	%	<0.01	<0.01
ME-ICP06	TiO2	%	0.17	0.42
ME-ICP06	MnO	%	0.06	0.06
ME-ICP06	P2O5	%	0.05	0.14
ME-ICP06	SrO	%	0.01	0.04
ME-ICP06	BaO	%	0.07	0.16
ME-MS81	C	%	0.13	0.08
ME-MS81	S	%	0.01	0.01
C-IR07	LOI	%	1.56	2.72
S-IR08	Total	%	100.12	99.63
ME-MS81	Ba	ppm	641	1405
ME-MS81	Ce	ppm	136	145
ME-MS81	Cr	ppm	10	10
ME-MS81	Cs	ppm	5.59	4.42
ME-MS81	Dy	ppm	4.59	4.56
ME-MS81	Er	ppm	2.47	2.35
ME-MS81	Eu	ppm	0.99	1.45
ME-MS81	Ga	ppm	20.2	20.6
ME-MS81	Gd	ppm	5.85	6.34
ME-MS81	Ge	ppm	<5	<5
ME-MS81	Hf	ppm	6	7.3
ME-MS81	Ho	ppm	0.94	0.93
ME-MS81	La	ppm	64.7	76.2
ME-MS81	Lu	ppm	0.43	0.32
ME-MS81	Nb	ppm	26.9	22
ME-MS81	Nd	ppm	45.7	52.3
ME-MS81	Pr	ppm	13.45	14.95
ME-MS81	Rb	ppm	283	189
ME-MS81	Sm	ppm	7.56	8.59
ME-MS81	Sn	ppm	2	3
ME-MS81	Sr	ppm	147	355
ME-MS81	Ta	ppm	2.3	1.4
ME-MS81	Tb	ppm	0.91	0.87
ME-MS81	Th	ppm	48.3	32.5
ME-MS81	Tm	ppm	0.37	0.3
ME-MS81	U	ppm	4.68	6.04
ME-MS81	V	ppm	13	28
ME-MS81	W	ppm	4	1
ME-MS81	Y	ppm	26.5	25.5
ME-MS42	Yb	ppm	2.68	2.13
ME-MS42	Zr	ppm	204	268
ME-MS42	As	ppm	2.8	0.8
ME-MS42	Bi	ppm	0.05	0.1
ME-MS42	Hg	ppm	0.009	0.02
ME-MS42	In	ppm	0.023	0.014
ME-MS42	Re	ppm	<0.001	<0.001
ME-MS42	Sb	ppm	2.44	4.88
ME-MS42	Se	ppm	<0.2	<0.2
OA-GRA05	Te	ppm	0.01	0.01
TOT-ICP06	Tl	ppm	0.19	0.14
ME-4ACD81	Ag	ppm	1.7	3.3
ME-4ACD81	Cd	ppm	<0.5	<0.5
ME-4ACD81	Co	ppm	<1	4
ME-4ACD81	Cu	ppm	7	10
ME-4ACD81	Li	ppm	40	10
ME-4ACD81	Mo	ppm	2	2
ME-4ACD81	Ni	ppm	2	3
ME-4ACD81	Pb	ppm	39	40
ME-4ACD81	Sc	ppm	3	6
ME-4ACD81	Zn	ppm	67	75
Au-ICP21	Au	ppm	<0.001	<0.001
Ag-OG62	Ag	ppm		
Pb-OG62	Pb	%		
Zn-OG62	Zn	%		

Appendix D2: Geochemistry of Altered Igneous Rocks

		Sample No.	10065	10090	10092	10099	10100	10102	10114
		Rock Type	dacite	dacite	dacite	dacite	dacite	dacite	dacite
		Alteration	phyllic	chloritic	phyllic	phyllic	phyllic	phyllic	phyllic
		UTM E (NAD27)	682784	678610	678490	678165	678465	679107	679475
		UTM N (NAD27)	4423777	4417406	4417450	4421724	4421724	4422704	4419290
Method	**Analysis**	**Unit**							
ME-ICP06	SiO2	%	70.5	71.1	85.1	72.8	72.2	73.4	73.1
ME-ICP06	Al2O3	%	14.4	14.4	8.95	13.5	13.6	13.5	14
ME-ICP06	Fe2O3	%	2.74	2.94	2.4	2.15	2.04	2.16	2.25
ME-ICP06	CaO	%	1.56	1.07	0.1	2.06	2.78	1.63	0.21
ME-ICP06	MgO	%	0.49	0.37	0.33	0.43	0.44	0.27	0.47
ME-ICP06	Na2O	%	3.1	3.43	0.08	1.43	0.04	2.69	2.02
ME-ICP06	K2O	%	4.83	4.89	2.87	4.98	4.1	4.54	5.37
ME-ICP06	Cr2O3	%	<0.01	<0.01	<0.01	<0.01	<0.01	<0.01	<0.01
ME-ICP06	TiO2	%	0.35	0.28	0.22	0.23	0.23	0.24	0.27
ME-ICP06	MnO	%	0.04	0.06	0.01	0.04	0.04	0.05	0.04
ME-ICP06	P2O5	%	0.1	0.07	0.07	0.09	0.08	0.09	0.1
ME-ICP06	SrO	%	0.02	0.03	<0.01	0.02	<0.01	0.02	0.03
ME-ICP06	BaO	%	0.14	0.15	0.06	0.16	0.04	0.13	0.12
ME-MS81	C	%	0.38	0.11	0.08	0.42	0.61	0.33	0.05
ME-MS81	S	%	0.01	0.01	0.01	<0.01	<0.01	<0.01	<0.01
C-IR07	LOI	%	2.64	1.39	1.8	3.4	4.68	2.71	2.04
S-IR08	Total	%	100.91	100.18	101.99	101.29	100.27	101.43	100.02
ME-MS81	Ba	ppm	1165	1375	604	1460	391	1165	1155
ME-MS81	Ce	ppm	125	143.5	75.2	57.2	59.6	60	115.5
ME-MS81	Cr	ppm	20	20	30	20	20	20	20
ME-MS81	Cs	ppm	3.78	5.9	8.28	7.67	6.05	3.06	5.76
ME-MS81	Dy	ppm	4.21	4.75	2.94	3.32	3.1	3.43	3.83
ME-MS81	Er	ppm	2.16	2.58	1.49	1.76	1.87	1.92	2.06
ME-MS81	Eu	ppm	1.33	1.4	0.91	0.9	0.91	0.95	0.91
ME-MS81	Ga	ppm	19.8	21.2	13.9	20.2	19.5	20.1	19.8
ME-MS81	Gd	ppm	5.27	5.76	3.71	3.5	3.59	3.82	4.61
ME-MS81	Ge	ppm	<5	<5	<5	<5	<5	<5	<5
ME-MS81	Hf	ppm	6.7	9.7	4.4	5	4.6	5.1	6.4
ME-MS81	Ho	ppm	0.8	0.95	0.59	0.68	0.61	0.7	0.71
ME-MS81	La	ppm	68.4	79.3	41.7	31.2	32.9	32.9	59.7
ME-MS81	Lu	ppm	0.3	0.4	0.22	0.36	0.31	0.33	0.33
ME-MS81	Nb	ppm	21.6	23.7	12.9	18.4	18	19.1	23.1
ME-MS81	Nd	ppm	46.5	51.2	27.9	22.6	23	23.4	40.8
ME-MS81	Pr	ppm	13.3	14.7	7.92	6.03	6.33	6.59	11.55
ME-MS81	Rb	ppm	181	210	267	203	184.5	173.5	254
ME-MS81	Sm	ppm	7.35	8.17	4.56	4.4	4.34	4.54	7.3
ME-MS81	Sn	ppm	3	1	3	2	2	1	7
ME-MS81	Sr	ppm	184.5	279	15.4	174.5	29.1	165	193.5
ME-MS81	Ta	ppm	1.5	1.8	1.1	1.3	1.3	1.4	2.1
ME-MS81	Tb	ppm	0.78	0.91	0.58	0.55	0.57	0.59	0.7
ME-MS81	Th	ppm	36.1	37.7	19.45	15.85	15.9	16.6	40.4
ME-MS81	Tm	ppm	0.34	0.4	0.22	0.29	0.29	0.31	0.33
ME-MS81	U	ppm	6.24	6.83	4.11	4.65	4.15	4.43	8.17
ME-MS81	V	ppm	28	10	26	23	25	22	19
ME-MS81	W	ppm	2	2	11	2	5	233	5
ME-MS81	Y	ppm	21.5	24.4	16.2	17.7	17.4	19.2	19.2
ME-MS42	Yb	ppm	2.27	2.7	1.58	2.11	1.86	1.99	2.06
ME-MS42	Zr	ppm	235	351	149	146	146	150	197
ME-MS42	As	ppm	1.3	0.8	79.8	2.5	8.6	0.7	2.2
ME-MS42	Bi	ppm	0.05	0.08	2.18	0.05	0.04	0.03	0.44
ME-MS42	Hg	ppm	<0.005	0.009	0.021	0.013	0.011	0.028	0.055
ME-MS42	In	ppm	0.015	0.009	0.015	0.006	0.011	0.006	0.029
ME-MS42	Re	ppm	<0.001	<0.001	<0.001	<0.001	<0.001	0.001	<0.001
ME-MS42	Sb	ppm	0.8	0.49	1	0.37	0.95	2.46	0.13
ME-MS42	Se	ppm	0.4	0.3	<0.2	0.4	0.3	0.2	<0.2
OA-GRA05	Te	ppm	<0.01	<0.01	0.09	<0.01	<0.01	<0.01	0.01
TOT-ICP06	Tl	ppm	0.12	0.09	0.2	0.16	0.16	0.09	0.18
ME-4ACD81	Ag	ppm	2.3	3.5	1.5	0.8	2.2	2.8	2.2
ME-4ACD81	Cd	ppm	<0.5	0.6	<0.5	<0.5	<0.5	<0.5	1.1
ME-4ACD81	Co	ppm	3	1	2	2	2	2	3
ME-4ACD81	Cu	ppm	2	2	12	1	1	5	10
ME-4ACD81	Li	ppm	20	20	60	<10	10	10	20
ME-4ACD81	Mo	ppm	1	1	23	<1	<1	1	<1
ME-4ACD81	Ni	ppm	1	1	<1	1	<1	1	1
ME-4ACD81	Pb	ppm	30	50	43	22	29	24	50
ME-4ACD81	Sc	ppm	4	3	2	3	3	3	3
ME-4ACD81	Zn	ppm	52	121	61	34	36	36	222
Au-ICP21	Au	ppm	0.02	0.002	0.068	0.008	0.013	0.002	0.001
Ag-OG62	Ag	ppm							
Pb-OG62	Pb	%							
Zn-OG62	Zn	%							

		Sample No.	10123	10251	10255	10256	10264	10265	10275
		Rock Type	rhyolite	dacite	andesite	dacite	dacite	dacite	dacite
		Alteration	phyllic	phyllic	oxidized	phyllic	chloritic	phyllic	chloritic
		UTM E (NAD27)	680730	680895	680197	678163	681535	677994	682345
		UTM N (NAD27)	4420869	4421923	4422117	4421724	4423332	4423513	4425686
Method	**Analysis**	**Unit**							
ME-ICP06	SiO2	%	77.8	71.3	63.1	71.1	71.5	72.1	71
ME-ICP06	Al2O3	%	13.95	14.15	16.5	13.65	12.3	14.25	13.5
ME-ICP06	Fe2O3	%	1.71	2.14	4.03	1.85	1.23	1.25	1.84
ME-ICP06	CaO	%	0.11	0.5	2.82	2.52	4.44	0.36	2.6
ME-ICP06	MgO	%	0.44	0.3	0.79	0.43	0.25	0.51	0.79
ME-ICP06	Na2O	%	0.07	2.77	0.34	0.05	0.02	0.03	0.03
ME-ICP06	K2O	%	4.54	5	3.69	4.59	2.93	3.73	3.8
ME-ICP06	Cr2O3	%	<0.01	<0.01	<0.01	<0.01	<0.01	<0.01	<0.01
ME-ICP06	TiO2	%	0.25	0.3	0.72	0.23	0.12	0.48	0.27
ME-ICP06	MnO	%	0.01	0.03	0.08	0.04	0.02	0.05	0.02
ME-ICP06	P2O5	%	0.04	0.1	0.25	0.08	0.03	0.15	0.08
ME-ICP06	SrO	%	<0.01	0.02	0.01	<0.01	<0.01	0.04	<0.01
ME-ICP06	BaO	%	0.06	0.12	0.09	0.08	<0.01	3.52	0.03
ME-MS81	C	%	0.02	0.05	0.56	0.55	1.02	0.05	0.62
ME-MS81	S	%	<0.01	<0.01	0.01	0.02	0.01	0.77	0.01
C-IR07	LOI	%	2.26	2.09	6.6	4.44	6.58	3.78	5.28
S-IR08	Total	%	101.24	98.82	99.02	99.06	99.42	100.25	99.24
ME-MS81	Ba	ppm	559	1145	836	809	35.6	>10000	272
ME-MS81	Ce	ppm	111.5	149.5	139.5	69.7	121.5	107.5	134.5
ME-MS81	Cr	ppm	20	10	10	<10	10	10	10
ME-MS81	Cs	ppm	9.22	3.78	5.85	8.17	8.46	6.12	7.11
ME-MS81	Dy	ppm	3.82	3.89	5.89	3.29	5.12	2.72	4.05
ME-MS81	Er	ppm	2.12	2.19	2.99	1.93	2.7	1.25	2.1
ME-MS81	Eu	ppm	1.07	1.1	1.76	1.02	0.94	0.92	1.04
ME-MS81	Ga	ppm	20.6	21.1	23.2	20.3	19	24.1	20.4
ME-MS81	Gd	ppm	5.25	5.69	7.03	4.08	6.86	3.95	5.23
ME-MS81	Ge	ppm	<5	<5	<5	<5	<5	<5	<5
ME-MS81	Hf	ppm	6.3	6.3	7.9	5	4.8	6.1	5.8
ME-MS81	Ho	ppm	0.68	0.84	1.11	0.67	1	0.46	0.74
ME-MS81	La	ppm	61.9	62.4	71.9	37.6	61.6	54.3	71
ME-MS81	Lu	ppm	0.31	0.31	0.48	0.39	0.52	0.22	0.33
ME-MS81	Nb	ppm	23	24.5	24.7	20.4	30.5	22.1	23.2
ME-MS81	Nd	ppm	42.6	45.5	53.3	26	45.5	38.3	46.5
ME-MS81	Pr	ppm	11.85	13.45	14.95	7.59	13.05	11.25	13.95
ME-MS81	Rb	ppm	307	235	195	212	219	216	211
ME-MS81	Sm	ppm	7.23	7.96	8.54	4.8	7.99	6.26	7.16
ME-MS81	Sn	ppm	8	2	2	2	1	3	5
ME-MS81	Sr	ppm	11.2	182	101.5	39.4	64.9	417	32.5
ME-MS81	Ta	ppm	2.2	1.9	1.6	1.3	2.5	1.6	1.8
ME-MS81	Tb	ppm	0.74	0.77	1.13	0.65	0.97	0.5	0.8
ME-MS81	Th	ppm	39	44.3	29.3	17.85	46.7	26	40.8
ME-MS81	Tm	ppm	0.29	0.34	0.48	0.3	0.43	0.19	0.31
ME-MS81	U	ppm	8.96	7.18	6.4	4.48	8.11	6.24	8.14
ME-MS81	V	ppm	18	28	69	25	5	59	19
ME-MS81	W	ppm	4	2	4	4	2	6	4
ME-MS81	Y	ppm	18.8	22.2	32.3	21.2	29.5	13.4	22.7
ME-MS42	Yb	ppm	1.97	2.31	3.09	2.31	2.88	1.31	2.19
ME-MS42	Zr	ppm	200	221	312	171	144	236	211
ME-MS42	As	ppm	1.1	7.8	5.6	9.4	8.6	119	22.9
ME-MS42	Bi	ppm	0.1	0.03	0.06	0.02	0.02	0.11	0.27
ME-MS42	Hg	ppm	<0.005	0.021	0.035	0.024	0.35	0.033	0.054
ME-MS42	In	ppm	0.009	0.014	0.042	<0.005	0.005	0.019	0.015
ME-MS42	Re	ppm	<0.001	<0.001	0.001	0.002	<0.001	<0.001	<0.001
ME-MS42	Sb	ppm	0.11	0.35	0.64	0.57	0.89	0.97	1.72
ME-MS42	Se	ppm	0.4	<0.2	<0.2	0.2	0.3	<0.2	<0.2
OA-GRA05	Te	ppm	<0.01	<0.01	0.01	0.01	0.02	0.01	0.01
TOT-ICP06	Tl	ppm	0.28	0.12	0.12	0.17	0.26	0.17	0.14
ME-4ACD81	Ag	ppm	<0.5	0.7	0.6	<0.5	0.8	0.7	3.2
ME-4ACD81	Cd	ppm	<0.5	<0.5	<0.5	<0.5	3.6	0.5	0.8
ME-4ACD81	Co	ppm	2	3	7	2	<1	2	1
ME-4ACD81	Cu	ppm	3	3	4	1	4	3	21
ME-4ACD81	Li	ppm	10	20	30	10	20	10	20
ME-4ACD81	Mo	ppm	1	1	1	1	<1	2	1
ME-4ACD81	Ni	ppm	2	4	3	1	1	4	5
ME-4ACD81	Pb	ppm	36	36	22	26	37	27	52
ME-4ACD81	Sc	ppm	3	3	8	3	3	3	3
ME-4ACD81	Zn	ppm	23	65	70	37	212	61	171
Au-ICP21	Au	ppm	<0.001	0.005	<0.001	<0.001	<0.001	0.002	<0.001
Ag-OG62	Ag	ppm							
Pb-OG62	Pb	%							
Zn-OG62	Zn	%							

		Sample No.	10283	10285	10055	10068	10075	10094	10106
		Rock Type	dacite	dacite	granite	tonalite	tonalite	monzonite	quartz monzonite
		Alteration	phyllic	chloritic	phyllic	chloritic	chloritic	phyllic	phyllic
		UTM E (NAD27)	682133	681496	680110	682667	682700	678498	679301
		UTM N (NAD27)	4425567	4423278	4418807	4424048	4423999	4417546	4417821
Method	Analysis	Unit							
ME-ICP06	SiO2	%	78	75	78.6	59.2	61.4	83.7	74
ME-ICP06	Al2O3	%	13.1	14.3	12.35	14.4	16.95	8.59	12.55
ME-ICP06	Fe2O3	%	2.17	1.85	1.38	5.3	5.38	1.69	2.56
ME-ICP06	CaO	%	0.05	1.11	0.24	7.07	5.03	1.19	1.65
ME-ICP06	MgO	%	0.49	0.56	0.17	1.12	2.83	0.14	0.55
ME-ICP06	Na2O	%	0.03	0.03	2.22	1.26	3.34	0.1	0.11
ME-ICP06	K2O	%	4.44	4.39	5.06	3.43	2.57	1.68	4.87
ME-ICP06	Cr2O3	%	<0.01	<0.01	<0.01	0.01	0.01	<0.01	<0.01
ME-ICP06	TiO2	%	0.27	0.26	0.13	0.78	0.82	0.22	0.33
ME-ICP06	MnO	%	0.02	0.02	0.02	0.08	0.08	0.03	0.11
ME-ICP06	P2O5	%	0.04	0.07	0.04	0.2	0.21	0.04	0.11
ME-ICP06	SrO	%	<0.01	<0.01	0.01	0.01	0.07	<0.01	0.01
ME-ICP06	BaO	%	0.06	0.05	0.07	0.06	0.13	0.06	0.11
ME-MS81	C	%	0.04	0.23	0.13	1.51	0.03	0.28	0.37
ME-MS81	S	%	0.02	0.02	<0.01	0.01	0.01	0.03	0.13
C-IR07	LOI	%	2.28	3.77	1.35	8.35	1.12	3.71	3.36
S-IR08	Total	%	100.95	101.41	101.64	101.27	99.94	101.15	100.32
ME-MS81	Ba	ppm	570	468	576	517	1135	602	959
ME-MS81	Ce	ppm	125	154	32.5	76.5	75.5	42.8	103.5
ME-MS81	Cr	ppm	10	10	30	50	60	30	20
ME-MS81	Cs	ppm	6.01	8.06	5.09	4.63	1.75	3.61	6.64
ME-MS81	Dy	ppm	3.81	5.15	3.3	3.75	4.13	2.27	3.13
ME-MS81	Er	ppm	2.15	2.97	1.6	1.98	2.37	1.13	1.43
ME-MS81	Eu	ppm	1.06	1.21	0.55	1.56	1.46	0.76	1.03
ME-MS81	Ga	ppm	21.1	21.4	16.5	18.4	23.4	14.6	19.1
ME-MS81	Gd	ppm	4.94	6.57	3.29	4.08	4.94	2.75	4.55
ME-MS81	Ge	ppm	<5	<5	<5	<5	<5	<5	<5
ME-MS81	Hf	ppm	6	6.8	3.5	4.8	5.5	3.7	5.5
ME-MS81	Ho	ppm	0.75	1.05	0.58	0.71	0.81	0.43	0.53
ME-MS81	La	ppm	66	81.8	14.9	41.6	38.7	23.8	57.1
ME-MS81	Lu	ppm	0.3	0.42	0.26	0.29	0.31	0.17	0.24
ME-MS81	Nb	ppm	22.8	26.7	21.3	14.2	17.1	14.5	18.4
ME-MS81	Nd	ppm	43.2	53.9	14.8	32.2	32.9	18	38.4
ME-MS81	Pr	ppm	12.7	15.95	3.68	8.41	8.75	4.81	10.8
ME-MS81	Rb	ppm	247	229	213	144	82.8	95	291
ME-MS81	Sm	ppm	7.16	8.64	3.54	5.85	6.5	3.63	6.45
ME-MS81	Sn	ppm	1	3	2	2	2	5	6
ME-MS81	Sr	ppm	56.7	24.1	85.1	73.6	595	65.4	75.7
ME-MS81	Ta	ppm	1.8	2.2	2.1	0.7	0.8	1.2	1.5
ME-MS81	Tb	ppm	0.73	0.95	0.52	0.6	0.67	0.41	0.57
ME-MS81	Th	ppm	39.6	44.9	24.9	12.6	10.55	14.25	31.4
ME-MS81	Tm	ppm	0.31	0.42	0.25	0.29	0.33	0.17	0.22
ME-MS81	U	ppm	6.82	8.34	5.82	2.21	1.34	4.83	5.44
ME-MS81	V	ppm	28	16	12	103	98	26	28
ME-MS81	W	ppm	2	4	4	1	1	23	9
ME-MS81	Y	ppm	23.5	28.4	16.8	18.5	21	12	13.9
ME-MS42	Yb	ppm	2.02	2.53	1.73	1.93	2.28	1.13	1.48
ME-MS42	Zr	ppm	210	252	85	190	219	113	175
ME-MS42	As	ppm	5.9	4.7	1.8	10.7	0.3	106	19.1
ME-MS42	Bi	ppm	0.05	0.11	0.17	0.06	0.03	1.86	0.34
ME-MS42	Hg	ppm	0.006	0.021	0.017	0.008	<0.005	1.775	0.115
ME-MS42	In	ppm	<0.005	0.006	0.006	0.034	0.022	0.039	0.038
ME-MS42	Re	ppm	<0.001	0.001	<0.001	<0.001	<0.001	<0.001	<0.001
ME-MS42	Sb	ppm	0.33	0.22	0.28	0.3	0.05	5.62	0.66
ME-MS42	Se	ppm	<0.2	<0.2	0.4	0.4	0.4	0.2	0.2
OA-GRA05	Te	ppm	0.01	<0.01	0.02	<0.01	<0.01	0.25	0.01
TOT-ICP06	Tl	ppm	0.15	0.13	0.18	0.19	0.33	0.35	0.24
ME-4ACD81	Ag	ppm	<0.5	<0.5	1.1	1	<0.5	1	1.4
ME-4ACD81	Cd	ppm	<0.5	<0.5	<0.5	<0.5	<0.5	<0.5	0.7
ME-4ACD81	Co	ppm	4	2	2	10	12	1	3
ME-4ACD81	Cu	ppm	4	3	21	4	2	23	13
ME-4ACD81	Li	ppm	<10	<10	10	20	20	30	20
ME-4ACD81	Mo	ppm	2	2	8	1	<1	19	1
ME-4ACD81	Ni	ppm	3	2	2	5	10	<1	2
ME-4ACD81	Pb	ppm	32	33	36	18	16	60	121
ME-4ACD81	Sc	ppm	3	4	2	9	12	2	3
ME-4ACD81	Zn	ppm	38	50	37	63	71	34	266
Au-ICP21	Au	ppm	<0.001	<0.001	0.001	0.003	0.001	0.004	0.238
Ag-OG62	Ag	ppm							
Pb-OG62	Pb	%							
Zn-OG62	Zn	%							

		Sample No.	10107	10113	10121	10069	10070	10081	10083
		Rock Type	quartz monzonite	quartz monzonite	quartz monzonite	tonalite	tonalite	granite	granite aplite
		Alteration	chloritic	phyllic	chloritic	veins, chloritic	veins, chloritic	veins, phyllic	phyllic
		UTM E (NAD27)	678259	679747	680712	682690	682690	678283	677968
		UTM N (NAD27)	4419595	4419444	4420931	4424071	4424071	4419597	4418214
Method	**Analysis**	**Unit**							
ME-ICP06	**SiO2**	**%**	73.3	79.2	70.5	74.8	71.2	71.1	83.9
ME-ICP06	**Al2O3**	**%**	12.6	12.65	13.4	11.7	12.7	13.95	8.01
ME-ICP06	**Fe2O3**	**%**	2.45	1.55	3.44	4.09	4.67	4.13	2.71
ME-ICP06	**CaO**	**%**	1.77	0.22	2.84	1.5	1.47	0.11	0.24
ME-ICP06	**MgO**	**%**	0.51	0.56	0.66	1.11	1.21	0.77	0.07
ME-ICP06	**Na2O**	**%**	0.1	0.05	0.06	0.06	0.06	0.02	0.05
ME-ICP06	**K2O**	**%**	4.88	4	4.59	3.25	3.7	4.58	0.56
ME-ICP06	**Cr2O3**	**%**	<0.01	<0.01	<0.01	0.01	0.01	<0.01	<0.01
ME-ICP06	**TiO2**	**%**	0.33	0.42	0.42	0.6	0.67	0.42	0.21
ME-ICP06	**MnO**	**%**	0.11	0.03	0.07	0.22	0.15	0.02	0.02
ME-ICP06	**P2O5**	**%**	0.11	0.15	0.13	0.14	0.16	0.05	0.18
ME-ICP06	**SrO**	**%**	0.01	<0.01	0.02	<0.01	<0.01	<0.01	0.02
ME-ICP06	**BaO**	**%**	0.11	0.04	0.09	0.05	0.05	0.04	0.08
ME-MS81	**C**	**%**	0.38	0.03	0.71	0.33	0.3	0.04	0.14
ME-MS81	**S**	**%**	0.14	0.01	0.11	0.06	0.01	0.33	0.05
C-IR07	**LOI**	**%**	3.36	2.06	4.62	3.45	3.73	3.38	3.91
S-IR08	**Total**	**%**	99.64	100.93	100.84	100.98	99.78	98.57	99.96
ME-MS81	**Ba**	**ppm**	997	328	868	399	430	425	698
ME-MS81	**Ce**	**ppm**	105	101.5	86.8	60.4	66.1	102	41.1
ME-MS81	**Cr**	**ppm**	20	30	20	40	50	20	20
ME-MS81	**Cs**	**ppm**	7.02	7.18	10.25	3.53	3.99	3.94	4.41
ME-MS81	**Dy**	**ppm**	3.15	3.86	3.57	2.77	3.11	1.89	1.68
ME-MS81	**Er**	**ppm**	1.61	1.89	1.92	1.4	1.75	0.79	0.8
ME-MS81	**Eu**	**ppm**	1.1	1.29	1.1	0.84	1	0.72	0.62
ME-MS81	**Ga**	**ppm**	19.5	19.7	19.7	16.4	17.3	22.8	16.9
ME-MS81	**Gd**	**ppm**	4.63	5.13	4.89	3.18	4.05	3.28	2.17
ME-MS81	**Ge**	**ppm**	<5	<5	<5	<5	<5	<5	<5
ME-MS81	**Hf**	**ppm**	5.5	5.3	6.1	4	4.7	6.2	3.5
ME-MS81	**Ho**	**ppm**	0.59	0.74	0.63	0.5	0.57	0.34	0.27
ME-MS81	**La**	**ppm**	57.9	56.7	48	32.5	35.3	57.2	22.5
ME-MS81	**Lu**	**ppm**	0.25	0.26	0.27	0.18	0.24	0.14	0.14
ME-MS81	**Nb**	**ppm**	19.5	19.8	22.7	11.4	12.8	23.1	13.9
ME-MS81	**Nd**	**ppm**	37.9	40.4	35.3	24.9	27	38.3	16.9
ME-MS81	**Pr**	**ppm**	10.85	10.8	9.45	6.8	7.4	10.65	4.41
ME-MS81	**Rb**	**ppm**	300	366	294	160.5	177	328	37
ME-MS81	**Sm**	**ppm**	6.58	6.89	6.28	4.11	4.75	5.97	3.27
ME-MS81	**Sn**	**ppm**	7	15	3	4	6	20	2
ME-MS81	**Sr**	**ppm**	78.3	10.6	148.5	18	23.1	13.4	141.5
ME-MS81	**Ta**	**ppm**	1.7	1.5	2.2	0.6	0.7	2.2	1
ME-MS81	**Tb**	**ppm**	0.61	0.74	0.69	0.43	0.52	0.37	0.31
ME-MS81	**Th**	**ppm**	31.3	24.3	23.5	10.5	10.65	20.3	13.6
ME-MS81	**Tm**	**ppm**	0.24	0.28	0.26	0.17	0.2	0.13	0.11
ME-MS81	**U**	**ppm**	5.61	3.16	6.31	1.84	2.08	2.63	6.8
ME-MS81	**V**	**ppm**	29	37	39	141	105	37	33
ME-MS81	**W**	**ppm**	18	24	5	4	4	10	25
ME-MS81	**Y**	**ppm**	14.9	20.2	19.3	12.8	15.3	8.3	8.8
ME-MS42	**Yb**	**ppm**	1.48	1.48	1.82	1.13	1.71	0.89	0.75
ME-MS42	**Zr**	**ppm**	185	178	197	159	171	200	105
ME-MS42	**As**	**ppm**	16.9	1.5	3.6	31.7	71.6	146	170
ME-MS42	**Bi**	**ppm**	0.5	0.76	1.55	0.05	0.04	2.13	0.11
ME-MS42	**Hg**	**ppm**	0.136	0.017	0.016	0.031	0.017	0.044	2.79
ME-MS42	**In**	**ppm**	0.048	0.033	0.056	0.04	0.013	0.042	0.013
ME-MS42	**Re**	**ppm**	<0.001	<0.001	<0.001	<0.001	<0.001	<0.001	<0.001
ME-MS42	**Sb**	**ppm**	1.14	0.16	0.09	0.5	0.24	2.12	15.05
ME-MS42	**Se**	**ppm**	<0.2	<0.2	0.6	0.4	0.5	<0.2	<0.2
OA-GRA05	**Te**	**ppm**	<0.01	<0.01	0.05	<0.01	<0.01	0.03	0.01
TOT-ICP06	**Tl**	**ppm**	0.24	0.27	0.23	0.16	0.21	0.28	0.49
ME-4ACD81	**Ag**	**ppm**	1.4	1.1	1.1	>100	25.5	19.7	<0.5
ME-4ACD81	**Cd**	**ppm**	0.7	<0.5	<0.5	19.7	2.7	<0.5	<0.5
ME-4ACD81	**Co**	**ppm**	2	1	3	6	9	1	2
ME-4ACD81	**Cu**	**ppm**	21	13	42	47	25	19	5
ME-4ACD81	**Li**	**ppm**	20	20	30	20	20	10	30
ME-4ACD81	**Mo**	**ppm**	1	1	1	1	1	57	23
ME-4ACD81	**Ni**	**ppm**	3	2	2	3	3	<1	1
ME-4ACD81	**Pb**	**ppm**	125	35	140	1400	336	968	16
ME-4ACD81	**Sc**	**ppm**	3	4	5	9	10	5	2
ME-4ACD81	**Zn**	**ppm**	264	43	70	1130	486	54	36
Au-ICP21	**Au**	**ppm**	0.008	0.001	0.001	0.794	0.767	0.061	0.01
Ag-OG62	**Ag**	**ppm**				116			
Pb-OG62	**Pb**	**%**							
Zn-OG62	**Zn**	**%**							

		Sample No.	10086	10087	10088	10104	10268	10269	10270
		Rock Type	quartz monzonite	quartz monzonite	quartz monzonite	granite aplite	granite	granite	quartz monzonite
		Alteration	polymetallic veins	phyllic	phyllic		greisen	greisen	phyllic
		UTM E (NAD27)		678398	678398	678572	678429	678468	678533
		UTM N (NAD27)		4420011	4420011	4417260	4415429	4415593	4419943
Method	**Analysis**	**Unit**							
ME-ICP06	SiO2	%	51.3	82.5	81.2	69.2	79.4	68.6	67.8
ME-ICP06	Al2O3	%	6.37	7.06	8.68	19.4	10.15	13.7	14.3
ME-ICP06	Fe2O3	%	25.5	3.79	3.76	1.06	1.48	1.84	3.24
ME-ICP06	CaO	%	8.76	0.07	0.06	0.37	1.82	2.69	2.41
ME-ICP06	MgO	%	0.43	0.42	0.51	0.18	0.24	0.61	0.52
ME-ICP06	Na2O	%	0.03	0.06	0.04	0.15	0.04	0.58	2.76
ME-ICP06	K2O	%	0.72	2.23	2.75	6.79	2.18	7.87	3.62
ME-ICP06	Cr2O3	%	<0.01	0.01	0.01	<0.01	<0.01	<0.01	<0.01
ME-ICP06	TiO2	%	0.14	0.69	0.48	0.19	0.25	0.36	0.45
ME-ICP06	MnO	%	0.3	0.01	0.02	0.02	0.01	0.03	0.07
ME-ICP06	P2O5	%	0.06	0.03	0.06	0.04	0.07	0.12	0.17
ME-ICP06	SrO	%	0.04	<0.01	<0.01	0.01	0.01	0.03	0.02
ME-ICP06	BaO	%	0.07	0.02	0.03	0.07	0.45	0.18	0.11
ME-MS81	C	%	0.07	0.03	0.03	0.13	0.06	0.1	0.51
ME-MS81	S	%	0.01	2.43	2.26	0.02	0.1	0.02	0.01
C-IR07	LOI	%	4.67	2.8	3.15	2.98	3.51	2.63	3.67
S-IR08	Total	%	98.39	99.69	100.75	100.46	99.61	99.24	99.14
ME-MS81	Ba	ppm	693	207	281	598	4010	1810	1035
ME-MS81	Ce	ppm	138.5	59.9	57.7	33	47.6	97.9	122.5
ME-MS81	Cr	ppm	40	120	60	20	10	10	10
ME-MS81	Cs	ppm	13.6	3.06	2.97	6.26	6.33	6.48	7.41
ME-MS81	Dy	ppm	3.52	8.03	5.37	8.35	1.75	3.62	3.63
ME-MS81	Er	ppm	1.87	4.63	2.85	5.17	0.88	1.77	1.64
ME-MS81	Eu	ppm	2.26	1.75	1.13	0.52	0.64	2.07	1.34
ME-MS81	Ga	ppm	19.4	12.1	14.2	25.5	21.4	22.5	22.4
ME-MS81	Gd	ppm	3.71	6.19	4.12	5.53	2.16	4.66	4.96
ME-MS81	Ge	ppm	12	<5	<5	<5	<5	<5	<5
ME-MS81	Hf	ppm	5.1	15.1	8.5	2.3	3.1	4.8	5.7
ME-MS81	Ho	ppm	0.7	1.7	1.07	1.7	0.34	0.61	0.64
ME-MS81	La	ppm	68.4	27.1	30.2	17.1	24.4	52.2	65.6
ME-MS81	Lu	ppm	0.29	0.7	0.43	0.96	0.14	0.29	0.27
ME-MS81	Nb	ppm	3.7	20.5	17.8	119	11.7	20.3	21
ME-MS81	Nd	ppm	41.1	24.7	22.5	15.4	16.5	36.8	43.9
ME-MS81	Pr	ppm	12.6	6.36	6.07	3.94	4.91	10.6	12.9
ME-MS81	Rb	ppm	38.8	155.5	186.5	376	175	567	198
ME-MS81	Sm	ppm	5.45	5.28	3.95	4.51	2.89	6.19	7.02
ME-MS81	Sn	ppm	298	7	22	7	2	107	4
ME-MS81	Sr	ppm	294	7.3	7.1	71	75.8	274	146
ME-MS81	Ta	ppm	0.3	1.6	1.6	36.7	0.9	1.7	1.6
ME-MS81	Tb	ppm	0.64	1.26	0.75	1.26	0.33	0.74	0.76
ME-MS81	Th	ppm	5.17	9.68	8.98	16.9	14.05	24.4	29.1
ME-MS81	Tm	ppm	0.29	0.7	0.43	0.94	0.14	0.24	0.23
ME-MS81	U	ppm	4.72	3.93	4.02	15.45	3.47	5.48	5.04
ME-MS81	V	ppm	27	39	34	20	26	40	46
ME-MS81	W	ppm	40	38	21	262	13	1200	8
ME-MS81	Y	ppm	20.3	48.9	30.4	54.5	11	20.2	18.5
ME-MS42	Yb	ppm	1.81	4.45	2.62	6.84	0.97	1.74	1.52
ME-MS42	Zr	ppm	170	611	300	34	117	178	208
ME-MS42	As	ppm	83.7	160.5	208	7.8	26.4	9.4	6
ME-MS42	Bi	ppm	1.02	12.75	8.65	44.5	0.65	4.94	0.24
ME-MS42	Hg	ppm	0.047	0.178	0.089	0.122	0.08	0.034	0.009
ME-MS42	In	ppm	2.64	0.027	0.081	0.316	0.008	0.068	0.024
ME-MS42	Re	ppm	<0.001	0.017	0.005	0.001	<0.001	0.003	<0.001
ME-MS42	Sb	ppm	0.84	44.3	38.2	41.5	3.61	1.75	0.25
ME-MS42	Se	ppm	1.1	0.7	0.5	0.5	<0.2	0.2	<0.2
OA-GRA05	Te	ppm	0.36	0.52	0.25	0.32	0.05	0.07	0.01
TOT-ICP06	Tl	ppm	0.2	0.18	0.23	0.15	0.38	0.52	0.12
ME-4ACD81	Ag	ppm	3.4	>100	>100	21.4	3	0.8	<0.5
ME-4ACD81	Cd	ppm	8.2	1.3	1.1	<0.5	<0.5	0.7	<0.5
ME-4ACD81	Co	ppm	65	7	5	1	1	2	3
ME-4ACD81	Cu	ppm	704	35	29	2790	4	58	14
ME-4ACD81	Li	ppm	10	30	30	20	70	40	20
ME-4ACD81	Mo	ppm	1	522	192	39	18	2	1
ME-4ACD81	Ni	ppm	27	14	5	<1	2	3	4
ME-4ACD81	Pb	ppm	91	1310	1680	67	25	62	24
ME-4ACD81	Sc	ppm	2	7	5	2	2	4	4
ME-4ACD81	Zn	ppm	577	116	113	74	38	58	94
Au-ICP21	Au	ppm	0.006	0.349	0.302	0.212	0.417	<0.001	<0.001
Ag-OG62	Ag	ppm		1030	835				
Pb-OG62	Pb	%							
Zn-OG62	Zn	%							

Appendix D3: Geochemistry of Mineralized Sedimentary Rocks

		Sample No.	10052	10058	10061	10062	10071	10073A	10073B
		Rock Type	quartz vein	skarn	calcite vein	quartz vein	quartz vein	skarn	skarn
		Alteration		garnet-epidote				hornfels	hornfels
		UTM E (NAD27)	682689	677468	680940	680948	680880	682579	682579
		UTM N (NAD27)	4425658	4417780	4421676	4421690	4421848	4424240	4424240
Method	Analysis	Unit							
ME-ICP06	SiO2	%	92.9	39.4	11.8	96.6	90.2	60	60.2
ME-ICP06	Al2O3	%	3.76	10.3	3.84	1.25	0.86	16.6	16.6
ME-ICP06	Fe2O3	%	1.74	18.7	16.4	1.6	2.57	6.68	6.84
ME-ICP06	CaO	%	0.12	26.7	20.5	0.1	1.1	3.89	3.95
ME-ICP06	MgO	%	0.18	0.81	8.48	0.08	0.12	2.12	2.12
ME-ICP06	Na2O	%	0.02	0.03	0.02	0.04	0.03	3.27	3.34
ME-ICP06	K2O	%	1.11	0.13	0.37	0.36	0.25	4.13	4.13
ME-ICP06	Cr2O3	%	0.01	0.01	<0.01	0.01	<0.01	<0.01	<0.01
ME-ICP06	TiO2	%	0.18	0.28	0.14	0.05	0.19	0.93	0.93
ME-ICP06	MnO	%	0.01	0.67	2.8	0.01	0.05	0.1	0.1
ME-ICP06	P2O5	%	0.02	0.04	0.02	0.01	0.01	0.37	0.37
ME-ICP06	SrO	%	<0.01	0.06	0.12	<0.01	<0.01	0.06	0.06
ME-ICP06	BaO	%	0.02	0.03	0.01	0.02	0.01	0.21	0.21
ME-MS81	C	%	0.07	0.04	9.15	0.04	0.32	0.24	0.24
ME-MS81	S	%	0.04	0.01	2.78	0.92	2.69	0.02	0.03
C-IR07	LOI	%	1.03	1.56	27.2	0.95	2.63	2.89	2.69
S-IR08	Total	%	101.1	98.72	91.7	101.08	98.02	101.25	101.54
ME-MS81	Ba	ppm	201	229	45.1	172	57.4	1815	1845
ME-MS81	Ce	ppm	32.6	55.1	14.3	6.8	8.6	127.5	128.5
ME-MS81	Cr	ppm	40	50	40	60	30	20	20
ME-MS81	Cs	ppm	1.12	1.15	0.51	0.56	0.37	1.89	2.5
ME-MS81	Dy	ppm	2.22	5.37	6.32	0.39	0.33	5.53	5.85
ME-MS81	Er	ppm	1.4	2.17	3.6	0.16	0.17	3.03	3
ME-MS81	Eu	ppm	0.45	2.75	1.75	0.08	0.11	1.84	1.81
ME-MS81	Ga	ppm	5.8	29.2	6.8	2.7	1.9	21.9	22.4
ME-MS81	Gd	ppm	1.95	8.97	7.1	0.36	0.42	7.24	7.21
ME-MS81	Ge	ppm	5	22	<5	7	6	<5	<5
ME-MS81	Hf	ppm	4.4	5.5	1.1	0.3	0.8	6.9	7.1
ME-MS81	Ho	ppm	0.47	0.92	1.24	0.07	0.07	1.08	1.08
ME-MS81	La	ppm	14.1	18.9	6.9	4.1	4.7	65.9	67.8
ME-MS81	Lu	ppm	0.23	0.35	0.49	0.02	0.03	0.38	0.44
ME-MS81	Nb	ppm	4.6	8.5	3.4	1.2	3.2	20.5	20.7
ME-MS81	Nd	ppm	13.4	39.1	11	2.5	3	52.9	53.4
ME-MS81	Pr	ppm	3.42	7.3	2.06	0.74	0.88	14.35	14
ME-MS81	Rb	ppm	53.9	7.9	20.6	15.2	10.3	144	146
ME-MS81	Sm	ppm	2.38	11.35	5.42	0.35	0.43	8.86	9.28
ME-MS81	Sn	ppm	6	237	2	1	6	4	5
ME-MS81	Sr	ppm	35.4	552	1035	7.4	8.2	511	520
ME-MS81	Ta	ppm	0.3	0.5	0.2	<0.1	0.1	1.1	1.1
ME-MS81	Tb	ppm	0.38	1.07	1.15	0.05	0.04	0.94	0.96
ME-MS81	Th	ppm	5.14	10	2.64	0.71	0.75	27.4	28.3
ME-MS81	Tm	ppm	0.23	0.34	0.47	0.02	0.03	0.41	0.44
ME-MS81	U	ppm	1.6	4.52	0.76	0.24	0.27	4.19	4.23
ME-MS81	V	ppm	31	60	34	11	16	145	148
ME-MS81	W	ppm	8	55	20	2	6	2	5
ME-MS81	Y	ppm	13.2	25.6	34.1	1.7	2.1	27.9	28.8
ME-MS42	Yb	ppm	1.59	2.09	3.18	0.17	0.19	2.77	2.8
ME-MS42	Zr	ppm	172	199	45	12	26	262	270
ME-MS42	As	ppm	22.4	3.9	>250	63.2	107.5	3.5	3.3
ME-MS42	Bi	ppm	1.88	0.33	0.3	0.04	0.07	0.13	0.13
ME-MS42	Hg	ppm	0.031	<0.005	0.024	0.067	0.463	0.008	<0.005
ME-MS42	In	ppm	0.144	1.47	0.061	0.025	0.025	0.037	0.035
ME-MS42	Re	ppm	<0.001	<0.001	<0.001	<0.001	<0.001	<0.001	<0.001
ME-MS42	Sb	ppm	18.75	0.19	3.68	>250	>250	0.82	2.05
ME-MS42	Se	ppm	0.6	0.4	0.9	1.2	0.8	0.8	0.6
OA-GRA05	Te	ppm	0.05	<0.01	0.06	0.01	0.03	<0.01	0.01
TOT-ICP06	Tl	ppm	0.13	0.04	0.05	0.05	0.04	0.08	0.17
ME-4ACD81	Ag	ppm	>100	<0.5	23.7	>100	>100	1.4	3.4
ME-4ACD81	Cd	ppm	0.5	0.6	1.9	10.1	220	<0.5	0.6
ME-4ACD81	Co	ppm	1	4	4	<1	4	14	15
ME-4ACD81	Cu	ppm	376	3	31	306	1200	13	14
ME-4ACD81	Li	ppm	<10	10	20	<10	<10	30	30
ME-4ACD81	Mo	ppm	4	4	<1	1	5	<1	<1
ME-4ACD81	Ni	ppm	1	8	10	4	5	<1	<1
ME-4ACD81	Pb	ppm	1090	9	89	1370	6360	37	52
ME-4ACD81	Sc	ppm	2	4	12	1	1	10	10
ME-4ACD81	Zn	ppm	39	44	212	1280	>10000	100	126
Au-ICP21	Au	ppm	0.396	0.007	>10.0	>10.0	>10.0	0.004	0.008
Ag-OG62	Ag	ppm	420			1025	1200		
Pb-OG62	Pb	%							
Zn-OG62	Zn	%					2.05		

		Sample No.	10095	10097	10101	10103	10115	10117	10257
		Rock Type	quartzite breccia	quartzite breccia	calcite vein	calcite vein	gossan	quartz vein	quartz vein
		Alteration							
		UTM E (NAD27)	677943	680191	679099	680886	677546	678606	678488
		UTM N (NAD27)	4418249	4422292	4422730	4421873	4416625	4416333	4422064
Method	Analysis	Unit							
ME-ICP06	SiO2	%	85.4	97.1	61.4	7.78	8.28	77.4	84.1
ME-ICP06	Al2O3	%	7.98	0.86	0.63	3.73	2.64	4.83	0.43
ME-ICP06	Fe2O3	%	3.09	2.28	1.24	22.2	76	11.8	0.41
ME-ICP06	CaO	%	0.14	0.04	15.5	18.95	0.12	0.11	7.57
ME-ICP06	MgO	%	0.07	0.06	2.61	8.52	0.39	0.27	0.63
ME-ICP06	Na2O	%	0.07	0.03	0.03	0.03	0.03	0.08	0.01
ME-ICP06	K2O	%	0.88	0.25	0.17	0.3	0.52	2.55	0.08
ME-ICP06	Cr2O3	%	<0.01	<0.01	<0.01	<0.01	<0.01	<0.01	<0.01
ME-ICP06	TiO2	%	0.19	0.03	0.01	0.16	0.17	0.12	0.01
ME-ICP06	MnO	%	0.02	0.01	0.08	2.35	0.02	0.15	0.01
ME-ICP06	P2O5	%	0.03	0.02	0.04	0.04	0.09	0.12	0.01
ME-ICP06	SrO	%	0.01	<0.01	0.12	0.1	<0.01	0.01	0.01
ME-ICP06	BaO	%	0.09	0.01	<0.01	<0.01	0.01	0.15	<0.01
ME-MS81	C	%	0.06	0.07	3.98	8.04	0.18	0.06	1.88
ME-MS81	S	%	0.17	0.02	0.1	10.1	0.09	0.05	0.03
C-IR07	LOI	%	3.67	0.66	15.15	20.5	10.9	1.45	6.92
S-IR08	Total	%	101.64	101.35	96.98	84.66	99.17	99.04	100.19
ME-MS81	Ba	ppm	826	128	30.6	36.6	122	1355	22.9
ME-MS81	Ce	ppm	39	6.4	3.7	11.4	13.5	21.1	1.7
ME-MS81	Cr	ppm	30	40	30	30	30	30	30
ME-MS81	Cs	ppm	4.62	0.36	0.23	0.38	1.18	1.06	0.28
ME-MS81	Dy	ppm	1.7	0.39	0.34	6.73	0.95	1.18	0.12
ME-MS81	Er	ppm	0.84	0.24	0.18	3.3	0.57	0.61	0.04
ME-MS81	Eu	ppm	0.61	0.13	0.11	1.81	0.17	0.36	0.05
ME-MS81	Ga	ppm	17.8	1.5	2.8	7.3	8.5	9.9	0.9
ME-MS81	Gd	ppm	2.24	0.45	0.33	7.82	0.94	1.23	0.12
ME-MS81	Ge	ppm	<5	<5	9	<5	<5	<5	10
ME-MS81	Hf	ppm	2.9	0.7	<0.2	1.5	4.5	1.6	<0.2
ME-MS81	Ho	ppm	0.31	0.05	0.06	1.28	0.21	0.24	0.02
ME-MS81	La	ppm	21.3	3.2	2	5.3	7.6	12.8	0.8
ME-MS81	Lu	ppm	0.15	0.03	0.02	0.47	0.13	0.08	0.01
ME-MS81	Nb	ppm	11.9	0.8	0.3	4	3.8	5.4	0.4
ME-MS81	Nd	ppm	16.1	2.8	1.8	10	5.8	9	0.8
ME-MS81	Pr	ppm	4.21	0.71	0.43	1.72	1.6	2.39	0.22
ME-MS81	Rb	ppm	54.3	10.7	4.3	15.3	21.5	92.3	3.7
ME-MS81	Sm	ppm	2.89	0.59	0.48	5.45	1	1.58	0.13
ME-MS81	Sn	ppm	2	58	1	5	7	48	1
ME-MS81	Sr	ppm	107.5	4.4	1015	885	19.5	136.5	159
ME-MS81	Ta	ppm	1	0.1	0.1	0.3	0.4	0.4	<0.1
ME-MS81	Tb	ppm	0.34	0.07	0.05	1.22	0.17	0.19	0.04
ME-MS81	Th	ppm	12.65	1.01	0.96	2.96	4.34	6.88	0.41
ME-MS81	Tm	ppm	0.13	0.04	0.04	0.51	0.12	0.1	0.01
ME-MS81	U	ppm	9.02	0.85	1.97	0.92	5.41	23.3	0.7
ME-MS81	V	ppm	35	6	31	32	39	369	5
ME-MS81	W	ppm	20	12	>10000	37	26	19	1
ME-MS81	Y	ppm	9.2	1.7	2.5	36.1	5.9	6.4	0.7
ME-MS42	Yb	ppm	0.85	0.18	0.11	3.26	0.84	0.66	0.05
ME-MS42	Zr	ppm	90	19	<2	48	174	54	4
ME-MS42	As	ppm	231	87.9	15.4	>250	>250	58.1	11.4
ME-MS42	Bi	ppm	0.08	4.73	0.01	1.14	219	126	0.05
ME-MS42	Hg	ppm	5.9	0.086	4.93	0.031	2.49	0.198	10.95
ME-MS42	In	ppm	0.011	1.31	0.012	0.063	0.03	3.86	<0.005
ME-MS42	Re	ppm	0.001	<0.001	0.002	<0.001	<0.001	<0.001	<0.001
ME-MS42	Sb	ppm	17.8	59.4	235	8.53	28.7	2.39	>250
ME-MS42	Se	ppm	0.2	0.3	0.3	0.7	3.1	3.1	<0.2
OA-GRA05	Te	ppm	0.01	2.47	<0.01	0.16	1.4	5.28	0.02
TOT-ICP06	Tl	ppm	0.51	0.02	0.12	0.03	0.06	0.08	0.12
ME-4ACD81	Ag	ppm	1.2	>100	>100	77.6	5.9	88.5	>100
ME-4ACD81	Cd	ppm	1	1.8	12	2.6	3.5	5.3	8.6
ME-4ACD81	Co	ppm	2	1	1	8	80	32	<1
ME-4ACD81	Cu	ppm	6	180	1020	26	709	3940	639
ME-4ACD81	Li	ppm	40	<10	20	10	<10	20	30
ME-4ACD81	Mo	ppm	26	11	1	<1	62	117	2
ME-4ACD81	Ni	ppm	<1	2	6	19	19	1	2
ME-4ACD81	Pb	ppm	16	1370	354	242	2710	>10000	924
ME-4ACD81	Sc	ppm	2	<1	<1	9	1	1	<1
ME-4ACD81	Zn	ppm	52	360	202	286	493	1160	254
Au-ICP21	Au	ppm	0.02	>10.0	0.025	>10.0	0.034	0.006	0.097
Ag-OG62	Ag	ppm		657	518				1460
Pb-OG62	Pb	%						1.13	
Zn-OG62	Zn	%							

		Sample No.	10258	10259	10262	10263	10266	10271	10274
		Rock Type	calcite vein	carbonate breccia	carbonate breccia	carbonate breccia	carbonate breccia	gossan	quartz vein
		Alteration					decalcification		
		UTM E (NAD27)	678478	678430	680726	680766	677995	678416	682321
		UTM N (NAD27)	4422053	4421967	4425400	4425461	4423513	4420106	4425687
Method	Analysis	Unit							
ME-ICP06	SiO2	%	16.6	47	95.7	5.77	13.7	84.9	97.8
ME-ICP06	Al2O3	%	1.61	0.71	0.83	0.59	1.08	4.31	0.9
ME-ICP06	Fe2O3	%	4.01	0.24	0.48	11.15	1.15	6.73	0.42
ME-ICP06	CaO	%	43.5	27.6	1.12	44.1	42.9	0.12	0.05
ME-ICP06	MgO	%	0.48	0.6	0.1	0.31	4.47	0.15	0.04
ME-ICP06	Na2O	%	0.02	0.01	0.01	0.01	0.02	0.05	0.02
ME-ICP06	K2O	%	0.47	0.18	0.17	0.09	0.26	1.23	0.27
ME-ICP06	Cr2O3	%	<0.01	<0.01	<0.01	<0.01	<0.01	0.01	0.01
ME-ICP06	TiO2	%	0.04	0.02	0.03	0.01	0.07	0.24	0.05
ME-ICP06	MnO	%	0.03	0.01	0.01	0.16	0.05	0.01	<0.01
ME-ICP06	P2O5	%	0.02	0.01	0.1	0.06	0.03	0.11	0.03
ME-ICP06	SrO	%	0.06	0.08	<0.01	0.02	<0.01	<0.01	<0.01
ME-ICP06	BaO	%	<0.01	<0.01	0.02	0.03	0.02	0.03	<0.01
ME-MS81	C	%	9.12	6.02	0.28	9.32	10.2	0.08	0.04
ME-MS81	S	%	0.02	0.04	0.02	0.05	0.01	0.06	0.03
C-IR07	LOI	%	33.9	22.2	1.21	36.3	37.4	1.93	0.4
S-IR08	Total	%	100.74	98.66	99.78	98.6	101.15	99.82	99.99
ME-MS81	Ba	ppm	36	47.3	164	319	139	246	34.5
ME-MS81	Ce	ppm	17.7	2.1	4.7	3.1	15.4	44.7	15.6
ME-MS81	Cr	ppm	10	10	30	<10	10	70	60
ME-MS81	Cs	ppm	1.12	0.34	0.49	0.85	0.9	1.24	0.42
ME-MS81	Dy	ppm	2.24	0.24	0.2	0.44	1.2	1.95	0.47
ME-MS81	Er	ppm	1.1	0.11	0.08	0.23	0.53	1.05	0.37
ME-MS81	Eu	ppm	0.91	0.05	0.08	0.1	0.33	0.72	0.12
ME-MS81	Ga	ppm	3.2	1.5	1.6	2	2.4	7.8	2.2
ME-MS81	Gd	ppm	2.73	0.23	0.24	0.42	1.23	2.63	0.7
ME-MS81	Ge	ppm	<5	6	5	<5	<5	<5	<5
ME-MS81	Hf	ppm	0.2	<0.2	0.2	<0.2	1	5.4	2
ME-MS81	Ho	ppm	0.47	0.05	0.05	0.09	0.2	0.42	0.1
ME-MS81	La	ppm	8.3	1.4	2.2	2.2	7.1	21.6	6.6
ME-MS81	Lu	ppm	0.12	0.03	0.02	0.04	0.06	0.18	0.06
ME-MS81	Nb	ppm	1.4	0.7	1.2	0.4	3	5	1.4
ME-MS81	Nd	ppm	10	1.3	2.4	2.3	7.3	17.7	5.1
ME-MS81	Pr	ppm	2.31	0.32	0.55	0.51	1.89	4.77	1.46
ME-MS81	Rb	ppm	23.5	8.6	8.4	4.2	13.1	57.1	11.8
ME-MS81	Sm	ppm	2.7	0.21	0.4	0.38	1.58	3.18	0.63
ME-MS81	Sn	ppm	<1	5	1	<1	<1	14	3
ME-MS81	Sr	ppm	590	715	20.7	161.5	48.8	45.2	6.9
ME-MS81	Ta	ppm	0.1	<0.1	0.1	<0.1	0.2	0.3	0.1
ME-MS81	Tb	ppm	0.46	0.05	0.03	0.06	0.19	0.37	0.09
ME-MS81	Th	ppm	1.54	0.31	0.6	0.42	1.49	5.5	1.42
ME-MS81	Tm	ppm	0.14	0.04	<0.01	0.03	0.07	0.18	0.05
ME-MS81	U	ppm	1.45	2.19	0.39	0.86	1.65	2.55	0.75
ME-MS81	V	ppm	10	20	<5	5	41	28	10
ME-MS81	W	ppm	4	30	2	3	5	30	4
ME-MS81	Y	ppm	13.7	1.4	0.9	3.1	6.4	11.3	3.2
ME-MS42	Yb	ppm	0.9	0.08	0.05	0.2	0.49	1.21	0.28
ME-MS42	Zr	ppm	9	5	8	4	40	213	73
ME-MS42	As	ppm	53.6	34.1	15	103.5	52	>250	13.6
ME-MS42	Bi	ppm	0.04	0.04	0.37	0.02	0.13	51.3	0.43
ME-MS42	Hg	ppm	0.268	>25.0	0.246	0.293	1.35	0.076	0.173
ME-MS42	In	ppm	0.021	0.006	0.007	0.7	0.01	0.186	0.055
ME-MS42	Re	ppm	<0.001	<0.001	<0.001	<0.001	<0.001	<0.001	<0.001
ME-MS42	Sb	ppm	17.2	>250	37.3	8.94	2.54	3.76	>250
ME-MS42	Se	ppm	0.5	0.4	<0.2	1.7	1.8	0.3	<0.2
OA-GRA05	Te	ppm	<0.01	0.02	0.01	<0.01	0.01	0.47	0.03
TOT-ICP06	Tl	ppm	0.09	1.5	0.03	0.04	0.14	0.15	0.03
ME-4ACD81	Ag	ppm	10.9	>100	37.5	5.5	0.6	5	>100
ME-4ACD81	Cd	ppm	<0.5	50	0.8	230	0.7	3.2	5.8
ME-4ACD81	Co	ppm	3	<1	1	3	<1	1	1
ME-4ACD81	Cu	ppm	21	2120	52	719	3	133	2020
ME-4ACD81	Li	ppm	<10	20	40	<10	<10	10	<10
ME-4ACD81	Mo	ppm	1	2	3	2	1	10	3
ME-4ACD81	Ni	ppm	24	1	3	3	5	3	2
ME-4ACD81	Pb	ppm	24	3330	172	4480	25	364	1040
ME-4ACD81	Sc	ppm	2	<1	<1	1	2	3	<1
ME-4ACD81	Zn	ppm	54	834	140	>10000	75	321	61
Au-ICP21	Au	ppm	0.04	0.057	0.018	0.003	0.02	0.009	0.102
Ag-OG62	Ag	ppm		1360					341
Pb-OG62	Pb	%							
Zn-OG62	Zn	%				1.595			

		Sample No.	10276	10277	10278	10279	10281	10289	10252
		Rock Type	gossan	quartz vein	quartz vein	jasperoid breccia	jasperoid	dolomite lens	quartz vein
		Alteration							
		UTM E (NAD27)	677470	677462	677479	680727	671104	676502	680554
		UTM N (NAD27)	4415986	4415975	4416074	4425399	4420041	4422533	4422037
Method	Analysis	Unit							
ME-ICP06	SiO2	%	17.2	75.7	94.1	91.2	96.3	1.01	90.4
ME-ICP06	Al2O3	%	0.48	13.7	1.01	0.71	1.63	0.33	0.68
ME-ICP06	Fe2O3	%	70.9	2.49	3.03	0.85	0.91	0.41	6.19
ME-ICP06	CaO	%	0.12	0.14	0.01	2.03	0.09	55.9	0.04
ME-ICP06	MgO	%	0.33	0.49	0.03	1.21	0.11	0.63	0.03
ME-ICP06	Na2O	%	0.01	0.03	0.01	0.01	0.02	0.02	0.02
ME-ICP06	K2O	%	0.05	4.73	0.32	0.14	0.38	0.06	0.15
ME-ICP06	Cr2O3	%	<0.01	<0.01	0.01	<0.01	0.01	<0.01	<0.01
ME-ICP06	TiO2	%	0.02	0.29	0.02	0.04	0.09	0.02	0.03
ME-ICP06	MnO	%	0.02	0.02	<0.01	0.03	<0.01	0.02	0.01
ME-ICP06	P2O5	%	0.05	0.09	<0.01	0.13	0.02	0.03	0.04
ME-ICP06	SrO	%	<0.01	<0.01	<0.01	<0.01	0.01	0.01	<0.01
ME-ICP06	BaO	%	0.04	0.05	0.04	<0.01	0.04	<0.01	<0.01
ME-MS81	C	%	0.1	0.04	0.01	0.84	0.24	11.6	0.06
ME-MS81	S	%	0.04	0.01	1.82	0.07	0.04	0.01	0.03
C-IR07	LOI	%	10.1	2.45	1.62	3.08	1.03	43.4	1.46
S-IR08	Total	%	99.32	100.18	100.2	99.43	100.64	101.84	99.05
ME-MS81	Ba	ppm	388	504	373	48.8	357	22.9	38.1
ME-MS81	Ce	ppm	4.8	143	4	4.4	11	3	3.9
ME-MS81	Cr	ppm	20	10	40	30	100	10	20
ME-MS81	Cs	ppm	0.14	8.04	0.4	0.29	5.19	0.27	0.31
ME-MS81	Dy	ppm	0.36	4.02	0.15	0.23	0.34	0.16	0.27
ME-MS81	Er	ppm	0.22	2.07	0.07	0.09	0.23	0.08	0.12
ME-MS81	Eu	ppm	0.05	1.09	0.03	0.05	0.1	0.04	0.07
ME-MS81	Ga	ppm	3.7	22.3	2.7	2.3	3.7	1.6	3.6
ME-MS81	Gd	ppm	0.4	5.95	0.19	0.37	0.37	0.2	0.29
ME-MS81	Ge	ppm	<5	<5	<5	7	17	<5	5
ME-MS81	Hf	ppm	0.4	6.8	0.5	0.3	0.7	0.2	0.3
ME-MS81	Ho	ppm	0.09	0.78	0.02	0.03	0.06	0.04	0.05
ME-MS81	La	ppm	2.6	75.4	1.8	2	5.4	1.5	2
ME-MS81	Lu	ppm	0.03	0.35	0.02	0.02	0.04	0.02	0.02
ME-MS81	Nb	ppm	0.7	24.9	0.6	2	2.4	0.5	0.8
ME-MS81	Nd	ppm	2.2	49.5	1.3	2.2	4.1	1.3	1.9
ME-MS81	Pr	ppm	0.54	14.45	0.38	0.56	1.16	0.33	0.46
ME-MS81	Rb	ppm	2.3	294	20.7	6.7	21.6	3.1	7.1
ME-MS81	Sm	ppm	0.46	7.7	0.21	0.34	0.67	0.18	0.38
ME-MS81	Sn	ppm	8	1	4	1	<1	<1	98
ME-MS81	Sr	ppm	13.7	9	13.5	50.9	108.5	69.2	6.3
ME-MS81	Ta	ppm	<0.1	1.8	<0.1	0.1	0.1	<0.1	<0.1
ME-MS81	Tb	ppm	0.07	0.84	0.03	0.05	0.06	0.03	0.05
ME-MS81	Th	ppm	1.21	42.3	0.63	0.64	1.53	0.38	0.68
ME-MS81	Tm	ppm	0.03	0.3	<0.01	0.01	0.04	0.01	<0.01
ME-MS81	U	ppm	11.9	7.14	0.25	0.71	1.11	1.32	2.43
ME-MS81	V	ppm	44	25	<5	<5	11	5	50
ME-MS81	W	ppm	32	2	1	2	3	2	1
ME-MS81	Y	ppm	2.9	23	0.9	1	1.8	1.1	1.5
ME-MS42	Yb	ppm	0.17	2.23	0.11	0.06	0.22	0.11	0.13
ME-MS42	Zr	ppm	17	245	18	12	26	5	11
ME-MS42	As	ppm	>250	4.9	65.3	86	31.9	12.3	171
ME-MS42	Bi	ppm	>250	1.57	1.2	1.03	0.09	0.02	0.45
ME-MS42	Hg	ppm	1.695	0.009	0.164	1.47	1.945	0.022	0.384
ME-MS42	In	ppm	0.07	<0.005	0.008	0.046	<0.005	<0.005	0.266
ME-MS42	Re	ppm	<0.001	<0.001	<0.001	<0.001	0.001	<0.001	<0.001
ME-MS42	Sb	ppm	18.45	0.94	1.89	>250	36.5	0.67	>250
ME-MS42	Se	ppm	0.2	<0.2	0.2	0.2	<0.2	0.5	3.6
OA-GRA05	Te	ppm	1.52	0.03	0.1	0.19	0.02	0.01	0.04
TOT-ICP06	Tl	ppm	0.03	0.18	0.03	0.02	0.19	0.06	0.02
ME-4ACD81	Ag	ppm	29	0.8	4.7	>100	0.8	<0.5	>100
ME-4ACD81	Cd	ppm	2.1	<0.5	<0.5	22.7	<0.5	<0.5	2.5
ME-4ACD81	Co	ppm	35	2	3	<1	<1	1	<1
ME-4ACD81	Cu	ppm	993	10	41	1830	8	4	403
ME-4ACD81	Li	ppm	<10	<10	<10	40	90	<10	10
ME-4ACD81	Mo	ppm	42	1	5	2	6	1	7
ME-4ACD81	Ni	ppm	15	3	6	2	4	<1	2
ME-4ACD81	Pb	ppm	4070	39	151	2630	6	6	3280
ME-4ACD81	Sc	ppm	1	3	<1	<1	1	<1	<1
ME-4ACD81	Zn	ppm	407	44	25	1830	7	9	1070
Au-ICP21	Au	ppm	0.411	0.003	0.012	0.16	<0.001	<0.001	2.43
Ag-OG62	Ag	ppm				1480			222
Pb-OG62	Pb	%							
Zn-OG62	Zn	%							

		Sample No.	10261	10089	10077
		Rock Type	calcite vein	jasperoid	quartzite
		Alteration			
		UTM E (NAD27)	678540	672758	682649
		UTM N (NAD27)	4422508	4421544	4423807
Method	Analysis	Unit			
ME-ICP06	SiO2	%	0.45	97.7	86.4
ME-ICP06	Al2O3	%	0.1	0.46	6.27
ME-ICP06	Fe2O3	%	0.2	0.78	3.49
ME-ICP06	CaO	%	56.5	0.9	0.1
ME-ICP06	MgO	%	0.45	0.04	1.18
ME-ICP06	Na2O	%	0.01	0.02	0.23
ME-ICP06	K2O	%	0.01	0.08	1.13
ME-ICP06	Cr2O3	%	<0.01	0.01	0.01
ME-ICP06	TiO2	%	<0.01	0.02	0.36
ME-ICP06	MnO	%	0.01	0.01	0.04
ME-ICP06	P2O5	%	0.01	0.05	0.03
ME-ICP06	SrO	%	0.03	<0.01	<0.01
ME-ICP06	BaO	%	<0.01	0.01	0.02
ME-MS81	C	%	11.7	0.24	0.03
ME-MS81	S	%	0.02	0.03	<0.01
C-IR07	LOI	%	43.8	0.92	1.77
S-IR08	Total	%	101.57	101	101.03
ME-MS81	Ba	ppm	17.4	68.8	150
ME-MS81	Ce	ppm	1	6.2	31.3
ME-MS81	Cr	ppm	<10	90	60
ME-MS81	Cs	ppm	0.06	0.63	1.79
ME-MS81	Dy	ppm	0.09	0.32	2.35
ME-MS81	Er	ppm	0.04	0.2	1.47
ME-MS81	Eu	ppm	0.03	0.15	0.42
ME-MS81	Ga	ppm	0.8	1	8.6
ME-MS81	Gd	ppm	0.15	0.44	2.38
ME-MS81	Ge	ppm	<5	<5	<5
ME-MS81	Hf	ppm	<0.2	0.3	6.6
ME-MS81	Ho	ppm	0.03	0.08	0.5
ME-MS81	La	ppm	0.5	8.7	15.7
ME-MS81	Lu	ppm	<0.01	0.02	0.22
ME-MS81	Nb	ppm	<0.2	0.7	7
ME-MS81	Nd	ppm	0.6	5.8	13.6
ME-MS81	Pr	ppm	0.13	1.46	3.58
ME-MS81	Rb	ppm	0.4	3.4	37.4
ME-MS81	Sm	ppm	0.1	0.86	2.36
ME-MS81	Sn	ppm	<1	2	1
ME-MS81	Sr	ppm	277	50.5	13.3
ME-MS81	Ta	ppm	<0.1	0.1	0.5
ME-MS81	Tb	ppm	0.02	0.05	0.37
ME-MS81	Th	ppm	<0.05	0.57	6.55
ME-MS81	Tm	ppm	0.01	0.03	0.23
ME-MS81	U	ppm	0.36	0.72	1.29
ME-MS81	V	ppm	<5	7	31
ME-MS81	W	ppm	1	2	1
ME-MS81	Y	ppm	0.9	3	13.1
ME-MS42	Yb	ppm	0.03	0.16	1.58
ME-MS42	Zr	ppm	<2	4	255
ME-MS42	As	ppm	2.4	17.5	5.3
ME-MS42	Bi	ppm	<0.01	0.1	0.05
ME-MS42	Hg	ppm	0.263	0.155	<0.005
ME-MS42	In	ppm	0.005	0.022	0.011
ME-MS42	Re	ppm	<0.001	<0.001	<0.001
ME-MS42	Sb	ppm	10	6.39	0.06
ME-MS42	Se	ppm	0.2	0.3	0.2
OA-GRA05	Te	ppm	0.01	0.01	0.02
TOT-ICP06	Tl	ppm	<0.02	0.3	0.06
ME-4ACD81	Ag	ppm	6	6.6	<0.5
ME-4ACD81	Cd	ppm	<0.5	<0.5	<0.5
ME-4ACD81	Co	ppm	<1	1	9
ME-4ACD81	Cu	ppm	7	8	12
ME-4ACD81	Li	ppm	<10	10	20
ME-4ACD81	Mo	ppm	1	5	1
ME-4ACD81	Ni	ppm	<1	3	17
ME-4ACD81	Pb	ppm	17	14	12
ME-4ACD81	Sc	ppm	<1	<1	5
ME-4ACD81	Zn	ppm	7	35	47
Au-ICP21	Au	ppm	<0.001	0.003	<0.001
Ag-OG62	Ag	ppm			
Pb-OG62	Pb	%			
Zn-OG62	Zn	%			